# POTENTIAL IMPACTS OF CLIMATE CHANGE ON WIND ENERGY RESOURCES IN TÜRKİYE

A THESIS SUBMITTED TO
THE GRADUATE SCHOOL OF NATURAL AND APPLIED SCIENCES
OF
MIDDLE EAST TECHNICAL UNIVERSITY

BY

İREM IŞIK ÇETİN

IN PARTIAL FULFILLMENT OF THE REQUIREMENTS
FOR
THE DEGREE OF DOCTOR OF PHILOSOPHY
IN
EARTH SYSTEM SCIENCE

MARCH 2023

Approval of the thesis:

**POTENTIAL IMPACTS OF CLIMATE CHANGE ON WIND ENERGY RESOURCES IN TÜRKİYE**

submitted by **İREM IŞIK ÇETİN** in partial fulfillment of the requirements for the degree of **Doctor of Philosophy** i**n Earth System Science, Middle East Technical University** by,

Prof. Dr. Halil Kalıpçılar
Dean, Graduate School of **Natural and Applied Sciences** _____

Prof. Dr. İsmail Ömer Yılmaz
Head of the Department, **Earth System Sciences** _____

Prof. Dr. İsmail Yücel
Supervisor, **Earth System Sciences, METU** _____

Assoc. Prof. Dr. İzzet Arı
Co-Supervisor, **Energy Economics and Management, Social Sciences Uni. of Ankara** _____

**Examining Committee Members:**

Assoc.Prof.Dr. Tuğrul Yılmaz
Civil Engineering, METU _____

Prof. Dr. İsmail Yücel
Civil Engineering, METU _____

Assoc. Prof. Dr. Barış Önol
Meteorological Engineering, Istanbul Technical University _____

Assoc. Prof. Dr. Nejan Huvaj
Civil Engineering, METU _____

Assoc. Prof.Dr. Hakan Aksu
Meteorological Engineering, Samsun University _____

Date: 02.03.2023

**I hereby declare that all information in this document has been obtained and presented in accordance with academic rules and ethical conduct. I also declare that, as required by these rules and conduct, I have fully cited and referenced all material and results that are not original to this work.**

Name Last name : İrem Işık Çetin

Signature :

# ABSTRACT

## POTENTIAL IMPACTS OF CLIMATE CHANGE ON WIND ENERGY RESOURCES IN TÜRKİYE

Işık Çetin, İrem
Doctor of Philosophy, Earth System Science
Supervisor : Prof. Dr. İsmail Yücel
Co-Supervisor: Assoc. Prof. Dr. İzzet Arı

March 2023, 227 pages

Increasing the use of renewable energy is crucial in reducing the adverse effects of climate change. However, climate change will also affect weather-dependent renewable energy resources. Therefore, this study aims to identify the effects of climate change on the wind energy resources in Türkiye, which is in the Mediterranean hotspot, in the next century by using recent climate projections (CMIP6) with two different scenarios. The study includes four different results for wind resources in Türkiye. First, two multi-model ensemble techniques (random forest [RF] and multiple linear regression) are applied to 28 CMIP6 models by using ERA5, MERRA2, and observation data during the historical period (1980-2014). Secondly, the RF method is applied to future projections from CMIP6 models with two scenarios (SSP2-4.5 and SSP5-8.5) using extrapolated wind speeds to 100 m. Thirdly, mesoscale model outputs were used to identify the wind resource over the study area to avoid the low resolution of general circulation models, for the SSP5-8.5 scenario. The results showed that climate change is likely to have an impact on wind energy resources in Türkiye. While there may be increases in wind speeds in the Aegean Sea (5.9%), Aegean Region (7.2%), Marmara Region (10%) and the

Marmara Sea (14.7%) in summer, decreases was determined in winter season in Türkiye (-4.1%). In addition to analysis, energy yield estimation for two selected wind farms were calculated using mesoscale model outputs. Overall results were also evaluated within the framework of climate and energy policies.

Keywords: Climate Change, Wind Resource, Wind Energy, Climate Modeling.

# ÖZ

## İKLİM DEĞİŞİKLİĞİNİN TÜRKİYE RÜZGAR ENERJİ KAYNAĞINA OLASI ETKİLERİ

Işık Çetin, İrem
Doktora, Yer Sistem Bilimleri
Tez Yöneticisi: Prof. Dr. İsmail Yücel
Ortak Tez Yöneticisi: Doç. Dr. İzzet Arı

Mart 2023, 227 sayfa

İklim değişikliğinin olumsuz etkilerinin azaltılmasında yenilenebilir enerji kullanımının artırılması büyük önem taşımaktadır. Ancak iklim değişikliği, havaya bağlı yenilenebilir enerji kaynaklarını da etkileyecektir. Bu nedenle bu çalışmada, iki farklı senaryo ile güncel iklim projeksiyonlarını (CMIP6) kullanarak iklim değişikliğinin önümüzdeki yüzyılda Akdeniz sıcak noktasında yer alan Türkiye'nin, rüzgar enerjisi kaynakları üzerindeki etkilerini belirlemeyi amaçlamaktadır. Çalışma, Türkiye'deki rüzgar kaynakları için dört farklı sonuç içermektedir. İlk olarak, geçmiş dönemde (1980-2014) ERA5, MERRA2 ve gözlem verileri kullanılarak 28 CMIP6 modeline iki çoklu model buket tekniği (rastgele orman [RF] ve çoklu doğrusal regresyon) uygulanmıştır. İkinci olarak, RF yöntemi, 100 m'ye ekstrapole edilen rüzgar hızları kullanılarak iki senaryo (SSP2-4.5 ve SSP5-8.5) ile CMIP6 modelleri gelecek projeksiyonlarına uygulanmıştır. Üçüncüsü, SSP5-8.5 senaryosu için genel sirkülasyon modellerinin düşük çözünürlüğünü önlemek amacıyla çalışma alanı üzerindeki rüzgar kaynağını belirlemek için orta ölçekli model çıktıları kullanılmıştır. Sonuçlar, iklim değişikliğinin Türkiye'deki rüzgar enerjisi kaynakları üzerinde etkili olabileceğini göstermiştir. Yaz aylarında Ege Denizi (%5,9), Ege Bölgesi (%7,2), Marmara Bölgesi (%10) ve Marmara Denizi (%14,7)'nde rüzgar hızlarında artış olabilirken, Türkiye'de kış sezonunda azalış (%

-4,1) saptanmıştır. Analizlere ek olarak, seçilen iki rüzgar çiftliği için enerji üretim tahminleri, orta ölçekli model çıktıları kullanılarak hesaplanmıştır. Genel sonuçlar, iklim ve enerji politikaları çerçevesinde de değerlendirilmiştir.

Anahtar Kelimeler: İklim Değişikliği, Rüzgar Kaynağı, Rüzgar Enerjisi, İklim Modelleme

To my beloved cat, Mario and my husband

## ACKNOWLEDGMENTS

I would like to thank my supervisor, Prof. Dr. İsmail YÜCEL, for his patience, scientific guidance and support. I would have never been able to complete the study without his precious contributions, kind support and encouragement. I have been extremely lucky to have a supervisor who cared so much about my work, and who responded to my questions and queries so promptly.

I would like to thank to my co-supervisor Assoc. Prof.Dr. İzzet ARI for his comments and advice on my thesis. I would like to express my gratitude and appreciation to Assoc. Prof.Dr. Barış Önol for his valuable contribution to the study. I also would like to thank Assoc. Prof.Dr. Tuğrul Yılmaz for his critical contribution to the study.

I would like to thank Soner Ç. Bağçacı for providing the mesoscale model outputs. I would like to thank TUBITAK ULAKBIM for allowing us to calculate/analyze mesoscale model outputs. The numerical calculations for the mesoscale modeling part reported in this study were partially performed at TUBITAK ULAKBIM, High Performance and Grid Computing Center (TRUBA resources). I would like to thank the Turkish State of Meteorological Servies for providing us observed wind speed data for the entire Türkiye; ECMWF for ERA5 products; NASA for MERRA2 products; WCRP for CMIP6 products and Copernicus services to provide ERA5 and CMIP6 data.

I would like to thank my sister, Dr.Göksu IŞIK for her support and academic perspective. I would like to thank my parents Ertan IŞIK and Hatice IŞIK for their encouragement and support. I would also like to thank my parents-in-law İbrahim ÇETİN and Ayser ÇETİN for their support. Finally, I would like to thank my husband Sinan ÇETİN for his patience, inspiration, endless support and critical comments during my entire PhD journey. Without his support, this thesis does not exist.

## TABLE OF CONTENTS

ABSTRACT ..... v

ÖZ ..... vii

ACKNOWLEDGMENTS ..... x

TABLE OF CONTENTS ..... xi

LIST OF TABLES ..... xiv

LIST OF FIGURES ..... xv

LIST OF ABBREVIATIONS ..... xxiv

CHAPTERS

1 INTRODUCTION ..... 1

1.1 Significance of the study ..... 5

1.2 Objectives and Scope of the Study ..... 7

1.3 Thesis Format ..... 8

2 LITERATURE REVIEW ..... 9

2.1 Climate Change ..... 9

2.1.1 Climate Modeling ..... 11

2.2 Wind Energy ..... 13

2.2.1 Wind Resource ..... 15

2.2.2 Wind Atlas Studies ..... 21

2.2.3 Wind Climatology of Türkiye ..... 23

2.3 Policy Perspective of Climate Change and Energy in Türkiye ..... 27

2.3.1 Climate Change Policy of Türkiye ..... 27

2.3.2 Energy Policy of Türkiye ..... 29

2.3.3 Wind Energy in Türkiye ..... 34
2.4 Impacts of Climate Change on the Wind Energy Resources ..... 36
3 DATA AND METHOD ..... 47
3.1 Data ..... 47
3.1.1 Observation Data ..... 48
3.1.2 Global Re-Analysis Data ..... 59
3.1.3 Coupled Model Intercomparison Project Phase 6 (CMIP6)- Data ..... 62
3.2 Study Area ..... 67
3.3 Method ..... 69
3.3.1 Validation ..... 69
3.3.2 Trend-Analysis ..... 71
3.3.3 Data Processing ..... 72
3.3.4 Wind Power Density ..... 73
3.3.5 Multi-Model Ensemble ..... 73
3.3.6 Mesoscale Model Outputs ..... 76
3.3.7 Microscale modeling of a selected onshore/offshore area ..... 77
4 RESULTS ..... 81
4.1 Evaluation of the reference data ..... 81
4.1.1 Trends in the Observation Data ..... 85
4.1.2 Trends in the Re-analysis data ..... 88
4.2 Multi-model ensemble results for historical period (1980-2014) ..... 91
4.2.1 Model Performances ..... 91
4.2.2 Dynamic Vegetation model effect ..... 100
4.2.3 Multi-model ensemble (MME) development for CMIP6 ..... 101

4.2.4 Performance of hindcast results ..... 105
4.3 Multi-model ensemble results for future period (2014-2100)..... 112
4.3.1 Changes in the offshore wind resource in Türkiye (at 100 m.a.g.l) 112
4.3.2 Changes in the wind resource on existing onshore Wind Power Plants (at 100 m.a.g.l) ..... 127
4.4 Mesoscale Model Output Analysis Results..... 151
4.4.1 Model performances ..... 151
4.4.2 Calculation of Wind Speeds at Hub heights ..... 161
4.4.3 Inter-annual changes during the historical wind resource ..... 164
4.4.4 Projected changes in the mesoscale wind resource..... 168
4.5 Micro-scale modeling results of a selected WPPs ..... 171
4.5.1 Offshore Area..... 172
4.5.2 Onshore WPP..... 180
5 DISCUSSION .....187
6 SUMMARY, CONCLUSIONS and RECOMMENDATIONS .....193
6.1 Summary and Conclusions..... 193
6.2 Recommendations ..... 202
REFERENCES .....203
CURRICULUM VITAE.....227

## LIST OF TABLES

TABLES

Table 1 Overview of widely used Wind Atlas Studies in Türkiye and Europe.....23
Table 2 Regional Distribution of Wind Power Potential of Türkiye [74]. .....27
Table 3 Summary of the relevant topics in the literature .....43
Table 4 General Overview of the Data.....47
Table 5 Number of Zero Values in the data .....50
Table 6 Missing Observations in the Monthly Data.....51
Table 7 List of Deleted Stations .....55
Table 8 Overview of CMIP6 historical period models .....64
Table 9 CMIP6 Models in the onshore WPPs future projections study.....65
Table 10 CMIP6 Models used in the offshore wind resource part of the study.....66
Table 11 CMIP6 Models used in the WRF-PGW .....66
Table 12 Wind field simulation conditions .....78
Table 13 Regional- Seasonal Error Metrics and Descriptive Statistics of Re-analysis data and Observations for Onshore Regions .....83
Table 14 NREL Wind Classes [263]. .....85
Table 15 Number of Stations for Seasonal Trend Analysis Results for each Region .....87
Table 16 Monthly Trends for Observation Stations .....88
Table 17 Test and Train Period MLR Results.....103
Table 18 Test and Train Period RF Results.....104
Table 19 Seasonal errors for RF predictions in terms of each sea .....118
Table 20 SSP5-8.5 Trends for Regions and Models .....123
Table 21 Averages of regional error for all WPPs .....142
Table 22 Statistical error metrics calculated for the closest WRF-ERA5 grid points .....156
Table 23 Statistical error metrics with observations and closest WRF-ERA5 grid points .....158

## LIST OF FIGURES

FIGURES

Figure 1 Modern direct $CO_2$ measurements of well-mixed $CO_2$ [55] ..... 10
Figure 2 Development of global wind power installed capacities [3] ..... 14
Figure 3 Wind turbine power curve [63] ..... 15
Figure 4 Wind Power Density Distribution of Türkiye [74] ..... 22
Figure 5 Elevation Map of Türkiye [100] ..... 24
Figure 6 Corine 2018 Land Cover Map of Türkiye [101] ..... 24
Figure 7 ERA5 Re-Analysis seasonal and annual mean temperature ( $^0$C) (1979-2020 period) ..... 26
Figure 8 Wind Speed Distribution over Türkiye [74]. ..... 26
Figure 9 Share of Installed capacities by resource in Türkiye [4]. ..... 30
Figure 10 Türkiye Demand Projections [117]. ..... 31
Figure 11 Annual and cumulative wind energy installations by years of Türkiye [129] ..... 34
Figure 12 Locations of Wind Power Plants in Türkiye [134]. ..... 36
Figure 13 Surface winds change according 20C warming scenario relative to 1850-1900 [169] ..... 39
Figure 14 Amount of the data with all stations obtained from TSMS ..... 48
Figure 15 Location of the 239 stations ..... 49
Figure 16 Inhomogenity and gradual decrease (17085) examples from the stations ..... 52
Figure 17 An example of deleted station ..... 53
Figure 18 Example of Cropped Station ..... 53
Figure 19 Mean Wind Speeds from Daily Data at 239 Stations ..... 56
Figure 20 Maximum Wind Speeds from Daily Data at 239 Stations ..... 57
Figure 21 Annual Mean Wind Speeds without cropped data ..... 57
Figure 22 Seasonal mean wind speeds ..... 58
Figure 23 Annual maximum wind speeds for each station at each year ..... 59

Figure 24 Seasonal average wind speeds (m/s) of ERA5 data over the study area. 60
Figure 25 Seasonal avarage wind speed (m/s) of MERRA2 data over the study area ..... 61
Figure 26 Diurnal Averages for all regions with 3 reference data ..... 62
Figure 27 Available periods for all data: CMIP6 data is obtained at monthly avarages, observation data is available at daily avarages and ERA5 and MERRA2 data is obtained at hourly avarages ..... 62
Figure 28 Study Area and location of Observation Stations ..... 68
Figure 29 Offshore study area including the seas surrounding Türkiye (I: Black Sea, II: Marmara Sea, III: Aegean Sea, IV: Mediterranean Sea) ..... 68
Figure 30 Locations of Wind Power Plants (associated with centroids, polygon borders and turbines) in Türkiye and Study area, Geographical regions are also numbered as I: Marmara Region, II: Aegean Region, III: Mediterranean Region, IV: Anatolia Region, V: Black Sea Region, VI: East Anatolia Region, VII: Southeast Anatolia Region. ..... 69
Figure 31 Summary of the researh method and design ..... 79
Figure 32 Seasonal averages of global re-analysis data ..... 81
Figure 33 Wind Power Density ($W/m^2$) at 10 m with ERA5 and MERRA2 data .. 84
Figure 34 Wind Power Density ($W/m^2$) ERA5 at 100 m and MERRA2 at 50 m ... 85
Figure 35 Annual Mann-Kendall Trend Test Results ..... 86
Figure 36 Seasonal Mann-Kendall Trend Test Results ..... 87
Figure 37 Annual maximum wind speeds' trend results ..... 88
Figure 38 Trend slopes (ms-1/decade) from daily averaged near surface wind speed across seven different geographical regions and Aegean offshore area for ERA5, MERRA2, and observation. Slopes of each region are calculated from annual and seasonal avarage wind speeds and interpolated to each grid resolution for global re-analysis data. All of 178 observation stations are not used in observed trend analysis due to the availability of some missing periods during the entire period (only 22 station is used with full period data) Significant trends are also signed in the figure where p-value is $< 0.05$. ..... 90

Figure 39 Corr. Coefficients for grid-based observations..... 92
Figure 40 Correlation Coefficients between CMIP6 and MERRA2 data..... 92
Figure 41 Correlation Coefficients between CMIP6 and MERRA2 data..... 93
Figure 42 RMSE for grid-based observations ..... 94
Figure 43 RMSE between CMIP6 and MERRA2 data ..... 94
Figure 44 RMSE between CMIP6 and ERA5 data..... 95
Figure 45 Bias for observations ..... 96
Figure 46 Bias between CMIP6 and MERRA2 data ..... 96
Figure 47 Bias between CMIP6 and ERA5 data ..... 97
Figure 48 Taylor Diagram for Observations..... 98
Figure 49 Taylor Diagram for ERA5..... 98
Figure 50 Taylor Diagram for MERRA2..... 99
Figure 51 Taylor diagrams for all models and MERRA2 data with ERA5 for each region and entire onshore Türkiye (“All”)..... 100
Figure 52 Comparison of EC-Earth Models and Re-analysis data ..... 101
Figure 53 Regional Errors for ALL- MLR and RF Predictions..... 105
Figure 54 DVM Models Results ..... 106
Figure 55 WDVM Models Results ..... 106
Figure 56 Boxplots for Entire Time Series and MLR Results for Each Region... 107
Figure 57 MLR-based MME estimates using ERA5, MERRA 2 and Observation as reference data over three onshore (Marmara, Aegean, and Mediterranean) and Aegean offshore regions. ..... 108
Figure 58 RF-based MME estimates using ERA5, MERRA2 and Observation as reference data over three onshore (Marmara, Aegean, and Mediterranean) and Aegean offshore regions. ..... 109
Figure 59 All Models MME Results for Monthly Means..... 110
Figure 60 DVM Models MME Results for Monthly Means ..... 111
Figure 61 WDVM Models MME Results for Monthly Means..... 111
Figure 62 Entire Period MLR and RF Results and GCM Means vs Observations-ERA5-MERRA2 for Onshore and Offshore regions ..... 112

Figure 63 Calculated heights for AWI-CM-1-1-MR Model between surface and 1000 mb ..... 113
Figure 64 Calculated heights for AWI-CM-1-1-MR Model between surface and 925, and surface and 850 mb ..... 113
Figure 65 The 100 m calculated wind speed results from 1000 mb wind speeds and 1000 mb raw wind speed for AWI-CM-1-1-MR Model ..... 114
Figure 66 The 100 m calculated wind speed results from 925 mb wind speeds and 925 mb raw wind speed for AWI-CM-1-1-MR ..... 114
Figure 67 The 100 m calculated wind speed results from 850 mb wind speeds and 850 mb raw wind speed for AWI-CM-1-1-MR ..... 115
Figure 68 Errors between ERA5 and CMIP6 models during the train period (1980-2014) for all model grids at each region (dots represents the grid points errors associated with each model). ..... 116
Figure 69 Train period wind speeds for individual models, GCM means, ERA5 and RF predictions ..... 117
Figure 70 Regional scatter plots for RF prediction and GCM means versus ERA5 data ..... 119
Figure 71 RF Predictions for entire period (SSP5-8.5) together with ERA5 re-analysis data and GCM means (Each boxplot represents a year which contains 12 months wind speed data) ..... 120
Figure 72 Averaged monthly wind speed changes (%) between three future periods and reference periods based on ERA5 for two scenarios. ..... 121
Figure 73 SSP2-4.5 Scenario 3 Months Rolling Means for RF Predictions, ERA5 and GCM Means ..... 123
Figure 74 SSP2-4.5 Scenario 6 Months Rolling Means for RF Predictions, ERA5 and GCM Means ..... 124
Figure 75 SSP2-4.5 Scenario 8 Months Rolling Means for RF Predictions, ERA5 and GCM Means ..... 124
Figure 76 SSP2-4.5 Scenario 12 Months Rolling Means for RF Predictions, ERA5 and GCM Means ..... 125

Figure 77 SSP 5-8.5 Scenario 3 Months Rolling Means for RF Predictions, ERA5 and GCM Means ..... 125
Figure 78 SSP 5-8.5 Scenario 6 Months Rolling Means for RF Predictions, ERA5 and GCM Means ..... 126
Figure 79 SSP 5-8.5 Scenario 8 Months Rolling Means for RF Predictions, ERA5 and GCM Means ..... 126
Figure 80 SSP 5-8.5 Scenario 12 Months Rolling Means for RF Predictions, ERA5 and GCM means ..... 127
Figure 81 Shear exponent calculation from ERA5 Re-analysis data..... 128
Figure 82 100 m wind speed comparisons for ERA5 re-analysis data ..... 128
Figure 83 Histograms of ERA5 Wind Speeds at 100 m.a.g.l ..... 129
Figure 84 An example of 100-m wind speed from AWI-CM-1-1-MR calculated with extrapolation using the shear exponent and 10-m wind speed (m/s). ..... 130
Figure 85 Difference between 10 m and 100 m wind speeds (m/s)..... 130
Figure 86 Statistics between GCMs and ERA5 data at 100 m.a.g.l. for each WPP ..... 131
Figure 87 Taylor diagram for all WPPs at each GCMs vs ERA5..... 132
Figure 88 Seasonal Taylor diagrams for 27 GCMs with ERA5 (as an “observed”) included all WPPs nearest grids in historical period (1980-2014)..... 133
Figure 89 Seasonal average wind speeds (m/s) at historical period for selected 15 GCMs which has higher correlation with ERA5 at 100 m.a.g.l. ..... 134
Figure 90 Seasonal average wind power density ($W/m^2$) at historical period for selected 15 GCMs which has higher correlation with ERA5 at 100 m.a.g.l. ..... 135
Figure 91 Entire study period RF results together with individual GCMs and ERA5 data ..... 136
Figure 92 Histogram of train period with two scenarios and ERA5 data in terms of regions and seasons ..... 137
Figure 93 Histogram of wind speed differences between prediction and ERA5 data during the train period with two scenarios in terms of regions and seasons..... 138

Figure 94 Corr. Coefficients between RF prediction and ERA5 during the train period, closed stations are zooms in some parts of the Marmara, Aegean and Mediterranean region.....139
Figure 95 RMSE for all WPPs for train period .....139
Figure 96 RMSE for Çanakkale, İzmir, Balıkesir cities.....140
Figure 97 for all WPPs for train period .....140
Figure 98 for Çanakkale, İzmir, Balıkesir cities.....141
Figure 99 Train period errors of entire study area for each WPPs in terms of regions .....142
Figure 100 Regional and seasonal errors for RF predictions during the train period for each WPP, each point represents the each WPP and rows shows the seasons while the columns show the errors .....143
Figure 101 Annual average time series analysis for regional wind speed predictions during the entire period (shaded area shows the confidence interval related to ERA5 annual avarages with standard deviation).....144
Figure 102 Monthly average time series analysis for regional wind speed predictions during the entire period (shaded areas shows the confidence interval with standard deviation) with ERA5 entire period averages .....145
Figure 103 Changes in the wind speed (%) between RF predictions and ERA5 reference data for three period at SSP2-4.5 scenario: each boxplot includes WPPs, columns show the geographical regions while the rows show the near-term (2014-2045), mid-term (2045-2075), long-term (2075-2100) average differences from the reference data.....146
Figure 104 Same as figure 103 but for SSP5-8.5 scenario.....147
Figure 105 Trend results for scenarios and historical periods in terms of number of significant trends (p value < 0.05) and “no trends” for percentage of GCMs among 27 GCMs .....148
Figure 106 Wind power densities ($W/m^2$) at 100 m for 14 CMIP6 models in the Table-9, together with SSP5-8.5 scenario (Part-1).....149

Figure 107 Wind power densities (W/m$^2$) at 100 m for 14 CMIP6 models in the table-9, together with SSP5-8.5 scenario (Part-2)..... 150
Figure 108 Wind speed and direction of 13 GCMs and WRF-ERA5 ..... 152
Figure 109 WRF and reference data comparisons at seasonal and annual scale .. 153
Figure 110 Detailed illustration of REPA [74], (100 m) and WRF-ERA5 (80 m.a.g.l) data ..... 154
Figure 111 WRF topography and observation station heights (m.a.g.l.) ..... 154
Figure 112 Regional Taylor Diagrams for between CMIP6 Models, WRF-ERA5, and two reanalysis data (MERAA2 and ERA5) ..... 155
Figure 113 Error heatmaps prepared for CMIP6 Models, MERRA2, ERA5, WRF-ERA5 through and observation stations ..... 156
Figure 114 Wind speed and direction of 13 GCMs and WRF-PGW ..... 159
Figure 115 Annual and seasonal averages for future period for WRF-PGW and CMIP6 ensembles with 13 GCMs. ..... 160
Figure 116 Annual and seasonal variability (variance) during the future period for WRF-PGW and CMIP6 ensembles with 13 GCMs. ..... 160
Figure 117 Annual and seasonal standart deviation for future period for WRF-PGW and CMIP6 ensembles with 13 GCMs..... 161
Figure 118 Mean height (m) at level-1 (bottom_top=0) ..... 162
Figure 119 Mean height (m) at level-2 (bottom_top=1) ..... 162
Figure 120 Mean height (m) at level 3 (bottom_top=2) ..... 162
Figure 121 Wind Speeds at 80 m for seasonal time scale (1995-2014)..... 163
Figure 122 Air density at 80 m for seasonal time scale (1995-2014) ..... 163
Figure 123 Wind power density at 80 m for seasonal time scale (1995-2014) .... 163
Figure 124 Annual mean wind speeds at 80 m ..... 164
Figure 125 Annual standard deviation of monthly wind speed data at 80 m ..... 165
Figure 126 Annual variability (variance) of monthly wind speed data at 80 m ... 165
Figure 127 Annual mean wind power density at 80 m ..... 166
Figure 128 Annual standart deviation of monthly WPD at 80 m ..... 167
Figure 129 Annual variability of monthly wind power density at 80 m..... 167

Figure 130 Difference between WRF-PGW and WRF-ERA5 (at 10 m) ..... 168
Figure 131 Projected wind speed changes in percentage (at 10 m) ..... 168
Figure 132 Simple mean ensemble and WRF outputs anomalies at seasonal and annual time scale (at 10 m) ..... 169
Figure 133 Changes in the future wind speeds (m/s) ..... 169
Figure 134 Changes in the future wind speeds (%) ..... 170
Figure 135 Wind power density ($W/m^2$) changes ..... 171
Figure 136 Wind power density changes (%) ..... 171
Figure 137 Vestas v90 wind turbine power curve and trust coefficient from WindSIM program ..... 172
Figure 138 10 MW-DTU wind turbine power curve and trust coefficient from WindSIM ..... 172
Figure 139 Wind speed distribution together with bathymetry data taken from GEBCO [269]. ..... 173
Figure 140 WPD distribution together with bathymetry data ..... 174
Figure 141 Wind Power Density ($W/m^2$) and wind speed (m/s) information over the selected area ..... 174
Figure 142 Overview of the WRF grid points and the selected area ..... 175
Figure 143 Terrain model set-up “a” is the horizontal mesh and “b” is the vertical gridding from surface to 800 m with 10 different vertical level ..... 175
Figure 144 Wind rose and Weibull distribution of wind speeds for grid point at 80 m (WRF-ERA5 Grids) ..... 176
Figure 145 Wind rose and Weibull distribution of wind speeds for grid point at 80 m (WRF-PGW-GRIDS) ..... 176
Figure 146 Wind speed distribution over the area with WRF-ERA5 from WindSIM program ..... 177
Figure 147 Wind speed distribution over the area with WRF-PGW from WindSIM program ..... 177
Figure 148 Wind farm layout from WindSIM program ..... 179

Figure 149 Wind Speed distribution with WRF-ERA5 outputs from WindSIM program ..... 179
Figure 150 Wind Speed distribution with WRF-ERA5 outputs from WindSIM program ..... 180
Figure 151 Selected onshore WPP layout and locations of the WRF grids and observation station ..... 181
Figure 152 Terrain (left) and roughness maps (right) of the WPP ..... 181
Figure 153 Terrain model setup ..... 182
Figure 154 Obsevation at 80 m ..... 182
Figure 155 WRF-ERA5 Grids at 80 m ..... 183
Figure 156 WRF-PGW Grids at 80 m ..... 183
Figure 157 Observation wind speed ..... 184
Figure 158 ERA5 all grids wind speed ..... 184
Figure 159 WRF-PGW all grid wind resource distribution ..... 185
Figure 160 Regional changes (%) for offshore RF prediction anomalies ..... 196
Figure 161 Regional avarages for onshore RF prediction anomalies (%) ..... 198
Figure 162 Regional avarages for WRF-PGW prediction anomalies (wind speed-%) ..... 200
Figure 163 Regional avarages for WRF-PGW prediction anomalies (WPD-%).. 200
Figure 164 Summary of the mesoscale model outputs with the nearest onshore WPPs ..... 201

## LIST OF ABBREVIATIONS

ABBREVIATIONS

AEP: Annual Energy Production

AOS: Automatic Observation Station

AR: Assessment Report

CM: Coupled Model

CMIP6: Coupled Model Intercomparison Project 6

$CO_2$: Carbon dioxide

COP: Conference of Parties

DVM: Dynamic Vegatation Model

ERA5: 5th generation ECMWF re-analysis

GCM: Global Circulation Model

GW: Gigawatt

IPCC: Intergovernmental Panel on Climate Change

m.a.g.l: meter above the ground level

MENR: Ministry of Energy and Natural Resources in Türkiye

MERRA2: Modern-Era Retrospective analysis for Research and Applications, Version 2

MLR: Multiple Linear Regression

MME: Multi-model ensemble

MW: Megawatt

NetCDF: Network Common Data Form

RCM: Regional Climate Model

REPA: Turkish Wind Energy Potential Atlas

RF: Random Forest

SRTM: Shuttle Radar Topographic Mission

TSMS: Turkish State of Meteorological Services

WCRP: World Climate and Research Program

WG: Working Group

WPP: Wind Power Plant

WRF: Weather Research and Forecast Model

YEKA: Renewable Energy Resource Zone (the tender model in Türkiye)

# CHAPTER 1

# INTRODUCTION

The energy sector is responsible for increasing $CO_2$ emissions due to the overuse of fossil fuels. According to Intergovernmental Panel on Climate Change (IPCC), 25 % of total direct emissions reasoned from energy and heat production [1]. $CO_2$ levels have reached the highest level since the pre-industrial era. Hence, renewable energy resources have become significant alternative energy resources over the last decades. Wind, solar, ocean, geothermal, and biomass are the most widely used renewable energy resources. The countries have also targeted to increase the share of renewables in the near-, mid- and long-term future to increase the use of alternative resources by keeping temperatures around $1.5^0$C within the scope of the Paris Agreement. European Union (EU) leads to the development of renewable energy, particularly in wind power, which aims to become carbon neutral in 2050 and increase the share of renewables by at least % 55 by 2030 [2].

It is a well-known fact that wind energy has one of the most critical energy resources for reducing Greenhouse Gas (GHG) emissions. Wind energy has dramatically increased since the early 2000s. The world reached 837 GW installed wind power capacity at the end of 2021, and 93.6 GW of this capacity was installed in 2021 worldwide [3]. Türkiye also reached the 11.396 MW installed wind power capacity at the end of December 2022 [4] and also aimed to reach 29.9 GW installed wind power capacity at 2035 [5]. There are many reasons for increased wind power all over the world. However, price is one of the most critical factor. Wind power capital expenditures have become competitive with fossil fuels over the last decades. It is also expected that offshore wind power will be cheaper in upcoming years, depending on the technology [6].

On the other hand, known as a hotspot of climate change Mediterranean region is expected to see the highest rates of change in hydrometeorological variables and its climate [7, 8]. Located on the eastern shores of the Mediterranean region and having complex topographical terrain surrounded by seas, Türkiye may potentially suffer rapid changes in the variability and availability of its wind energy resources. However, in the latest released IPCC Report (2022), it was shown that the impact of climate change on wind resources have low agreement with high confidence [9]. This low agreement are reasoned from both using different models and limited studies over the region about predicting the existing wind resources. On the other hand, extremes is expected to continue to increase at high confidence level for the Mediterranean region [10]. Together with the Assesment Report (AR) 6, an interactive global atlas, which also includes surface wind as well, published by IPCC [11] using 31 Coupled Model Intercomparison Project (CMIP) 6 where the models showed low agreement over the continental Türkiye. Continuing uncertainty about climate change impacts in changing world prevents better decision-making necessary for proper and adaptive wind resources management in this region.

Wind speed trend analysis using ground observations may have a tendency toward significant decreasing trend. However, relating this decreasing trend solely to climate change might be suspicious because of global terrestrial stilling that is dominated by increasing surface friction [12]. Similarly, using observational stations of the Turkish State Meteorological Service (TSMS) distributed over Türkiye from 1975 to 2006, Dadaser-Celik and Cengiz, E. (2014) also found negative trends for observed wind speeds [13]. Therefore, it is also essential to understand the possible causes of these trends by investigating the relationship between re-analysis data, climate models and observation data [12]. Yet, such a study has been missing in the literature. Accordingly, dedicated renewable energy potential variability analyses over Türkiye should be done in the climate change framework utilizing the latest climate projections.

The potential of the wind resource is also commonly determined using the Global Circulation Models (GCMs) for long-term planning of variable energy resources.

Some difficulties arise from predicting wind climate because each GCM has unique features of different initial conditions, model physics and dynamics, and resolution. The fundamentals for evaluating the utility of these models require calibration and verification studies. Hence, they can be reliable in extending their utility to solve important practical questions. The latest version of the CMIP (the sixth phase; CMIP6) models [14] uses Shared Socio-economic Pathways (SSPs), different from the Representative Concentration Pathways (RCPs) in CMIP5. Although radiative forcing is same as the RCPs, SSPs also include land use changes and aerosol forcing (including optical properties) [14].

Recent studies have increasingly focused on using CMIP6 models to assess global historical and future climate change impacts on precipitation and temperature [15, 16]. However, the use of CMIP6 models for investigating the climate change impacts on wind resources is limited in the literature [17–20]. Therefore, studies which use CMIP6 over Türkiye for wind resource determination are very limited. Carvalho et al. (2021) used CMIP6 data over Europe, including Türkiye with the multi-model ensemble (MME) and found that there could be a wind speed increase over Türkiye around 15-30 % according to the SSP2.4-5 scenario at the end of the 21$^{st}$ century [18]. Most MME studies focusing on the climate change impact on wind speed have included simple averaging with the CMIP5 and prior versions of CMIPs [21–28].

The intermittency of wind speed causes nonlinear patterns. Thus, it is generally difficult to predict the wind accurately and efficiently using a simple average ensemble lacking the weights among models and using a multi-model ensemble considering linear assumption. As a low agreement among CMIP6 models on wind speed analysis is highlighted over the Mediterranean region, the use of performance-based weights in forming the MME becomes critical. Besides, as a supervised machine learning algorithm, Random Forest (RF) can identify and formulate inherently the nonlinear structure of the wind speed. The RF has been used widely in regression problems, including wind energy applications and short-term wind power forecasts over the last decade [29–32]. However, the application of the RF method on long-term wind speed assessments using the number of CMIP6 climate

models and its comparison with the weighted average multiple linear regression (MLR) method has not been performed yet. Moreover, downscaling techniques are widely used in the literature to determine climate resources. However, the studies about wind in this manner are also limited.

On the other hand, there is no offshore wind farm yet in Türkiye. However, the potential is high and expected to be tapped in the future, especially for offshore floating foundations [33]. Offshore wind resource assessment studies are also limited for Türkiye and performed on a regional basis [34–36]. Over the Aegean Sea region, some studies focus on offshore wind potential and corresponding wind energy resources associated with the Etesian winds [37–40]. In addition, multiple re-analysis data sets were compared with observation for predicting wind power production over localized wind farms in France [41]. Some studies targeting the site selection for wind turbines using ground stations over generally the region or city scale were also performed in Türkiye [42–45]. However, the studies using multiple GCMs, different re-analysis data, and ground observations together for comprehensive surface wind analysis over topographically complex regions and rough surfaces have still been limited.

Human systems will also be negatively affected by climate change. Besides, there will be unequal risks for all countries [46]. Particularly weather-dependent resources such as wind and solar will also be affected by future climate change effects. The changing global climate will affect wind energy in terms of resource magnitude, icing, and extreme wind speeds in the future [47, 48].

The nature of the wind is also affected by local topographies, roughness, obstacles [49]. Consequently, micro-meteorological effects should be considered in wind resource estimations. Moreover, the hub heights of wind turbines are getting bigger with technological advances. The atmospheric boundary layer must be accurately modeled in consideration of the increasing size of wind turbines [50]. Therefore, downscaling techniques need to be applied to decrease the uncertainties about future wind resource estimation, similar to wind atlas studies. However, high-resolution

future wind resource information with dynamical downscaling techniques is also missing in Türkiye.

In this study, firstly, a MME approach utilizing 28 CMIP6-based monthly surface wind speed predictions is generated using random forest (RF) and multiple linear regression (MLR) methods between 1980 and 2014 period over seven geographical regions with different topographic complexity in Türkiye and an offshore area. MMEs are also generated separately for groups of climate models with and without including dynamic vegetation growth in their land surface models. Performances of MME- and benchmark (ERA5 and MERRA2)-based predictions are compared against station-based predictions. Secondly, the RF method was applied to two different climate scenarios (SPP2-4.5 and SSP5-8.5) by using CMIP6 data and ERA5 data as reference data. Due to the complex topographical structure of Türkiye, onshore and offshore parts are separated into two parts using different wind speed extrapolation methods (power law and hypsometric equation). 330 RF predictions are developed for 330 WPPs already existing in Türkiye. Thirdly, mesoscale model outputs are analyzed and compared with the reference period. Model performances of mesoscale model outputs are evaluated with ERA5, MERRA2 and observations. Wind speeds and wind power density at the hub heights of the wind turbines are also calculated, and the second model level is used as the hub height of the wind turbines. Inter and intra-annual changes in the mesoscale wind resource are calculated and analyzed. Eventually, two different areas are selected for micro-scale modeling. The offshore area is chosen using mesoscale model outputs and bathymetry information and run in the WindSIM [51] program. An existing onshore wind power plant is also run with future and historical data.

## 1.1 Significance of the study

The use of climate models that provide long-term prediction is crucial for determining wind energy potential and its future planning. Several statistical and

dynamic methodologies are used in this work to apply and assess historical and projected wind resources in Türkiye.

There aren't many modeling studies that concentrate on how climate change will affect the wind resources over Turkiye, which is part of the Mediterranean hotspot. This study fills the gap in this area. Besides, this study, for the first time, investigates the following:

- The difference between the performance skills of MMEs of GCMs established using two different methods (MLR and RF) and 3 different benchmark datasets (two re-analysis and ground observation) for estimating monthly wind speed where the skills are compared against simple ensemble mean approach.
- The expected future change in wind speed potential over topographically complex onshore regions and an offshore region possessing high wind potential in the Eastern Mediterranean utilizing the latest generation GCMs. In forming MLR- and RF-based MMEs, two different re-analysis datasets, 5$^{th}$ generation ECMWF re-analysis (ERA5) and The Modern-Era Retrospective Analysis for Research and Applications, Version 2 (MERRA2) over the period of 1980-2014 are utilized. After testing the appropriateness of developed models, they are used for prediction through the entire evaluation period. This assessment hints at whether the models developed using CMIP6 are skillful enough to project future wind speed for long-term planning of wind energy resources.
- High-resolution (mesoscale model) future onshore and offshore wind resource availability and variability over Türkiye.

This study is also contributes to long term wind energy planning of Türkiye, which aims to increase the share of renewables in electricity production and reach net zero emission in 2053.

## 1.2 Objectives and Scope of the Study

This study aims to identify the effects of climate change on the wind energy resources in Türkiye in the next century by using CMIP6 outputs with two different climate scenarios. Due to the consideration of high-resolution from the regional models, Weather Research and Forecast Model (WRF) outputs are also used at 4 km horizontal resolution. ERA5, MERRA2 re-analysis data and observation data from the Turkish State of Meteorological Services are used as reference data over the period of 1980-2014. The objectives of the study can be summarised as follows:

- To evaluate future wind energy resources using multi-model ensemble methods and high-resolution numerical weather prediction and micro-scale model.
- To determine the variability and availability of future wind resources in two different climate scenarios for Türkiye.
- To identify forthcoming wind energy potential in Türkiye
- To test several methodologies for investigating wind resource

The study also aims to analyze future wind resources and the potential of Türkiye and find out whether there will be a feasible wind energy potential in Türkiye in the future by using the CMIP6 GCM model outputs which are recently released climate change projections.

The following questions are answered during this study.

- What will the future variability of wind resources in Türkiye be due to changing climate conditions?
- Türkiye aims to increase wind energy investments. However, there are already lower wind speeds compared to Northern European Countries. Will these wind speeds stay stable in the 21st century?
- Which CMIP6 models are better at simulating the wind climatology of Türkiye?

- How well do re-analysis data represent the current wind resource conditions in Türkiye?
- Current literature about climate change effects on wind energy resources is limited by model resolution and uncertainties. How could these uncertainties be decreased for Türkiye?

## 1.3 Thesis Format

The first chapter of the thesis defines the scope and significance of the work and summarizes the study. Chapter 2 frames the work in the context of climate change and wind energy, including the policy perspective of those both globally and in Türkiye, together with similar studies related to the impact of climate change on wind energy or wind resources. Chapter 3 concentrates specifically on the data and method used in this study and study area. Chapter 4 includes results from the multi-model ensemble, mesoscale, and micro-model. Chapter 5 discusses the results from the policy perspective on wind energy in Türkiye. Chapter 6 summarizes and concludes the research findings by seeking information about the changes in wind speeds and wind power density for future wind energy investments in Türkiye.

# CHAPTER 2

# LITERATURE REVIEW

## 2.1 Climate Change

IPCC was established under the auspices of the UN (composed of UNEP and WMO) in 1988, aims to collect the state of the art information about climate change for policymakers. IPCC (2022) defines climate change as "A change in the state of the climate that can be identified (e.g., by using statistical tests) by changes in the mean and/ or the variability of its properties and that persists for an extended period, typically decades or longer" [52]. However, climate can also be changed by both natural (volcanic eruptions, changes in the solar cycles) or human-related activities (resulting in the changes in the composition of the atmosphere) as it is defined in the UNFCCCs Article 1: "change of climate which is attributed directly or indirectly to human activity that alters the composition of the global atmosphere and which is in addition to natural climate variability observed over comparable time periods" [53].

Yet, the current scientific knowledge about climate change is based on the increasing greenhouse gas emissions that are mostly reasoned human-based activities such as land-use change, fossil fuel combustion, deforestation, etc. Depletion of natural resources by human activities and consuming more and more is causing the imbalance of natural feedback mechanisms, general circulation of the atmosphere, degradation of the environment, and loss of biodiversity. Since all elements of the climate system (hydrosphere, biosphere, atmosphere, geosphere) depend on each other with feedback mechanisms, any changes in one affect another and cause a snowball effect on the Earth.

On the other hand, climatic impact drivers are the solar and orbital forcing, volcanic aerosol forcings, greenhouse gases (well-mixed and halogenated), short-lived gases,

aerosols, land use, and land cover. Changes in the climate drivers degrade the Earth's energy balance, where the warming causes positive "Radiative Forcing" while the cooling causes negative radiative forcing. On the other hand, changes in the climate drivers are not only reasoned by human activities but also natural activities. For example, solar forcing and volcanic aerosol forcings are forced by the solar cycle and volcanic activities. However , changes in solar activities since the 1900s was high but not outstanding compared to the last 9000 year. Volcanic aerosol forcing is also similar to the previous 2500 years, and there are no notable changes [54].

However, changes in the gas content of the atmosphere are dramatically increased since the industrial revolution due to the combustion of fossil fuels to produce energy. Figure 1 shows the dramatic increase in $CO_2$ emissions since the mid-1900s according to the three measurements.

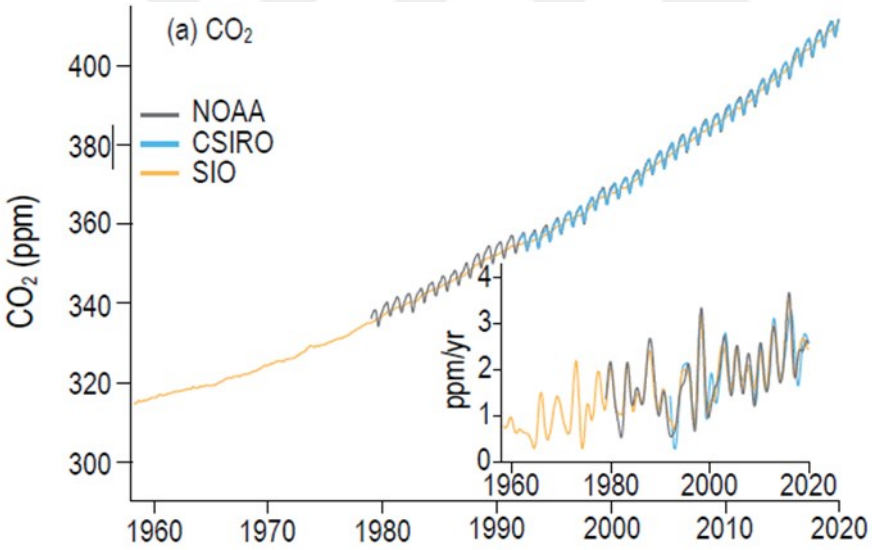



Figure 1 Modern direct $CO_2$ measurements of well-mixed $CO_2$ [55]

On the other hand, IPCC collects recently published research about climate change and regularly publishes reports about the topic every 4-6 years. According to "AR6 Physical Science Basis Report", most of the climatic impact drivers, including seven parameters (heat & cold, wet & dry, wind, snow&ice, coastal, open ocean, other [air pollution weather, atmospheric $CO_2$ at surface, radiation at surface]) of physical

climate systems will be changed by depending on region. Human-induced effects on the atmosphere system are also examined in the report. It found that the global mean surface temperature is 0.9-1.2°C increased while only −0.1°C to +0.1°C of this warming came from the natural forcings. However, this warming is not equally distributed to the world. For example, the land is warmed more quickly than the oceans [55].

With the medium confidence level in the AR6, Hadley Circulation has been extended in the Northern hemisphere since 1980 because this variability can be evaluated in the internal variability range. However, this enlargement with human influence has high confidence in the Southern hemisphere [52].

### 2.1.1 Climate Modeling

Climate models have been used to understand the general circulation of the atmosphere and climatology since the beginning of the 1900s. Most of the literature believes that the first climate modeling started with Bjerkness, which uses equations such as Newton's laws of motion, the hydrodynamic state, conservation of mass, momentum, thermodynamic energy equation, etc. Richardson has utilized Bjerkness's equations by using a "finite difference grid." Due to the error in the input data and apparent mistakes in the surface pressure, numerical modeling had been postponed for twenty years. However, the first numerical modeling started using Richardson's approach after World War II by using cartesian grids and energy transfer between those grids. Those models were regional models which did not model the entire globe [56].

GCMs are then started to use with the same equations that are mentioned above for more extended periods for the entire globe or a hemisphere. Depending on the developments in computers, GCMs started to develop, and many meteorological research institutions were established (after the three modeling institutions NCAR (National Center for Atmospheric Research), GFDL (Geophysical Fluid Dynamics

Laboratory), and UCAR (University Corporation for Atmospheric Research) at the beginning of the 1970s. Atmosphere-Ocean GCMs started to develop as coupled models in the 1980s. GCMs are widely used for calculating regional wind energy potential at seasonal to decadal time scales. Depending on the developments of the models, there are several climate models which use different components of the climate system. After that Earth System model, which includes land-surface interactions, cryosphere, all elements of the hydrological cycle, vegetation, etc., started to develop and be used in climate science [56].

After the establishment of the IPCC in 1988, modeling groups have come together and used standardized approaches with intercomparison projects (Atmosphere Modelling Intercomparison Project).

Coupled Models (CM) or Atmosphere-Ocean General Circulation Models (AOGCM)s are the "standard models" which determine the physical composition of the climate system [57]. The models were assessed in IPCC Assessment Report IV in 2007 [58].

Earth System Models (ESMs) are the new generation models which use all elements in the Earth System such as biosphere, atmosphere, land, ice, and ocean and their interactions with each other through various ways such as carbon, sulfur, ozone, etc. cycles and feedbacks, chemical reactions, etc. The difference between climate models and ESMs is the carbon cycle which means ESMs take into account captured $CO_2$ by the oceans, trees, or emitted $CO_2$ by anthropogenic resources. IPCC Assessment Report V assessed these models in 2013 [59]. Thus, changes in the land cover or changes in the aerosol content are also included in these models.

CMIPs have been developed by a working group of climate modeling in the World Climate and Research Program (WCRP) to understand the past, present, and future of the Earth's climate since the beginning of 1995. Lots of modeling groups from all over the world contribute to the CMIPs with the same experiment protocols, forcing, and outputs [14].

CMIP6s are the recent climate data with new scenarios. There are two types of models in the CMIP6 GCM outputs: coupled models (Atmosphere-Ocean) and Earth System Models. SSP is new scenario approach for climate projections which includes impact, vulnerability, adaptation, and mitigation [60]. SSPs also use radiative forcing like RCPs, but the difference comes from the impact, vulnerability, adaptation, and mitigation. SSPs includes energy system, emissions and climate change, and land use changes, as well as the climate and energy policies in the world. There are five SSP scenarios with four radiative forcings (2.6, 4.5, 6.0, and 8.5 $W/m^2$ are the radiative forcings, same with the RCPs). 5 SSP represents the *"Sustainability: Taking the Green Road (Low challenges to mitigation and adaptation), Middle of the Road (Medium challenges to mitigation and adaptation), Regional Rivalry: A Rocky Road (High challenges to mitigation and adaptation), Inequality – A Road Divided (Low challenges to mitigation, high challenges to adaptation), Fossil-fueled Development: Taking the Highway (High challenges to mitigation, low challenges to adaptation)"* respectively [60].

## 2.2 Wind Energy

Among the other renewables, the wind has one of the fastest growing renewables due to the rapid developments of technology and the abundancy of resources all over the world. Wind energy installed capacities which are dramatically increased over the last two decades, now reached 894 GW [3] % 7 of this installed capacity belongs to offshore wind energy with 57 GW installed capacity (see fig.2).

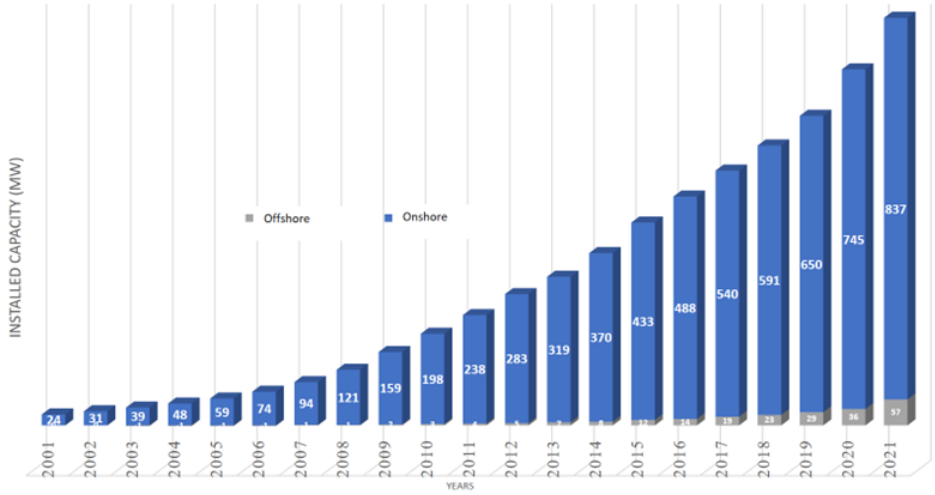



Figure 2 Development of global wind power installed capacities [3]

Modern wind turbines are composed of three blades and start to rotate with the wind and convert this kinetic energy to electrical energy. The power in the Equation (1) that is produced by wind basically depends on the air density and cube of the wind speeds.

$$\mathbf{P}=\frac{\mathbf{1}}{\mathbf{2}}\boldsymbol{x\rho xAxv^{3}} \qquad (1)$$

Wind turbines are rapidly developing depending on technological advances and increasing energy demand. The first commercialized wind turbines had a 100 kW installed capacity in the 1980s with a 20 m blade. At the beginning of the 1990s, MW-based wind turbines were produced [61]. Over the last decade, hub-heights weighted averages have been increasing. Türkiye is ranked with the third highest increase in the weighted average hub heights, with 44 % over the last decade [62].

On the other hand, according to Global Wind Energy Council (GWEC), around 4700 wind turbines in Europe and 25% of the onshore turbines will be decommissioned. New regulation and policy studies are also being performed in Europe to use wind resources efficiently [3]. Therefore, repowering wind turbines is another option for installed wind turbines that reach their end of life. Moreover, small wind turbines with older technology could be changed with new ones to produce more electricity from wind power.

However, produced power from wind turbines can vary with the type of the turbine, wind speeds, and power curve, which is specific to each manufacturer. A power curve is a function of wind speed at hub height and produced electricity. Figure 3 shows an example power curve of a wind turbine where the "cut-in" is the wind speed that the wind turbine started to produce electricity, "rated power" is the wind speed that reached maximum produced power and the "cut out" is the maximum wind speed that this wind turbine can continue to produce electricity [63].

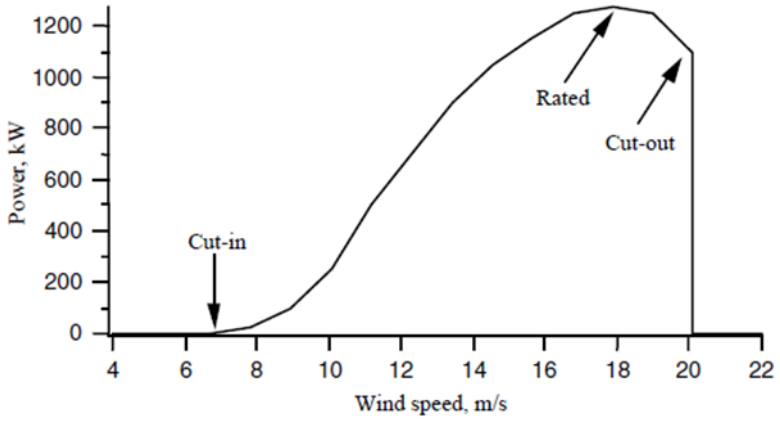



Figure 3 Wind turbine power curve [63]

When the cut-out wind speed is exceeded, turbines are usually shut down due to security purposes. Hence, it is important to know if there is any kind of variability in the wind speeds to predict wind power or plan produced power for future energy system reliability.

### 2.2.1 Wind Resource

Like all energy resources, the formation of the winds starts with the incoming energy from the Sun. Due to the unequal distribution of the heat on Earth, different pressure sources occur. In addition to solar radiation, the rotation of the Earth is also a primary resource of the general circulation of the atmosphere. These circulations have an impact on pressure differences which move from high-pressure to low-pressure areas. "Pressure forces," the "Coriolis force" (reasoned from the Earth's rotation),

“inertial forces due to large-scale circular motion,” and “frictional forces” are the four main atmospheric forces that drive the motion of winds. Smaller circulations such as hurricanes, monsoon circulation, and extratropical cyclones take place due to the heat changes at high- and low-pressure centers. Land and sea breezes; valley and mountain winds; monsoon-like flow; foehn winds; thunderstorms; tornadoes come off from local winds on a smaller scale. These types of motions arise from the heating of surfaces due to the topographic structure at a smaller time scale [63]. For example, land breeze occurs at nighttime because the land cooling is quicker than the sea. Cooler air on the land moves over the land from the sea. Sea breeze also occurs and vice versa. These motions have resulted from regional winds.

The atmospheric boundary layer creates the available wind resource on the local scale. Wind profile, wind shear, turbulence and gusts, and extreme winds are the main elements of this layer. Those elements are affected by the topography, which includes roughness, obstacles, and orography [64].

Wind resource information not only helps to forecast produced energy output of a wind farm but also helps to make turbine design, micro-siting of the turbines, and operation purposes [63].

Wind resources could be determined using various sources such as re-analysis data, measurements, or synoptic network stations [49]. Wind resource assessment is also required for the wind energy industry to sit wind turbines at efficient locations. In order to achieve this, collecting reliable data, analyzing this data, identifying uncertainties, predicting wind farm production, and modeling should be included in the assessment of the wind resource [65].

In the first step, the reliability and availability of wind resources depend on wind resource modeling studies which cover global to micro-scale meteorological modeling techniques. Global models can be downscaled with mesoscale models to increase the models’ resolution. Mesoscale models can help to understand the Atmospheric Boundary Layer.

Determination of wind resource studies also requires local scale knowledge, including surface roughness, obstacles, stability of the atmosphere, turbulence effects, wind profile, wakes between each turbine, etc.[66]. It is well-known fact that orography, obstacles, roughness, stability, and thermal flow should be modeled properly by micro and mesoscale models to consider all effects over a wind farm and to understand local flow over a terrain [49].

***Downscaling Techniques***

Due to the coarse resolution of the GCMs, downscaling of the wind is important to accurately model wind speed, which is affected by all micro, meso, and macro effects. Since wind is affected many parameters such as roughness, elevations, etc., in the micro-scale, GCMs have to be downscaled to the mesoscale and then micro-scale. This downscaling could be done by using two different approaches. These are statistical and dynamical (physical) downscaling [50]. Dynamical downscaling uses regional climate models, mesoscale models, or micro-scale models to increase the resolution of the wind resource. In the statistical downscaling (empirical), similar statistical properties of GCM model grids are used [67].

Downscaling techniques are mostly used in the literature to enhance the reliability of the GCMs. Dynamical downscaling (nested) techniques are the most appropriate method for wind energy applications however, due to the computer expenses, statistical (semi-empirical) methods are also widely used in the current literature [68–71].

#### 2.2.1.1 Mesoscale Modeling for Wind Energy Applications

Mesoscale models are widely used to determine the site conditions and medium-term predictability of wind resources. It also contributes to understanding sub-seasonal changes in wind resources. Those models also require initial boundary conditions from global circulation models. Although mesoscale models are not explicitly produced for wind energy applications, they are widely used in this area to increase

the resolution of the GCMs [72]. For example, most of the Atlas studies use re-analysis data as an initial condition for mesoscale models [73–76].

Mesoscale models are based on conservation equations: conservation of mass, heat, motion, water, and other gases and aerosols. The disadvantage of these models at the micro-scale is that they can not have the capability of modeling the obstacles [49].

WRF [77] is most widely used for both Atlas and short-term prediction of wind speeds. An application of this method is also studied in Türkiye [78, 79]. Those models dynamically downscale the climatic parameters. WRF is used for both operational forecasting and atmospheric research purposes. The model has a data assimilation module as well. WRF has different versions for different purposes. WRF-ARW is a compressible, Eulerian, and non-hydrostatic version of the WRF. Vertical levels of the model are terrain-following, hybrid sigma-pressure vertical coordinates, with the top of the model being a constant pressure surface. The horizontal grid is the Arakawa-C grid. 3rd order Runge-Kutta scheme is used for time integration. The model with several boundary conditions supports idealized and real-data applications. There are also nesting options as well with one/two ways. WRF has different physics options: micro-physics, cumulus physics, planetary boundary layer, surface layer, land surface model, longwave radiation, short wave radiation, urban surface model, shallow cumulus, and ocean physics. The options for each of them can be used with sensitivity studies [77].

#### 2.2.1.2 Microscale Models

Micro-scale modeling at the wind farm level is used to understand the interaction between each wind turbine and terrain effects over a wind farm [50]. Micro models are also used for calculating Annual Energy Production (AEP), capacity factor, etc., and micro-siting of wind turbines for efficient locations. Capacity factor is the amount of time a power plant operates at rated power given a time reference, which

is often the number of hours in a period [80]. For example by using annual energy production (MWh), annual capacity factor can be calculated as :

$$\text{Capacity Factor} = \frac{\text{Annual Energy Production (MWh)}}{8760\ (h) x\ Installed\ Capacity\ (MW)} \qquad (2)$$

Those calculations are most widely used in the wind energy sector for preparing feasibility or bankability reports. There is a considerable number of micro models in the wind energy market which have been used for many years. Some of them are commercial, and some of them are used for in-house purposes for turbine manufacturers. Wind flow models can be examined under two categories: Linear and Computational Fluid Dynamic Models (CFD). Linear Models such as Wind Atlas Simulation Program (WAsP) [81] and Wind Pro [82] are mostly commercial models. CFD models can properly model all local effects using Reynold Average Navier Stokes (RANS) equations. However, it requires higher computer capacity and time. Linear models are good at modeling all effects except thermal flow. Mesoscale models can not consider obstacles [83]. Therefore, these models can be coupled to minimize the disadvantage of each. Those coupling techniques are already used to produce wind atlas studies. WindSIM [51], OpenFOAM [84], WAsP CFD, OfWind CFD [85] etc., can be examples of CFD models. CFD models are better at modeling complex terrains properly, while linear models are good at modeling flat terrains or offshore wind sites. Moreover, in recent years, WRF-CFD coupled models are also used to accurately determine all local conditions and turbulence effects [86].

Mesoscale and microscale models are coupled to properly model atmospheric boundary layers. Those coupling techniques are mostly based on downscaling techniques [50].

#### 2.2.1.3 Wind Speed Extrapolation Methods for different Heights

It is a well-known fact that the wind speeds in the atmospheric boundary layer are affected by many micro-scale factors such as surface roughness, thermal flow, horizontal temperature, pressure gradients, earth's rotation, heating and cooling

differences between day and night, length of the planetary boundary layer which defines the wind shear, surface topography, momentum, heat exchange, etc. [87]

Therefore, changes in the wind speed vertically/horizontally require further micro-meteorological knowledge about the area. In the current literature, there are a couple of methods that can be used to calculate wind speed at different heights. These methods are given in this chapter.

***Logarithmic Wind Profile***

The method is one of the most common methods which uses Monin-Obukhov Length [88] for extrapolating wind speeds at the desired height depending on the stability conditions in the atmosphere. Equation (3) shows the logarithmic wind speed profile formula where U_z is the wind speed, z0 is the roughness length, k is the Karman constant, u* is the friction velocity, L is the Monin-Obukhov length, ψ_m is the stability function. There are also other methods in the literature [89].

$$\boldsymbol{U_z = \frac{u_*}{k}\left(\ln\frac{z}{z_0} - \psi_m\left(\frac{z}{L}\frac{z_0}{L}\right)\right)} \qquad (3)$$

This method is also embedded in the CFD wind flow and mesoscale models.

***Hellmann Exponential (Power) Law***

The method also known as power law defines the wind speed changes with height. The formula of the method is given in the Equation (4).

$$\boldsymbol{WS_2 = WS_1\left(\frac{Z_2}{Z_1}^{\alpha}\right)} \qquad (4)$$

where:

WS1 = wind speed (m/s) at height Z1

WS2 = wind speed (m/s) at height Z2

Z1 = Height 1 (lower height)

Z2 = Height 2 (upper height)

α = a is the friction coefficient or Hellmann exponent

Shear exponent can vary during the day and night depending on the topography. It is assumed as 0.143 in open land [90]. Using power law in higher levels of the boundary layer are not recommended due to changes in stability and other conditions in the higher levels [87].

### 2.2.2 Wind Atlas Studies

Current wind energy climatology is determined by various wind atlas studies providing high-resolution information about regional or country-level wind energy potential using re-analysis data. These studies also help to find past inter-annual, seasonal, and diurnal variability [73, 75, 91]. Country-level Atlas studies for Türkiye [74], South Africa [76], Algeria [92], Brazil [93] and Russia [94] are available in the literature.

Most of the atlas studies start with downscaling re-analysis data to the mesoscale. It could also be downscaled to the microscale by using statistical/dynamical approaches. For instance, Global Wind Atlas (GWA) [75], New European Wind Atlas (NEWA) [73] , Turkish Wind Energy Potential Atlas [74] are generally calculated by using global climate models and downscaling them by using mesoscale models. GWA and Turkish wind atlas are generated using micro-scale linear models to downscale mesoscale model outputs.

European Wind Atlas, the first atlas study in Europe, determined the Atlas conditions, wind resource determination, modeling techniques, etc., in 1989 [91]. Many former atlas studies have been created with a similar approach based on wind measurements. Roughness and elevation information are important for these studies to consider local effects. However, measurement data is not available for all locations. Even if the data exists, reliability and homogeneity of this data are also other concerns for producing wind atlas. Therefore, mesoscale models or mesoscale

coupled micro-model techniques have been used for the last decades to produce wind atlases [76].

Turkish Wind Energy Potential Atlas (REPA-2006) [95] was created by using GCMs, mesoscale model (WRF) and micro-scale model at 200 m horizontal resolution [96]. The new version of the Turkish Wind Energy Potential Atlas (REPA) is also published (see fig. 4) which is produced with higher resolution (100 m) at 7 different heights above the ground level [74].

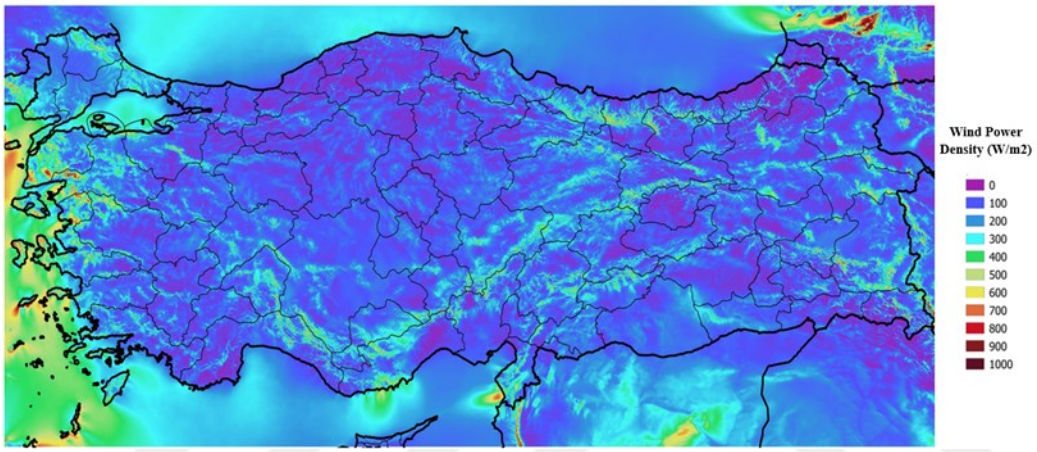



Figure 4 Wind Power Density Distribution of Türkiye [74]

NEWA is the recent Atlas study that covers Europe and Türkiye with high-resolution mesoscale modeling (3 km resolution) and micro-scale modeling with statistical downscaling techniques. WRF model sensitivity studies with observation data for the study area are also being implemented in the first part of the study [73]. Forty-four stations from Türkiye have also been used to validate this Atlas study [97]. Global Wind Atlas (GWA) generated using MERRA re-analysis data for the globe. The aim of the GWA is to give an idea about the country's wind energy potential [75].

These studies also found past inter-annual, intra-annual, seasonal, and diurnal variability. However, they do not contain information about future wind energy resources. Those studies aimed to understand resource availability in a region and

give an idea to investors and policymakers about existing wind resource. Table 1 gives the summary of all the atlas studies mentioned above.

Table 1 Overview of widely used Wind Atlas Studies in Türkiye and Europe

| ATLAS | Year | Re-analysis data | Resolution of the Mesoscale model (km) | Resolution of the Microscale Model (m) | Downscaling technique |
|---|---|---|---|---|---|
| European Wind Atlas | 1989 | Observation data | | | |
| NEWA | 2019 | ERA5 | 3 | 50 | WASP |
| GWA | | MERRA2 | 2.5 | 250 | statistical |
| REPA (TÜRKİYE | 2006 | | 5 | 200 | statistical |
| NEW REPA (TÜRKİYE) | 2020 | ERA5 | 3 | 100 | statistical |

### 2.2.3 Wind Climatology of Türkiye

Türkiye is located in the mid-latitudes where it is affected by different climate types and weather patterns due to the global atmospheric circulation and its complex topography, such as mountains, surrounded by seas and high-altitude mountain regions, which shows variability from region to region.

It is also known that the country is already vulnerable to climate change due to its geographical location. According to the Turkish State of Meteorology Services (TSMS) mean temperature of Türkiye was $14.9^0$C which is above the 1981-2010 normal mean value $13.5^0$C [98]. Based on the observations, in the last decades, the frequency, intensity, and duration of meteorological disasters are already increased in Türkiye [99]. It is inevitable that Türkiye will most likely be negatively affected by climate change during the upcoming century. Therefore, Türkiye has to take immediate action to adapt and mitigate climate change.

On the otherhand, wind climate and wind resources are affected by global atmospheric circulations on the macro scale, synoptic-scale weather patterns, and land-sea interactions in the mesoscale, which is supported by the local terrain,

obstacles, and roughness on the microscale. Elevation and land cover maps of Türkiye are illustrated respectively in Figures 5 and 6 respectively.

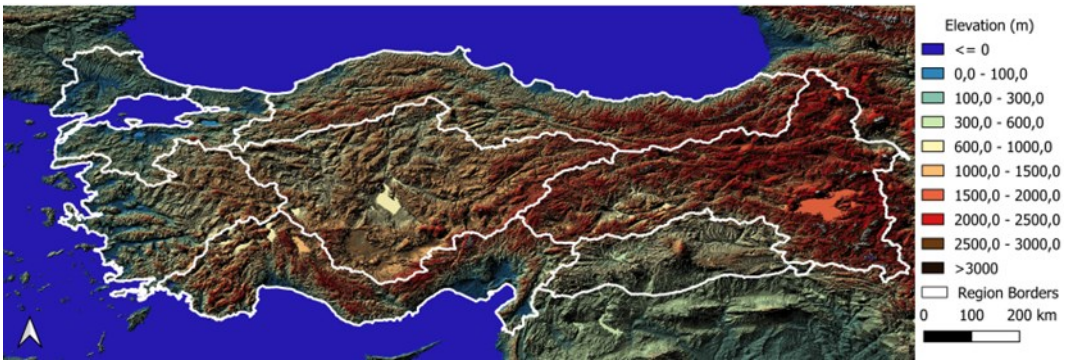



Figure 5 Elevation Map of Türkiye [100]

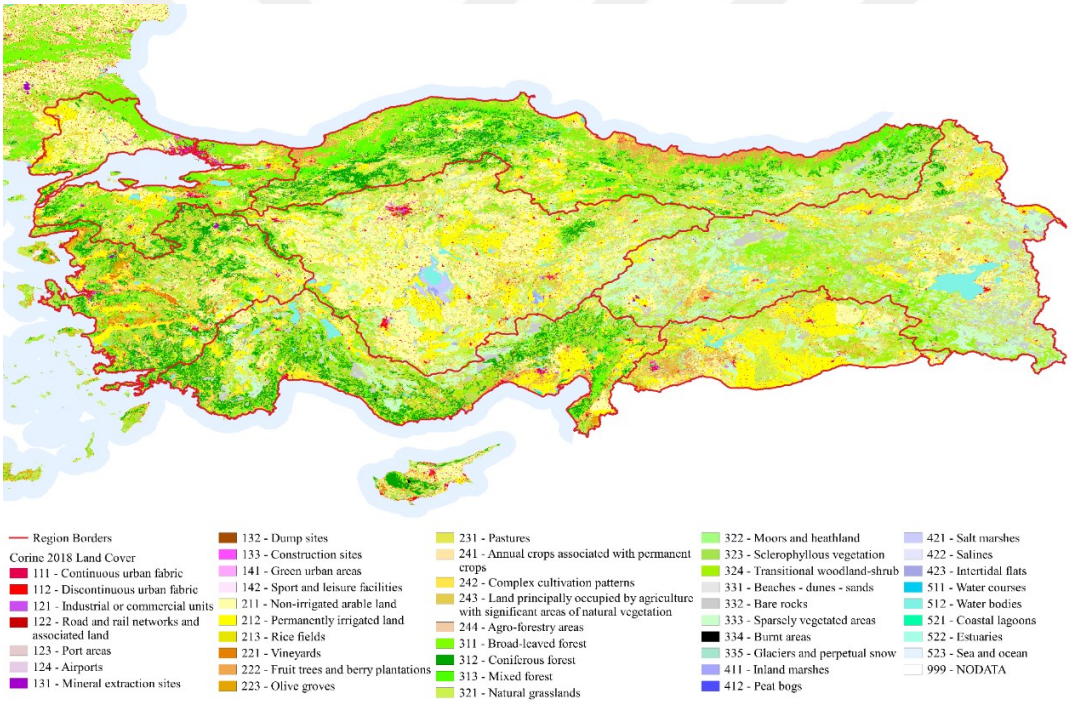



Figure 6 Corine 2018 Land Cover Map of Türkiye [101]

Türkiye is affected by the tropical and polar air masses depending on those factors. In the winter time, the Siberian High and Basra Low-Pressure System affects the Türkiye's climate, and also, polar front cold air mass from Balkan regions brings rainy and cold weather to the Türkiye, and low pressure occurs in the Mediterranean with frontal passages towards the east. Azores High and Island Low-Pressure system

affects Türkiye for all seasons. Islandic Low-Pressure System brings warm and heavy rain, Basra Low-Pressure System affects the Southern-Eastern part of Türkiye and brings dry and hot air from the South. In summer, cold fronts go into the north and Azores High-Pressure System and tropical air masses start to be effective [102].

All these meteorological and geographical factors show that each region of Türkiye has different climate types. The Mediterranean Region has warm and rainy winters and hot and dry summers; the vegetation type is maquis which is the main flora type for the Mediterranean. Aegean Region: same with the Mediterranean climate. The Marmara Region: This region has a moderate climate. Sometimes temperatures can drop below 00C. The Black Sea Region has high humidity, but the region must be evaluated in 2 different parts because of the Eastern part of the Black sea's topographic structure and intense monthly and annual precipitation. The central part of the Black Sea has intense precipitation. Central Anatolia is widely dry and has sub-humid conditions. However, because of the Taurus Mountains that are close to the coast and rain clouds cannot penetrate Central Anatolia even if they penetrate, they already had lost their humidity. That is why Central Anatolia has dry and hot summers without humidity and because their continental structure causes the difference between day and night temperatures. Eastern Anatolia is affected by the Eastern Black Sea Region's high mountains, which prevent to reach precipitation in the region. This region also has very high mountains where their elevation exceeds 2500-3000 m (see fig.5). Long and cold winters can be seen in the region. The minimum temperature can reach -38 C, and it prevents snow from melting. Gradient winds are also low here due to sudden topographical changes in small areas and friction [103]. The South-Eastern Anatolia Region has a steppe climate. Great temperature differences between day and night can be observed in the region. Precipitation is low, but it usually takes the form of snow [104]. The average temperature is 29.8°C in July and 3.7°C in January [105].

Figure 7 shows the long-term (1979-2020) annual and seasonal temperature ($^0$C) values at 2 m obtained from ERA5 re-analysis data from 1979-2020. Lower surface

temperatures in the East Anatolia and higher temperatures in the Southern part of Türkiye can be seen from the figure.

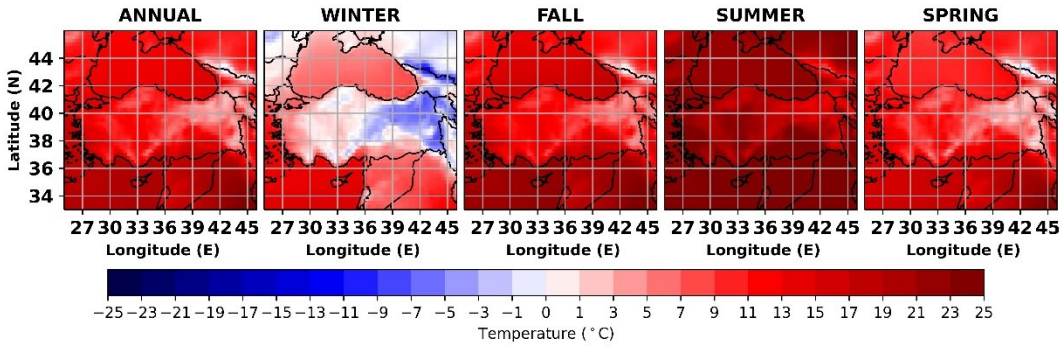



Figure 7 ERA5 Re-Analysis seasonal and annual mean temperature ( $^{0}$C) (1979-2020 period)

Depending on all these factors explained above, wind speeds are higher in the western part of the Türkiye and lower in the inner parts of Anatolia. The following figure shows Türkiye's wind speed distribution at 100 m spatial resolution, which was published by the Ministry of Energy and Natural Resources (MENR) in 2020 [74].

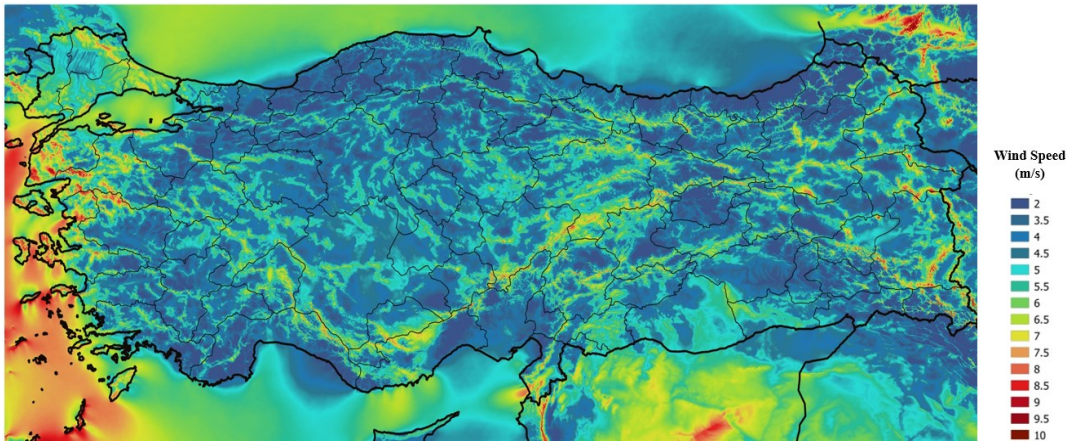



Figure 8 Wind Speed Distribution over Türkiye [74].

Since Türkiye has complex and variable topography, regionality is an important parameter in terms of wind speed distribution and analysis. According to MENR's Wind Energy Potential Atlas, the regional distribution of wind speeds and wind

power potential is given in Table 2. Marmara Region has the highest mean wind speed, capacity factor and wind power density. This could be explained by the Marmara Sea's effect on cooling. Colder currents from the Black Sea also increase thermal differences between land and sea [103]. The Black Sea has the lowest wind speed and power capacity.

Table 2 Regional Distribution of Wind Power Potential of Türkiye [74].

| Region | Wind Speeds (m/s) | | | Capacity Factor (%) | | | Wind Power Density (W/m$^2$) | | |
|---|---|---|---|---|---|---|---|---|---|
| | Mean | Variance | Std.Dev | Mean | Variance | Std.Dev | Mean | Variance | Std.Dev |
| Mediterrenean | 4.46 | 1.28 | 1.13 | 18.3 | 72.250 | 8.5 | 162.194 | 9.811.695 | 99.054 |
| Agean | 4.81 | 1.3 | 1.14 | 21.3 | 106.090 | 10.3 | 176.89 | 13573.42 | 116.505 |
| Marmara | 5.24 | 1.23 | 1.11 | 25.7 | 104.040 | 10.2 | 201.765 | 10428.29 | 102.119 |
| East Anat. | 4.61 | 1.3 | 1.14 | 18.4 | 67.240 | 8.2 | 152.67 | 8537.39 | 92.398 |
| South-East Anat. | 4.59 | 0.59 | 0.77 | 18.6 | 39.438 | 6.28 | 137.229 | 3.401.222 | 58.32 |
| Anatolia | 4.53 | 0.55 | 0.74 | 17.3 | 32.490 | 5.7 | 128.537 | 3.602.881 | 60.024 |
| Black Sea | 4.01 | 1.08 | 1.04 | 14.4 | 49.985 | 7.07 | 121.152 | 7.015.738 | 83.76 |

## 2.3 Policy Perspective of Climate Change and Energy in Türkiye

### 2.3.1 Climate Change Policy of Türkiye

In 1992, Earth Summit was held in Rio De Janeiro in Brazil, where the 197 countries signed the first climate change negotiation. The negotiation aims to regulate the obligations of state parties who have responsibilities regarding greenhouse gas emissions and prevent anthropogenic effects on the climate system. According to UNFCC, Annex-I countries are obliged to reduce greenhouse gas emissions and Annex-II countries also have the responsibility to reduce greenhouse gas emissions and support developing countries in climate change mitigation and adaptation [53]. As a founding member of the Organisation for Economic Co-operation and Development (OECD) in 1992, Türkiye is placed in both Annex-I and Annex-II. However, in 2001, in Marrakech (COP7), Türkiye's different situation was recognized and excluded from Annex II. At the same time, in 1997, Türkiye signed

the Kyoto Protocol as well. During the Conference of Parties (COPs) and negotiations, it is also determined that Türkiye has a different situation than other Annex-I countries and has a right to utilize the adaptation, technology development and transfer, capacity building, and finance funding as well. After a couple of decisions in the COPs, Türkiye has utilized the Green Environment Fundings. However, Türkiye still cannot utilize the Green Climate Fundings [106].

Finally, Paris Agreement was accepted in December 2015 at the 21st conference of parties (COP). Türkiye signed the agreement on 22 April 2016 and ratified the Agreement on 6 October 2021 [107]. Before ratifying the Agreement, countries submit their Intended Nationally Determined Contributions (INDC). Within INDCs, Türkiye aims to reduce 21% of GHGs by 2030. The INDC also includes increasing the current solar power capacity to 10 GW and wind power capacity to 16 GW by 2030 [108].

However, there are two crucial subjects for Türkiye in the Paris Agreement. First, Türkiye needs to be treated like other countries, which is similar to Türkiye's situation, in order to utilize financial and technological support. Secondly, it is not possible to reduce emissions when measures such as Türkiye's economic growth and demographic increase are considered [109]. The Ministry of Environment, Urbanization and Climate Change has identified Türkiye's climate strategy. Those strategies are supported by several goals and strategies together with the stakeholders. First, climate change mitigation and adaptation policies are expected to be integrated into the national development plans. That integration is applied under the "common but differentiated responsibilities" principle in the UNFCCC. Secondly, greenhouse gas reductions will be supported by considering the development plans within the scope of sustainable development goals. Türkiye also aims to be prepared for the negative impacts of climate change by increasing stakeholder engagement and supporting research. Maximum utilization of wind energy is already included in this strategy [110].

#### 2.3.1.1 Current status

Climate Council was held on 21-25 February 2022 with the participation of all public and private sectors. Two hundred seventeen decisions are made in this council. In the energy part of the decisions, it is declared that to reach the net zero emissions target in 2053, a long-term energy planning agenda should be prepared before COP27 in 2022. It is also recommended that the use of renewables should be increased. The council also recommended that it should be ensured that hybrid renewable energy technologies with high efficiency and low energy cost, more compatible with its habitat, and can be used for multi-purposes with appropriate designs are developed [111]. In the COP27, the latest climate summit held in Egypt's Sharm el-Sheikh city, Türkiye has also declared the Nationally Distributed Contributions, aiming to bring its greenhouse gas emissions to 41% below business-as-usual levels by 2030, raising the target from 21%. The peak year is determined in 2038 for Türkiye's emissions [112].

In light of all this information and the development plans of Türkiye, the country has started to build net zero targets and green development plans. Based on the recent changes in Türkiye's situation with the climate change negotiations, the country has also set ambitions of net-zero targets.

### 2.3.2 Energy Policy of Türkiye

Energy production of Türkiye is highly dependent on the import and fossil fuels, which dominate the energy sector with 83 % of TPES in 2019 [113]. Therefore, the energy sector is also an emission-intensive sector that requires a new policy framework after the ratification of the Paris Agreement and net-zero targets. On the other hand, Türkiye aims to increase the use of domestic resources in energy production. 31 % of energy production in Türkiye was provided by domestic energy supply in 2019 [113]. Energy policies and regulations in the last years have supported these aims. According to the “National Energy and Mining Policy”, announced in

April 2017 by MENR, Türkiye energy strategies have been built on "energy supply security, bringing domestic resources into economy, reliable and foreseeable energy markets" [114]. Several policies have been implemented within this context, including renewable energy supporting mechanisms, auction models, local incentives, etc., to increase the share of renewables in electricity production. The installed capacity of Türkiye has reached 103,868 MW by the end of December 2022 [4]. Figure 9 shows the distribution of installed capacities in terms of resources in Türkiye. % 51 of this capacity belongs to natural gas and thermic resources not produced in Türkiye. The share of wind is still low in the electricity installed capacity (11 % approx.).

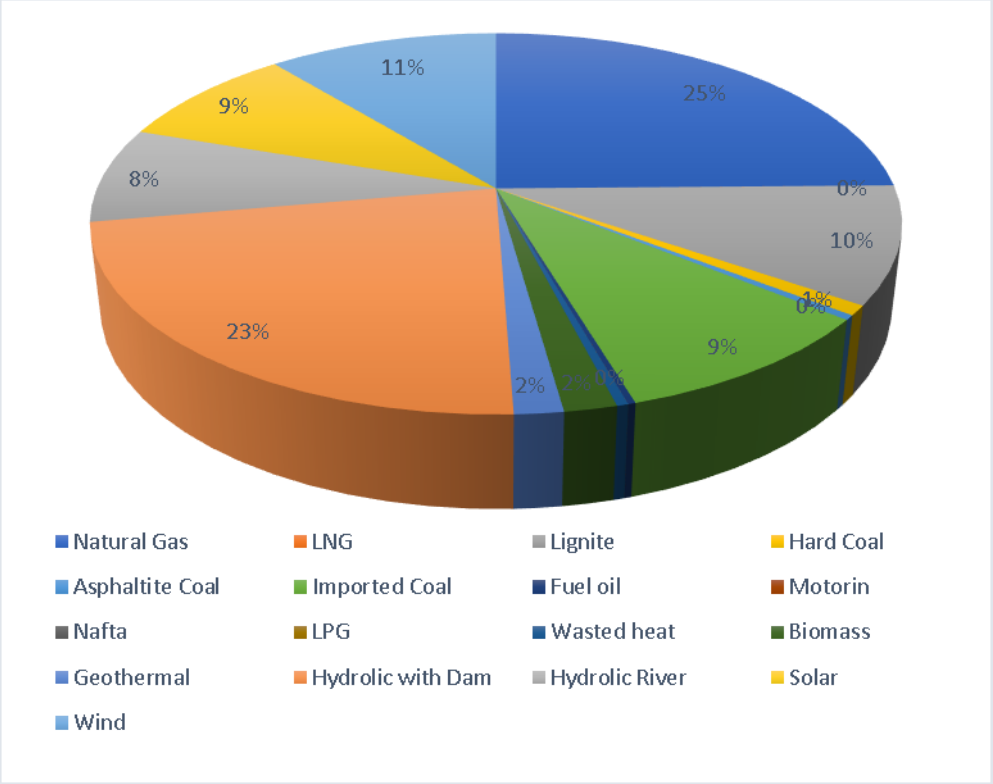



Figure 9 Share of Installed capacities by resource in Türkiye [4].

Moreover, Türkiye also set long-term targets for renewables by publishing "National Energy Plan" at the beginning of 2023. According to plan, Türkiye aims to reach 29.6 GW (24.6 onshore, 5 GW offshore) wind and 52.9 GW solar installed capacity by 2035 [5]. There is already a mature onshore wind industry in Türkiye.

Manufacturing factories and R&D facilities are increasing with local content incentives and subsidies. However, Türkiye has a high import dependency because of using foreign natural gas and coal, which means wind and solar power will be essential players in the Turkish energy sector in the near- or long-term future. Moreover, International Energy Agency (IEA) advised that Türkiye could increase the targets, especially for wind energy, due to decreasing prices of wind energy investments [113]. The 11th Development Plan (2019-2023) of Türkiye also aimed to increase the share of renewable electricity production from 32.5% in 2018 to 38.8% in 2023 [115]. This aim was already achieved with 133.4 TWh of electricity produced from renewables which means 43.8% of total electricity generation was renewables [113].

According to OECD, Türkiye's economy has grown 4.1 % over the last five years, which is crucial proof of increasing demand [116]. Türkiye's energy production still depends on natural gas and oil. Moreover, according to Türkiye Electricity Demand Projections in Figure 10, Türkiye's electricity demand will be doubled in 2040 [117].

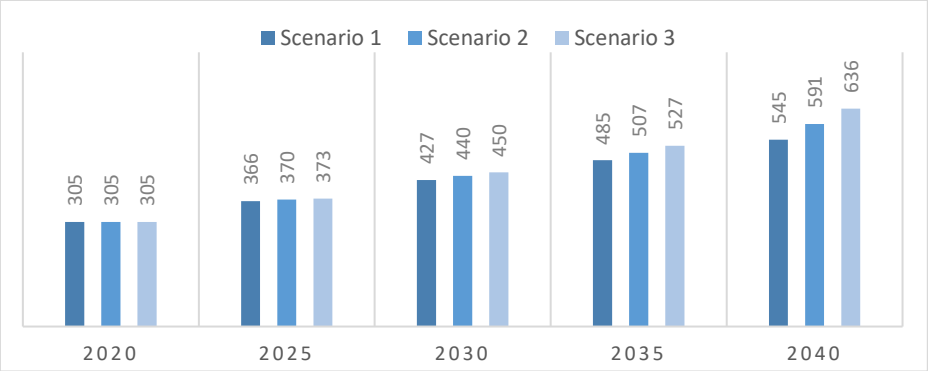



Figure 10 Türkiye Demand Projections [117].

#### 2.3.2.1 Renewable Energy

The share of energy in the total greenhouse gas emissions in Türkiye is reached 70 % by the end of 2020. The increase in the energy sector emissions is % 163.3 when compared to the 1990 emissions [118]. Türkiye's greenhouse gas emissions are

belowed the OECD member's averages however has ranked as one of the fastest-growing countries in the OECD [119]. Therefore, for both combating climate change and reducing import dependency, Türkiye has increased its share of renewable energy in the last two decades with both regulations and policy frameworks.

MENR and Energy Market Regulatory Authority (EMRA) are two of the main regulatory bodies which are responsible for the legal and regulatory framework for renewable energy projects in Türkiye. There are three different approval systems in place for renewable energy installations:

- Unlicensed
- Licensed
- Renewable Energy Resource Zones (RE-Zone / YEKA-model) [120]

Renewable energy incentives are based on the "Law on Utilization of Renewable Energy Sources for the Purposes of Generating Electrical Energy (known as YEK Law, No:5346)". The purpose of the law is *"to expand the use of renewable energy resources for electrical energy production, to bring these resources to the economy in a reliable, economical and high-quality manner, to increase the diversity of resources, to reduce greenhouse gas emissions, to evaluate waste, to protect the environment and to develop the manufacturing sector needed for the realization of these goals"* [121]. Renewables and local content incentives have been supported with feed-in-tariffs within this law since 2005, with Renewable Energy Supporting Mechanism (YEKDEM with Turkish acronym). YEKDEM was valid from 2005 to 31.12.2020 with the US dollar-based prices for each renewable energy resource. Presidential Decree No: 2949 was published in the Official Gazette No. 31248 on September 18$^{th}$, 2020, the current renewable energy support mechanism's (YEKDEM) duration was extended from December 31$^{st}$, 2020, to June 30$^{th}$, 2021. By Law No. 7257 amending the Renewable Energy Law No. 5346, which was published in the Official Gazette No. 3122 on December 2$^{nd}$, 2020, a new renewable energy support mechanism will be forced on July 1st, 2021, is formed. After that,

with Presidential Decree No. 3453 was published in the Official Gazette No. 31380, YEKDEM was enlarged for the electricity producers who will start to operate from 01.07.2021 to 31.12.2025, and the prices were changed from US dollar to Turkish Liras, and the prices are escalated on the basis of source within a period of 3 months each year, according to Domestic Producer Price Index, Consumer Price Index, the average daily US dollar and Euro forex buying rates [122].

Regulation on RE-Zones (YEKA with Turkish acronym) was published in the Official Gazette on October 9, 2016, by the MENR. The primary purpose of introducing this new model is to support large-scale renewable energy investments and incentivize local manufacturing of renewable power plants [123]. In 2017, two YEKA tenders for solar and wind energy with 1 GW capacity each were held. The first YEKA onshore wind includes an R&D center and manufacturing company as well [124]. The first offshore wind RE-Zones was announced in 2018 and postponed due to no bids [125] . In 2019, a new onshore wind energy tender covering four regions (Aydın, Çanakkale, Muğla, Balıkesir) with a total installed capacity of 1GW was completed [124]. In 2020, a new solar tender was announced in the Official Gazette for 1 GW capacity. Applications for 74 projects for 10, 15, and 20 MW capacities in 36 cities were submitted on 8 -12 March 2021. In June 2022, a new wind energy tender was completed at 20 connection regions with 850 MW capacity (YEKA RES-3), and contracts were signed on 20/07/2022 by the winner of the tenders and MENR [126].

There is also another renewable energy supporting system which is published in the Official Gazette dated 14/11/2020, numbered 31304 [127] called Renewable Energy Guarantees of Origin System “YEK-G.” The companies who obtained the YEK-G document can consume their electricity from renewable energy resources. This is a voluntary based system that is managed by Energy Exchange Istanbul (EXIST).

### 2.3.3 Wind Energy in Türkiye

Türkiye has started to build wind farms at the end of the 1990s. Figure 11 illustrates the cumulative and annual installation of wind energy in Türkiye. Moreover, Türkiye already achieved more than 11 GW of wind power installed capacity by the end of December 2022 [4]. According to IEA's prediction, 48.1 TWh consumption is expected in 2026 in Türkiye from wind energy [128].

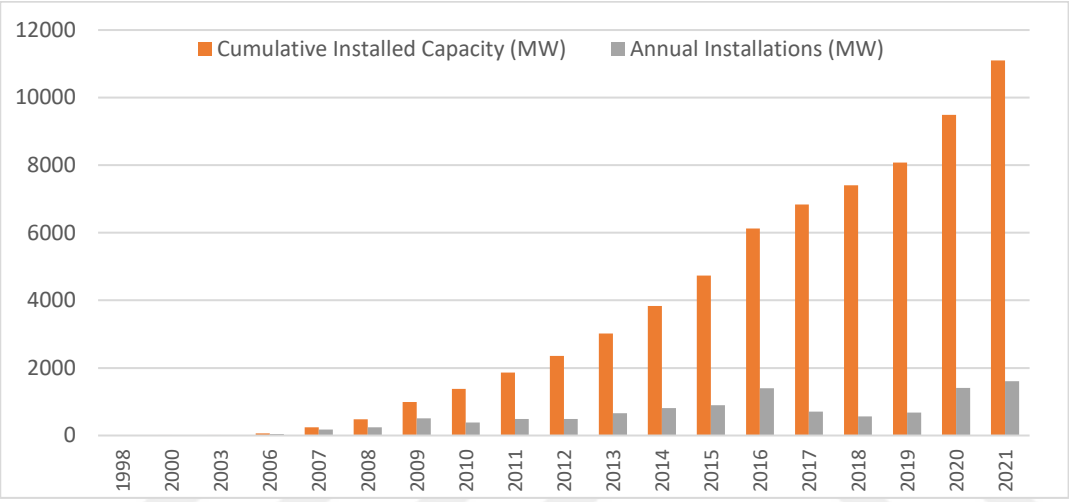



Figure 11 Annual and cumulative wind energy installations by years of Türkiye [129]

On the other hand, wind energy potential in Türkiye has 47,850 MW wind power capacity, according to the 2006 Wind Energy Potential Atlas of Türkiye [130]. Moreover, a new wind energy potential atlas [74] has been published by the MENR, but the new potential in terms of MW has not been announced yet. Offshore wind projects can only be established following the YEKA process [131]. Morever, Energy Sector Management Program (ESMAP)'s report indicates that there is a 69 GW (57 GW floating and 12 GW fixed foundation) offshore wind potential over Türkiye [33].

The onshore wind market, among the other renewables, is nearly mature, and there are 358 wind power plants with 11.396 MW capacity installed by the end of 2022 in Türkiye [4]. Besides, with the new auction model called Renewable Energy

Resource Zone (REZ) Model, 2000 MW wind energy auction has been completed [132].

Wind Power Plants (WPPs) in Türkiye are subject to the Electricity Market Law (No:6446), which provides licenses to build WPPs or pre-license to complete permissions before licensing procedure. Energy Market Regulatory Authority (EMRA) approves the licenses/pre-licenses. A pre-license has a maximum of 36 month-duration to complete all permission processes. After completing a pre-license, the company can build and operate with a license. Even though pre-licensed projects cannot obtain their permits, a pre-licensed area requires at least one year of measurement and a couple of feasibility studies that prove the potential of the site [133]. Therefore, pre-licensed WPPs are also considered in this study to evaluate the potential of existing potential sites. On the other hand, the license gives the right to WPP owners to use wind power plant area for 49 years even if a wind turbine lifetime is limited to 20-30 years. Repowering is an option for those wind turbines to efficiently utilize the wind power potential.

The location of licensed and pre-licensed wind power plants is given in Figure 12 [134]. Most of the wind farms are in the Aegean and the western part of the Marmara Region. The highest wind power capacity is in the Marmara Region, with a total of 4632 MW installed capacity, and the Aegean Region, which has about 3718 MW installed wind power capacity [135].

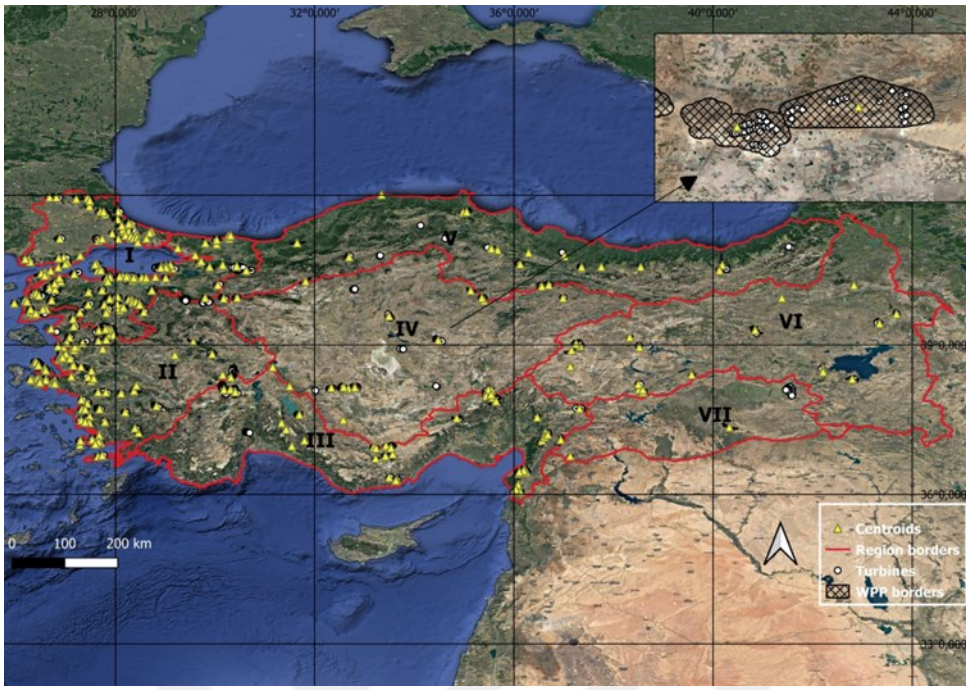



Figure 12 Locations of Wind Power Plants in Türkiye [134].

To meet increasing energy demand and to reduce energy imports, the increase in the use of domestic resources becomes essential from an energy supply security and economic perspective for Türkiye. Within these policies and needs, it is expected that Türkiye will continue to increase the use of wind energy resources in the future with its growing demand and promising potential.

## 2.4 Impacts of Climate Change on the Wind Energy Resources

It is a well-known fact that the energy sector is vulnerable to climate change due to increased demand, supply, resource availability, and increasing risks from extreme weather events. Climate change is expected to impact energy supply, resource, transmission, distribution and transfer of energy, design, operation, and indirect effects on the other sectors. Those sectors will be negatively affected by increasing/decreasing air temperatures. As a result of climate change, uncertainties will also be increased [136].

It is emphasized by the IPCC's Special Report on Renewable Energy Resources that the distribution of available wind resources will be affected by climate change. Not only the magnitude of the wind speed will be affected but also extreme winds and gusts, icing, and inter-annual and intra-annual variability of wind resources will be negatively affected. Increasing extreme winds and gusts or icing conditions will cause high loads on the wind turbines. Therefore, the design of the wind turbine should be changed depending on these extremes. On the other hand, changes in the magnitude of the wind resource will directly affect the final production. The report also summarizes that there will be changes in the multi-year annual winds multi-year more than a maximum of ±25% for most of Europe and North America [48].

On the other hand, observed changes in wind speed are also widely studied in the current literature, by investigating long-term trends mostly using re-analysis data [12, 23, 40, 137–141] and measurements [137, 138]. Moreover, Dadaser-Celik, F., & Cengiz, E. (2014) studied wind speed trend analysis using observational stations from the TSMS distributed over Türkiye and found that there are negative trends from 1975 to 2006 [13]. However, decreasing wind speeds over the last decades over the lands are called terrestrial global stilling may have many reasons, such as changes in the atmospheric circulation, surface roughness, surface friction, urbanization, etc. Previous studies investigated these reasons by using long-term re-analysis data. However, the results show that it is suspicious to relate these decreasing trends to climate change as they can result from the existence of the obstacles (trees, urbanization, etc.) growing with time around the measurement station. Zhang et al. (2019) found that global terrestrial stilling is also dominated by increasing surface friction [12]. Therefore, it is also important to understand the possible causes of these trends through the investigation of the relationship between re-analysis data, climate models, and observation data [36]. Wind speed as a climatic impact driver will be decreased depending on the region or land and ocean. Surface winds are decreased since the 1970s on land with high confidence and increased over the ocean with low confidence [55].

Artificial intelligence methods have also been extensively used in wind energy applications over the last decade [29]. Random forest regression is one of these methods, which is considerably used for short-term wind power forecasting methods [32]. Li. et al. (2021) studied RF, linear regression, and simple mean of multi-model to determine climate indices over China by using 24 CMIP6 models [142]. However, no study has been found for wind resource assessment with random forest regression with CMIP6 models. It is important to assess model skill using multiple diagnostics because inter-comparison projects show that no single model consistently outperforms all others [143, 144] Ensemble approaches are also used in the literature for the determination of wind resources [22, 24, 27, 145, 146]. However, most multi-model ensemble studies focusing on the climate change impact on wind resources have included simple averaging in the literature with the CMIP5 and prior versions of CMIPs [17, 22–28]. On the other hand, as a supervised machine learning algorithm, random forest (RF) has been used widely in regression problems, including wind energy applications and short-term wind power forecasts over the last decade [29-32]. Nevertheless, a regression-based multi-model ensemble approach delivered by multi-linear and RF that includes weights optimized for each model needs to be applied to provide a comparative assessment of long-term wind speed predictions.

Recent studies have increasingly focused on using CMIP6 models to assess historical and future climate change impacts on precipitation and temperature [15, 16]. However, studies using CMIP6 models for wind resource determination over Türkiye are very limited. Carvalho et al. (2021) used CMIP6 data over Europe, including Türkiye found that the wind speed will be increased over Türkiye around % 15-30 according to the SSP2.45 scenario at the end of the 21$^{st}$ century [18]. Deng et al. (2021) found that surface winds will decrease over China according to SSP scenarios [21]. Another study that uses CMIP6 and ensemble mean methods for predicting future wind resources was published in 2021 by Akinsanola A.A. et al. [147]. The study is based on calculating wind power density from multi-CMIP6 models at the wind turbine level without any downscaling technique. Similar studies

for West Africa and China have been performed respectively by [17] and [23, 28] with the simple mean ensemble. Krishnan and Bhaskaran (2020) studied CMIP5 and CMIP6 data for the Bay of Bengal using a simple mean ensemble [148]. Another study that used 14 different CMIP6 models with the simple mean ensemble belongs to Akinsola and Ogunjobi et al. (2021). They also calculated wind power density over West Africa [17]. Hahhmann et al. (2022) used 18 different CMIP6 for predicting North Sea offshore wind resources at 100 m [19].

There are also country-based studies in the literature about the effect of climate change in the future wind energy resources for USA [69, 149–153], Europe [22, 68, 70, 154–159], Africa [160, 161], Brazil [162, 163], Ireland [164], Japan [165], France [70], Germany [166] and Greece [167]. There are also few studies which covers entire globe and uses GCM models [24, 168].

According to AR6. there is a low agreement in the CMIP6 models which it can be seen in the Figure 13.

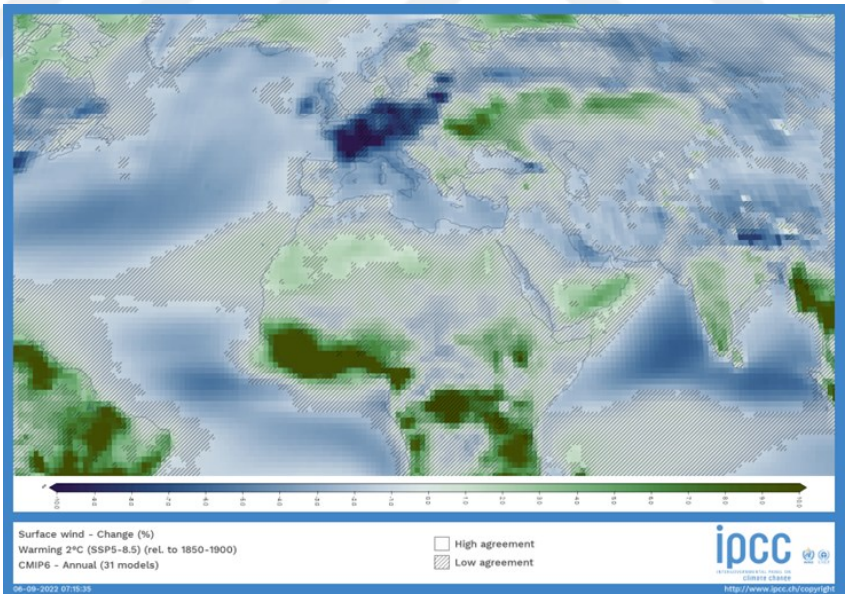



Figure 13 Surface winds change according 20C warming scenario relative to 1850-1900 [169]

Since the beginning of the 2000s, similar studies have been conducted depending on the advances in climate models and the increasing share of wind energy all over the

World. Most studies focus on Global Climate Model (GCM) results by modeling the surface winds [69, 149, 149, 160, 163]. The common characteristic of these studies was downscaling GCM outputs.

On the other hand, a couple of studies have been performed using regional climate models [150–152, 154, 162] [153, 161] . Some of the studies for Europe also include Türkiye [146, 154, 156, 159]. As a result of those studies, it is expected that Southern Europe's wind speeds will be decreased while Northern Europe will have slightly higher wind speeds. A study which is performed for East Mediterranean found that there will be an increase in the Aegean Sea, in contrast to a decrease in lands in the Mediterranean Sea [170].

A study also focuses on micro-scale calculation of wind farms, such as Levelized Cost of Energy (LCOE) [171]. Multi-model ensemble approaches are also used in these studies [22, 27, 147]. A neurol network approach have been used for [172]. Statistical downscaling techniques are also used to increase the resolutions of GCMs [69]. Multi-model ensemble approaches are also used in some of these studies [22, 24, 27, 145, 146].

In addition, only a master thesis study was done by using an MPI-EMS-MR model from CMIP3 outputs and Regional Climate Model (RegCM) for Türkiye in 2016 with two different RCP scenarios at 10 km spatial resolution. The study also includes micro-scale modeling by using WaSP for a selected location in the Bandırma region [173].

All these studies are summarized in Table 3 depending on their methods, climate models, downscaling techniques, resolution, model type, and study area. To sum up, there have been many studies about the effect of climate change on wind resources since the beginning of the 2000s. Most of them have coarse resolution and do not consider mesoscale to micro scale effects. Moreover, the majority of them use CMIP5 GCM model outputs, mostly using evaluation techniques.

Different from those studies, this study aims to analyze high-resolution mesoscale model outputs in order to consider all mesoscale effects by using the dynamical downscaling of GCMs. Before the mesoscale modelings, two multi ensemble approach is developed for 28 CMIP6 models, which may also contribute to the current literature to increase the accuracy of climate projections.

Since the beginning of the 2000s, similar studies have been conducted depending on the advances in climate models and the increasing share of wind energy all over the World. Most studies focus on Global Climate Model (GCM) results by modeling the surface winds [69, 149, 149, 160, 163]. The common characteristic of these studies was downscaling GCM outputs.

On the other hand, a couple of studies have been performed using regional climate models [150–152, 154, 162] [153, 161] . Some of the studies for Europe also include Türkiye [146, 154, 156, 159]. As a result of those studies, it is expected that Southern Europe's wind speeds will be decreased while Northern Europe will have slightly higher wind speeds. A study which is performed for East Mediterranean found that there will be an increase in the Aegean Sea, in contrast to a decrease in lands in the Mediterranean Sea [170].

A study also focuses on micro-scale calculation of wind farms, such as Levelized Cost of Energy (LCOE) [171]. Multi-model ensemble approaches are also used in these studies [22, 27, 147]. A neurol network approach have been used for [172]. Statistical downscaling techniques are also used to increase the resolutions of GCMs [69]. Multi-model ensemble approaches are also used in some of these studies [22, 24, 27, 145, 146].

In addition, only a master thesis study was done by using an MPI-EMS-MR model from CMIP3 outputs and Regional Climate Model (RegCM) for Türkiye in 2016 with two different RCP scenarios at 10 km spatial resolution. The study also includes micro-scale modeling by using WaSP for a selected location in the Bandırma region [173].

All these studies are summarized in Table 3 depending on their methods, climate models, downscaling techniques, resolution, model type, and study area. To sum up, there have been many studies about the effect of climate change on wind resources since the beginning of the 2000s. Most of them have coarse resolution and do not consider mesoscale to micro scale effects. Moreover, the majority of them use CMIP5 GCM model outputs, mostly using evaluation techniques.

Different from those studies, this study aims to analyze high-resolution mesoscale model outputs in order to consider all mesoscale effects by using the dynamical downscaling of GCMs. Before the mesoscale modelings, two multi ensemble approach is developed for 28 CMIP6 models, which may also contribute to the current literature to increase the accuracy of climate projections.

Table 3 Summary of the relevant topics in the literature

| Model | Resolution | Method | Study Area | Ref. |
|---|---|---|---|---|
| RCM | 50 x 50 km | Delta method, wind power potential calculated | Brazil | [163] |
| RCM-GCM | 2.5° x 3.75° | Dynamical downscaling, nested the high-grid-resolution regional climate model (RegCM2) into the low-grid-resolution GCM (HadCM2) | USA | [152] |
| GCM | 0.5° x 0.5° | Regrided and compared with the historical runs | USA | [149] |
| GCM, | ~2 degree | Weibull parameters and energy density calculated and interannual, intra-annual variability compared | Northern Europe | [157] |
| 4 GCMs | variable | Empirical downscaling of 5 state-of-the-art AOGCMs | Northern Europe | [68] |
| 4 GCM | ~2.5° x 2.5° | Statistical downscaling | Northwest United States | [69] |
| GCMs | 50 km x 50 km | Validated and compared | Ontario | [153] |
| CMIP5 | 20 km x 20 km | HADGEM2-ES, MICRO5, CANESM2 GCMs, RCMs for South american regional model(downscaled version of GCMs) | Brazil | [162] |
| CMIP 5 | ~2.5° x 2.5° | Multi-model ensemble | European | [22] |
| 9 GCMs in Euro-Cordex | 12 km x 12 km | The bias-corrected 10 m wind speeds are extrapolated to the hub height of a wind turbine, future wind energy outputs calculated, Model ouputs compared | Europe, partially Türkiye | [156] |
| RCM | 0.44° x 0.44° | analyze simulations from RCMs nested within lateral boundary conditions from three AOGCMs | USA | [151] |
| CMIP-3 | variable | Sparman rank correlation calculated to find out relationship between temperature and wind speed and global horizontal irradiance | South Africa | [160] |
| ENSEMBLES European FP6 project GCM-RCM Model outputs | 25 km x 25 km | 15 regional climate projections from 10 Regional Climate Models downscaling six Global Climate Models, bias correction by using Cumulative Distribution Function-transform, Multi-model ensemble averages compared for wind power (ENSEMBLES project) | Europe | [159]. |
| 14 GCMs from CMIP-3 | 2-3° | statistical and dynamical downscaling approach (mesoscale model and wind class classification) | France | [174] |
| RCM | 0.5 x 0.5° | RCMs with 12 different GCMs inputs were compared in terms of WPD, MME mean also calculated | North America | [150] |

Table-3 continued

| | | | | |
|---|---|---|---|---|
| RCM | 2.8° x 2.8° | RCM outputs analysed for afforrestration effect on wind power | Nigeria | [161] |
| 6 CMIP5 model and d4PDF (large ensemble data) | 20 km x 20 km | Annual wind power calculated from ensemble data and CMIP6 models by using power curve | Japan | [165] |
| Dynamical RCM | 18 km x 18km | Dynamical downscaling, CCLM runned. Wind power production calculated by using turbine power curve, dynamical downscaling | Germany | [175] |
| RCA3 | 13 km x 13 km | Dynamical downscaling: RCM model runned for both control and future periods, dynamical downscaling | Ireland | [164] |
| CMIP-5 CORDEX | 12 km x 12 km | 10 m wind speeds extrapolted with The friction velocity which is calculated from the surface wind stress | Europe-Black Sea | [154] |
| 10 coupled GCM | The coarsest: 4° x 5°, The finest : 1.875°x 1.875° | Statistical downscaling models of Weibull A and k at each site | Northern Europe-Scadinavia | [176] |
| 5 GCM from CMIP5 | variable | Analyzed | North America | [155] |
| 4 GCM/RCM combinations | variable | compared models and calculated WPDs | USA | [177] |
| 8 GCM from CMIP3 | variable | determine warming and wind power, power law calculated | China | [178] |
| ECHAM5-MPIOM and dynamically downscaled by the RegCM | 10-15 km | Wind power density calculated for observations and RCM and analysed | Crotia | [179] |
| CMIP3-19 model | 2.5° x 2.5° | Averaged multi-model ensemble, compared with re-analysis (regrided all models) | Global | [24] |
| Earth System Model 2 (ESM2G) from CMIP5 | 2° x 2.5° | 10 m wind speeds extrapolated to 80 m, weibull parameters calculated, AEP, CP and LCOE calculated | UK | [171] |
| HAPPI, 'Inter-Sectoral Impact MIP | 0.5° × 0.5° | Bias corrected, WPD calculated | UK, EU | [180] |
| Arpege/IFS | 30 km x 30 km | Dynamical downscaling, Same model set up arranged for 4 model with reference period and ensembled. WPD calculated from ensemble projections | N Europe | [145] |
| RCM | 0.44°x 0.2° | Dynamical downscaling, wind energy density calculated for each model | EU, Türkiye included partially | [146] |

Table-3 continued

| | | | | |
|---|---|---|---|---|
| REGCM | 20 km x 20 km | Dynamical downscaling, micro model used for specific locations, dynamical downscaling | Türkiye | [173] |
| MIROC3.2-medres, ECHAM5, CCCMA3.1, and 86 CSIRO-Mk3.0 | 50 km x 50 km | Dynamical downscaling, 4 GCM downscaled with WRF to 12 ensembled model, LCOE calculated | Australia | [181] |
| 14 CMIP6s | 2.81° x 2.81° | MME mean, WPD calculated | West Africa | [17] |
| PRECIS Regional Climate Model | 0.22° ×0.22° | RCM compared with the ERA40s | Greece-Western Türkiye | [182] |
| NCAR CCM3 (GCM) | - | Feedforward neural networks, downscaled with semi-empirical downscale approach | 3 points in USA | [183] |
| 4 GCMs | | Wind gust analysis | Canada | [184] |
| EURO-CORDEX | 12 km x 12 km | MME mean | Europe | [27] |
| RCM | 50 km x 50 km | Coupled with re-analysis, analyzed with measurements and re-analysis data | 3 sites in California | [185] |
| 31 GCMs from CMIP5 | 2.5° × 2.5° | Statistical downscaling, 31 models ensembled, WPD calculated, extreme winds evaluated | Suriname | [71] |
| 30 GCMs from CMIP6 | Variable | MME mean | China | [21] |
| 15 GCM from CMIP6 | Variable | MME mean | Europe | [18] |
| 18 GCMs from CMIP6 | Variable | Multiple CMIP6 models analysized at 100 m together with observations and NEWA, ERA5, MERRA2, 20CRv3 data | Northern Europe | [19] |
| 1 GCM | 5 km x 5 km | Dynamically downscaled with WRF | Greece | [167] |
| CORDEX-SA | 0.5° × 0.5° | Regional climate model results analysized | India | [20] |

# CHAPTER 3

# DATA AND METHOD

## 3.1 Data

In this study, observation data at 10 m obtained from the TSMS to validate the models. In addition to observation data, two re-analysis data (MERRA2, ERA5) are used for validation and multi-model ensemble development.

GCMs from CMIP6 models for surface winds and pressure level parameters (temperature, specific humidity, surface specific humidity, surface pressure, u and v component of the wind speed) is also obtained from the WCRP [14] and Copernicus databases [186] and validated with the observations and re-analysis data. CMIP6 models include approximately 100 different GCMs. Depending on the availibity of required parameters for calculating the wind speeds at different heights with different methods with different scenarios, different CMIP6 models is used in this study which is explained in Chapter 3.1.3.

All reference data and model data sets summarized in the Table-4 in terms of resolution, available period, model type, and institute available heights above the ground level. The details of the data that is used in this study are given in the following chapters.

Table 4 General Overview of the Data

| DATA | MERRA-2 | ERA5 | OBSERVATION | CMIP6 MODELS |
|---|---|---|---|---|
| **Institution** | NASA | ECMWF | TSMS | Variable |
| **Model** | GEOS v5 12.4 | IFS Cycle 41r2 | - | Variable |
| **Resolution** | 0.5 ° x 0.625 ° | 0.25 ° x 0.25 ° | - | Variable |
| **Heights above the ground level** | 10:50 | 10:100 | 10 | 10: pressure levels |
| **Available time period** | 1980-present | 1979-present | 1979-2020 | 1979-2014 |

### 3.1.1 Observation Data

Observation data for monthly, daily and hourly time scales have been obtained from TSMS at 10 m. Monthly and daily average data covers the period from 1979 to 2020. However, hourly data only covers a 5-year period from 2015 to 2020. Although there are 2093 observation stations, 239 of them have continuous data for monthly and daily average time series. Figure 14 shows the number of available days for each station. As is shown in the figure, stations that start with "17" have the most consistent data.

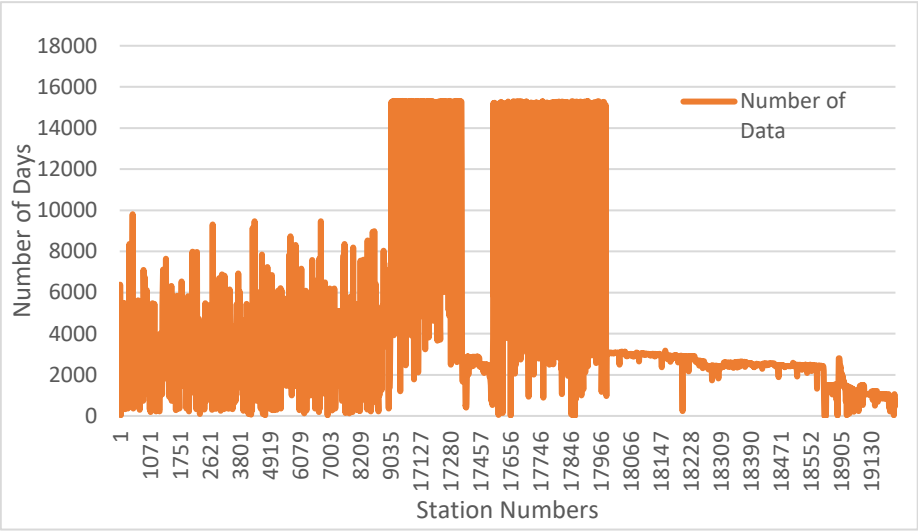



Figure 14 Amount of the data with all stations obtained from TSMS

Approximately 15341 data should exist for each station between Jan.1, 1979, to Dec. 31, 2020. Therefore, the percentage of available data has been calculated from entire stations. 249 stations found where has 90 % or higher data availability and 239 stations with 95 % or higher data availability. The situation was similar in the monthly data. Therefore, those 239 stations are selected for the initial analysis. Figure 15 shows the locations and station numbers of those selected stations over Türkiye.




Figure 15 Location of the 239 stations

Missing values and zero values belonging to daily data have also been investigated. Missing values were very low among the entire data for daily averages; therefore, those stations are also included in the analysis. Zero values are also counted and summarized in table 5. Thirty-three stations have missing daily wind speeds bigger than the 720 days. 39 Station has no zero values.

Table 5 Number of Zero Values in the data

| **Number of Zero Values (Day)** | **Number of Stations** |
|---|---|
| 0 | 39 |
| <30 | 94 |
| 30-60 | 23 |
| 60-120 | 21 |
| 120-360 | 23 |
| 360-720 | 7 |
| > 720 | 33 |

Therefore, to increase and understand the quality of validations, the following processes have been performed for the stations where monthly and daily average data are available. Although daily average data is selected according to the availability of the data, monthly data is also analyzed for availability. 68 stations that have missing values were determined from the 1979 to 2020 period from monthly data. The number of missing data among the entire data is very low. Therefore, those stations are also included in the validations. Table 6 shows the number of stations and the missing observation percentage among the data.

Table 6 Missing Observations in the Monthly Data

| Number of Stations | Missing Observations (% in entire data) |
|---|---|
| 1 | 4,37 |
| 1 | 4,17 |
| 5 | 2,19 |
| 1 | 2,39 |
| 2 | 2,78 |
| 3 | 1,79 |
| 1 | 1,59 |
| 2 | 1,19 |
| 5 | 0,99 |
| 3 | 0,80 |
| 5 | 0,60 |
| 14 | 0,40 |
| 14 | 0,20 |

#### 3.1.1.1 Inhomogeneities and Gradual Decrease in the Observation Data

In addition to stations with missing values, there is also obvious heterogeneity and gradual decrease in the monthly and daily time series at some of the stations. The reasons for inhomogeneities based on the literature could be explained by the changes in location, anemometer hub height, Automatic Observations Stations (AOS), or measurement protocols [187]. Gradual decreases can also be reasoned from rising temperatures, increase in surface roughness such as urbanization, an increase in forest areas and height or an increase in cultivated land area, changes in atmospheric circulation [188], cyclonic and anticyclonic activity, instrumentation, observation, and exposure biases [189].

Figure 16 shows a couple of example stations with inhomogeneities and gradual decreases. The reasons for those kinds of changes in the entire data are most probably changes in the location of the stations or changes in the roughness around the station

[190]. 44 stations are determined with inhomogeneities among the entire stations in the monthly data.

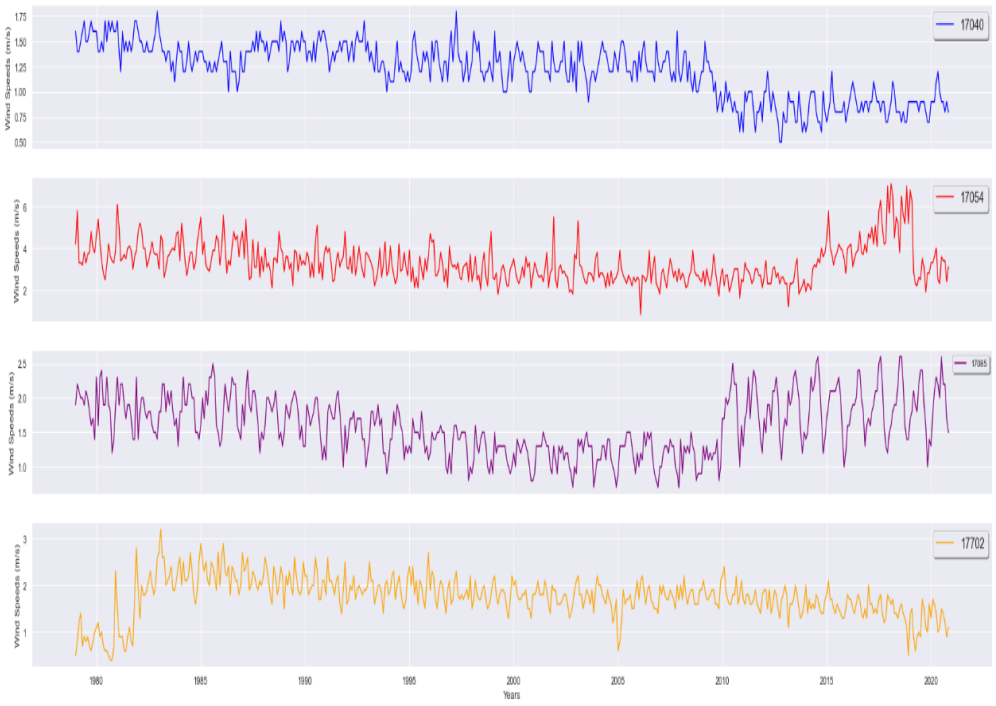



Figure 16 Inhomogenity and gradual decrease (17085) examples from the stations

Moreover, station data that do not follow the same variation with ERA5 re-analysis data are also analyzed, and some of them are cropped in order to minimize uncertainties. Figure 17 shows an example of this deleted station.

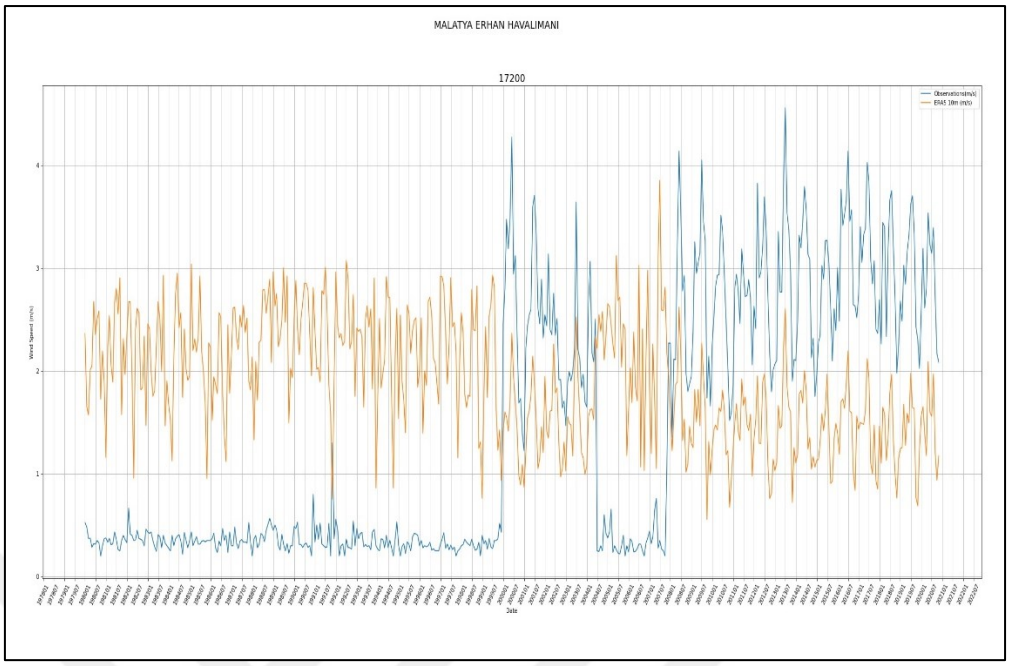



Figure 17 An example of deleted station

An example from the cropped station is given in Figure 18 that is cropped before 2010.

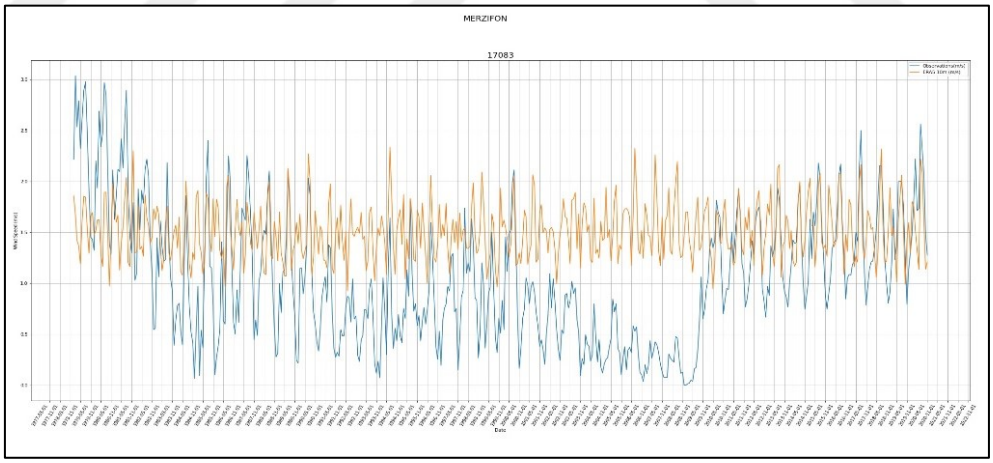



Figure 18 Example of Cropped Station

Dadaser-Celik and Cengiz (2014) also investigated wind speed trends over Türkiye based on TSMS meteorological data and determined a decreasing trend, while the temperatures have an increasing trend. The study found that most observation stations were not located in the city centers. However, they explained that rapid

urbanization from 1979 to 2006 could also be the reason for this decreasing trend [13] It is also known that changes in the roughness around the station could also be another reason for those changes. No metadata or location change information was received from TSMS. Therefore, in a Ph.D. thesis study: Demircan (2019) explained the stations with location changes and instrumental changes in the TSMS stations. 21 stations where the locations were changed after 1979 are found in Demircan's study, which matches this study [191]. However, those stations were not subject to these inhomogeneities or gradual decreases. TSMS also changed the manual observation stations to (AOS) after 2008. The noticeable alterations that occurred around the year 2008 can therefore be attributed to this transition. There are also other changes, such as anemometer or location change which are not explained in the data which is obtained from TSMS. Therefore, since there is no metadata information, inhomogeneities and gradual decreases in the observation data are eliminated by cropping those data station by station. Finally, 26% of the observation data is cropped. Airport stations are also deleted due to high inhomogeneity in those stations, and stations with obvious inhomogeneity and gradual decrease are not used. Finally, 178 stations stayed among all stations used in the validation and analysis together with ERA5 and MERRA2 re-analysis data. Table 7 gives information about deleted stations.

Table 7 List of Deleted Stations

| Station ID | Region | Station name | City | Latitude | Longitude | Elevation above the sea level (m) |
|---|---|---|---|---|---|---|
| **17020** | Black Sea | BARTIN | Bartın | 416.248 | 323.569 | 33 |
| **17033** | Black Sea | ORDU | Ordu | 409.838 | 378.858 | 5 |
| **17066** | Marmara | KOCAELI | Kocaeli | 407.663 | 299.173 | 74 |
| **17082** | Black Sea | AMASYA MERZIFON HAVALIMANI | Amasya | 408.357 | 355.258 | 535 |
| **17092** | East Anatolia | ERZINCAN HAVALIMANI | Erzincan | 39.716 | 39.525 | 1154 |
| **17096** | East Anatolia | ERZURUM HAVALIMANI | Erzurum | 399.529 | 411.897 | 1758 |
| **17115** | Marmara | BANDIRMA HAVALIMANI | Balıkesir | 403.245 | 279.737 | 42 |
| **17170** | East Anatolia | VAN FERIT MELEN HAVALIMANI | Van | 38.469 | 43.337 | 1665 |
| **17172** | East Anatolia | VAN BOLGE | Van | 384.693 | 43.346 | 1675 |
| **17180** | Aegean | DIKILI (IZMIR) | İzmir | 390.737 | 26.888 | 3 |
| **17195** | Anatolia | KAYSERI ERKILET HAVALIMANI | Kayseri | 38.773 | 354.908 | 1053 |
| **17200** | East Anatolia | MALATYA ERHAN HAVALIMANI | Malatya | 384.343 | 380.934 | 849 |
| **17202** | East Anatolia | ELAZIG HAVALIMANI | Elazıg | 386.058 | 392.973 | 881 |
| **17204** | East Anatolia | MUS | Muş | 387.509 | 415.023 | 1322 |
| **17205** | East Anatolia | TATVAN | Bitlis | 385.033 | 422.808 | 1665 |
| **17210** | South East Anatolia | SIIRT | Siirt | 379.319 | 419.354 | 895 |
| **17220** | Aegean | IZMIR BOLGE | İzmir | 383.949 | 270.819 | 29 |
| **17270** | South-East Anatolia | SANLIURFA | Şanlıurfa | 371.608 | 387.863 | 550 |
| **17285** | East Anatolia | HAKKARI | Hakkari | 375.745 | 437.388 | 1727 |
| **17310** | Mediterranean | ALANYA (ANTALYA) | Antalya | 365.507 | 319.803 | 6 |
| **17320** | Mediterranean | ANAMUR (MERSİN) | Mersin | 360.686 | 328.649 | 2 |
| **17340** | Mediterranean | MERSIN | Mersin | 367.808 | 346.031 | 7 |
| **17350** | Mediterranean | INCIRLIK MEYDAN (ADANA) | Adana | 370.005 | 354.183 | 65 |
| **17375** | Mediterranean | FINIKE | Antalya | 363.024 | 301.458 | 2 |
| **17606** | Black Sea | KASTAMONU/BOZKURT | Kastamonu | 419.597 | 340.037 | 167 |
| **17652** | Anatolia | OSMANCIK (CORUM) | Çorum | 409.787 | 348.011 | 419 |
| **17662** | Marmara | GEYVE (SAKARYA) | Sakarya | 405.214 | 30.296 | 100 |
| **17664** | Anatolia | KIZILCAHAMAM (ANKARA) | Ankara | 404.729 | 326.441 | 1033 |
| **17666** | East Anatolia | ISPIR (ERZURUM) | Erzurum | 404.868 | 409.997 | 1223 |
| **17668** | East Anatolia | OLTU (ERZURUM) | Erzurum | 405.497 | 419.951 | 1312 |
| **17679** | Anatolia | NALLIHAN (ANKARA) | Ankara | 401.733 | 31.332 | 650 |
| **17681** | Anatolia | ZILE(TOKAT) | Tokat | 40.296 | 358.905 | 719 |
| **17684** | Anatolia | SUSEHRI (SIVAS) | Sivas | 401.623 | 380.752 | 1164 |
| **17695** | Marmara | KELES (BURSA) | Bursa | 39.915 | 292.313 | 1063 |
| **17720** | East Anatolia | DOGUBEYAZIT (AGRI) | Ağrı | 395.396 | 44.018 | 1640 |
| **17768** | East Anatolia | CEMISGEZEK (TUNCELI) | Tunceli | 390.401 | 389.177 | 898 |
| **17774** | East Anatolia | KARAKOCAN (ELAZIG) | Elazığ | 389.425 | 400.428 | 1090 |
| **17776** | East Anatolia | SOLHAN (BINGOL) | Bingöl | 389.597 | 410.503 | 1366 |
| **17784** | East Anatolia | ERCIS (VAN) | Van | 390.197 | 433.382 | 1678 |
| **17786** | East Anatolia | MURADIYE VAN | Van | 389.897 | 437.627 | 1706 |
| **17802** | Anatolia | KAYSERI/PINARBASI | Kayseri | 387.251 | 363.904 | 1542 |
| **17808** | East Anatolia | GENC (BINGOL) | Bingöl | 387.616 | 405.577 | 993 |
| **17810** | East Anatolia | AHLAT (BITLIS) | Bitlis | 387.487 | 42.475 | 1730 |
| **17824** | Aegean | GUNEY (DENIZLI) | Denizli | 381.515 | 290.587 | 825 |
| **17836** | Anatolia | DEVELI (KAYSERI) | Kayseri | 383.744 | 354.797 | 1204 |
| **17844** | East Anatolia | SIVRICE (ELAZIG) | Elazığ | 384.507 | 393.101 | 1240 |
| **17846** | East Anatolia | MADEN (ELAZIG) | Elazığ | 383.924 | 396.757 | 1047 |
| **17847** | Southeast Anatolia | ERGANI (DIYARBAKIR) | Diyarbakır | 38.267 | 39.766 | 986 |
| **17854** | Aegean | SELCUK (IZMIR) | İzmir | 379.423 | 273.669 | 18 |
| **17864** | Mediterranean | ULUBORLU (ISPARTA) | Isparta | 38.086 | 304.582 | 1025 |
| **17884** | Aegean | MILAS (MUGLA) | Muğla | 373.027 | 277.804 | 57 |
| **17886** | Aegean | YATAGAN (MUGLA) | Muğla | 373.395 | 281.369 | 365 |
| **17898** | Anatolia | SEYDISEHIR (KONYA) | Konya | 374.267 | 31.849 | 1129 |
| **17900** | Anatolia | CUMRA (KONYA) | Konya | 375.658 | 32,79 | 1014 |
| **17912** | South-East Anatolia | SIVEREK (SANLIURFA) | Şanlıurfa | 377.522 | 393.291 | 801 |
| **17928** | Anatolia | HADIM (KONYA) | Konya | 369.893 | 324.557 | 1552 |
| **17936** | Mediterranean | KARAISALI (ADANA) | Adana | 372.506 | 350.628 | 240 |
| **17958** | Mediterranean | ERDEMLI (MERSIN) | Mersin | 366.268 | 34.338 | 7 |
| **17962** | Mediterranean | DORTYOL (HATAY) | Hatay | 368.244 | 361.981 | 29 |
| **17974** | Mediterranean | GAZIPASA (ANTALYA) | Antalya | 362.715 | 323.045 | 21 |
| **17986** | Mediterranean | SAMANDAG (HATAY) | Hatay | 360.814 | 359.492 | 4 |

### 3.1.1.2 General Statistics of the Observation Data

To understand the structure of the available data, average, standard deviation, maximum and minimum values of daily data is calculated from 239 stations before cropping the data. Maximum average wind speeds have been found for the 17111 station with 5.75 m/s. This station is located in the Bozcaada/Çanakkale region, which has Türkiye's highest wind power potential. The lowest mean wind speeds are calculated in Tokat Zile (Station number 17681), which is located in the internal Anatolia region. The mean wind speeds belonging to each station were interpolated by using Inverse Distance Weighting (IDW) interpolation method in QGIS [192] to understand the geographical distribution of mean surface winds (fig.19). There are also some stations where wind speeds are lower but have extreme maximum wind speeds. Those stations are also excluded from validation data sets.

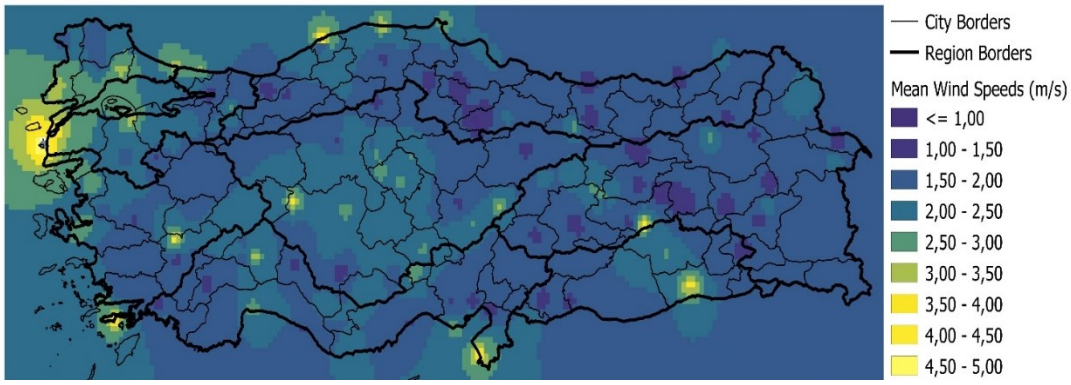



Figure 19 Mean Wind Speeds from Daily Data at 239 Stations

Maximum wind speeds are also interpolated in Figure 20. Most cities with lower average wind speeds also have lower maximum wind speeds, like the eastern Marmara or the South-West part of Türkiye. Only a few extremes, such as Konya (high maximum wind speed, low mean wind speed), Şanlıurfa has been determined.

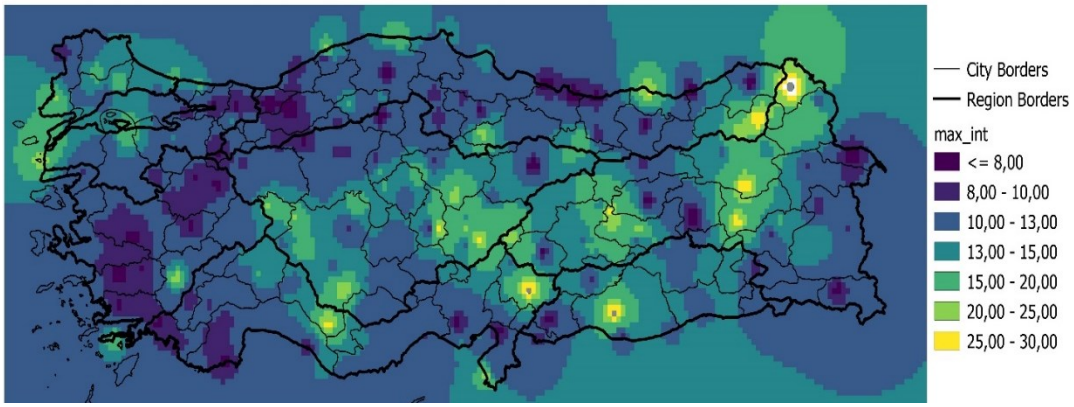



Figure 20 Maximum Wind Speeds from Daily Data at 239 Stations

The heatmap in Figure 21 shows the annual average from daily data for each station from 1979 to 2020. There is consistency in the wind speed averages until specific years; after these years, those averages are decreased/increased with specific values. The relocation of the stations is probably the reason for these sudden changes. Moreover, there is a noticeable wind speed increase for some stations after 2000 (for stations between 17015 to 17195). Those stations are also excluded from the validation of the models.

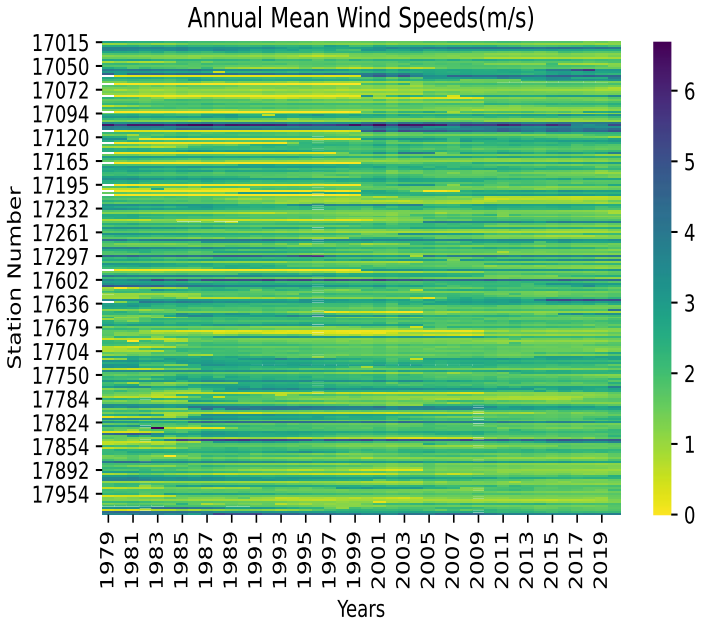



Figure 21 Annual Mean Wind Speeds without cropped data

Same analysis has been done for the seasonal averages in figure 22. Seasonality is obvious for all stations. Summer (JJA) and Spring (MMA) months have higher wind speed averages than fall and winter seasons.

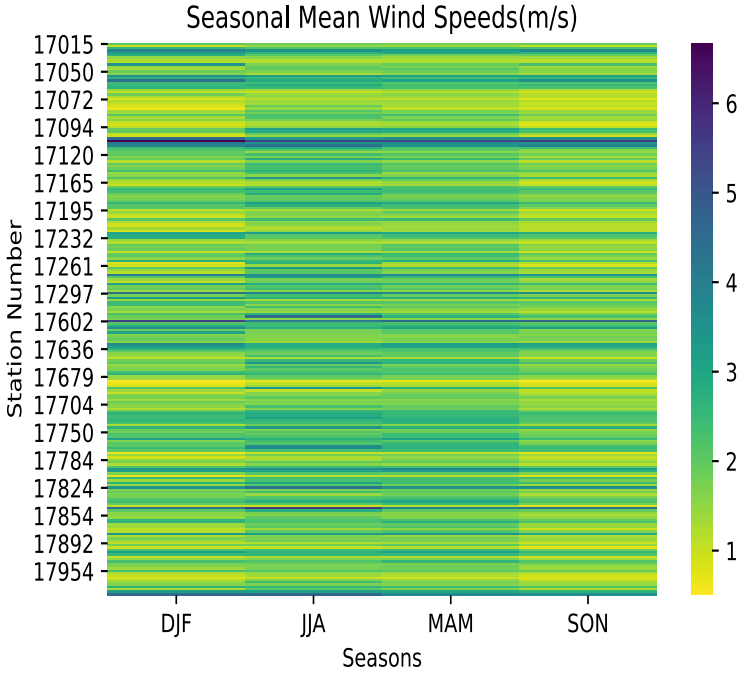



Figure 22 Seasonal mean wind speeds

Maximum wind speeds for each year at each station are also determined to understand the trend of the maximum wind speeds during the 41 years. In 2010, maximum wind speeds were increased for many stations. Some stations (the station numbers are between 17100-17119) have higher maximum wind speeds than others. Those stations are located in Bandırma, Çanakkale, Bozcaada, Gökçeada, and Bursa cities, which have Türkiye's highest wind energy potential.

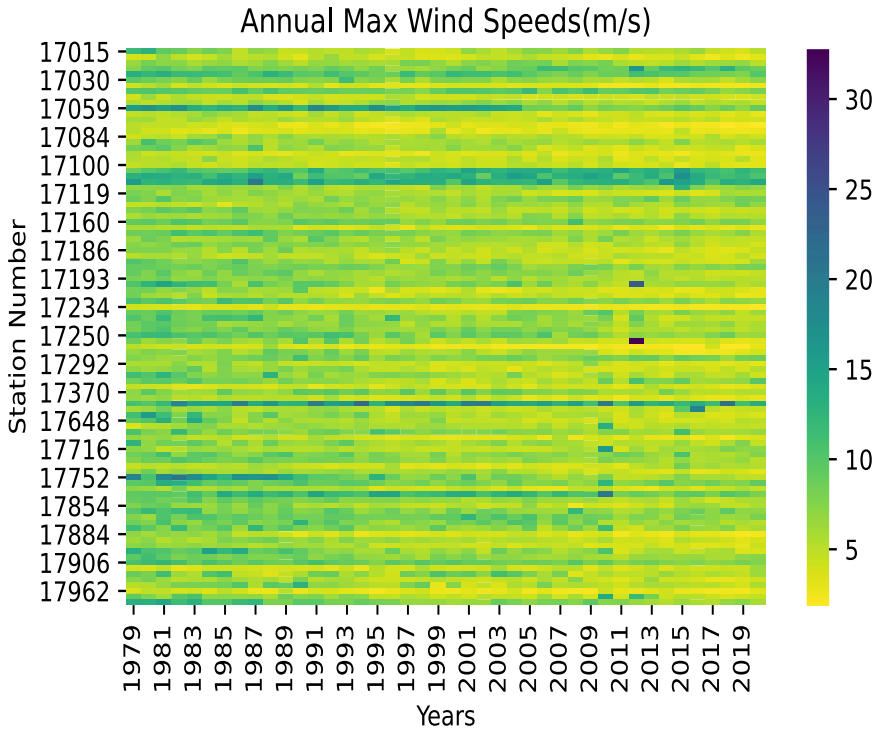



Figure 23 Annual maximum wind speeds for each station at each year

### 3.1.2 Global Re-Analysis Data

#### 3.1.2.1 5th Generation ECMWF re-analysis (ERA5)

ERA5 re-analysis data has been used for many years to determine available wind resources in the literature and wind energy market. The data is also 100 m above the ground level (m.a.g.l.) wind speeds. Monthly and hourly single-level wind speeds at 10 and 100 m have been obtained from Copernicus Services for this study with a 0.25-degree spatial resolution from 1979 to the present at NetCDF format [193]. Since the wind turbines are now approximately installed 100 m above the ground level, those data are also used in the further steps of this study. The seasonal average of the spatial distribution of 10 and 100 m wind speeds is illustrated in Figure 24.

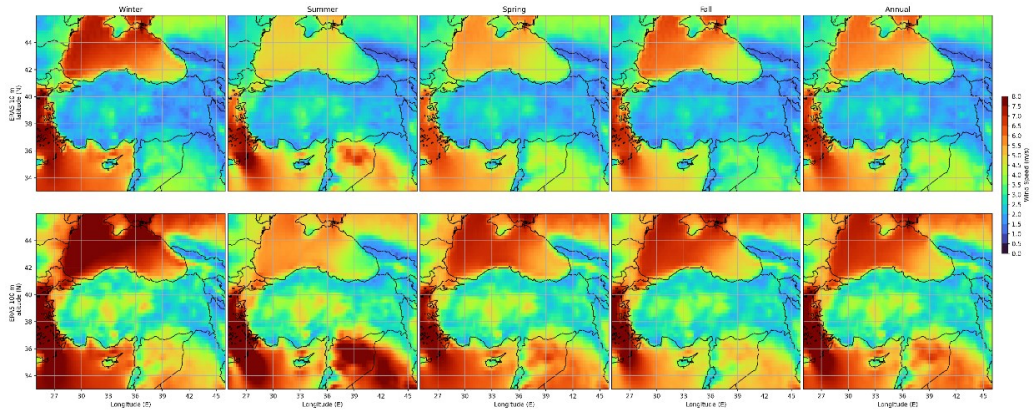



Figure 24 Seasonal average wind speeds (m/s) of ERA5 data over the study area

### 3.1.2.2 Modern-Era Retrospective analysis for Research and Applications, Version 2

Since observation data have inhomogeneities and gradual decreases, another re-analysis data are also used to evaluate model performances for both onshore and offshore wind resources of Türkiye. NASA's Modern-Era Retrospective analysis for Research and Applications, Version 2 (MERRA-2) data, has also been obtained from NASA servers. MERRA2 has 0.5° x 0.625° horizontal resolution, and the vertical height of the data is 10 m and 50 m above the ground level [194]. The seasonal and annual distribution of MERRA2 wind speeds obtained from hourly data is illustrated in Figure 25.

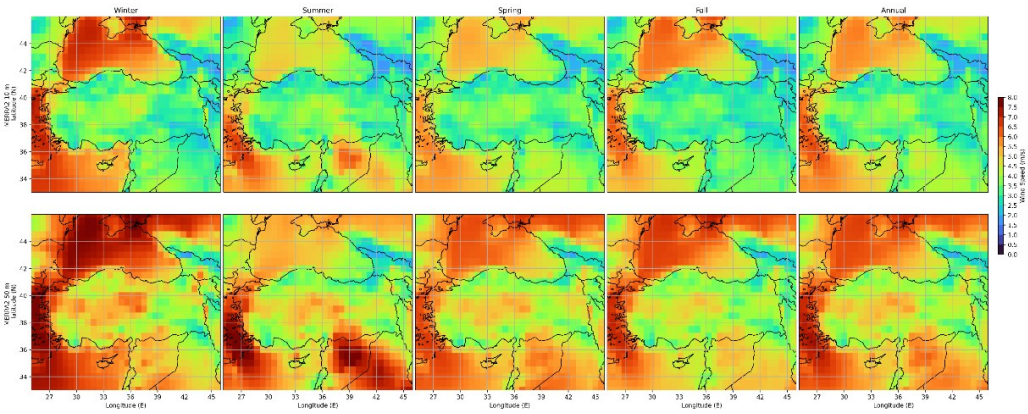



Figure 25 Seasonal avarage wind speed (m/s) of MERRA2 data over the study area

***Hourly Data***

5-year hourly data have also been examined in terms of geographical regions in Figure 26 for all three reference data. The data starts in 2015 and ends in December 2020 for the same cropped stations. Therefore, these data are not included in the study period (1980-2014) due to the availability of the CMIP6 models' historical outputs. ERA5 and MERRA2 hourly mean wind speeds have also been obtained from the hourly data for the same years. The data have been extracted from each grid point which is the closest to the observation stations, and averaged for each geographical region. Figure 26 shows the mean wind speeds for each hour between the 2015-2020 years at 10 m wind speeds(m/s) for observations, ERA5 and MERRA2. It shows the diurnal variation of wind speed is the same for all the reference data. However, MERRA2 wind speeds are higher than both ERA5 and observations. Marmara region has the highest wind speeds, where the Aegean Region follows it for ERA5 and MERRA2. The Anatolia region has higher wind speeds than the Aegean region in the observations. This could be reasoned by the missing data in the region. The general diurnal variation of wind is similar to the temperature variation in a typical day, which reaches the highest values in the mid of the day, and the lowest values are seen in the nocturnal hours.

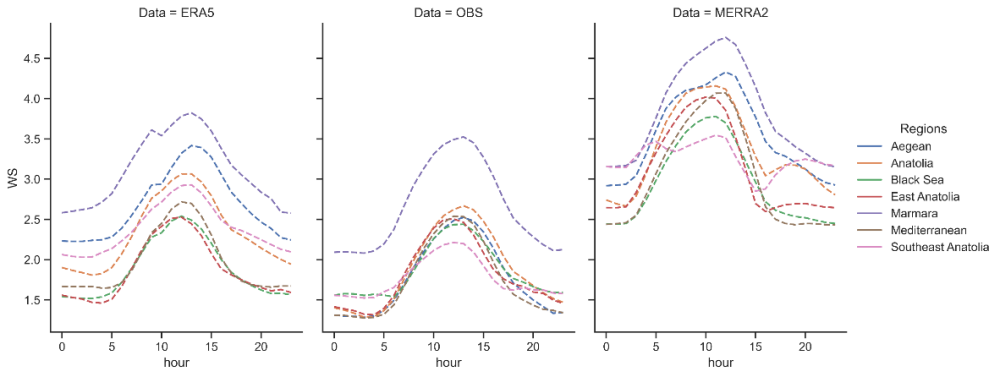



Figure 26 Diurnal Averages for all regions with 3 reference data

### 3.1.3 Coupled Model Intercomparison Project Phase 6 (CMIP6)- Data

The recent version of the CMIPs is used in this study with the historical period and two different scenarios (SSP2-4.5 and SSP5-8.5). Figure 27 summarizes the available data periods for observations, ERA5, MERRA2, and CMIP6 models.

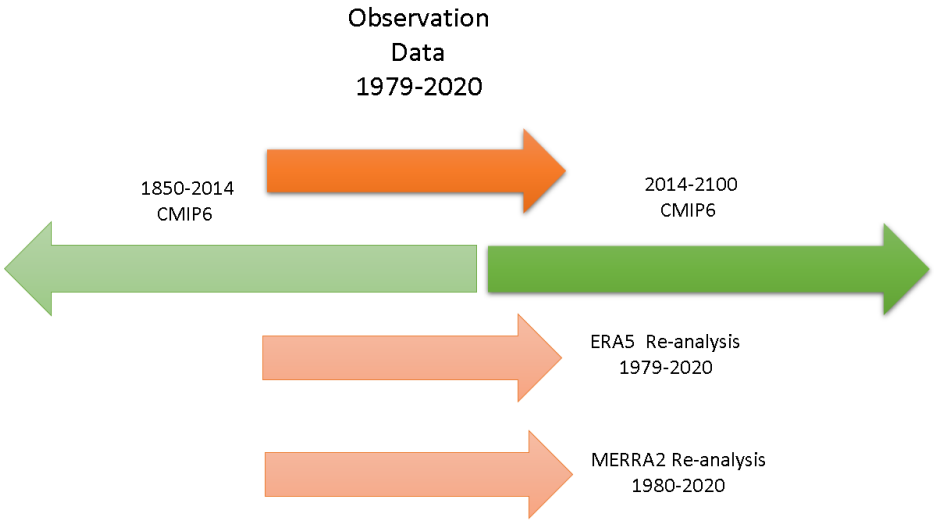



Figure 27 Available periods for all data: CMIP6 data is obtained at monthly avarages, observation data is available at daily avarages and ERA5 and MERRA2 data is obtained at hourly avarages

Since the study covers different wind speed calculation methods at 100 m, different CMIP6 models are used and classified due to the availability of CMIP6s with

different parameters and scenarios. Therefore the methods and models are classified as follows:

***I-Historical:*** 1850–2014 (1979–2014 is used to compare with ERA5 and observations) 48 models were available for monthly surface wind speeds. 28 GCMs have been obtained from the CMIP6 database depending on the same initial conditions for surface wind. An overview of the CMIP6 models used in the historical part of the study is given in Table 8. Variant labels are selected for all models r1i1p1f1 (r: realization: initialization method, p: physics: forcing). The models are also classified depending on model types. Land use explanations are also given to understand the effect of dynamic vegetation on wind resources. 14 ESMs and 14 coupled models were used for this study. Dynamic vegetation is used mostly in the ESM models. Coupled models mostly include land-surface models, which consider energy fluxes, biosphere-atmosphere interactions, photosynthesis, etc.

***II-Future projections:*** The multi-model ensemble part of the study contains two different methods for calculating the 100 m wind speeds, which is explained in Chapter 3.3. Therefore, for the onshore part of Türkiye, all available CMIP6 models (27) for surface winds parameters at historical, SPP2-4.5, and SSP5-8.5 scenarios are used and given in Table 9. Secondly, for the offshore wind resource at 100 m wind speed calculations, pressure level data is used to calculate the height of the 1000 m pressure level. Therefore, the availability of those parameters was also different at a three-time scale. Those models used in the offshore multi-model ensemble are explained in Table 10.

***III- Mesoscale model outputs:*** 13 CMIP6 models are used as an input of the WRF-PGW method. Those models (see Table 11) are also used to measure the performance of the WRF outputs.

Table 8 Overview of CMIP6 historical period models

| GCM No | Model Name | Resolution | Model Type | DVM | Instution | Reference |
|---|---|---|---|---|---|---|
| GCM1 | BCC-CSM2-MR | 1.1°x1.1° | CM | ? | Beijing Climate Center | [195] |
| GCM2 | BCC-ESM1 | 2.81°×2.81° | ESM | No | Beijing Climate Center | [196] |
| GCM3 | CAMS-CSM1-0 | 1.1°x1.1° | CM | ? | Chinese Academy of Meteorological Sciences | [197] |
| GCM4 | CanESM5 | 2.8°x2.8° | ESM | No | Canadian Centre for Climate Modeling and Analysis, Canada | [198] |
| GCM5 | CAS-ESM2 | 1.4° x 1.4° | ESM | Yes | Chinese Academy of Sciences | [199] |
| GCM6 | CESM2 | 1.3°x0.9° | ESM | Yes | National Center for Atmospheric Research | [200] |
| GCM7 | CESM2-FV2 | 1.9°x2.5° | CM | Yes | National Center for Atmospheric Research | [201] |
| GCM8 | CESM2-WACCM | 1.3°x0.9° | CM | Yes | National Center for Atmospheric Research | [202] |
| GCM9 | E3SM1-0 | 1° x1° | fully CM, ESM | No | U.S. Department of Energy (DOE) | [203, 204] |
| GCM10 | EC-Earth3 | 0.7°x0.7° | ESM | No | EC-EARTH consortium | [204] |
| GCM11 | EC-Earth3-Veg | 0.7°x0.7° | ESM | Yes | EC-EARTH consortium | [205] |
| GCM12 | FGOALS-f3-L | 1°x1° | CM | Yes | Chinese Academy of Sciences (CAS) | [206] |
| GCM13 | FGOALS-g3 | 2° x 2° | CM | Yes | Chinese Academy of Sciences (CAS) | [207] |
| GCM14 | GFDL-ESM4 | 1.3°x1° | ESM | Yes | The Geophysical Fluid Dynamics Laboratory of NOAA | [208] |
| GCM15 | GISS-E2-1-G | 2.5°x2° | CM | No | Goddard Institute for Space Studies (GISS), USA | [209] |
| GCM16 | GISS-E2-1-G-CC | 2.5°x2° | CM | Yes | Goddard Institute for Space Studies (GISS), USA | [210] |
| GCM17 | GISS-E2-1-H | 2.5°x2° | CM | No | Goddard Institute for Space Studies (GISS), USA | [211] |
| GCM18 | INM-CM4-8 | 2°x1.5° | CM | ? | Russian Institute for Numerical Mathematics Climate Model Version 4 | [212] |
| GCM19 | IPSL-CM6A-LR | 2.5° × 1.3° | CM | No | Institut Pierre Simon Laplace (IPSL) | [213] |
| GCM20 | KACE-1-0-G | 1° x1° | CM | Yes | National Institute of Meteorological Research, Republic of Korea | [214] |
| GCM21 | MIROC6 | 1.4° x 1.4° | CM | No | National Institute for Environmental Studies, The University of Tokyo, Japan | [215] |
| GCM22 | MPI-ESM1-2-HR | 1° x1° | ESM | No | Max Planck Instutue (Germany) | [216] |
| GCM23 | MPI-ESM1-2-LR | 1.9°x1.9° | ESM | Yes | Max Planck Instutue (Germany) | [217] |
| GCM24 | MRI-ESM2-0 | 1.1° x1.1° | ESM | No | Meteorological Research Institute (Japan) | [218] |
| GCM25 | NorESM2-LM | 2.5°x1.9° | ESM | Yes | Norwegian Climate Center | [219] |
| GCM26 | NorESM2-MM | 1.3°x0.9° | ESM | Yes | Norwegian Climate Center | [220] |
| GCM27 | SAM-0-UNICON | 1°x1° | AOGCM, BGC, AER | No | Seoul National University | [221] |
| GCM28 | MPI-ESM1-2-HAM | 1.9°x1.9° | ESM | Yes | Max Planck Instutue (Germany) | [222] |

Table 9 CMIP6 Models in the onshore WPPs future projections study

| No | Model Name | Resolution | Institution | Reference |
|---|---|---|---|---|
| GCM1 | ACCESS-CM2 | 1.875×1.25 | Commonwealth Scientific and Industrial Research Organisation (Australia) | [223] |
| GCM2 | AWI-CM-1-1-MR | 0.9 × 0.9 | Alfred Wegener Institute | [224] |
| GCM3 | BCC-CSM2-MR | 1.1x1.1 | Beijing Climate Center | [225] |
| GCM4 | CanESM5-CanOE | 2.8 × 2.8 | Canadan Earth System Model | [226] |
| GCM5 | CESM2 | 1.3x0.9 | National Center for Atmospheric | [200] |
| GCM6 | CMCC-ESM2 | 1.3x0.9 | Fondazione Centro Euro-Mediterraneo sui Cambiamenti Climatici (Italy) | [227] |
| GCM7 | EC-EARTH3 | 0.7x0.7 | EC-EARTH consortium | [204] |
| GCM8 | EC-EARTH3-CC | 0.7x0.7 | EC-EARTH consortium | [228] |
| GCM9 | EC-EARTH3-VEG-LR | 0.7 × 0.7 | EC-EARTH consortium | [229] |
| GCM10 | FGOALS-f3-L | 2 x 2 | Chinese Academy of Sciences (CAS) | [207] |
| GCM11 | FGOALS-g3 | 1.3x1.0 | Chinese Academy of Sciences (CAS) | [208] |
| GCM12 | GFDL-ESM4 | 1.3x1.0 | Geophysical Fluid Dynamics Laboratory | [208] |
| GCM13 | FIO-ESM-2-0 | 1.3x0.9 | First Institute of Oceanography, State Oceanic Administration (China) | [230] |
| GCM14 | HadGEM3-GC31-LL | 1.88° x 1.25° | Met Office Hadley Centre | [231] |
| GCM15 | IITM-ESM | 1.9 × 1.9 | Centre for Climate Change Research Indian Institute of Tropical Meteorology | [232] |
| GCM16 | INM-CM4-8 | 2.0x1.5 | Russian Institute for Numerical Mathematics Climate Model Version 4 | [212] |
| GCM17 | INM-CM5-0 | 1.5 × 2.0 | Russian Institute for Numerical Mathematics Climate Model Version 4 | [233] |
| GCM18 | IPSL-CM6A-LR | 2.5 × 1.3 | Institute Pierre-Simon Laplace | [213] |
| GCM19 | KACE-1-0-G | 1 x1 | National Institute of Meteorological Research, Republic of Korea | [214] |
| GCM20 | MIROC6 | 1.4x1.4 | National Institute for Environmental Studies, The University of Tokyo, Japan | [215] |
| GCM21 | MIROC-ES2L | 4.5 × 4.5 | National Institute for Environmental Studies, The University of Tokyo, Japan | [234] |
| GCM22 | MPI-ESM1-2-LR | 1.9x1.9 | Max Planck Instutue (Germany) | [217]. |
| GCM23 | MRI-ESM2-0 | 1.1x1.1 | Meteorological Research Institute (MRI) | [218] |
| GCM24 | NorESM2-LM | 2.5x1.9 | Norwegian Climate Center | [219] |
| GCM25 | NorESM2-MM | 1.3x0.9 | | [220]. |
| GCM26 | TaiESM1 | 1.25×0.94 | Research Center for Environmental Changes, Academia Sinica (Taiwan) | [235]. |
| GCM27 | UKESM1-0-LL | 1.9x1.3 | Met Office Hadley Centre | [236]. |

Table 10 CMIP6 Models used in the offshore wind resource part of the study

| No | Model Name | Resolution (degree) | Institution | References |
|---|---|---|---|---|
| GCM1 | AWI-CM-1-1-MR | 0.9 × 0.9 | Alfred Wegener Institute for Polar and Marine Research (Germany) | [237] |
| GCM 2 | CanESM5-CanOE | 2.8 × 2.8 | Canadian Climate Centre (Canada) | [238] |
| GCM 3 | CESM2 | 1.3x0.9 | National Center for Atmospheric Research (USA) | [200] |
| GCM 4 | CMCC-ESM2 | 1.3x0.9 | Fondazione Centro Euro-Mediterraneo sui Cambiamenti Climatici (Italy) | [239] |
| GCM 5 | GFDL-ESM4 | 1.3x1.0 | Geophysical Fluid Dynamics Laboratory (USA) | [208] |
| GCM 6 | FIO-ESM-2-0 | 1.3x0.9 | First Institute of Oceanography, State Oceanic Administration (China) | [240] |
| GCM 7 | INM-CM4-8 | 2.0x1.5 | Russian Institute for Numerical Mathematics Climate Model (Russia) | [212] |
| GCM 8 | INM-CM5-0 | 1.5 × 2.0 | Russian Institute for Numerical Mathematics Climate Model (Russia) | [241] |
| GCM 9 | IPSL-CM6A-LR | 2.5 × 1.3 | Institute Pierre-Simon Laplace (France) | [213] |
| GCM 10 | MIROC6 | 1.4x1.4 | National Institute for Environmental Studies, The University of Tokyo (Japan) | [215] |
| GCM 11 | MPI-ESM1-2-LR | 1.9x1.9 | Max Planck Institute (Germany) | [217] |
| GCM 12 | NorESM2-MM | 1.3x0.9 | Norwegian Climate Center (Norway) | [220] |
| GCM 13 | TaiESM1 | 1.25×0.94 | Research Center for Environmental Changes, Academia Sinica (Taiwan) | [235] |

Table 11 CMIP6 Models used in the WRF-PGW

| Model Name | Resolution | Institute | References |
|---|---|---|---|
| AWI-CM-1-1-MR | 0.9 × 0.9 | Alfred Wegener Institute | [237] |
| BCC-CSM2-MR | 1.1x1.1 | Beijing Climate Center (China) | [225] |
| CNRM-CM6-1-HR | 0.5 × 0.5 | Centre National de Recherches Meteorologiques (France) | [242] |
| CMCC-CM2-SR5 | 0.94x1.25 | Fondazione Centro Euro-Mediterraneo sui Cambiamenti Climatici (Italy) | [243] |
| CMCC-ESM2 | 1.3x0.9 | Fondazione Centro Euro-Mediterraneo sui Cambiamenti Climatici (Italy) | [239] |
| EC-EARTH3 | 0.7x0.7 | EC-EARTH consortium | [204] |
| EC-EARTH3-CC | 0.7x0.7 | EC-EARTH consortium | [228] |
| EC-EARTH3-VEG | 0.7x0.7 | EC-EARTH consortium | [205] |
| FGOALS-f3-L | 1.25 x 1 | Chinese Academy of Sciences (CAS) | [207] |
| GFDL-ESM4 | 1.3x1.0 | Geophysical Fluid Dynamics Laboratory | [208] |
| HadGEM3-GC31-MM | 0.83° x 0.54° | Met Office Hadley Centre | [244] |
| MPI-ESM1-2-HR | 0.935 × 0.935 | Max Planck Institute (Germany) | [245] |
| MRI-ESM2-0 | 1.1x1.1 | Meteorological Research Institute | [218] |

## 3.2 Study Area

The study area for the multi-model ensemble development of the historical period is given in Figure 28, which is the entire Türkiye located in mid-western Asia and Eastern Europe and bordered by the Mediterranean Sea from the South, the Black Sea from the North and Aegean Sea from the west. The onshore sites and the site in the Aegean Sea borders, which intersects with the rectangular frame (25 E,32 N,46 E,46 N coordinates), are included in the area. Türkiye's land surface is approximately 783.562 km2 which has a different topographical structure and complexity (see fig.5).

For the multi-model ensemble development over the historical period, the onshore parts of the study area are divided into seven geographical regions in Türkiye as Marmara (I), Agean (II), Black Sea (III), Anatolia (IV), East Anatolia (V), Mediterranean (VI), South East Anatolia (VII), and one offshore site where has the highest wind energy potential has also selected as Aegean Sea Offshore Region (VIII). Figure 28 also shows the study area and locations of the TSMS stations used in this study.

For the future projection calculations from GCMs, offshore sites are also included to understand the future offshore wind energy potential of Türkiye (see fig.29). However, since there are no offshore measurements in Türkiye, only onshore data validations are evaluated in the historical part of the study.

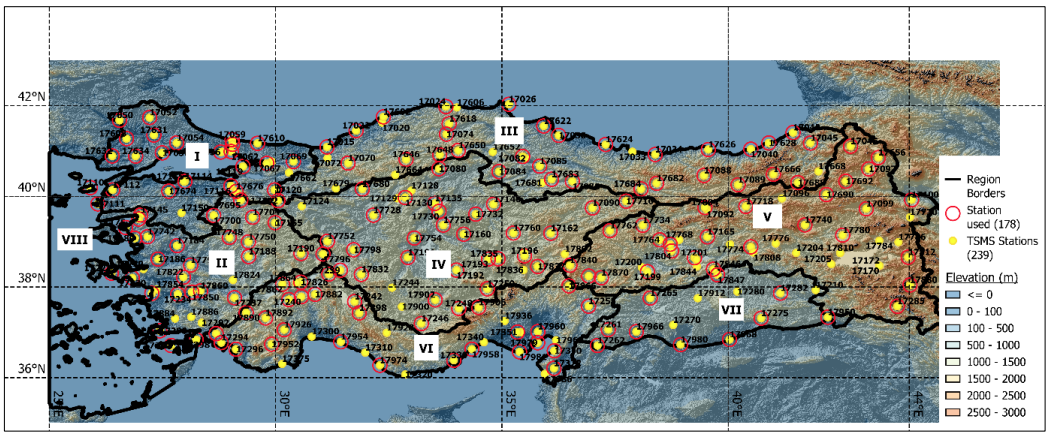



Figure 28 Study Area and location of Observation Stations

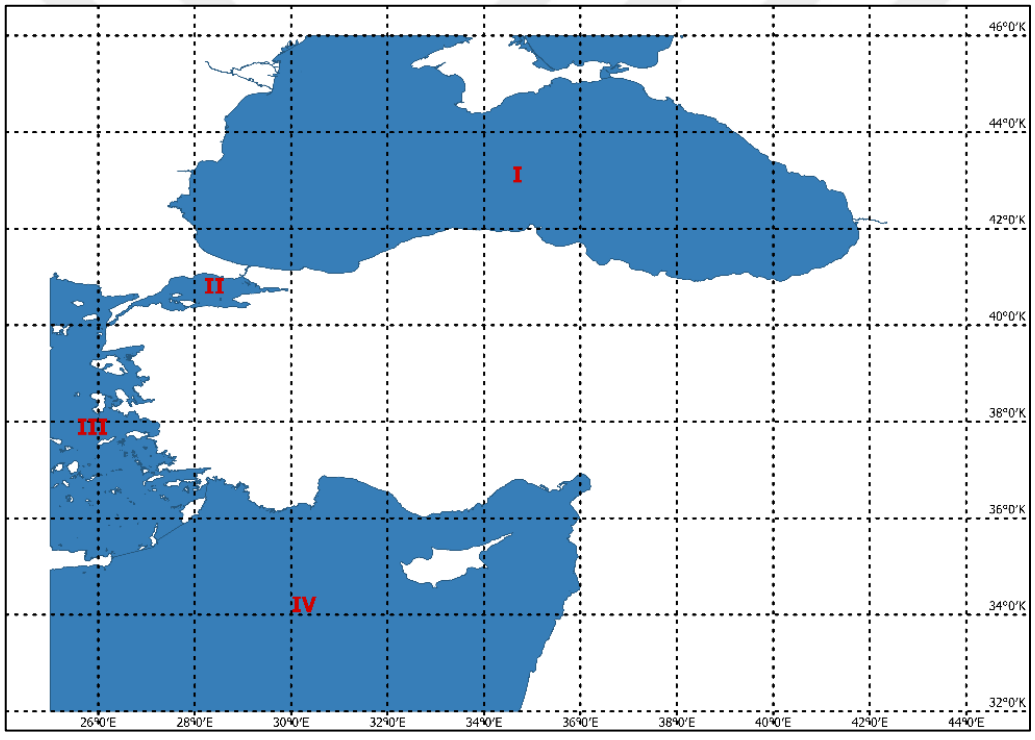



Figure 29 Offshore study area including the seas surrounding Türkiye (I: Black Sea, II: Marmara Sea, III: Aegean Sea, IV: Mediterranean Sea)

In this study, licensed [246] and pre-licensed [247] WPPs are obtained from the EMRA database with their wind power plant borders (see fig.30). The wind turbines are also associated with their boundary (dashed polygon in figure 30) according to "Legislation on Technical Evaluation on Electricity Production based on Wind Resource Applications" [248]. Therefore, individual wind turbine locations would

provide more grid points than each WPP area. Besides, since the turbines are too close to each other, most of them will be in the same GCM grid. Therefore, it is decided to use a single point for each licensed and pre-licensed WPPs that is obtained from the database. Those points are created in QGIS by using their center of gravity.

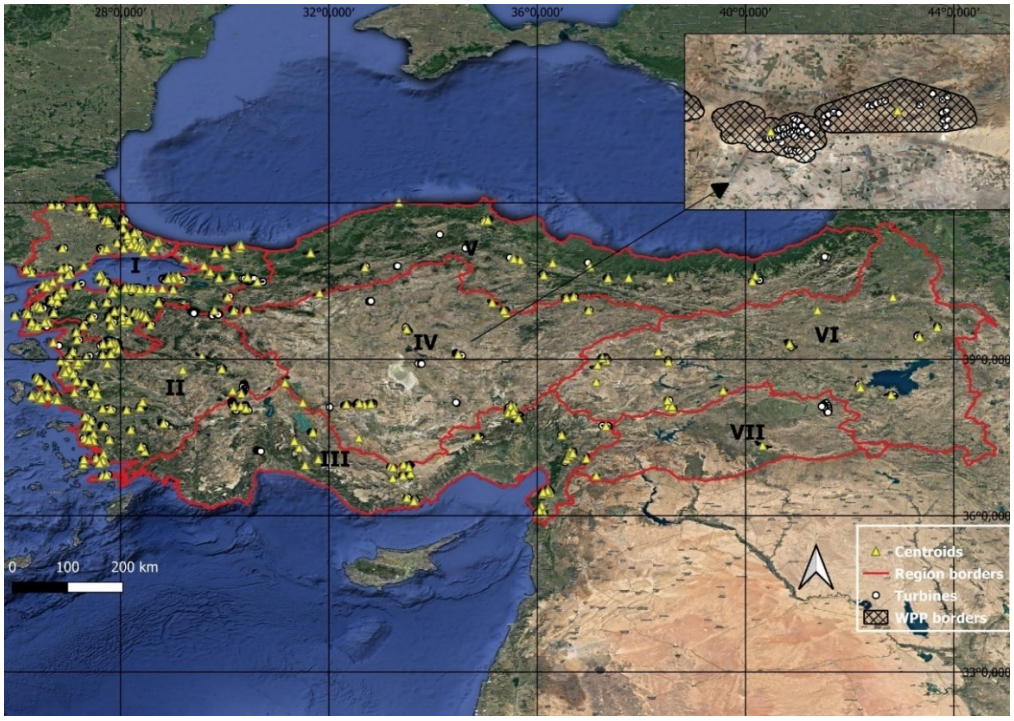



Figure 30 Locations of Wind Power Plants (associated with centroids, polygon borders and turbines) in Türkiye and Study area, Geographical regions are also numbered as I: Marmara Region, II: Aegean Region, III: Mediterranean Region, IV: Anatolia Region, V: Black Sea Region, VI: East Anatolia Region, VII: Southeast Anatolia Region.

## 3.3 Method

### 3.3.1 Validation

#### 3.3.1.1 Statistical Error Metrics

In order to determine the relationship between models and observations, classical error metrics, root mean square error (RMSE), Standard Deviation of Error (SDE),

Percent Bias (PBIAS) and Pearson correlation coefficient (r) have been calculated between CMIP6 models, ERA5 and MERRA2 grids and observations together with produced predictions from MME and mesoscale model results.

Equation (5) explains the RMSE formula, which includes "a" that is an actual value (production), "f" is a forecasted value, and "n" is the number of data. RMSE is widely used for determining error studies in literature because square errors show bigger errors with bigger values. The weight of errors is increased by using RMSE.

$$\boldsymbol{RMSE} = \sqrt{\frac{\mathbf{1}}{\boldsymbol{n}} \boldsymbol{x} \sum_{\boldsymbol{i=1}}^{\boldsymbol{n}} (\boldsymbol{a} - \boldsymbol{f})^{\mathbf{2}}} \quad (5)$$

Equation (6) defines bias for forecasted and actual values. Bias is also defined as an average error. Bias shows the average difference of forecast from actual values and determines over-under estimations.

$$\boldsymbol{BIAS} = \sum_{\boldsymbol{i=1}}^{\boldsymbol{n}} (\boldsymbol{f} - \boldsymbol{a}) \quad (6)$$

Equation (7) defines the correlation coefficient between two variables (forecast and actual). It is used for determining the linear relationship between variables.

$$\boldsymbol{r} = \frac{\sum((\boldsymbol{a_i} - \overline{\boldsymbol{a}}) \, \boldsymbol{x} \, (\boldsymbol{f_i} - \overline{\boldsymbol{f}})}{\sqrt{\sum \, (\boldsymbol{a_i} - \overline{\boldsymbol{a}})^{\mathbf{2}} \, \boldsymbol{x} \, \sum \, (\boldsymbol{f_i} - \overline{\boldsymbol{f}})^{\mathbf{2}}}} \quad (7)$$

Equation (8) shows the Standard Deviation of Error.

$$\text{SDE} = \boldsymbol{std} \sum_{\boldsymbol{i=1}}^{\boldsymbol{n}} (\boldsymbol{f} - \boldsymbol{a}) \quad (8)$$

Equation (9) shows the calculation of percent bias.

$$\boldsymbol{PBIAS} = \frac{\sum_{\boldsymbol{i=1}}^{\boldsymbol{n}} (\boldsymbol{f} - \boldsymbol{a})}{\sum_{\boldsymbol{i=1}}^{\boldsymbol{n}} (\boldsymbol{a})} \, \boldsymbol{x100} \quad (9)$$

Variance in equation (10) and standard deviation in equation (11) is also used to determine inter-annual and intra-annual relationships in the mesoscale modeling results by using Climate Data Operators (CDO) [249].

$$\textit{Variance} = \boldsymbol{n^{-1}} \sum_{\boldsymbol{i=1}}^{\boldsymbol{n}} (\boldsymbol{x_i} - \overline{\boldsymbol{x}})^2 \quad (10)$$

$$\text{Standart deviation} = \sqrt{\boldsymbol{n^{-1}} \sum_{\boldsymbol{i=1}}^{\boldsymbol{n}} \quad (\boldsymbol{x_i} - \overline{\boldsymbol{x}})^{\boldsymbol{2}}} \qquad (11)$$

### 3.3.2 Trend-Analysis

Before the downscaling/ensembling studies, observation and ERA5 re-analysis data were checked to determine the general trend in surface winds over Türkiye. Therefore, a non-parametric Mann-Kendall [250, 251] test has been applied to all observation stations, MERRA2 and ERA5 grids in the study area by using "pymannkendal" packages from python [252]. xi in Equation (12) represents each data, n is the number of available data sgn (equation [13]) is the function which is determined in the following equations.

$$\boldsymbol{S} = \sum_{\boldsymbol{i=1}}^{\boldsymbol{n=1}} \sum_{\boldsymbol{j=i+1}}^{\boldsymbol{n}} \boldsymbol{sgn}(\boldsymbol{x_j} - \boldsymbol{x_i}) \qquad (12)$$

$$\boldsymbol{sgn}(\boldsymbol{\theta}) = \begin{cases} \boldsymbol{1} & \boldsymbol{if\ \theta > 0} \\ \boldsymbol{0} & \boldsymbol{if\ \theta = 0} \\ \boldsymbol{-1} & \boldsymbol{if\ \theta < 0} \end{cases} \qquad (13)$$

Following equations shows the mean ($\mu$) and variance ($\sigma$) of *S*.

$$\mu = 0 \qquad (14)$$

$$\boldsymbol{\sigma} = \frac{\boldsymbol{n(n-1)(2n+5) - \sum_{i=1}^{n} (t_i - 1)(2_{ti} + 5)}}{\boldsymbol{18}} \qquad (15)$$

Test statistic $\boldsymbol{Z}$ is determined in the equation (16). It is assumed that $\boldsymbol{Z}$ is significant when $p < 0.05$.

$$\boldsymbol{Z} = \begin{cases} \frac{\boldsymbol{S-1}}{\sqrt{\boldsymbol{\sigma}}} & \boldsymbol{if\ S > 0} \\ \boldsymbol{0} & \boldsymbol{if\ S = 0} \\ \frac{\boldsymbol{S+1}}{\sqrt{\boldsymbol{\sigma}}} & \boldsymbol{if\ S < 0} \end{cases} \qquad (16)$$

Sen's Slope ($q_i$) [253] is also calculated (Equation [17]) for same data in order to determine the magnitude of the trend.

$$q_{i=\frac{xj-x_k}{j-k}} \quad \text{, where } j > k \qquad (17)$$

### 3.3.3 Data Processing

#### 3.3.3.1 Hypsometric Equation

In order to obtain CMIP6 wind speeds at 100 m, all available models are investigated. In order to calculate the thickness (m) between the surface and 1000 mb pressure level for offshore wind resources, the hypsometric equation in the equation (18) is used where h is the height between two levels, $p_1$ is the pressure of the surface level, $p_2$ is the 1000 mb, g is the gravity, $R_d$ is the ideal gas constant (287 J $K^{-1}$ $kg^{-1}$) and Tv is the virtual temperature.

$$\boldsymbol{h = z2 - z1 = \frac{R_d * T_v}{g} * \ln(\frac{p_1}{p_2})} \qquad (18)$$

Virtual temperature (Tv) is calculated by using specific humidty (q)(kg/kg) and temperature $(T)^0K$ at related level (see eq.19).

$$\mathbf{T_V = (1 + 0.61q) * T}s \qquad (19)$$

#### 3.3.3.2 3.4.2.2. Calculation of Shear Exponent

In the onshore part of the multi-model ensemble study, due to the complex topographical structure of Türkiye, the shear exponent (α) is calculated between 10 m and 100 m ERA5 wind speeds for the entire Türkiye by using the following formula:

$$\alpha = \frac{\ln(WS_{10}) - \ln(WS_{100})}{\ln(10) - \ln(100)} \qquad (20)$$

After calculating the shear exponent, ERA5 data is re-gridded to each CMIP6 model's resolution. Then, wind speeds at 100 m among each model are calculated using calculated shear exponents. In the offshore part of the study, the shear exponent is assumed as constant (0.14), because it is the general assumption of the shear exponent (1/7) and IEC also assumes 0.14 for offshore operational conditions [254].

### 3.3.4 Wind Power Density

Wind power density depends on wind speed and air density. The following equation explains available wind power and the relationship between wind speed and the produced power of wind energy. The WPD ($W/m^2$) in Equation (21) is power density per $m^2$ and V is wind speed (m/s) and the ρ ($kg/m^3$) density of the air.

$$\boldsymbol{WPD} = \frac{\mathbf{1}}{\mathbf{2}}\boldsymbol{x}\,\boldsymbol{\rho}\ \mathrm{x}\ \boldsymbol{V^3} \qquad (21)$$

This equation indicates that the wind power is directly proportional to the density of the air, the cube of the wind speed. It also explains that any small changes in the wind speed effects the available wind power. Even if produced wind power is affected by other factors, this equation determines the available wind power in the region. Atlas studies have also widely used this equation to give an idea to investors. Air density is assumed constant for individual GCM calculations. However, in the mesoscale wind power density calculations, air density is calculated by using the ideal gas law in Equation (22), where R is the dry air gas constant (287.0 J / kg K), T is the temperature (Kelvin), and P is the pressure (Pa).

$$\boldsymbol{\rho} = \frac{\boldsymbol{p}}{\boldsymbol{R}*\boldsymbol{T}} \qquad (22)$$

### 3.3.5 Multi-Model Ensemble

Climate models have different initial conditions, model formulations, and model types (ESM or coupled). These differences may also cause to increase in the uncertainties from each model. Therefore, combining these models with different

techniques are widely used in the literature for the determination of wind resource [22, 24, 27, 145, 146].

It is a well-known fact that uncertainties of climate models can be decreased by using ensemble approaches. Ensemble methods could be examined under three different methods: perturbated physics ensembles, multi-model ensembles, and super ensembles, which use linear regression. Two different types of multi-model ensemble methods are used in this study and explained in this chapter.

#### 3.3.5.1 Multiple Linear Regression based multi-model ensemble

Ensemble methods provide taking advantage of each model and eliminate the extremes from each model. A MME approach is used in this study by using CMIP6 model outputs at the historical period. Since the MERRA2 data starts from 1980 and CMP6 data is available up to 2014, all data is sliced from 1980 to 2014. % 75 of the data was selected as a train period, and % 25 of the data was selected as test period. First, the average value of all grids in each geographical region has been calculated in order to perform multiple linear regressions at the equal number of grids. Then MLR predictions are developed for each region in the study area by using "python sklearn.linear_model LinearRegression" packages.

For each observation data set, MLR model are set to determine the optimum weight for each CMIP6 model at seven regions and an offshore region for train period. Weights and errors are estimated by fitting the model and minimizing the sum of square errors (equation 23) with observations. R_k represents each region (k= 1,8) time series and x_i is associated with each ensemble member with 3 obervation data sets from y y_(1,2,3).

$$\boldsymbol{R_k = \sum_{i=1}^{28}\left(y_{1,2,3} - x_i\right)^2} \qquad (23)$$

Following equation (20) shows the basic equation for MLR predictions. a_i represents weights for each model, x_i represents surface wind speed value from

each model at each region, y is the observation data and b is the intercept (error). $y_1$ is observation, $y_2$ is ERA5 and $y_3$ is MERRA2 for all MLR results.

$$\boldsymbol{y_{1,2,3}} = \sum_{\boldsymbol{i=1}}^{\boldsymbol{28}} \boldsymbol{a_i x_i} + \boldsymbol{b} \qquad (24)$$

For the historical calculations: three different Multiple Linear Regression (MLR) predictions were calculated: (1) MLR for all models (MLR-All), (2) MLR for models with dynamic vegetation model (MLR-DVM), (3) MLR for models without dynamic vegetation model (MLR-WDVM) for train period. Results are compared with the simple mean ensembles obtained from the mean values of each time step for all models and at model classifications. After obtaining the weights from each model and each region, test period predictions are performed using those weights. The results are also calculated for the entire data (1980-2014), and single predictions are produced based on these approaches.

#### 3.3.5.2 Random Forest Regression based multi-model ensemble

The random forest (RF) method is used in this study to increase the individual model performances and determine the performance of the RF method among the other methods (multiple linear regression). RF is a machine-learning approach for producing multiple regressions with decision trees. The method creates decision trees based on the conditions in the model data. These trees are grown in each step, and compare results with the observation data. Multiple decision trees in the method provide to reduce uncertainties in the predictions. The method is also successful in large data sets [255]. Therefore, this study uses this method for both 28 CMIP6 model data from 1980 to 2014 (historical period) and future projections (SSP2-4.5 and SSP5-8.5 scenarios). The method can also detect non-linear relationships or composite demeanors in the data [142].

Python Scikit-learn Machine learning packages are used for calculating the random forest predictions [256]. Each decision tree's mean square error (MSE) is calculated to determine the best regression results from 100 decision trees as default. Equation (25) defines the MSE where f is the forecast and a is the observation data.

$$\mathbf{MSE} = \frac{1}{n}\sum_{i=1}^{n}(f - a)^2 \qquad (25)$$

In the historical period part of the study, RF Regression calculations are done for three different model classifications with observation, ERA5 and MERRA2 data. % 75 of the data was selected as the train period, and the model was created from this period. Then % 25 of the data was selected as the test period as it is applied in the multiple linear regression, and ensemble predictions were created for the test period. After test and train period calculations, entire data has also been predicted using the same model that is developed in the train period.

For the future projections part of the study, which is done as explained below by using only RF regression:

For the onshore WPPs in Türkiye, the closest model grids to each WPP are obtained for the entire period (1980-2100). CMIP6 models in Table 9 are used in this part of the study. Random Forest Regression calculations are done for two different scenarios (SSP2-4.5 and SSP5-8.5) by using historical data as a training period (1980-2014) and future projections as a test period (2014-2100). After test and train period calculations, entire data has also been predicted by using the same model which is developed in the train period.

For the offshore part, each model grid in each sea is averaged, and then the historical period (1980-2014) is used as a train period, and future scenarios from 2014-2100 are used as a test period. 13 GCMs from Table 10 are used for this part of the study.

### 3.3.6 Mesoscale Model Outputs

Mesoscale model outputs are also analyzed in this study. The data is analyzed in the TUBITAK ULAKBIM, High Performance and Grid Computing Center (TRUBA resources) servers for both historical and SSP5-8.5 scenarios.

WRF-PGW (Pseudo Global Warming) approach is used to downscale 13 CMIP6 ensemble models in Table 11. PGW is a downscaling method where it takes initial conditions from GCMs. PGW is a method that is used for regional climate modeling

studies which modify the initial boundary conditions. Due to high computer capacity and time requirements in mesoscale modeling, PGW can be an alternative for saving time for regional climate modeling. [257].

Since individual GCMs has different from each other, this could also create uncertainties. The ensemble mean of GCMs is used to reduce uncertainties. PGW method adds climate change information to re-analysis data [258]. The method are done under the following formula.

$$\text{WRF-PGW} = \boldsymbol{ERA5\ reanalysis} + \Delta_{\boldsymbol{CMIP6\ (SSP5-8.5)}} \qquad (26)$$

Climate change signals are derived from the 13 GCMs ensemble mean from CMIP6-SSP5-8.5 scenario for the 2080-2100 period relative to the 1994-2014 period (Δ) added to ERA5 re-analysis data and WRF model are run based on this conditions for the 2080-2100 period with 4 km spatial resolution. Baseline period are also run at same resolution with only ERA5 data. The results with WRF-PGW are compared with WRF5-ERA5 outputs.

### 3.3.7 Microscale modeling of a selected onshore/offshore area

Due to high computer expenses for dynamically downscaling the wind on a micro-scale, only two selected areas are run in the micro-model. After collecting the required information, the areas are run three times:

- Run with WRF-ERA5
- Run with WRF-PGW for future production.
- Run with observation data (only for onshore)

For each run, a wind atlas is obtained and compared with each other. This part aims to create a wind atlas with higher resolution for the future production of electricity from wind.

WindSIM 10.0 Evaluation version is used. The version is entirely the same as the commercial version except for the maximum number of cells (500) and vertical

layers (10). This creates smooth modeling of elevation and roughness, and discretization errors [259].

WindSIM uses Reynolds Average Navier Stoke (RANS) equations for solving the wind resource by utilizing roughness and elevation of the area. Since there is no offshore wind measurement in Türkiye, only WRF-ERA5 runs are used to determine reference wind resources. Due to computer expenses, 2-year hourly wind speed and direction data is obtained from WRF outputs.

Elevation and roughness maps are obtained from Aster GDEM [260] and Corine 2006 [261] are converted to a grid.gws file is an input of WindSIM [51] by using Global Mappper Evaluation Version [262]. The maximum number of cells is selected as 50000. Wind field simulations are done using the following conditions in table 12.

Table 12 Wind field simulation conditions

| | |
|---|---|
| Height of boundary layer (m) | 500.0 |
| Speed above boundary layer (m/s) | 10.0 |
| Boundary condition at the top | fix pres. |
| Potential temperature | No |
| Turbulence model | Standard |
| Solver | GCV |
| Maximum iterations | 100 |

Overall research method in this study is summarised in Figure 31 where it is separated into 4 main parts. The results of the each part are given in the Chapter 4.

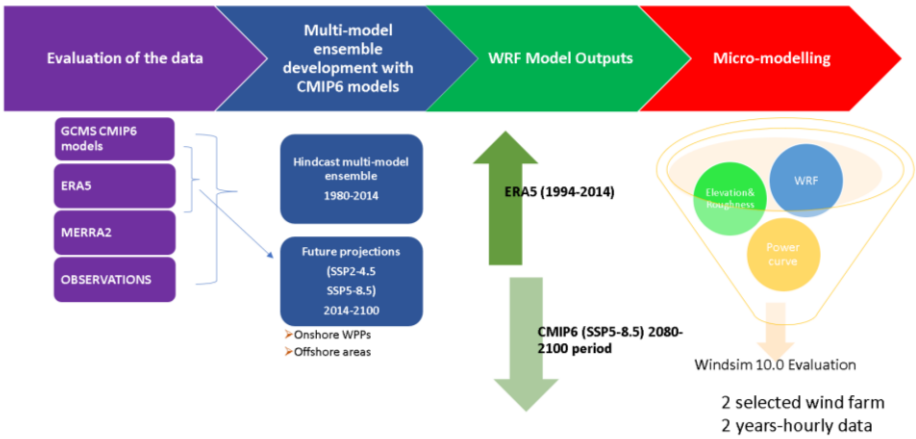



Figure 31 Summary of the researh method and design

# CHAPTER 4

# RESULTS

## 4.1 Evaluation of the reference data

This study uses two global re-analysis data to compare their reliability with observations and CMIP6 models. Figure 32 illustrates the seasonal and annual average during the study period (1980-2014). MERRA2 data overestimation over the land is obvious for all seasons and annual averages. ERA5 and observations are similar to each other. On the other hand, seasonality in offshore wind speeds is more obvious than in the onshore regions. High wind speeds over the Black Sea and Aegean Sea during the winter season reach the highest values. Summer season wind speeds in the Aegen Sea are the highest, which can be associated with the Etesian winds.

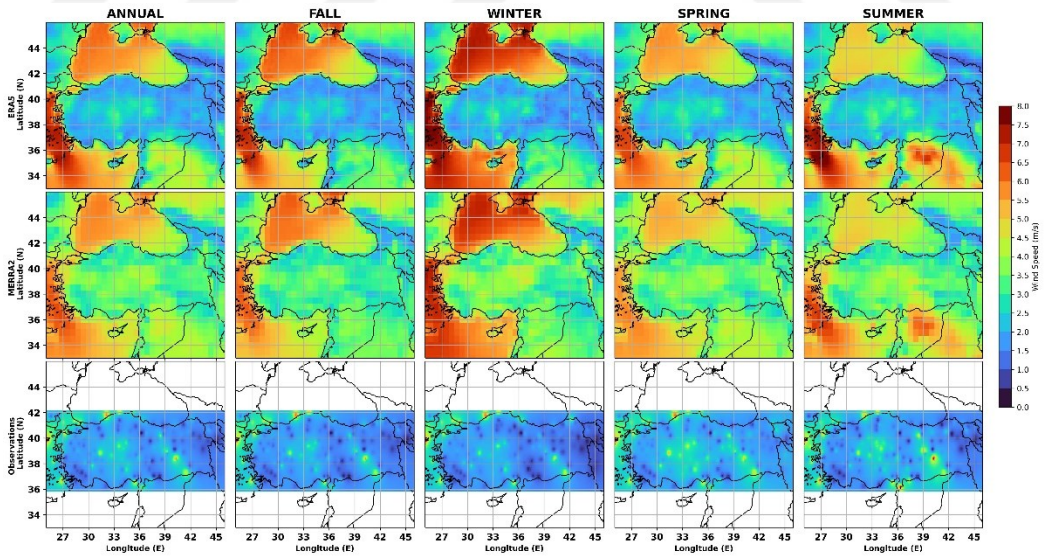



Figure 32 Seasonal averages of global re-analysis data

Various statistical measures have been calculated using the nearest ERA5 and MERRA2 grid points and observation station data to understand the relationship between ERA5, MERRA2 re-analysis data, and the observations. Regional and

seasonal descriptive statistics are also calculated to understand the wind climatology of Türkiye.

Table 13 shows the descriptive and error statistics for ERA5, MERRA2, and observation data at 10 m. Error statistics are obtained from observation stations and the closest grid from related re-analysis data. The highest onshore mean and maximum wind speeds are determined in the Marmara Region. MERRA2 data is higher than the observations and ERA5 for all regions. In addition to descriptive statistics, errors are also calculated for both ERA5 and MERRA2 re-analysis data. MERRA2 has the highest errors. ERA5 performed better than MERRA2 for all regions in all seasons. Both MERRA2 and ERA5 have low correlations in the Southeast Anatolia region. These low correlation coefficients could be explained by the lack of data or low-quality data for this region. The Black Sea and Mediterranean Regions, which have the highest complexity, have very close correlation results (changes between 0.46-0.56) for both re-analysis data. Marmara region, which has the highest mean wind speeds, has the lowest errors for both re-analysis data. Especially ERA5 has better results in the region. MERRA2 PBIAS (%) values are higher than the ERA5, which could be explained by higher wind speeds on the MERRA2.

Table 13 Regional- Seasonal Error Metrics and Descriptive Statistics of Re-analysis data and Observations for Onshore Regions

| Region | Season | ERA5 | | | | | | | | MERRA2 | | | | | | | | Observation | | | |
|---|---|---|---|---|---|---|---|---|---|---|---|---|---|---|---|---|---|---|---|---|---|
| | | RMSE | PBIAS | SDE | CORR | mean | std | min | max | RMSE | PBIAS | SDE | CORR | mean | std | min | max | mean | std | min | max |
| Mediterranean | DJF | 1.24 | 10.14 | 1.22 | 0.56 | 2.07 | 1.17 | 0.21 | 13.14 | 2.19 | 80.49 | 1.58 | 0.53 | 3.39 | 1.77 | 0.49 | 15.97 | 1.88 | 1.41 | 0.30 | 14.40 |
| | JJA | 1.04 | 3.43 | 1.04 | 0.50 | 2.24 | 0.81 | 0.36 | 9.45 | 1.69 | 54.45 | 1.21 | 0.41 | 3.34 | 1.06 | 0.61 | 13.47 | 2.16 | 1.17 | 0.30 | 12.00 |
| | MAM | 1.05 | -0.26 | 1.05 | 0.52 | 2.02 | 0.89 | 0.33 | 11.32 | 1.64 | 54.07 | 1.22 | 0.52 | 3.12 | 1.31 | 0.43 | 14.67 | 2.02 | 1.18 | 0.30 | 16.60 |
| | SON | 0.98 | 11.40 | 0.96 | 0.53 | 1.88 | 0.84 | 0.23 | 11.20 | 1.72 | 73.98 | 1.18 | 0.49 | 2.93 | 1.24 | 0.38 | 14.29 | 1.69 | 1.10 | 0.30 | 32.80 |
| East Anatolia | DJF | 1.31 | 1.20 | 1.31 | 0.45 | 1.64 | 0.63 | 0.16 | 5.98 | 2.21 | 88.67 | 1.69 | 0.33 | 3.05 | 1.45 | 0.45 | 14.99 | 1.62 | 1.47 | 0.30 | 15.20 |
| | JJA | 1.34 | -12.48 | 1.31 | 0.47 | 1.93 | 0.58 | 0.46 | 7.50 | 1.76 | 43.94 | 1.47 | 0.36 | 3.17 | 1.05 | 0.85 | 11.57 | 2.20 | 1.47 | 0.30 | 36.30 |
| | MAM | 1.12 | -11.29 | 1.10 | 0.48 | 1.85 | 0.66 | 0.21 | 8.70 | 1.85 | 55.19 | 1.45 | 0.37 | 3.24 | 1.33 | 0.63 | 13.16 | 2.08 | 1.25 | 0.30 | 26.00 |
| | SON | 1.12 | -1.08 | 1.12 | 0.46 | 1.67 | 0.60 | 0.20 | 5.88 | 1.79 | 68.39 | 1.37 | 0.37 | 2.84 | 1.16 | 0.52 | 13.75 | 1.69 | 1.26 | 0.30 | 23.30 |
| Aegean | DJF | 1.73 | 39.98 | 1.53 | 0.67 | 2.81 | 2.06 | 0.41 | 16.94 | 2.57 | 99.09 | 1.64 | 0.67 | 3.99 | 2.20 | 0.49 | 18.37 | 2.01 | 1.47 | 0.30 | 19.00 |
| | JJA | 1.58 | 34.20 | 1.40 | 0.59 | 2.89 | 1.73 | 0.60 | 12.59 | 2.08 | 77.12 | 1.26 | 0.62 | 3.81 | 1.60 | 0.61 | 13.90 | 2.15 | 1.15 | 0.30 | 23.70 |
| | MAM | 1.46 | 31.13 | 1.32 | 0.63 | 2.64 | 1.69 | 0.46 | 16.14 | 2.04 | 76.72 | 1.33 | 0.64 | 3.56 | 1.74 | 0.52 | 17.27 | 2.01 | 1.16 | 0.30 | 21.00 |
| | SON | 1.52 | 43.58 | 1.31 | 0.65 | 2.55 | 1.73 | 0.41 | 15.39 | 2.20 | 98.64 | 1.32 | 0.67 | 3.53 | 1.79 | 0.38 | 16.09 | 1.78 | 1.16 | 0.30 | 17.80 |
| SouthEast Anatolia | DJF | 1.38 | 15.23 | 1.35 | 0.48 | 2.21 | 0.98 | 0.54 | 8.18 | 2.21 | 71.16 | 1.73 | 0.31 | 3.27 | 1.44 | 0.72 | 16.30 | 1.92 | 1.52 | 0.30 | 14.40 |
| | JJA | 1.56 | 21.64 | 1.47 | 0.22 | 2.96 | 1.02 | 0.68 | 7.48 | 2.54 | 71.57 | 1.85 | 0.15 | 4.18 | 1.53 | 0.73 | 14.62 | 2.43 | 1.31 | 0.30 | 12.20 |
| | MAM | 1.30 | 15.84 | 1.26 | 0.39 | 2.44 | 0.95 | 0.60 | 8.88 | 1.94 | 54.54 | 1.56 | 0.23 | 3.25 | 1.24 | 0.75 | 16.07 | 2.10 | 1.28 | 0.30 | 12.40 |
| | SON | 1.24 | 22.60 | 1.17 | 0.38 | 2.13 | 0.80 | 0.52 | 7.90 | 2.08 | 81.91 | 1.51 | 0.24 | 3.17 | 1.23 | 0.67 | 15.31 | 1.74 | 1.22 | 0.30 | 11.90 |
| Anatolia | DJF | 1.25 | 6.06 | 1.24 | 0.58 | 2.15 | 1.09 | 0.17 | 9.78 | 2.30 | 81.85 | 1.60 | 0.56 | 3.68 | 1.86 | 0.46 | 15.18 | 2.03 | 1.50 | 0.30 | 19.00 |
| | JJA | 1.03 | 5.74 | 1.02 | 0.47 | 2.44 | 0.87 | 0.48 | 8.38 | 1.65 | 50.76 | 1.15 | 0.50 | 3.49 | 1.22 | 0.55 | 11.59 | 2.31 | 1.08 | 0.30 | 28.60 |
| | MAM | 1.12 | -0.43 | 1.12 | 0.54 | 2.31 | 0.98 | 0.28 | 9.68 | 1.77 | 49.39 | 1.34 | 0.55 | 3.46 | 1.53 | 0.56 | 13.81 | 2.32 | 1.29 | 0.30 | 20.70 |
| | SON | 1.00 | 10.27 | 0.99 | 0.54 | 2.03 | 0.88 | 0.24 | 9.27 | 1.78 | 70.33 | 1.22 | 0.54 | 3.14 | 1.38 | 0.47 | 12.90 | 1.84 | 1.13 | 0.30 | 25.50 |
| Black Sea | DJF | 1.59 | 24.62 | 1.50 | 0.58 | 2.67 | 1.59 | 0.19 | 13.81 | 2.38 | 71.79 | 1.82 | 0.44 | 3.68 | 1.75 | 0.46 | 16.43 | 2.15 | 1.69 | 0.30 | 22.30 |
| | JJA | 1.15 | 13.47 | 1.12 | 0.48 | 2.25 | 1.14 | 0.46 | 12.73 | 1.45 | 47.49 | 1.10 | 0.44 | 2.93 | 1.02 | 0.56 | 10.56 | 1.99 | 1.04 | 0.30 | 16.30 |
| | MAM | 1.23 | 16.92 | 1.18 | 0.53 | 2.32 | 1.24 | 0.27 | 15.21 | 1.64 | 49.15 | 1.32 | 0.45 | 2.95 | 1.32 | 0.58 | 14.17 | 1.98 | 1.21 | 0.30 | 16.60 |
| | SON | 1.35 | 22.31 | 1.29 | 0.55 | 2.32 | 1.39 | 0.21 | 14.04 | 1.72 | 58.61 | 1.31 | 0.50 | 3.01 | 1.32 | 0.58 | 13.85 | 1.90 | 1.30 | 0.30 | 25.80 |
| Marmara | DJF | 1.95 | 32.48 | 1.72 | 0.72 | 3.78 | 2.42 | 0.41 | 19.67 | 2.59 | 67.26 | 1.74 | 0.72 | 4.76 | 2.47 | 0.52 | 20.59 | 2.85 | 2.08 | 0.30 | 24.10 |
| | JJA | 1.48 | 28.11 | 1.29 | 0.69 | 3.35 | 1.74 | 0.59 | 13.35 | 2.05 | 60.46 | 1.31 | 0.70 | 4.19 | 1.81 | 0.54 | 13.86 | 2.61 | 1.45 | 0.30 | 13.70 |
| | MAM | 1.55 | 26.60 | 1.40 | 0.69 | 3.22 | 1.89 | 0.54 | 18.41 | 2.08 | 59.11 | 1.44 | 0.69 | 4.04 | 1.95 | 0.63 | 19.57 | 2.54 | 1.59 | 0.30 | 20.50 |
| | SON | 1.74 | 36.55 | 1.49 | 0.71 | 3.40 | 2.10 | 0.44 | 17.32 | 2.33 | 72.07 | 1.48 | 0.73 | 4.28 | 2.15 | 0.66 | 17.97 | 2.49 | 1.72 | 0.30 | 19.30 |
| TÜRKİYE | DJF | 1.53 | 20.40 | 1.47 | 0.62 | 2.53 | 1.74 | 0.16 | 19.67 | 2.38 | 80.12 | 1.69 | 0.59 | 3.77 | 2.02 | 0.45 | 20.59 | 2.12 | 1.68 | 0.30 | 24.10 |
| | JJA | 1.30 | 13.60 | 1.27 | 0.52 | 2.57 | 1.32 | 0.36 | 13.35 | 1.85 | 57.11 | 1.32 | 0.52 | 3.56 | 1.42 | 0.54 | 14.62 | 2.34 | 1.25 | 0.30 | 30.00 |
| | MAM | 1.28 | 11.13 | 1.25 | 0.56 | 2.43 | 1.37 | 0.21 | 18.41 | 1.86 | 57.08 | 1.38 | 0.56 | 3.43 | 1.59 | 0.43 | 19.57 | 2.24 | 1.30 | 0.30 | 26.00 |
| | SON | 1.32 | 22.13 | 1.25 | 0.60 | 2.32 | 1.46 | 0.20 | 17.32 | 1.96 | 74.39 | 1.35 | 0.60 | 3.32 | 1.63 | 0.38 | 17.97 | 1.94 | 1.33 | 0.30 | 32.80 |
| ALL-TÜRKİYE | | 1.36 | 14.63 | 1.32 | 0.58 | 2.46 | 1.48 | 0.16 | 19.67 | 2.02 | 66,.4 | 1.45 | 0,57 | 3.52 | 1.69 | 0.38 | 20.59 | 2.11 | 1.40 | 0.30 | 36.30 |

WPD has also been calculated by assuming air density is constant (1.225 kg/m$^3$) from ERA5 and MERRA2 daily data at 10 m and given in figure 33. It shows the wind power per m$^2$ for the entire study area. According to NREL's wind classes (see Table-14), wind power density should be bigger than 200 W/m$^2$ for suitable wind energy investments at 50 m. However, those are near surface wind speeds (10 m.a.g.l) which are expected to be lower than the turbine hub heights. The results are similar to the wind speeds as it is expected (see figure 33). MERRA2 wind speeds were higher over the lands in Türkiye. However, Aegean Sea wind speeds and WPD is higher in the ERA5.

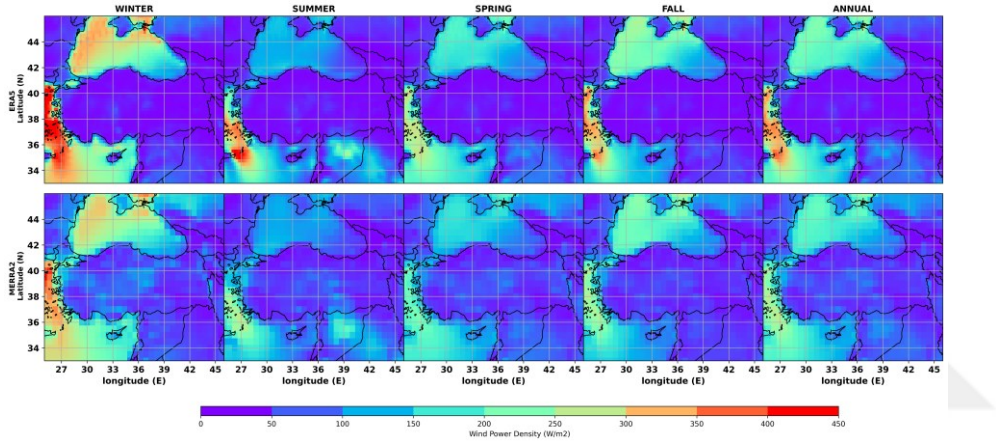



Figure 33 Wind Power Density (W/m$^2$) at 10 m with ERA5 and MERRA2 data

For ERA5 at 100 m and MERRA2 at 50 m, wind power density (fig 34) seems to have bigger than 400 W/m$^2$, especially in the western part of Türkiye, Aegean, and Marmara Region and around Hatay.

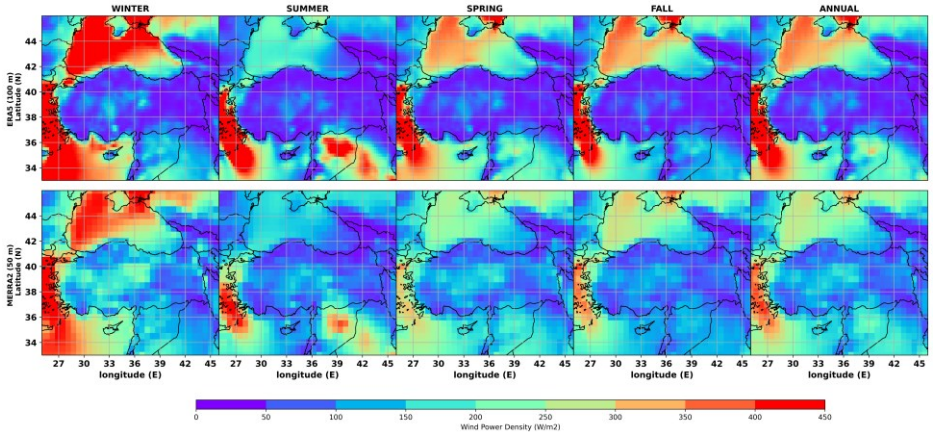



Figure 34 Wind Power Density (W/m$^2$) ERA5 at 100 m and MERRA2 at 50 m

NREL's wind classes are also given in Table 14 [263]. Compared to Türkiye's WPD results, there is no class 6 or 7 wind power in Türkiye for re-analysis data, even if these results are only valid for 30 m or 50 m above the ground levels. However, re-analysis data results could be downscaled by using dynamical downscaling techniques to determine these classes accurately.

Table 14 NREL Wind Classes [263].

| Wind Power Class | 30 m | | 50 m | |
|---|---|---|---|---|
| | Wind Power Density ($W$/m$^2$) | Wind Speed (m/s) | Wind Power Density ($W$/m$^2$) | Wind Speed (m/s) |
| 1 | ≤ 160 | ≤ 5.1 | ≤ 200 | ≤ 5.6 |
| 2 | ≤ 240 | ≤ 5.9 | ≤ 300 | ≤ 6.4 |
| 3 | ≤ 320 | ≤ 6.5 | ≤ 400 | ≤ 7.0 |
| 4 | ≤400 | ≤7.0 | ≤ 500 | ≤ 7.5 |
| 5 | ≤480 | ≤7.4 | ≤ 600 | ≤ 8.0 |
| 6 | ≤640 | ≤8.2 | ≤ 800 | ≤ 8.8 |
| 7 | ≤ 1600 | ≤11.0 | ≤ 2000 | ≤ 11.9 |

### 4.1.1 Trends in the Observation Data

Non-parametric Mann-Kendall Trend analysis has been applied to the entire data for monthly, seasonal, and annual results time scales to detect trends in the entire data. The following figure shows the results of the annual trends between 1979-2020 for

all 239 stations from daily data. According to the results given in the figure 35, 133 stations have decreasing trend, 36 stations have an increasing trend, and 70 stations are found with no trend among the 239 stations. Trend values are counted according to statistically significant p-value < 0.05.

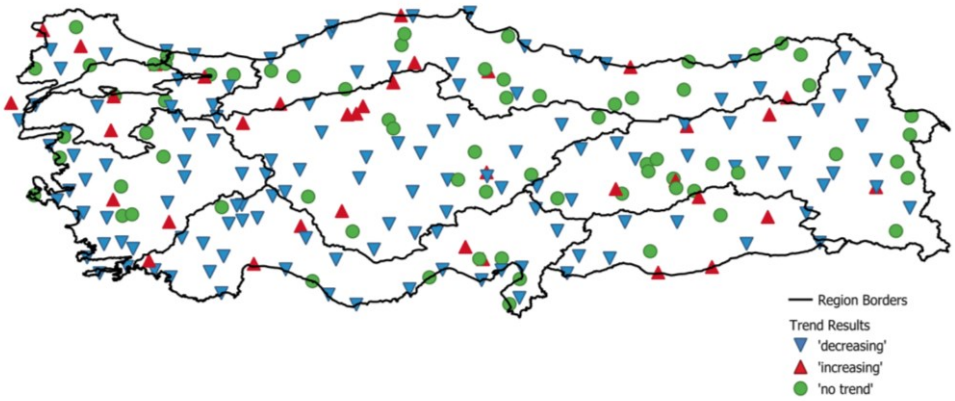



Figure 35 Annual Mann-Kendall Trend Test Results

Since seasonality is an important factor for Türkiye's wind climatology, monthly and seasonal trend analyses have also been calculated among the entire data. Seasonal results (see fig.36) also showed a similarity with the entire data. Seasonal and regional results are also summarized in Table 15. The lowest number of stations with "no-trend" has been found for the summer season. The majority of the stations have a decreasing trend. The highest number of stations with an increasing trend (totally 76 stations) is also determined for the summer season.

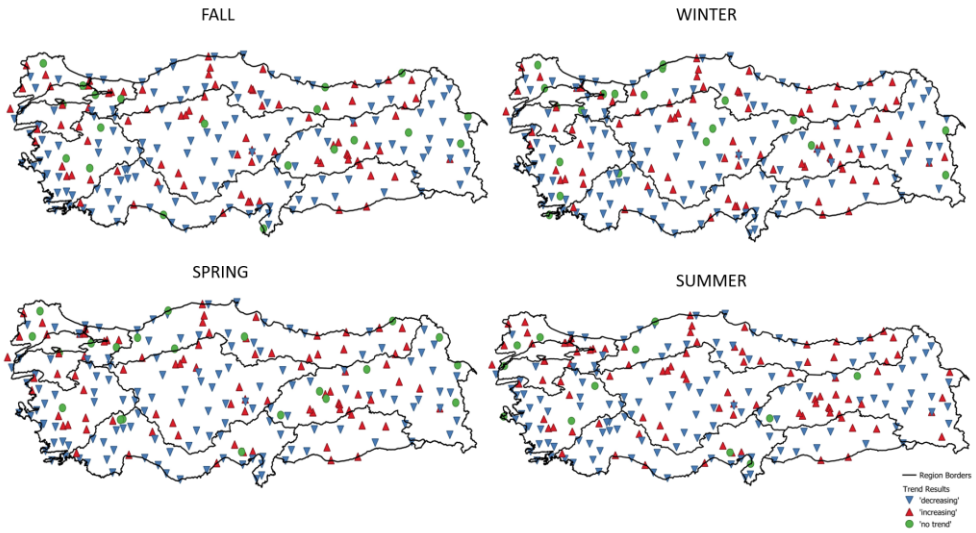



Figure 36 Seasonal Mann-Kendall Trend Test Results

Table 15 Number of Stations for Seasonal Trend Analysis Results for each Region

| Region | Trend | Winter | Spring | Summer | Fall |
|---|---|---|---|---|---|
| Mediterranean | Decreasing | 23 | 22 | 22 | 22 |
| | No trend | 1 | 4 | 3 | 3 |
| | Increasing | 7 | 5 | 6 | 6 |
| East-Anatolia | Decreasing | 22 | 20 | 23 | 22 |
| | No trend | 3 | 6 | 5 | 1 |
| | Increasing | 18 | 17 | 15 | 20 |
| Aegean | Decreasing | 25 | 26 | 26 | 25 |
| | No trend | 3 | 2 | 3 | 3 |
| | Increasing | 8 | 9 | 7 | 8 |
| South-East Anatolia | Decreasing | 7 | 7 | 8 | 8 |
| | No trend | 1 | - | - | - |
| | Increasing | 5 | 5 | 5 | 5 |
| Anatolia | Decreasing | 30 | 32 | 33 | 32 |
| | No trend | 4 | 1 | - | 2 |
| | Increasing | 19 | 20 | 20 | 19 |
| Black Sea | Decreasing | 11 | 12 | 11 | 13 |
| | No trend | 3 | 4 | 2 | 2 |
| | Increasing | 14 | 12 | 15 | 13 |
| Marmara | Decreasing | 17 | 14 | 12 | 14 |
| | No trend | 6 | 5 | 3 | 5 |
| | Increasing | 12 | 16 | 20 | 16 |

Monthly trends are also calculated from monthly average data. Table 16 summarizes the results of the monthly trends. The majority of the stations have shown decreasing trend for all months. The highest number of stations with a decreasing trend is

determined in the winter months. Stations with no trend (p-value> 0.05) are higher than the increasing trends. 75 stations have decreasing trend for all months.

Table 16 Monthly Trends for Observation Stations

| Trend / Month | Jan | Feb | Mar | Apr | May | Jun | Jul | Aug | Sept | Oct | Nov | Dec |
|---|---|---|---|---|---|---|---|---|---|---|---|---|
| Decreasing Trend | 115 | 115 | 104 | 124 | 112 | 104 | 117 | 113 | 107 | 112 | 126 | 127 |
| No Trend | 99 | 90 | 97 | 80 | 85 | 89 | 83 | 83 | 85 | 90 | 85 | 82 |
| Increasing Trend | 25 | 34 | 38 | 35 | 42 | 46 | 39 | 43 | 47 | 37 | 28 | 30 |

Trends for the maximum wind speed in each year are also determined from each station among the daily data to understand the inter-annual variability in the maximum wind speeds(see fig.37). Mann-Kendall trend test has been applied to these maximum wind speeds as well. The results showed that 157 stations' maximum wind speeds have decreasing trends, 22 stations have increasing trends, and 60 stations have no significant trends.

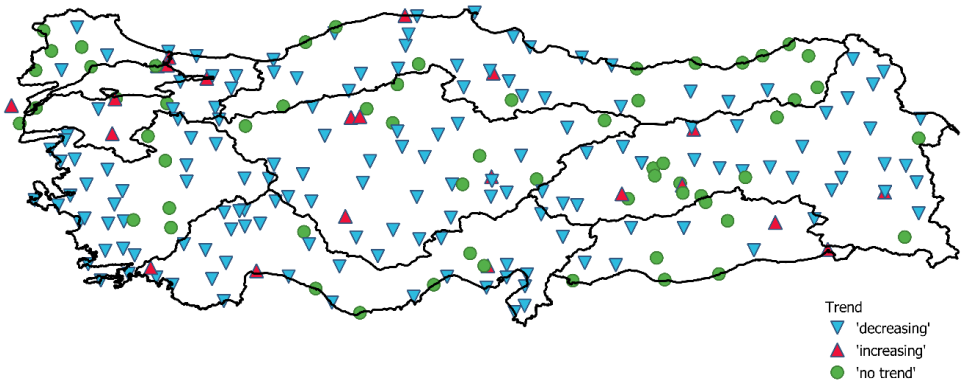



Figure 37 Annual maximum wind speeds' trend results

### 4.1.2 Trends in the Re-analysis data

Decadal trend slopes calculated for averaged magnitudes of seasonal and annual wind speeds for each reference data product are also shown in Figure 38. Entire observation data are not used in this part due to obtaining exact information from observation data without inhomogeneities or lack of data. Both re-analysis data show strong seasonality and spatial variability (-0.2 and +0.15 m/s per decade) in trend slopes. Both ERA5 and MERRA2 products consistently provide wintertime

significant decreasing slopes (-0.2 m/s/decade) over the western Marmara to the northwestern Black Sea and increasing significant slopes (+0.1- (+)0.15 m/s/decade) over the eastern Black Sea towards Georgia. Observed slope values over these regions also agree with this distribution. The directions of fall slopes over the Aegean Sea and winter slopes over inland Anatolia are the same for both products, but their magnitudes differ. Directions of spring and summer slopes from both re-analysis products contradict each other. For example, a significant increase in spring season's slopes over the southeastern part of inland Anatolia, eastern Anatolia, and in summer slopes over north and south of the Aegean region are acquired by ERA5, but MERRA2 shows negative slope values over these areas. Observed wind slope directions are in better agreement with ERA5 data, although they show more tendency toward higher negative slope values as consistent with the literature. ERA5 and MERRA2 show an increase in spring and summer time Aegean Sea offshore winds (Etesian winds), while this increase is not significant. It is also noticeable that both global products, especially MERRA2, yield significant increases in mean offshore wind speed over the eastern Black Sea throughout all four seasons. Besides, annual mean wind slopes are positive in Northern Aegean and eastern Anatolia regions by ERA5, while they are negative by MERRA2.

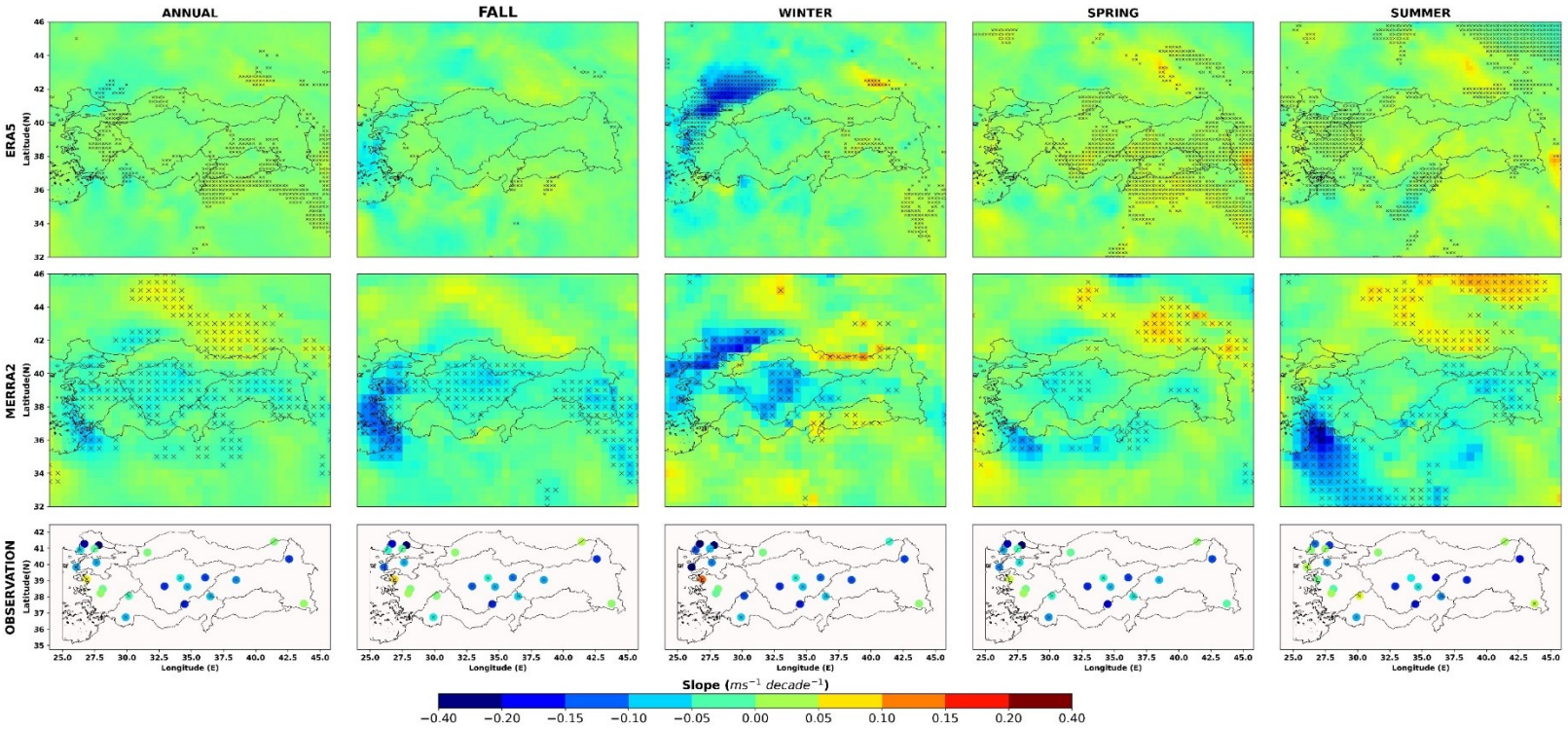



Figure 38 Trend slopes (ms-1/decade) from daily averaged near surface wind speed across seven different geographical regions and Aegean offshore area for ERA5, MERRA2, and observation. Slopes of each region are calculated from annual and seasonal avarage wind speeds and interpolated to each grid resolution for global re-analysis data. All of 178 observation stations are not used in observed trend analysis due to the availability of some missing periods during the entire period (only 22 station is used with full period data) Significant trends are also signed in the figure where p-value is < 0.05.

## 4.2 Multi-model ensemble results for historical period (1980-2014)

### 4.2.1 Model Performances

CMIP6 models in Table 8 have been compared with observation, ERA5, and MERRA2 data for the 1980-2014 period. The following heatmaps show the Pearson Correlation Coefficients, bias, and RMSE results between 27 models and observations, MERRA2 and ERA5 data, respectively. Time series data in each CMIP6 model grid closest to each reference data are obtained and error metrics are calculated. Then if there is more than one reference data grid in the CMIP6 model grid, the average value of those grids is calculated, and statistical errors are calculated for each. Therefore, depending on each CMIP6 model's resolutions, grid numbers in the heat maps are different.

The highest correlation coefficients are determined for GISS models (see fig. 39). However, EC-Earth3 and EC-Earth-Veg also have higher correlations for most grid points with the observations. MERRA2 data correlation coefficients (see fig.40) are higher than the ERA5 (figure 41) and observations, but similar models (EC-Earth3 and EC-Earth-Veg, MIROC6, MPI-ESM1-2-HR) in the ERA5 data had shown similar high resolutions.

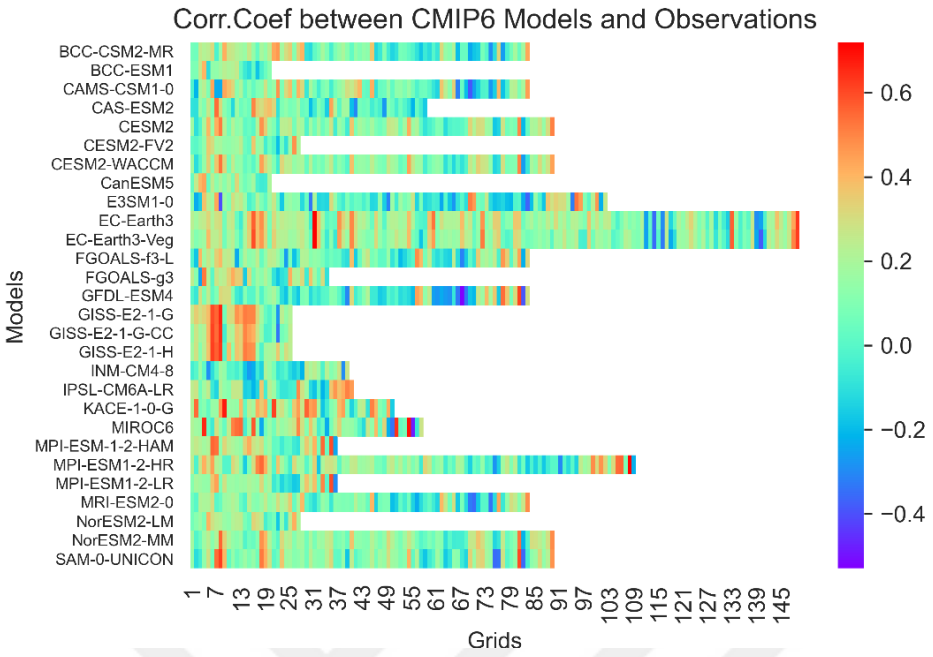



Figure 39 Corr. Coefficients for grid-based observations

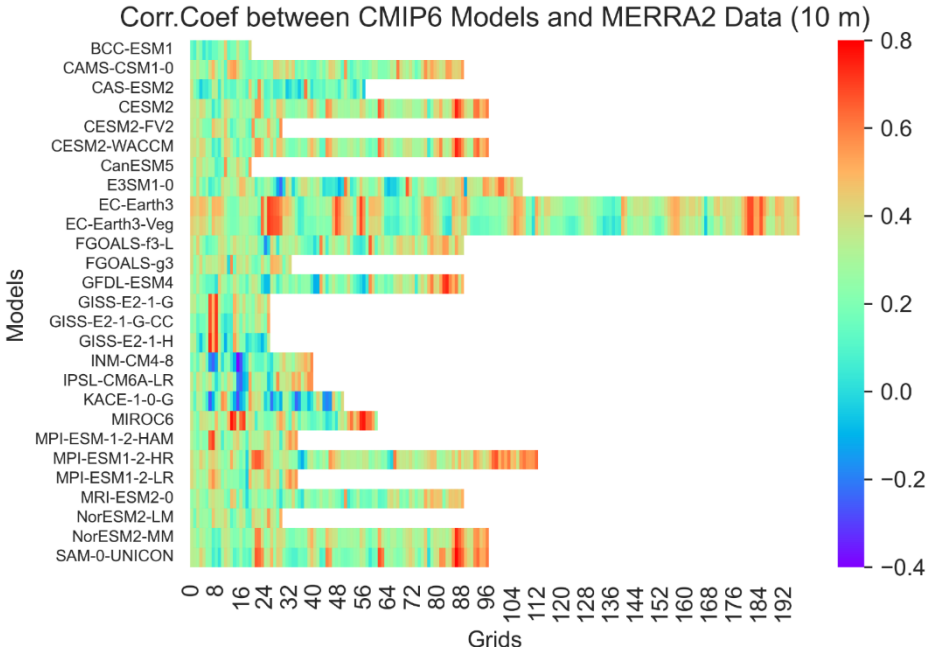



Figure 40 Correlation Coefficients between CMIP6 and MERRA2 data

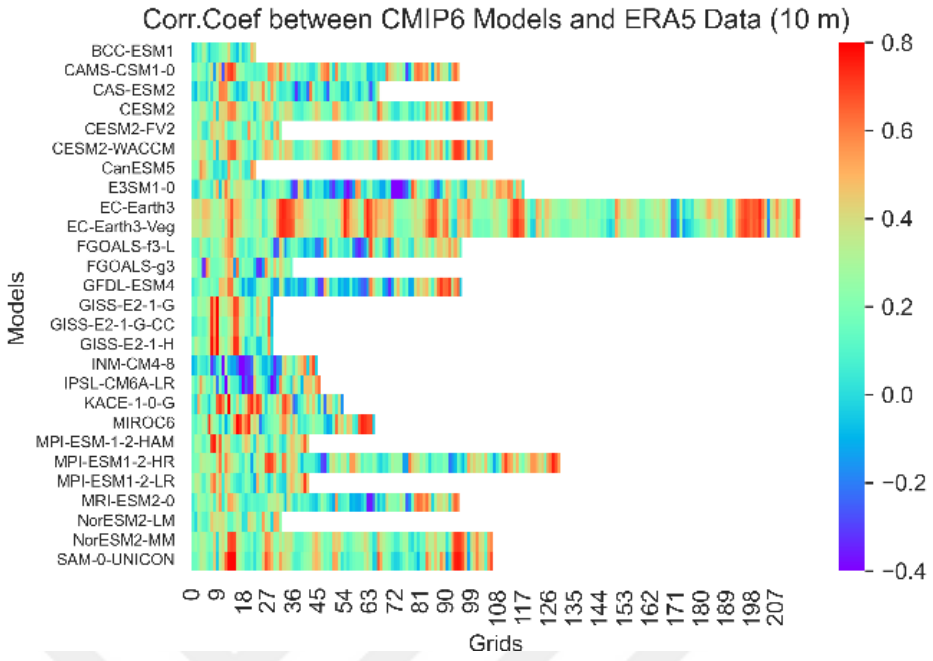



Figure 41 Correlation Coefficients between CMIP6 and MERRA2 data

RMSE in Figure 42 for the observations shows that EC-Earth3 and EC-Earth-Veg have lower RMSE than other models, such as CAMS-ESM2, KACE-1-0-G, and MIROC6 models. MERRA2 RMSE (fig. 43) results are lower for almost all models. However, MRI-ESM2-0, BCC-CSM2-MR, and FGOALS-F3-L have the highest errors with all reference data, including ERA5, in Figure 44.

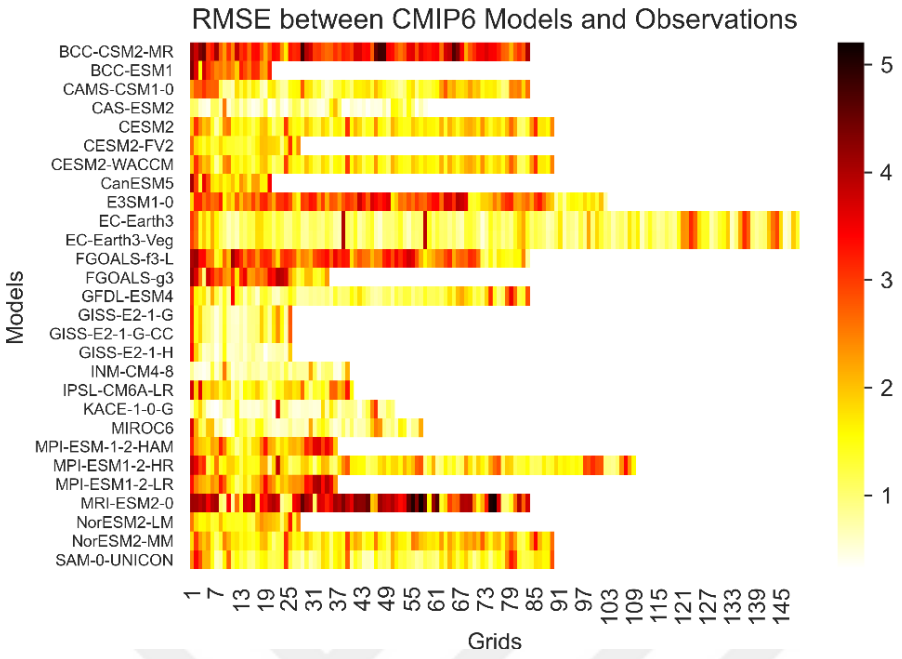



Figure 42 RMSE for grid-based observations

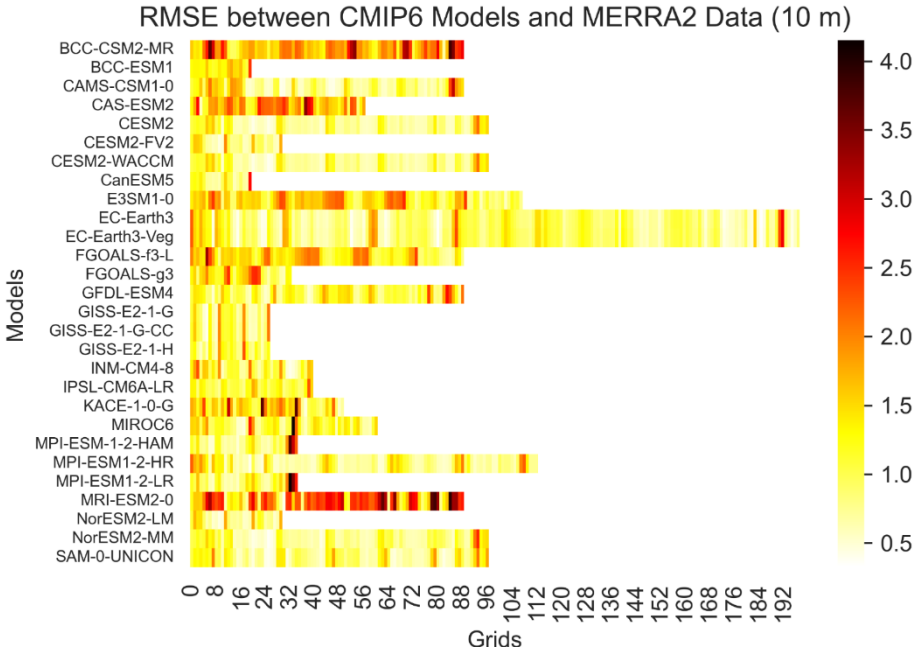



Figure 43 RMSE between CMIP6 and MERRA2 data

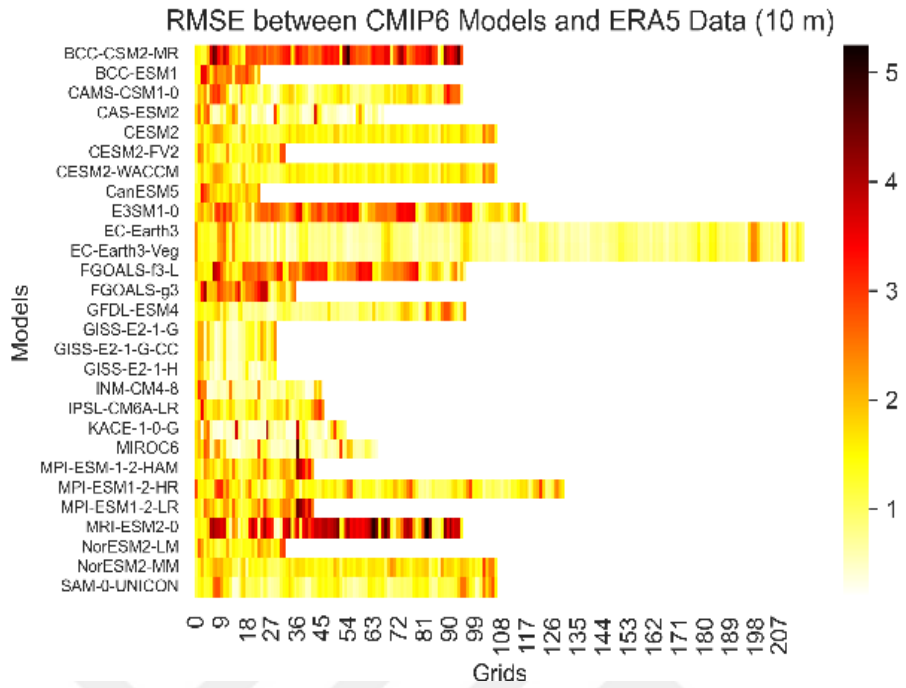



Figure 44 RMSE between CMIP6 and ERA5 data

The lowest bias values are calculated between observations (see fig. 45) for EC-Earth3 and EC-Earth-Veg, CAS-ESM2, GFDL-ESM4, GISS-E2-1-G, GISS-E2-1-G-CC, GISS-E2-1-G-H, INM-CM4-8, KACE-1-0-G, and MIROC6. Negative bias values are associated with the overestimation of models with those data. Bias is lower in the ERA5 (figure 47) than in the MERRA2 (figure 46). The same models with observations have lower bias than the others.

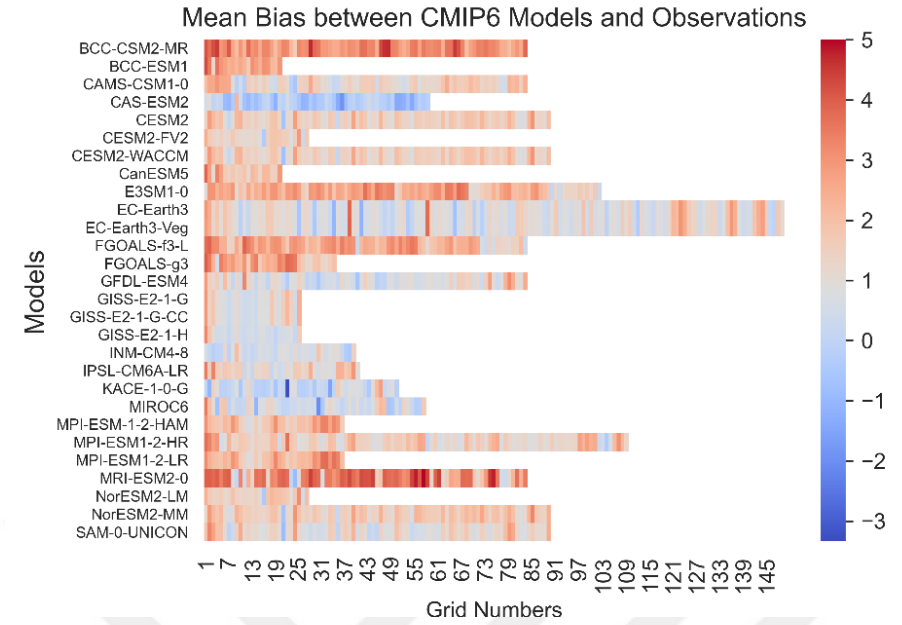



Figure 45 Bias for observations

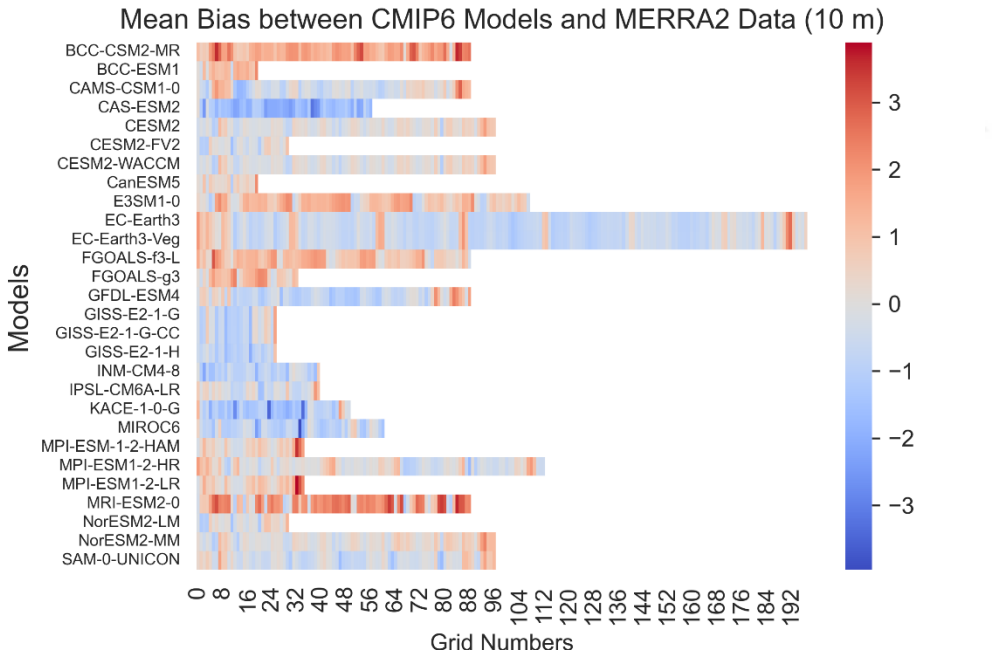



Figure 46  Bias between CMIP6 and MERRA2 data

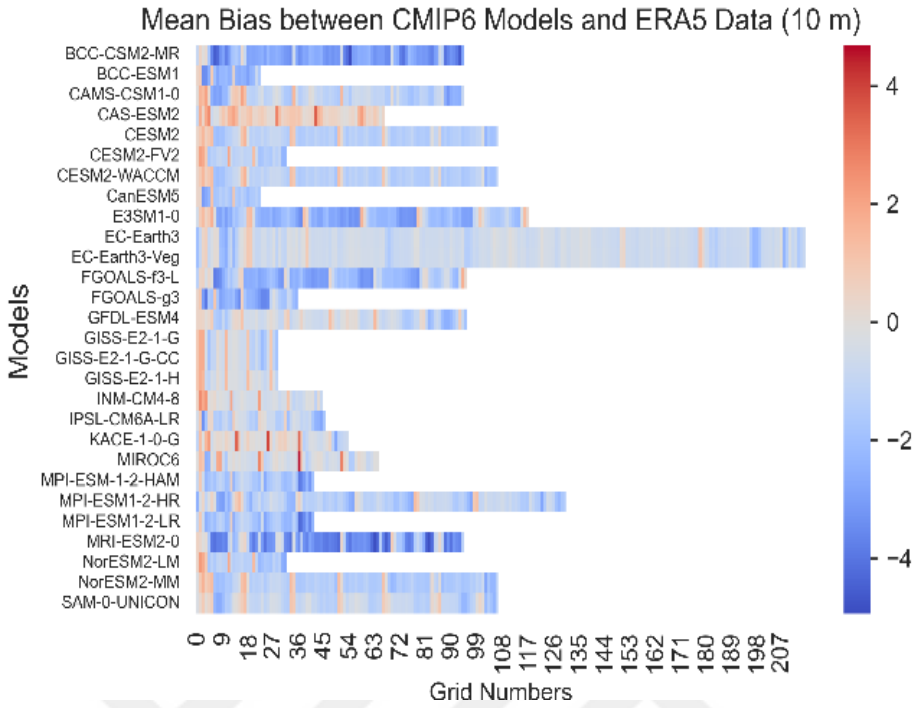



Figure 47 Bias between CMIP6 and ERA5 data

Individual model performances with global re-analysis data are also examined using Taylor Diagrams in the "opeanair" library of the R Project [264] for each region with each reference data (see fig.48,49,50). Correlations are lower than 0.6 in the observations for all regions except for Southeast Anatolia. GCM10 (EC-Earth3), GCM11 (EC-Earth3-Veg), GCM14 (GFDL-ESM4), GCM15 (GISS-E2-1-G) and GCM20 (KACE-1-0-G) are closer to observation for all regions. Since there is no observation data over the Aegean Sea, the performance of this region is given in Figures 49 and 50 with MERRA2 and ERA5 data respectively.

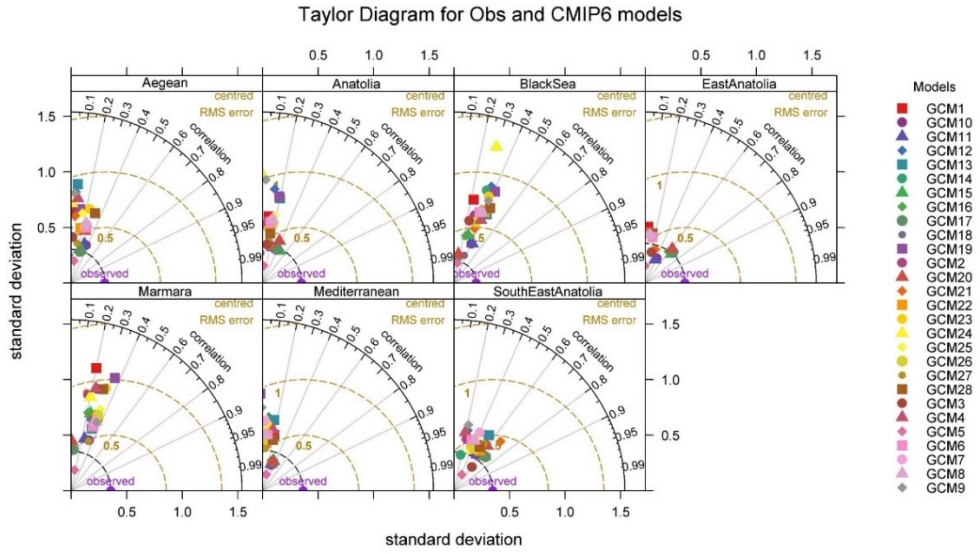



Figure 48 Taylor Diagram for Observations

ERA5 performances with each CMIP6 model are given in Figure 49. Aegean Sea errors are bigger than all regions, and this is the same in the MERRA2 in figure 50. GCM10 (EC-Earth3) and GCM11 (EC-Earth3-Veg) have the best results in this region for both MERRA2 and ERA5. The other region has similar errors in similar models.

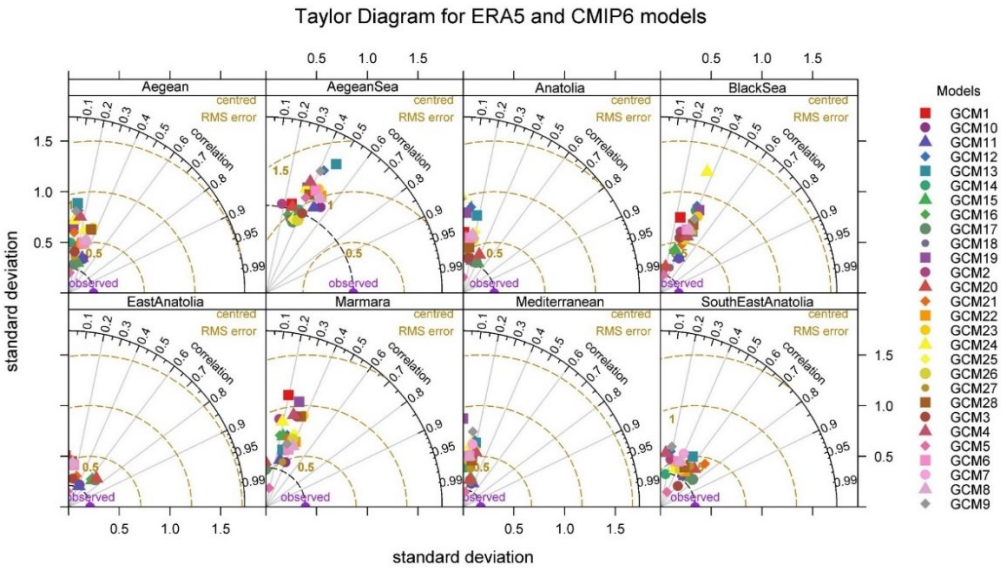



Figure 49 Taylor Diagram for ERA5

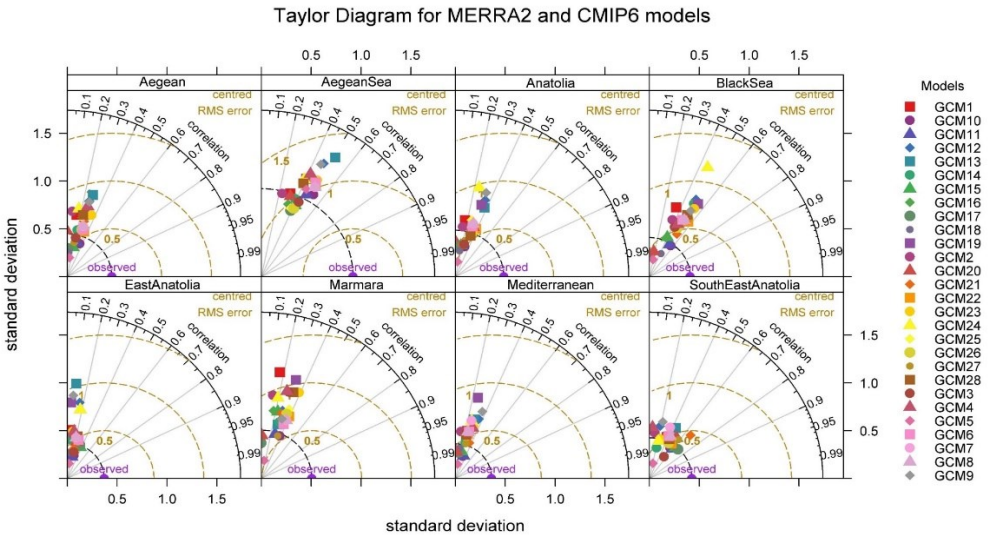



Figure 50 Taylor Diagram for MERRA2

The performances of all models for Türkiye and all regions without observation data are summarized in Figure 51. All models and ERA5 evaluations in the entire onshore parts of the Türkiye are also given in the same figure (the first row and the 3rd column) as "*All* ."GCM10 (EC-Earth3), GCM11 (EC-Earth3-Veg), and GCM20 (KACE-1-0-G) model performances with ERA5 are higher than the other models for all regions. The higher correlations are determined in the Aegean Sea offshore region, where the wind speeds are higher than any other onshore region. GCM20 (KACE-1-0-G) also has high correlations in Anatolia, the Black Sea, and East Anatolia. GCM10 (EC-Earth3), GCM27 (SAM-0-UNICON), and GCM11 (EC-Earth3-Veg) are also good in Marmara Region. GCM3 (CAMS-CSM1-0), GCM5 (CAS-ESM2), GCM14 (GFDL-ESM4), and GCM21 (MIROC6) are closest to observation (ERA5) for the Southeast Anatolia region. ERA5 and MERRA2 relationship are higher than any models for all regions, as it is expected.

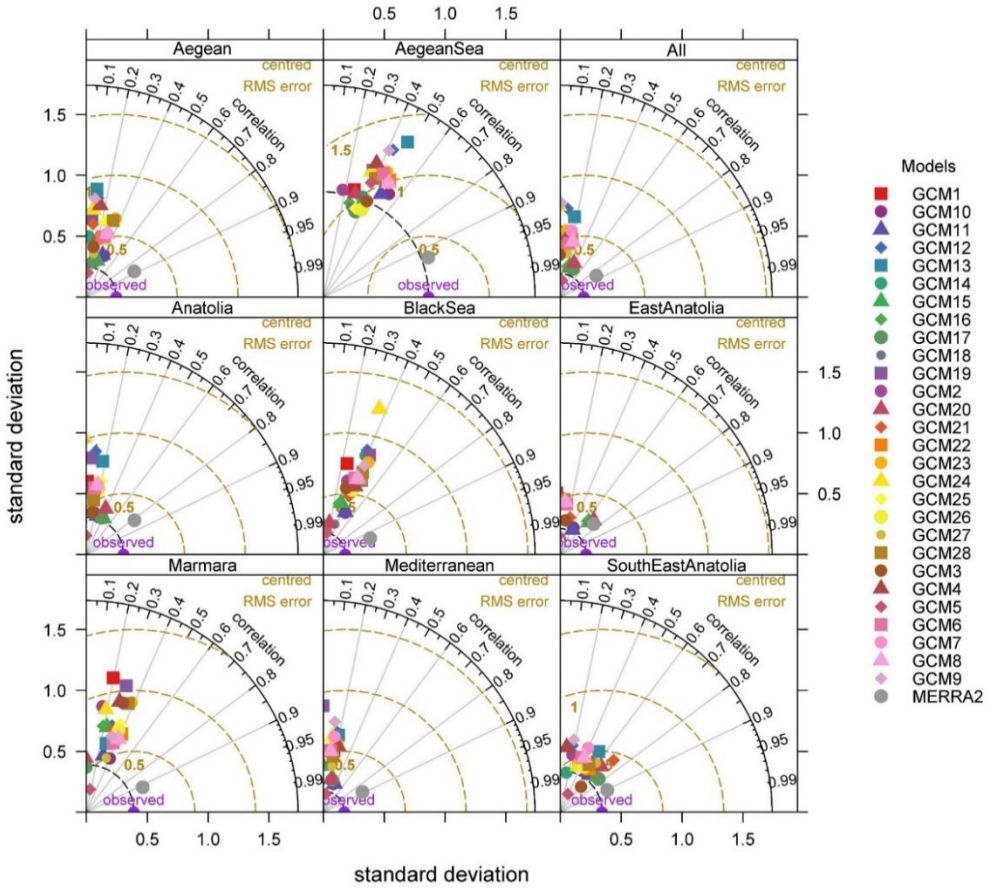



Figure 51 Taylor diagrams for all models and MERRA2 data with ERA5 for each region and entire onshore Türkiye ("All")

### 4.2.2 Dynamic Vegetation model effect

Some CMIP6 models consider vegetation growth in their land surface models. Transient surface roughness conditions induced by this representation affect the near-surface wind speed and direction. Changes in wind speed resulting from dynamic vegetation growth are investigated using the high resolution (0.70 x 0.70) EC-Earth3 model with (GCM11 in Table 8) and without (GCM10 in Table 8) dynamic global vegetation component. While both models are in the form of the earth system model (ESM), EC-Earth3-Veg (GCM11) differs from the EC-Earth3 model [265] through its 2$^{nd}$ generation dynamic global vegetation model called LPJ-GUESS [266]. The impact of vegetation growth on near-surface wind speed from

these two versions of EC-Earth models is compared with two re-analysis fields for February and July in Figure 52. Monthly average values are obtained from the period of 1980-2014. The effect of dynamic vegetation growth on wind speed is clearly seen between the two EC-Earth model versions in June, during which such impact is more dictated. The spatial pattern of June winds for the EC-Earth with dynamic vegetation growth provides a better match with both reanalysis data. Wind distributions of June over the Caucasian mountains, the Black Sea region, Anatolia, the Aegean coast, and the Mediterranean coast of Syria are more agreeable with both re-analysis data. The lower wind speeds over the continental Türkiye, as consistent with both re-analysis data, can be seen for the EC-Earth3-Veg (GCM11). This could be explained by vegetation growth that causes to increase in the surface roughness. However, the spatial wind pattern of February for both GCM models resembles each other. In addition, the MERRA2 product always results in higher surface wind speeds compared to the ERA5 product.

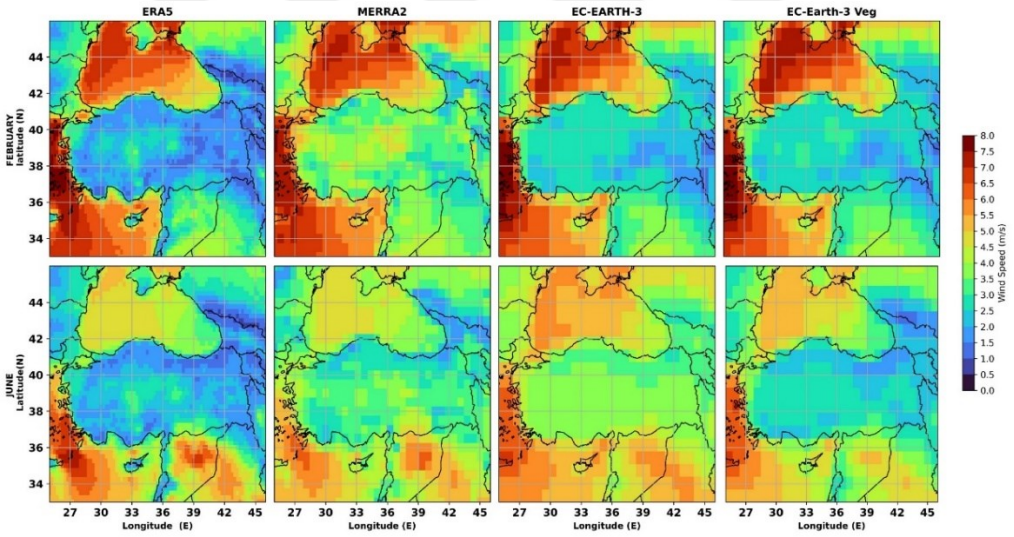



Figure 52 Comparison of EC-Earth Models and Re-analysis data

### 4.2.3 Multi-model ensemble (MME) development for CMIP6

As it is explained in Chapter III, multi-model ensemble results are calculated for the test and train period with three different classifications. Tables 17 and 18 show, respectively the results for MLR and RF. MLR-MERRA2 and MLR-ERA5

correlation coefficients showed better results than observations. ERA5 has slightly lower errors than MERRA2. Although RF-PBIAS values are higher than the MLR-PBIAS values, RF correlation coefficients are slightly higher than the MLR results. WDVM-MLR and DVM-MLR errors are very close to each other for all reference data.

Table 17 Test and Train Period MLR Results

| MLR RESULT | All Models MLR Result | | | | | | | | DVM Models MLR RESULT | | | | | | | | WDVM Models MLR RESULT | | | | | | | |
|---|---|---|---|---|---|---|---|---|---|---|---|---|---|---|---|---|---|---|---|---|---|---|---|---|
| | RMSE | | PBIAS | | STD-ERROR | | CORR. COEF. | | RMSE | | PBIAS | | STD-ERROR | | CORR. COEF. | | RMSE | | PBIAS | | STD-ERROR | | CORR. COEF. | |
| REGION | Train | Test | Train | Test | Train | Test | Train | Test | Train | Test | Train | Test | Train | Test | Train | Test | Train | Test | Train | Test | Train | Test | Train | Test |
| MERRA2 | | | | | | | | | | | | | | | | | | | | | | | | |
| Aegean Region | 0.38 | 0.37 | -0.01 | 2.81 | 0.38 | 0.35 | 0.55 | 0.47 | 0.40 | 0.37 | 0.00 | 4.15 | 0.40 | 0.34 | 0.48 | 0.49 | 0.40 | 0.36 | 0.00 | 2.72 | 0.40 | 0.34 | 0.48 | 0.50 |
| AegeanSea Offshore Region | 0.70 | 0.62 | 0.01 | 2.55 | 0.70 | 0.60 | 0.69 | 0.66 | 0.74 | 0.59 | 0.00 | 3.12 | 0.74 | 0.56 | 0.64 | 0.69 | 0.74 | 0.61 | 0.00 | 2.16 | 0.74 | 0.60 | 0.63 | 0.65 |
| Anatolia Region | 0.41 | 0.40 | 0.00 | 2.43 | 0.41 | 0.40 | 0.55 | 0.52 | 0.42 | 0.42 | 0.00 | 3.30 | 0.42 | 0.41 | 0.51 | 0.49 | 0.42 | 0.41 | 0.00 | 1.73 | 0.42 | 0.41 | 0.50 | 0.48 |
| BlackSea Region | 0.30 | 0.32 | 0.00 | 0.99 | 0.30 | 0.32 | 0.67 | 0.67 | 0.31 | 0.32 | 0.00 | 1.40 | 0.31 | 0.32 | 0.63 | 0.68 | 0.30 | 0.32 | 0.00 | 0.06 | 0.30 | 0.32 | 0.65 | 0.68 |
| East_Ant Region | 0.30 | 0.33 | 0.00 | 1.75 | 0.30 | 0.33 | 0.56 | 0.50 | 0.32 | 0.35 | 0.00 | 1.74 | 0.32 | 0.34 | 0.46 | 0.44 | 0.31 | 0.33 | 0.00 | 1.30 | 0.31 | 0.32 | 0.53 | 0.53 |
| Marmara Region | 0.42 | 0.40 | 0.05 | 1.76 | 0.42 | 0.39 | 0.59 | 0.53 | 0.44 | 0.39 | 0.00 | 3.09 | 0.44 | 0.37 | 0.54 | 0.58 | 0.44 | 0.41 | 0.00 | 1.32 | 0.44 | 0.40 | 0.53 | 0.48 |
| Med Region | 0.32 | 0.29 | 0.00 | 0.71 | 0.32 | 0.29 | 0.53 | 0.45 | 0.33 | 0.28 | 0.00 | 1.06 | 0.33 | 0.28 | 0.46 | 0.52 | 0.32 | 0.30 | 0.00 | 1.15 | 0.32 | 0.29 | 0.49 | 0.42 |
| SE_Ant Region | 0.26 | 0.31 | 0.00 | -0.88 | 0.26 | 0.31 | 0.79 | 0.69 | 0.30 | 0.32 | 0.00 | -0.83 | 0.30 | 0.32 | 0.72 | 0.66 | 0.26 | 0.32 | 0.00 | -0.89 | 0.26 | 0.32 | 0.78 | 0.68 |
| ERA5 | | | | | | | | | | | | | | | | | | | | | | | | |
| Aegean Region | 0.20 | 0.23 | 0.01 | -1.79 | 0.20 | 0.22 | 0.57 | 0.43 | 0.22 | 0.22 | 0.00 | -0.40 | 0.22 | 0.21 | 0.48 | 0.51 | 0.21 | 0.22 | 0.00 | -2.15 | 0.21 | 0.22 | 0.49 | 0.47 |
| AegeanSea Offshore Region | 0.63 | 0.65 | -0.01 | 0.00 | 0.63 | 0.65 | 0.70 | 0.61 | 0.68 | 0.62 | 0.00 | 0.70 | 0.68 | 0.62 | 0.63 | 0.63 | 0.67 | 0.65 | 0.00 | -0.38 | 0.67 | 0.65 | 0.65 | 0.59 |
| Anatolia Region | 0.24 | 0.26 | 0.00 | -1.22 | 0.24 | 0.26 | 0.59 | 0.61 | 0.26 | 0.28 | 0.00 | -0.05 | 0.26 | 0.28 | 0.52 | 0.52 | 0.25 | 0.27 | 0.00 | -1.92 | 0.25 | 0.26 | 0.54 | 0.59 |
| BlackSea Region | 0.14 | 0.15 | 0.01 | -1.32 | 0.14 | 0.15 | 0.61 | 0.52 | 0.15 | 0.15 | 0.00 | -0.97 | 0.15 | 0.15 | 0.55 | 0.54 | 0.15 | 0.15 | 0.00 | -1.86 | 0.15 | 0.15 | 0.58 | 0.54 |
| East_Ant Region | 0.13 | 0.15 | 0.00 | -0.78 | 0.13 | 0.15 | 0.79 | 0.72 | 0.14 | 0.16 | 0.00 | -0.74 | 0.14 | 0.16 | 0.76 | 0.67 | 0.13 | 0.14 | 0.00 | -1.22 | 0.13 | 0.14 | 0.77 | 0.74 |
| Marmara Region | 0.30 | 0.37 | 0.04 | 0.41 | 0.30 | 0.36 | 0.64 | 0.41 | 0.32 | 0.35 | 0.00 | 1.50 | 0.32 | 0.35 | 0.59 | 0.45 | 0.31 | 0.38 | 0.00 | -0.58 | 0.31 | 0.38 | 0.60 | 0.33 |
| Med Region | 0.15 | 0.16 | 0.00 | -1.38 | 0.15 | 0.15 | 0.53 | 0.43 | 0.16 | 0.15 | 0.00 | -0.72 | 0.16 | 0.15 | 0.41 | 0.50 | 0.15 | 0.16 | 0.00 | -1.14 | 0.15 | 0.16 | 0.50 | 0.37 |
| SE_Ant Region | 0.18 | 0.22 | 0.00 | -3.47 | 0.18 | 0.21 | 0.84 | 0.80 | 0.20 | 0.22 | 0.00 | -3.35 | 0.20 | 0.21 | 0.81 | 0.79 | 0.19 | 0.23 | 0.00 | -3.18 | 0.19 | 0.21 | 0.83 | 0.78 |
| OBSERVATION | | | | | | | | | | | | | | | | | | | | | | | | |
| Aegean Region | 0.26 | 0.24 | -0.02 | 5.97 | 0.21 | 0.26 | 0.58 | 0.36 | 0.27 | 0.25 | 0.00 | 8.45 | 0.27 | 0.19 | 0.50 | 0.47 | 0.27 | 0.24 | 0.00 | 5.70 | 0.27 | 0.22 | 0.49 | 0.29 |
| Anatolia Region | 0.26 | 0.30 | 0.00 | 7.77 | 0.26 | 0.26 | 0.65 | 0.59 | 0.29 | 0.34 | 0.00 | 10.17 | 0.29 | 0.27 | 0.54 | 0.54 | 0.27 | 0.30 | 0.00 | 7.06 | 0.27 | 0.26 | 0.62 | 0.58 |
| BlackSea Region | 0.17 | 0.14 | 0.00 | 1.66 | 0.14 | 0.17 | 0.59 | 0.49 | 0.18 | 0.15 | 0.00 | 1.80 | 0.18 | 0.15 | 0.53 | 0.42 | 0.18 | 0.14 | 0.00 | 1.01 | 0.18 | 0.14 | 0.55 | 0.47 |
| East_Ant Region | 0.23 | 0.28 | 0.00 | 11.35 | 0.20 | 0.23 | 0.77 | 0.79 | 0.25 | 0.32 | 0.00 | 12.43 | 0.25 | 0.23 | 0.71 | 0.69 | 0.24 | 0.26 | 0.00 | 10.46 | 0.24 | 0.19 | 0.74 | 0.82 |
| Marmara Region | 0.30 | 0.31 | 0.00 | 3.14 | 0.30 | 0.30 | 0.62 | 0.29 | 0.31 | 0.30 | 0.00 | 4.73 | 0.31 | 0.28 | 0.56 | 0.35 | 0.31 | 0.32 | 0.00 | 1.98 | 0.31 | 0.31 | 0.57 | 0.19 |
| Med Region | 0.30 | 0.34 | 0.00 | 13.71 | 0.23 | 0.30 | 0.59 | 0.48 | 0.32 | 0.35 | 0.00 | 15.86 | 0.32 | 0.22 | 0.48 | 0.53 | 0.31 | 0.33 | 0.00 | 13.66 | 0.31 | 0.23 | 0.54 | 0.49 |
| SE_Ant Region | 0.22 | 0.20 | 0.00 | 2.29 | 0.19 | 0.22 | 0.79 | 0.81 | 0.23 | 0.21 | 0.00 | 2.59 | 0.23 | 0.20 | 0.75 | 0.80 | 0.22 | 0.21 | 0.00 | 2.70 | 0.22 | 0.20 | 0.77 | 0.81 |

Table 18 Test and Train Period RF Results

| RANDOM FOREST | All Models RF Result | | | | | | | | DVM Models RF RESULT | | | | | | | | WDVM Models RF RESULT | | | | | | | |
|---|---|---|---|---|---|---|---|---|---|---|---|---|---|---|---|---|---|---|---|---|---|---|---|---|
| | RMSE | | PBIAS | | STD-ERROR | | CORR. COEF. | | RMSE | | PBIAS | | STD-ERROR | | CORR. COEF. | | RMSE | | PBIAS | | STD-ERROR | | CORR. COEF. | |
| REGION | Train | Test | Train | Test | Train | Test | Train | Test | Train | Test | Train | Test | Train | Test | Train | Test | Train | Test | Train | Test | Train | Test | Train | Test |
| MERRA2 | | | | | | | | | | | | | | | | | | | | | | | | |
| Aegean Region | 0.16 | 0.36 | 0.05 | 3.76 | 0.16 | 0.33 | 0.97 | 0.54 | 0.16 | 0.38 | -0.02 | 4.93 | 0.16 | 0.33 | 0.97 | 0.54 | 0.16 | 0.36 | -0.01 | 3.86 | 0.16 | 0.33 | 0.97 | 0.55 |
| AegeanSea Offshore Region | 0.28 | 0.60 | 0.13 | 3.32 | 0.28 | 0.57 | 0.97 | 0.69 | 0.30 | 0.57 | 0.15 | 3.28 | 0.29 | 0.54 | 0.97 | 0.72 | 0.29 | 0.63 | 0.07 | 3.19 | 0.29 | 0.60 | 0.97 | 0.65 |
| Anatolia Region | 0.17 | 0.40 | 0.04 | 2.44 | 0.17 | 0.40 | 0.97 | 0.53 | 0.17 | 0.40 | -0.07 | 2.85 | 0.17 | 0.38 | 0.97 | 0.57 | 0.17 | 0.42 | -0.07 | 2.58 | 0.17 | 0.41 | 0.97 | 0.45 |
| BlackSea Region | 0.12 | 0.31 | 0.05 | 0.83 | 0.12 | 0.31 | 0.97 | 0.70 | 0.12 | 0.32 | 0.00 | 1.21 | 0.12 | 0.32 | 0.97 | 0.68 | 0.13 | 0.32 | -0.02 | 0.87 | 0.13 | 0.32 | 0.96 | 0.69 |
| East_Ant Region | 0.12 | 0.34 | 0.10 | 2.00 | 0.12 | 0.33 | 0.97 | 0.52 | 0.12 | 0.35 | 0.06 | 1.48 | 0.12 | 0.35 | 0.97 | 0.43 | 0.13 | 0.32 | 0.04 | 2.19 | 0.13 | 0.32 | 0.97 | 0.57 |
| Marmara Region | 0.17 | 0.38 | 0.08 | 2.22 | 0.17 | 0.37 | 0.97 | 0.59 | 0.17 | 0.39 | 0.12 | 2.95 | 0.17 | 0.38 | 0.97 | 0.56 | 0.17 | 0.41 | 0.07 | 2.07 | 0.17 | 0.40 | 0.97 | 0.50 |
| Med Region | 0.13 | 0.30 | 0.10 | 1.50 | 0.13 | 0.29 | 0.97 | 0.43 | 0.14 | 0.29 | -0.04 | 1.26 | 0.14 | 0.29 | 0.97 | 0.46 | 0.13 | 0.32 | -0.03 | 1.89 | 0.13 | 0.31 | 0.97 | 0.36 |
| SE_Ant Region | 0.10 | 0.32 | 0.02 | 0.32 | 0.10 | 0.31 | 0.98 | 0.69 | 0.11 | 0.33 | 0.05 | -0.17 | 0.11 | 0.33 | 0.97 | 0.64 | 0.10 | 0.32 | 0.01 | 0.16 | 0.10 | 0.32 | 0.98 | 0.68 |
| ERA5 | | | | | | | | | | | | | | | | | | | | | | | | |
| Aegean Region | 0.08 | 0.21 | 0.01 | -1.19 | 0.08 | 0.21 | 0.97 | 0.55 | 0.08 | 0.21 | -0.03 | -0.27 | 0.08 | 0.21 | 0.97 | 0.56 | 0.09 | 0.21 | 0.06 | -1.26 | 0.09 | 0.21 | 0.97 | 0.53 |
| AegeanSea Offshore Region | 0.26 | 0.63 | -0.01 | 0.49 | 0.26 | 0.63 | 0.97 | 0.62 | 0.27 | 0.59 | 0.02 | 0.71 | 0.27 | 0.59 | 0.97 | 0.67 | 0.27 | 0.69 | 0.09 | 0.63 | 0.27 | 0.69 | 0.97 | 0.55 |
| Anatolia Region | 0.10 | 0.26 | 0.00 | -0.69 | 0.10 | 0.26 | 0.97 | 0.60 | 0.10 | 0.27 | 0.10 | -0.08 | 0.10 | 0.27 | 0.97 | 0.56 | 0.10 | 0.27 | 0.04 | -1.45 | 0.10 | 0.27 | 0.97 | 0.56 |
| BlackSea Region | 0.06 | 0.15 | 0.06 | -1.09 | 0.06 | 0.14 | 0.97 | 0.58 | 0.06 | 0.15 | -0.06 | -1.10 | 0.06 | 0.15 | 0.97 | 0.55 | 0.06 | 0.15 | -0.08 | -1.18 | 0.06 | 0.15 | 0.97 | 0.55 |
| East_Ant Region | 0.05 | 0.15 | 0.12 | -0.96 | 0.05 | 0.15 | 0.98 | 0.72 | 0.05 | 0.16 | 0.06 | -0.94 | 0.05 | 0.16 | 0.97 | 0.67 | 0.05 | 0.14 | 0.04 | -0.98 | 0.05 | 0.14 | 0.97 | 0.73 |
| Marmara Region | 0.12 | 0.35 | -0.04 | 0.30 | 0.12 | 0.35 | 0.97 | 0.45 | 0.13 | 0.33 | 0.07 | 0.96 | 0.13 | 0.33 | 0.97 | 0.50 | 0.13 | 0.37 | 0.12 | 0.11 | 0.13 | 0.37 | 0.97 | 0.33 |
| Med Region | 0.06 | 0.15 | 0.09 | -0.62 | 0.06 | 0.15 | 0.97 | 0.48 | 0.06 | 0.15 | 0.16 | -0.32 | 0.06 | 0.15 | 0.97 | 0.51 | 0.06 | 0.16 | 0.04 | -0.80 | 0.06 | 0.16 | 0.97 | 0.38 |
| SE_Ant Region | 0.07 | 0.20 | 0.05 | -2.41 | 0.07 | 0.19 | 0.98 | 0.82 | 0.08 | 0.23 | 0.04 | -3.07 | 0.08 | 0.22 | 0.98 | 0.76 | 0.07 | 0.22 | -0.03 | -2.25 | 0.07 | 0.21 | 0.98 | 0.79 |
| OBSERVATION | | | | | | | | | | | | | | | | | | | | | | | | |
| Aegean Region | 0.11 | 0.24 | -0.05 | 7.11 | 0.11 | 0.20 | 0.97 | 0.45 | 0.11 | 0.24 | 0.06 | 8.72 | 0.11 | 0.18 | 0.97 | 0.53 | 0.11 | 0.25 | 0.02 | 7.20 | 0.11 | 0.21 | 0.97 | 0.37 |
| Anatolia Region | 0.11 | 0.30 | -0.05 | 8.82 | 0.11 | 0.24 | 0.97 | 0.67 | 0.12 | 0.33 | 0.17 | 10.13 | 0.12 | 0.26 | 0.97 | 0.58 | 0.11 | 0.31 | 0.07 | 7.90 | 0.11 | 0.26 | 0.97 | 0.58 |
| BlackSea Region | 0.07 | 0.14 | -0.09 | 1.57 | 0.07 | 0.13 | 0.97 | 0.52 | 0.07 | 0.15 | 0.03 | 1.90 | 0.07 | 0.14 | 0.97 | 0.45 | 0.07 | 0.15 | -0.03 | 1.52 | 0.07 | 0.15 | 0.97 | 0.44 |
| East_Ant Region | 0.09 | 0.29 | 0.23 | 11.88 | 0.09 | 0.21 | 0.98 | 0.78 | 0.10 | 0.32 | 0.18 | 12.25 | 0.09 | 0.23 | 0.97 | 0.70 | 0.10 | 0.28 | 0.20 | 11.22 | 0.10 | 0.20 | 0.97 | 0.80 |
| Marmara Region | 0.12 | 0.31 | -0.01 | 3.12 | 0.12 | 0.30 | 0.97 | 0.28 | 0.12 | 0.30 | -0.01 | 2.96 | 0.12 | 0.29 | 0.97 | 0.29 | 0.12 | 0.29 | 0.13 | 3.64 | 0.12 | 0.28 | 0.97 | 0.35 |
| Med Region | 0.12 | 0.35 | 0.13 | 14.60 | 0.12 | 0.23 | 0.97 | 0.47 | 0.13 | 0.35 | 0.09 | 15.44 | 0.13 | 0.22 | 0.97 | 0.55 | 0.12 | 0.35 | 0.14 | 14.60 | 0.12 | 0.24 | 0.97 | 0.43 |
| SE_Ant Region | 0.08 | 0.21 | 0.08 | 3.86 | 0.08 | 0.19 | 0.98 | 0.82 | 0.09 | 0.21 | 0.13 | 3.10 | 0.09 | 0.20 | 0.98 | 0.80 | 0.09 | 0.20 | 0.03 | 3.40 | 0.09 | 0.19 | 0.98 | 0.82 |

### 4.2.4 Performance of hindcast results

#### 4.2.4.1 General evaluation

A general evaluation is performed for the full period of the reference dataset (1980-2014) after combining the training and testing periods. The RMSE, PBias, and correlation metrics for the MLR and RF estimate established by the observation, MERRA2, and ERA5 datasets are shown for All model, DVM, and WDVM classifications in Figure 53, Figure 54, and Figure 55, respectively. It is clearly indicated that the RF estimates from all model classifications and datasets at all regions are more accurate (higher correlation and lower error) than the MLR estimates. ERA5-derived estimates yielded the smallest error throughout regions, while the MERRA 2-based estimates provided the highest error. However, the percent biases (Pbias) of the observation-based estimates were the largest for all regions. While the correlation values of MLR estimates showed some regionality and reference data dependency, the RF estimates produced highly uniform correlation values for each region and dataset. Also, the results from All model classifications produced better statistics than the results from DVM and WDVM types, both of which released similar statistics.

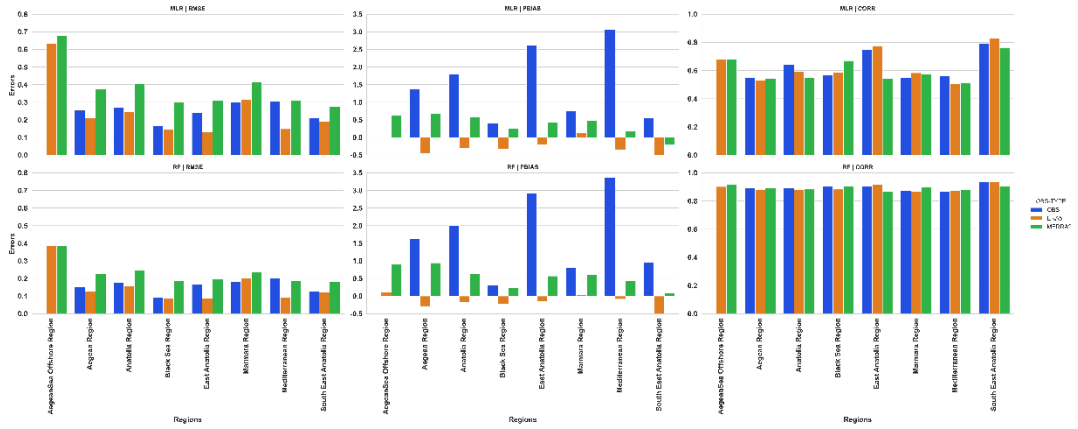



Figure 53 Regional Errors for ALL- MLR and RF Predictions

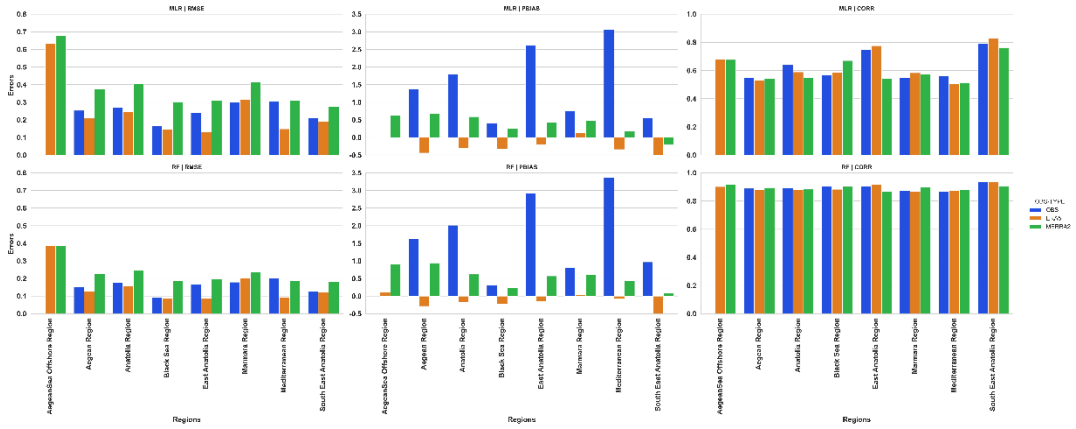


Figure 54 DVM Models Results

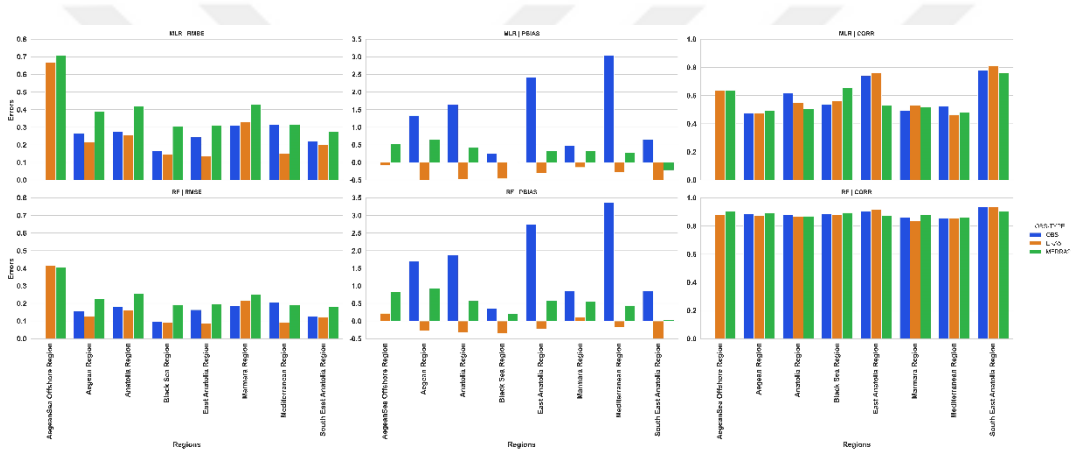


Figure 55 WDVM Models Results

Entire period results are also examined. Model overestimation can be seen in Figure 56. Both RF and MLR get better results than model means and individual model performances. MERRA2 data is closer to GCMs than the ERA5 and Observation. However, as it is determined in Figure 53 and Table 17,18: MME results with ERA5 also have lower errors than other reference data. This could be explained by MERRA2 wind speed ranges being wider than the ERA5, which could increase the MLR or RF results. Offshore region results are higher and wider than the onshore results, but the same success for RF and MLR is obvious. In contrast to onshore results, offshore wind speeds for ERA5 is higher than the MERRA2.

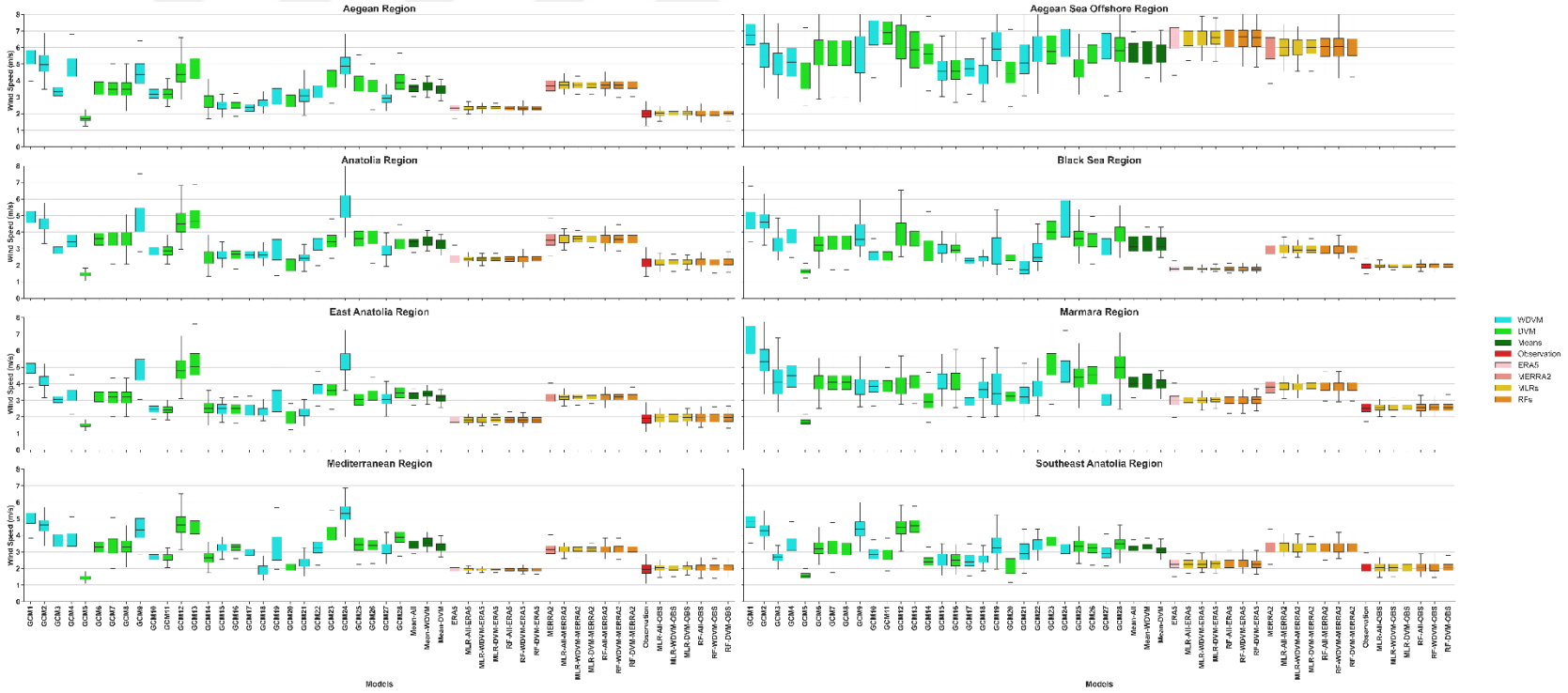



Figure 56 Boxplots for Entire Time Series and MLR Results for Each Region

#### 4.2.4.2 Series Analysis

Along with the entire reference period, monthly averaged wind speeds estimated using MLR-based MME in Figure 57 and RF-based MME in Figure 58 are shown as heatmaps for three onshore regions (Marmara, Aegean, and Mediterranean) and the Aegean offshore region. Lower winds in Spring (Apr-June) and Fall (Sep-Nov) and higher winds in the remaining part of the year throughout the reference period are persistently available for onshore regions. During the spring, the lower winds are also visible over the Aegean offshore area. The MERRA2 winds are higher than ERA5 and observation over onshore regions, while they are slightly lower than ERA5 winds over offshore regions. The high wind speed of offshore areas compared to onshore regions is highly remarkable.

Moreover, the onshore wind speed potential from high to low is ordered as the Marmara, the Aegean, and the Mediterranean regions. Both MME methods show no significant trend in the data series throughout the 34 years, although some interannual variability exists over both onshore and offshore regions. It seems that the RF estimates showed higher year-to-year variability. Area-averaged correction provided by the MLR and RF to the GCMs can diminish the positive or negative trends already observed in the reference data sets.

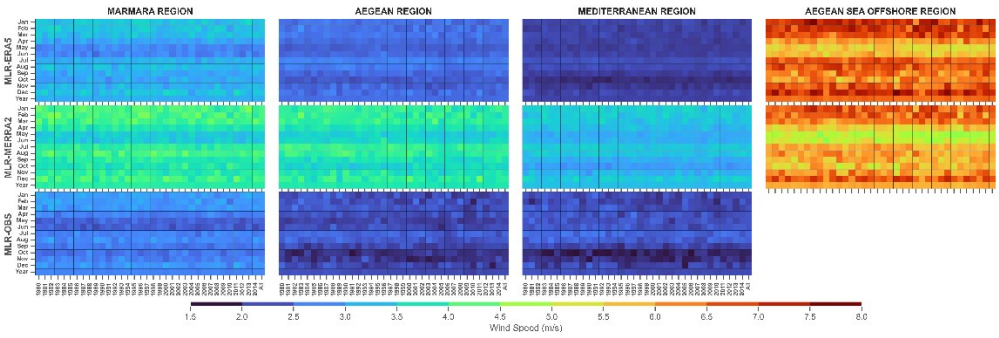



Figure 57 MLR-based MME estimates using ERA5, MERRA 2 and Observation as reference data over three onshore (Marmara, Aegean, and Mediterranean) and Aegean offshore regions.

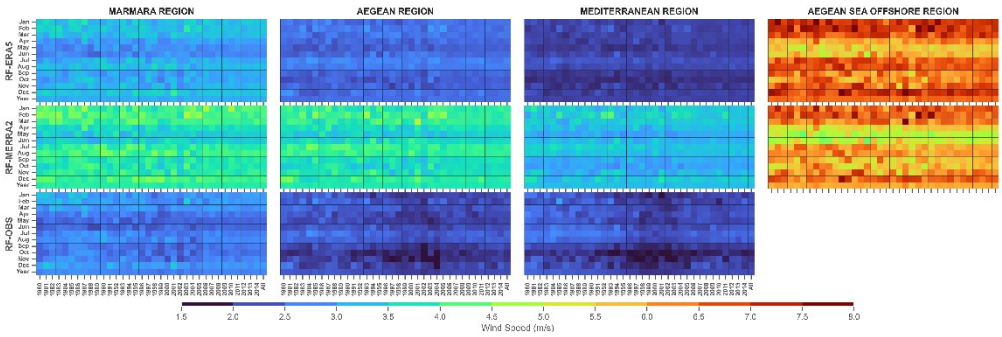



Figure 58 RF-based MME estimates using ERA5, MERRA2 and Observation as reference data over three onshore (Marmara, Aegean, and Mediterranean) and Aegean offshore regions.

Intra-annual MME variation generally varies with higher wind speeds during the summer and winter months and lower wind speeds during the Fall and Spring seasons for all models. Entire period MLR and RF results with their combination of model classifications (DVM, WDVM) are also illustrated in the following figures (fig 59,60,61). Figure 59 shows the All Models monthly average MLR Results for eight regions. Since no observation data exists for the offshore region, the Aegean Sea Offshore Region has only been calculated with ERA5 and MERRA2 data. The simple mean of GCMs always overestimates all reference data and MLR/RF results except for MERRA2. MERRA2 data is very close to all GCM mean for all regions at all months. ERA5 is also higher than the observations for the Aegean, Anatolia, Southeast Anatolia, and Marmara Regions at all months.

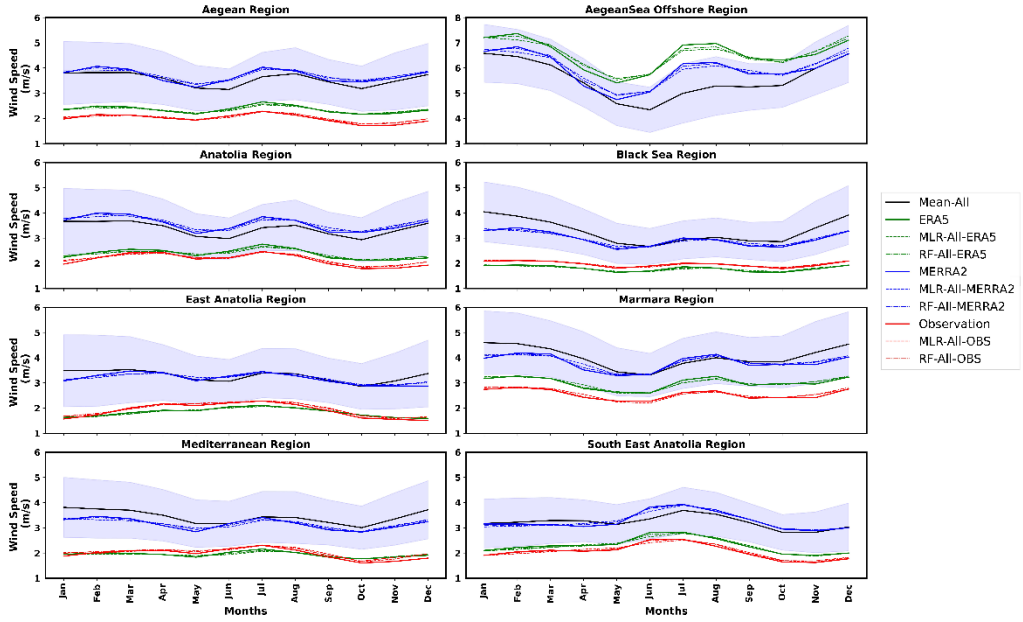



Figure 59 All Models MME Results for Monthly Means

Results with DVM models showed similar performance to MLR and RF-All results (see fig.60). Results in Aegean, Anatolia and Marmara Regions are close to catch simple mean variation during the summer months especially results with MERRA2 due to higher mean wind speeds in this data.

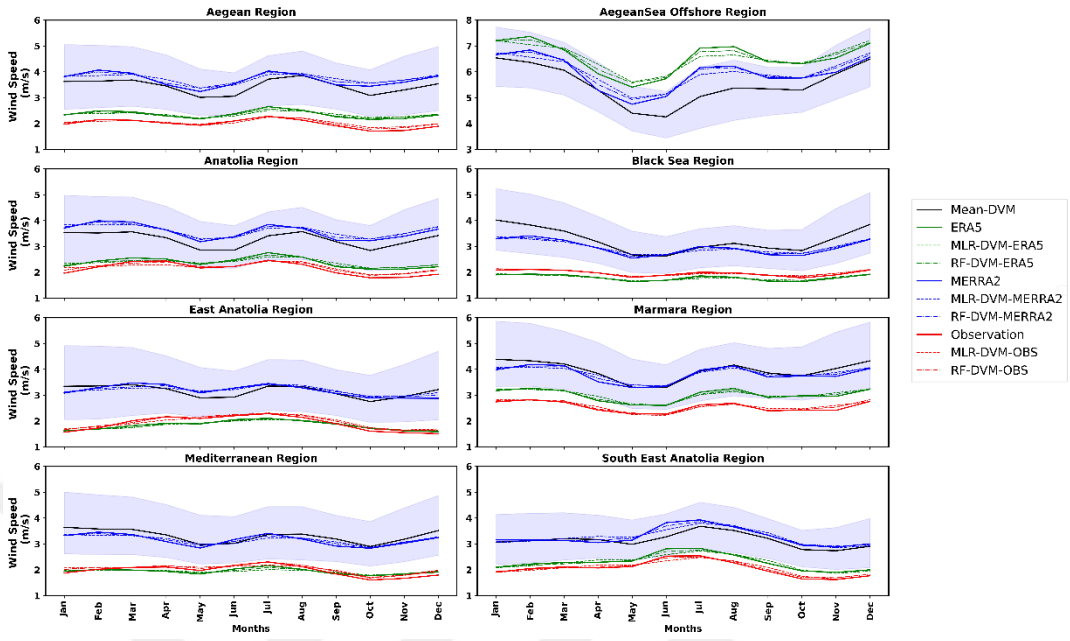



Figure 60 DVM Models MME Results for Monthly Means

WDVM Models results are also showed similar variation with DVMs (figure 61).

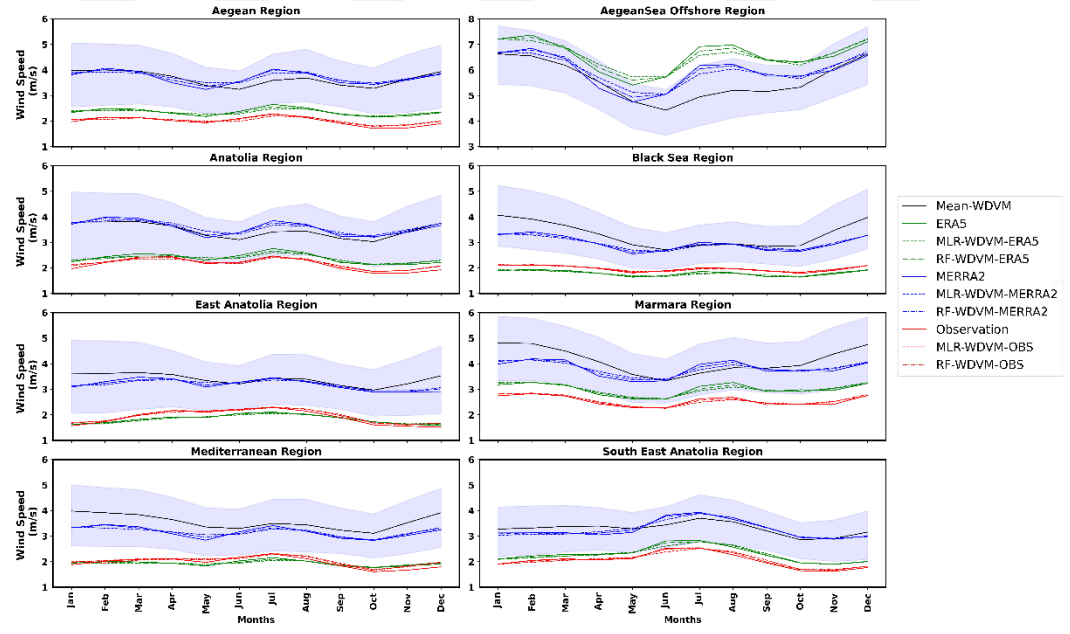



Figure 61 WDVM Models MME Results for Monthly Means

Overall RF results showed better performance than MLR performances. GCM Means are overestimated for all reference data except MERRA2. Figure 62 shows

scatter plots for the entire period (1980-2014), including MLR-All, RF-All, and 28 GCM Mean versus three reference data. Since offshore wind speeds are higher than onshore regions, this region is evaluated separately. Overall, onshore wind speed ranges between 0-8 m/s, while offshore wind speeds change between 4-11 m/s.

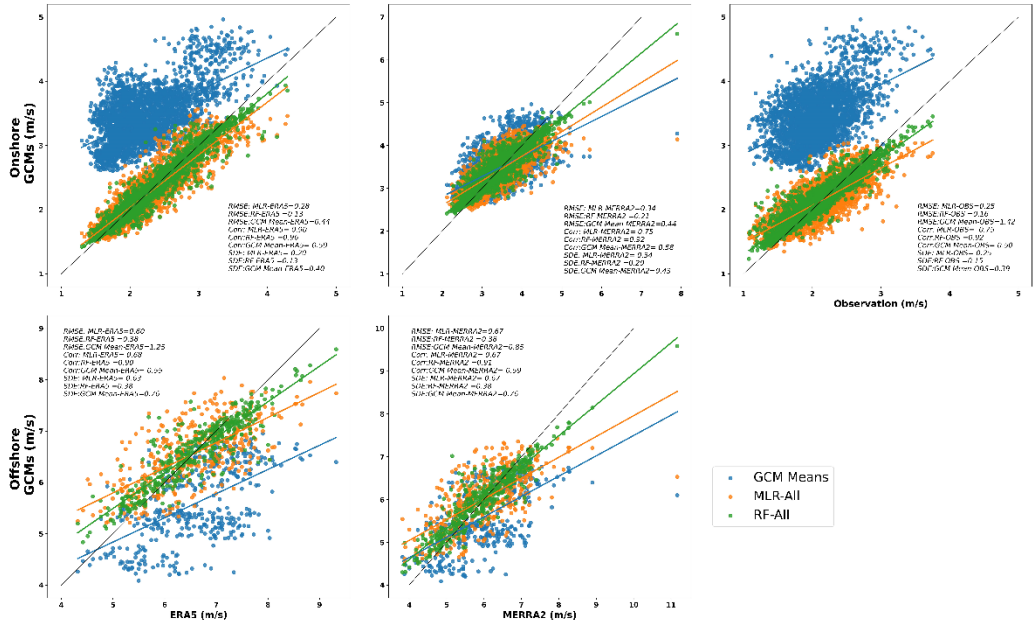



Figure 62 Entire Period MLR and RF Results and GCM Means vs Observations-ERA5-MERRA2 for Onshore and Offshore regions

## 4.3 Multi-model ensemble results for future period (2014-2100)

### 4.3.1 Changes in the offshore wind resource in Türkiye (at 100 m.a.g.l)

#### 4.3.1.1 Height calculation from pressure levels data

The heights between the surface and 1000 mb, 925 mb, and 850 mb are calculated using the hypsometric equation for each CMIP6 model in Table 10 to obtain wind speeds at 100 m. To test the height computation approach, the Alfred Wegener Institute AWI-CM-1-1-MR model [237] is utilized. The model has 0.9375x0.9272 0 horizontal resolution and is a coupled model.

The height between the surface (10 m.a.g.l) and 1000 mb is illustrated in figure 63. The height of the 1000 mb is negative except offshore and open land surfaces near the Aegean, Marmara, and Mediterranean shores.

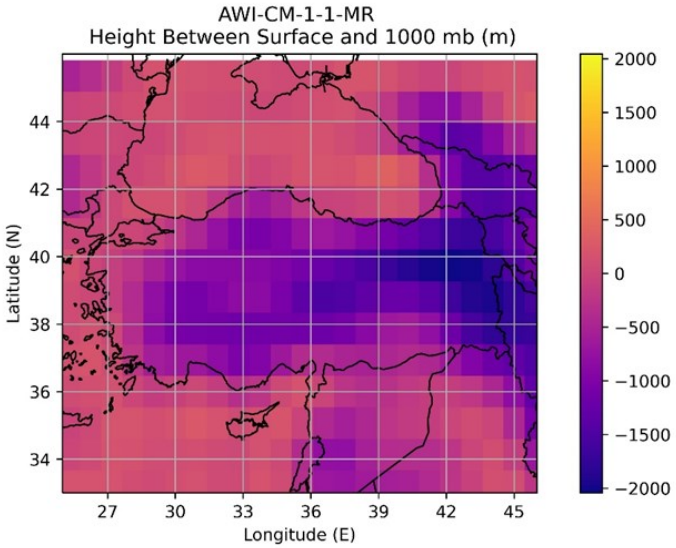



Figure 63 Calculated heights for AWI-CM-1-1-MR Model between surface and 1000 mb

925 mb and 850 mb pressure levels' heights from the surface are also calculated and illustrated in Figure 64 for the AWI-CM-1-1-MR model.

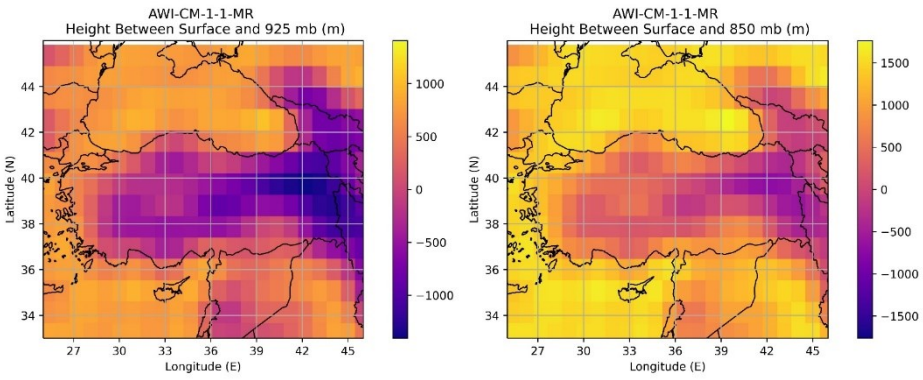



Figure 64 Calculated heights for AWI-CM-1-1-MR Model between surface and 925, and surface and 850 mb

Then, wind speeds are calculated using calculated heights between pressure and surface levels. However, the results for higher pressure levels are negative due to negative heights between those levels and 100 m.a.g.l. The following figures

(Figures 65,66 and 67) compare the calculated 1000, 925, and 850 mb wind speeds, depending on their heights above the surface layer. Even for the 850 mb level (figure 66), there are still missing values, especially for the mountainous regions over Eastern Anatolia.

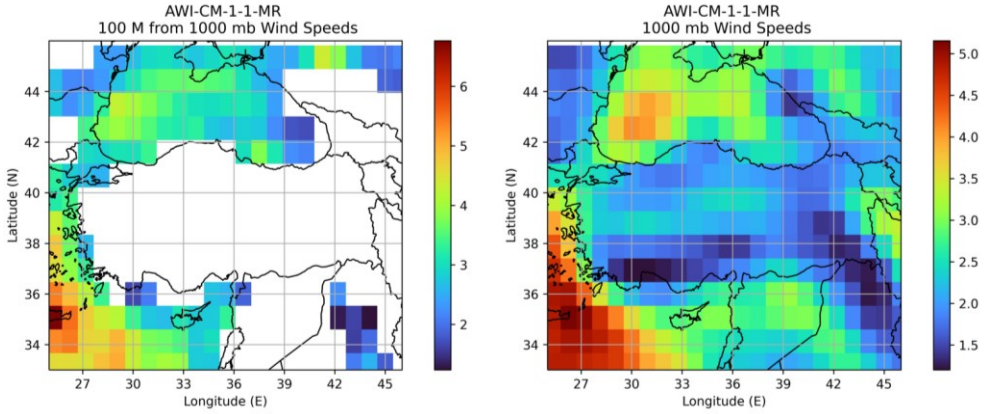



Figure 65 The 100 m calculated wind speed results from 1000 mb wind speeds and 1000 mb raw wind speed for AWI-CM-1-1-MR Model

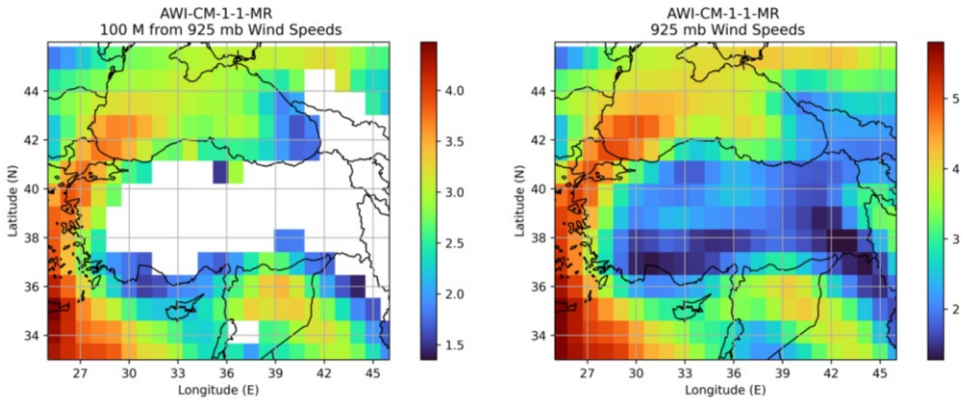



Figure 66 The 100 m calculated wind speed results from 925 mb wind speeds and 925 mb raw wind speed for AWI-CM-1-1-MR

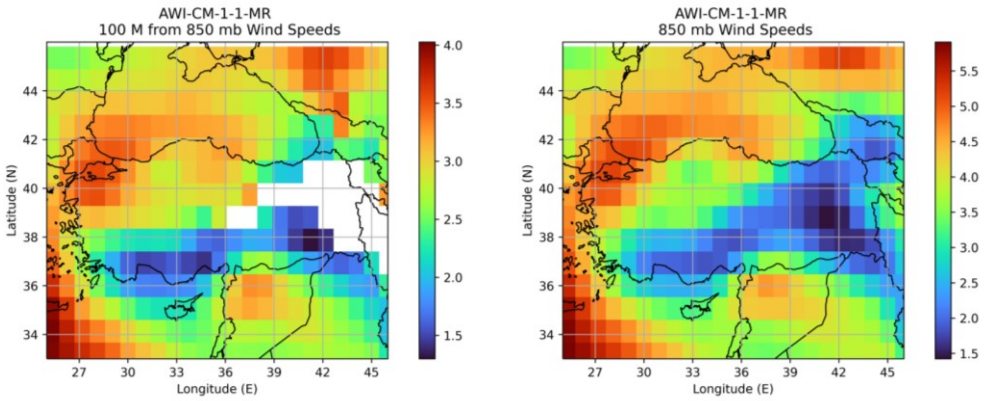



Figure 67 The 100 m calculated wind speed results from 850 mb wind speeds and 850 mb raw wind speed for AWI-CM-1-1-MR

Since the topography of Türkiye is not homogenous, this method will only be applicable for offshore regions due to the flat surface over the sea. Therefore, it is decided to separate future projections studies into two parts onshore and offshore. For the offshore regions, this method is applied to calculate wind speeds at 100 m. The first pressure level of each model' is obtained for the required parameters in the hypsometric equation. After calculating the height of the pressure level for the Aegean Sea, Marmara Sea, Black Sea, and Mediterranean Sea, these heights are used in the power law.

#### 4.3.1.2 Model Performances

The validation of offshore models is evaluated using the nearest GCM grid points to each ERA5 grid included in the region. After obtaining the nearest grid values for four regions, ERA5 wind speeds are averaged for each same model grid, and then the error metrics are calculated for each model and each sea. Figure 68 shows the correlation coefficients (CORR), RMSE, percent bias (PBIAS), and standard deviation error (SDE) for all four seas. Although the other models have relatively high positive correlations, INM-CM4-8 and INM-CM5-0 models have mostly negative correlations and the highest negative PBIAS for all seas. The lowest PBIAS values are calculated at the Mediterranean Sea for GFDL-ESM4 models. The highest correlations are found for the FIO-ESM-2-0 model and CMCC-ESM2 at the Black

Sea (> 0.63). The lowest and negative PBIAS is also valid for INM-CM4-8 and INM-CM5-0 at the Black Sea and Aegean Sea (< -80). The highest negative PBIAS values can be seen for the AWI-CM-MR2 model, which also has relatively high correlations at the Black Sea and the Aegean Sea. However, all models nearly underestimated the ERA5 at 100 m. Due to the low resolution of the models, Marmara Sea has lower model grids than other regions. Therefore, although model performances are calculated for all models for the Marmara Sea (using the closest grid point to ERA5), the region is represented with 9 CMIP6 models in the RF calculations, in contrast to other regions where they are represented with 13 GCM models.

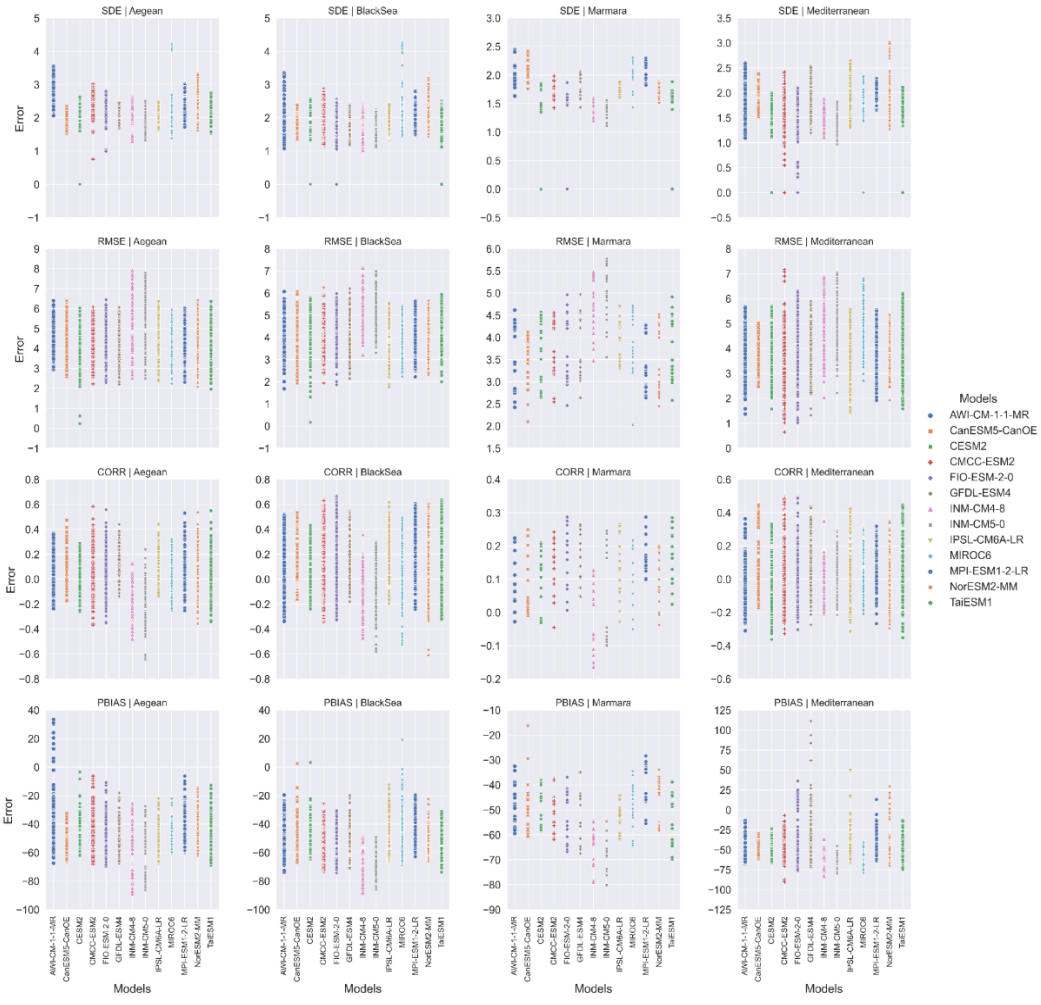



Figure 68 Errors between ERA5 and CMIP6 models during the train period (1980-2014) for all model grids at each region (dots represents the grid points errors associated with each model).

#### 4.3.1.3 Performance Evaluation of RF Results for Train Period

According to the outcomes of the earlier hindcast analysis in Chapter 4-2, ERA5 outperformed MERRA2 and observations, whereas RF projections outperformed MLR. As a result, ERA5 is chosen as the reference dataset, and only RF regression is used to compute all multi-model ensemble future predictions. Since the model data and reference data are available for the train period (1980-2014), RF predictions are evaluated with ERA5 data by using statistical error metrics at each region. GCM means are compared with ERA5 as well. Figure 69 shows the box plots of individual models, produced RF predictions and ERA5 data wind speeds at the train period. Underestimation of ERA5 can be seen from each raw model, but such biases are greatly reduced with the RF predictions for all seas.

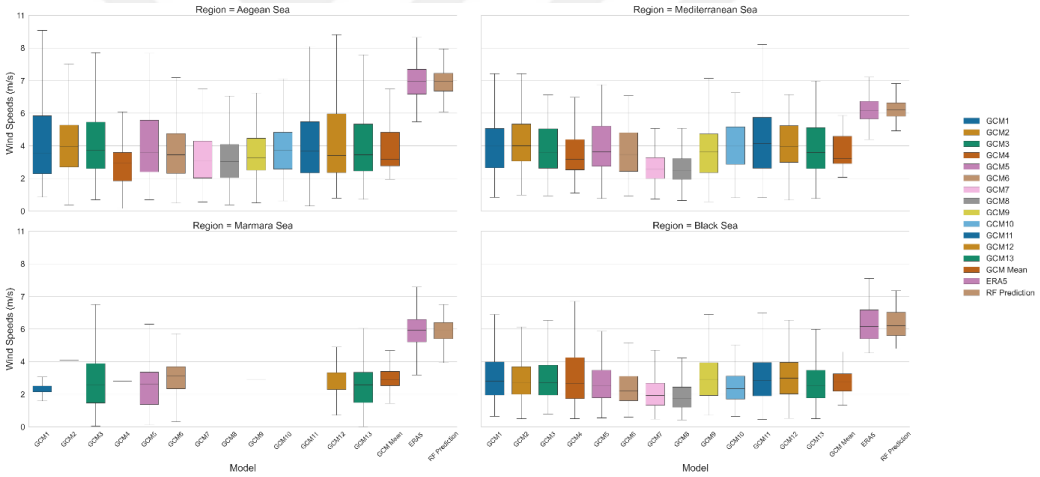



Figure 69 Train period wind speeds for individual models, GCM means, ERA5 and RF predictions

Seasonal RF performances during the train period are also examined, and the results are shown in Table 19. Marmara and the Mediterranean Sea have higher RMSE for the Summer and Fall seasons, respectively. Correlation coefficients are very close to each other. However, the Aegean Sea correlations for all seasons are higher than the other regions, especially for the fall and spring seasons. The lowest correlations are found for the Black Sea during the summer season. Moreover, individual model performances were obviously low PBIAS (changes from -75 to 40 % see figure 67) compared to the RF predictions (changes between -2.96 % and 3.78 %).

Table 19 Seasonal errors for RF predictions in terms of each sea

| REGION | SEASON | RMSE-RF | SDE-RF | PBIAS-RF | Corr-RF |
|---|---|---|---|---|---|
| Aegean Sea | DJF | 0.39 | 0.36 | -1.76 | 0.98 |
| | JJA | 0.33 | 0.33 | -0.46 | 0.97 |
| | MAM | 0.26 | 0.25 | 0.89 | 0.98 |
| | SON | 0.35 | 0.33 | 1.59 | 0.97 |
| Black Sea | DJF | 0.32 | 0.30 | -1.63 | 0.93 |
| | JJA | 0.28 | 0.20 | 3.69 | 0.85 |
| | MAM | 0.32 | 0.32 | -1.00 | 0.97 |
| | SON | 0.27 | 0.27 | -0.64 | 0.96 |
| Marmara Sea | DJF | 0.38 | 0.33 | -2.96 | 0.96 |
| | JJA | 0.40 | 0.40 | 0.92 | 0.95 |
| | MAM | 0.31 | 0.30 | 1.28 | 0.96 |
| | SON | 0.32 | 0.32 | 1.00 | 0.96 |
| Mediterranean Sea | DJF | 0.42 | 0.39 | -2.41 | 0.97 |
| | JJA | 0.17 | 0.17 | -0.35 | 0.95 |
| | MAM | 0.22 | 0.22 | -0.57 | 0.97 |
| | SON | 0.33 | 0.25 | 3.78 | 0.92 |

The distribution of the predicted wind speeds for the train period is illustrated in figure 70. The figure shows that Aegean and Black Sea RF prediction results performed better with the ERA5 data. However, the Marmara Sea results are worse than any other region. GCM means for the Marmara and Mediterranean Seas show negative correlations (-0.04 for the Marmara Sea, -0.05 for the Mediterranean Sea). These negative correlations could be reasoned by using a simple mean, which cannot represent the reference data correctly.

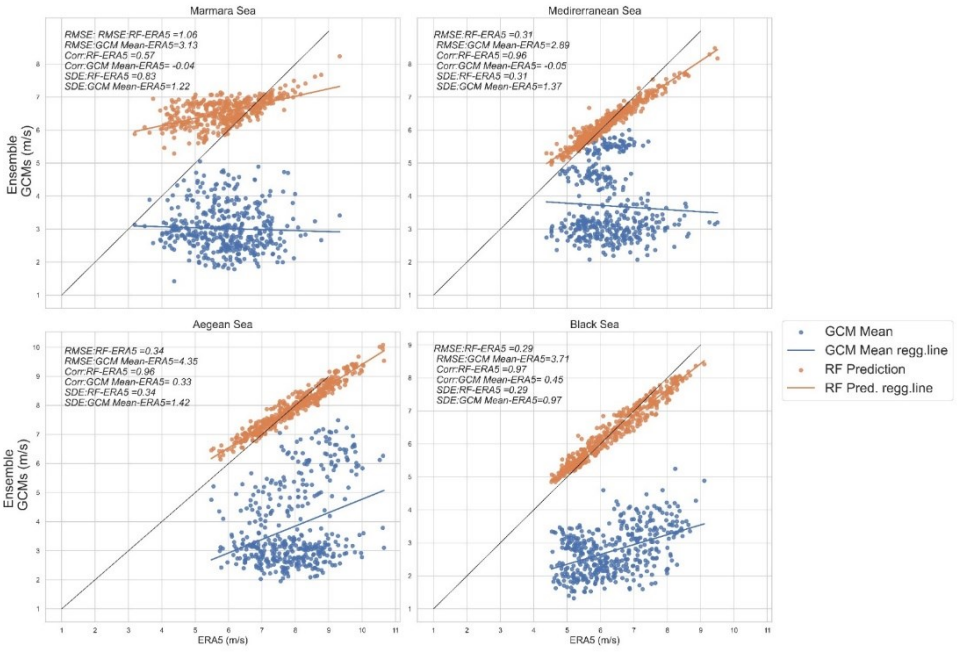



Figure 70 Regional scatter plots for RF prediction and GCM means versus ERA5 data

#### 4.3.1.4 Time Series Analysis

Time series results for each region are also produced for SSP2-4.5 and SSP5-8.5 scenarios at each region using ERA5 as reference data. As illustrated in Figure 71, ERA5 is higher than all models and model means. However, RF predictions are closer to ERA5. The Aegean Sea has the highest wind speeds. The variability of wind speeds in the region is high as well.

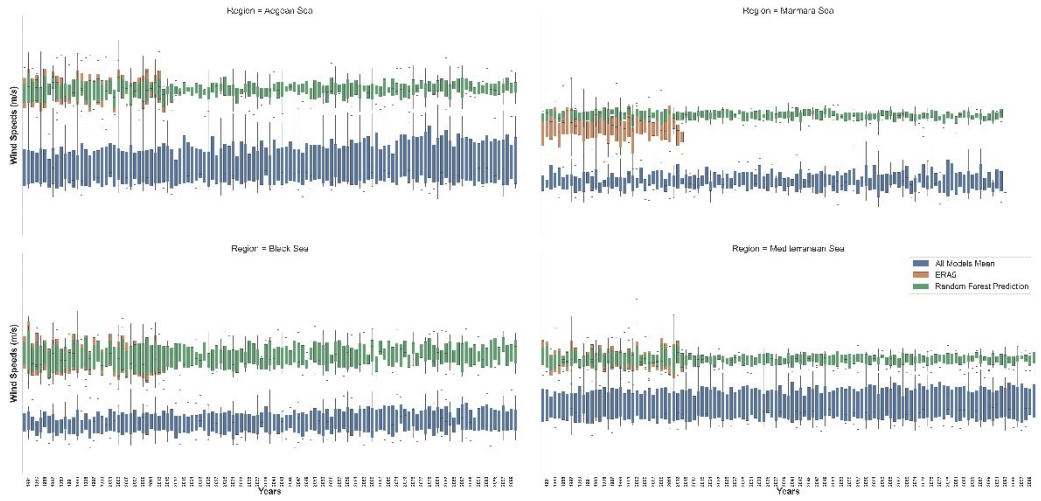



Figure 71 RF Predictions for entire period (SSP5-8.5) together with ERA5 re-analysis data and GCM means (Each boxplot represents a year which contains 12 months wind speed data)

Since the boxplots were nearly the identical for the two scenarios, SSP2-4.5 results are not illustrated in this part. However, detailed differences between scenarios can be seen in Figure 72. Produced RF predictions for the entire test period are also compared with the reference period monthly averages to obtain wind speed changes for near-term, mid-term, and long-term periods. Wind speeds are expected to increase in the summer months in the Black Sea (around % 10-20) for all three periods. Aegean Sea spring months are also expected to have higher wind speeds for both scenarios. The difference between SSP5-8.5 and SSP2-4.5 is smallish. However, it is obvious, especially in the Marmara Sea, where negative differences occurred in the summer months.

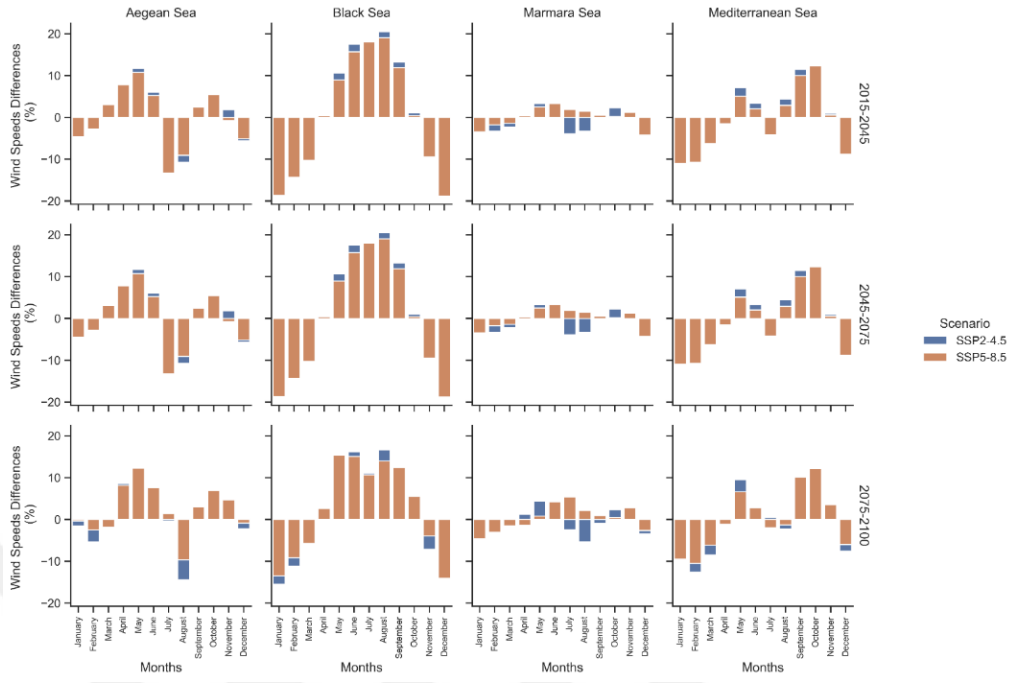



Figure 72 Averaged monthly wind speed changes (%) between three future periods and reference periods based on ERA5 for two scenarios.

To sum up, for the offshore wind resource evaluation, 100 m wind speeds are calculated at 100 above the sea level by using pressure level data from CMIP6 for surrounding seas around Türkiye. Two different climate change scenarios' results for RF prediction are produced, and results showed that using individual GCMs cannot represent ERA5 re-analysis data for a region.

CMIP6 models underestimate the ERA5 data over the study area. Aegean Sea wind speeds change between 7 m/s to 10 m/s for the entire study period for ERA5 and RF predictions which promises a good opportunity for offshore wind power installations during the upcoming years. Although Black Sea wind speeds change between 5-8 m/s, the winds in this region are also expected to increase by %20 in the near, mid, and long term, especially in the summer months. Mediterranean Sea wind speeds are expected to decrease in the winter months and increase in fall by approximately 10 %. Seasonal variability of wind speed changes is also considered due to the increasing electricity demand for those regions in the summer months. Projected

changes in the Marmara Sea are low, but the reasons can be varied due to the low number of grids in this region, or it may be reasoned because of the internal sea.

RF prediction results performed better than any GCMs, and correlations with the ERA5 data are found to be high (changes from 0.85 to 0.98). The difference between scenarios is also found to be very small. However, SSP2-4.5 are only higher than SSP5-8.5 for the summer months at Marmara and Black Sea.

However, this study only includes the GCMs with a coarse resolution which gives a rough estimation of offshore wind climatology. Therefore, further work is needed to establish to increase the resolution of the GCMs due to wind climatology requiring higher resolution for better representation of the area.

#### 4.3.1.5 Offshore Trends for Future Scenarios

Offshore wind speed trends are also investigated for all seas and models. First, for each region, each model's and scenario's trends are calculated.

For the SSP2-4.5 scenario AWI-CM-1-1-MR model has shown an increasing trend for the Marmara region. The FIO-ESM-2-0 model has shown an increasing trend for the Black Sea region. No trend was found for other models in all regions.

Table 20 lists more models with rising and falling trends for SSP5-8.5 scenarios than for SSP2-4.5 scenarios. Most models predict that the wind will increase by the end of the twenty-first century, as the table below shows.

Table 20 SSP5-8.5 Trends for Regions and Models

| Region | Model | Trend |
|---|---|---|
| Marmara Sea | CESM2 | 'decreasing' |
| Marmara Sea | TaiESM1 | 'increasing' |
| Aegean Sea | GFDL-ESM4 | 'increasing' |
| Aegean Sea | NorESM2-MM | 'increasing' |
| Aegean Sea | TaiESM1 | 'increasing' |
| Black Sea | AWI-CM-1-1-MR | 'increasing' |
| Black Sea | CESM2 | 'increasing' |
| Black Sea | CanESM5-CanOE | 'increasing' |
| Black Sea | FIO-ESM-2-0 | 'increasing' |
| Black Sea | GFDL-ESM4 | 'increasing' |
| Black Sea | MPI-ESM1-2-LR | 'increasing' |
| Black Sea | TaiESM1 | 'increasing' |
| Mediterranean Sea | INM-CM4-8 | 'decreasing' |
| Mediterranean Sea | CanESM5-CanOE | 'increasing' |

Since the offshore wind part of the multi-model ensemble study is based on averaging grids for each region, it is also better to investigate trends with moving averages. Therefore, moving averages for 3,6,8,12 months are also illustrated for two scenarios to determine the future variability of predictions and historical period in Figures 73,74,75, and 76, respectively. The 12-month moving averages for GCM means and RF projections for this scenario clearly shows an increasing trend (Figure 76) in the Aegean Sea.

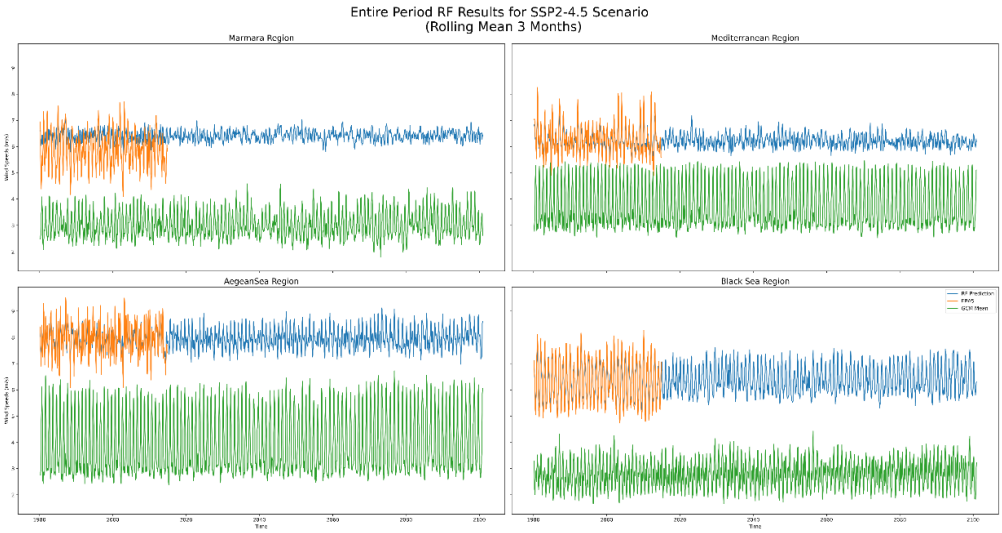



Figure 73 SSP2-4.5 Scenario 3 Months Rolling Means for RF Predictions, ERA5 and GCM Means

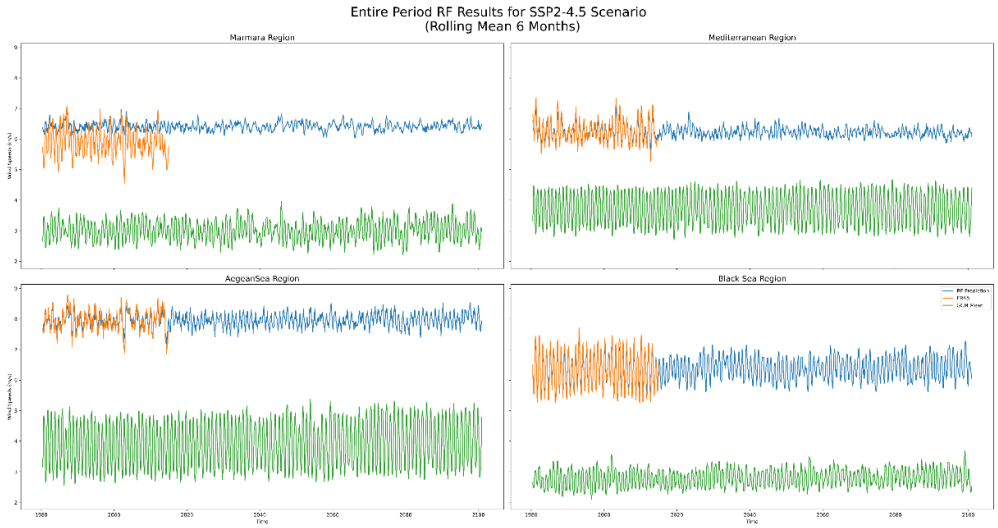



Figure 74 SSP2-4.5 Scenario 6 Months Rolling Means for RF Predictions, ERA5 and GCM Means

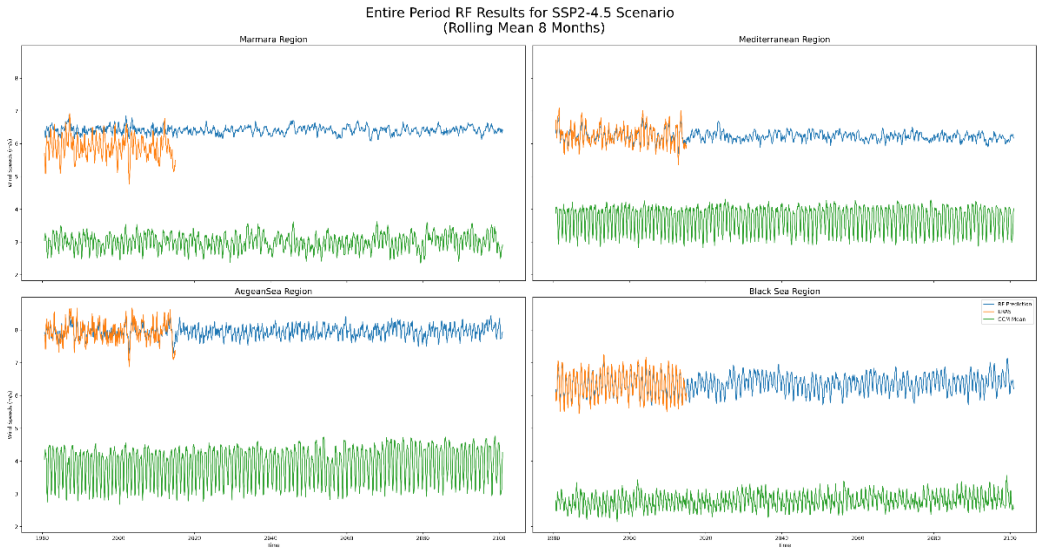



Figure 75 SSP2-4.5 Scenario 8 Months Rolling Means for RF Predictions, ERA5 and GCM Means

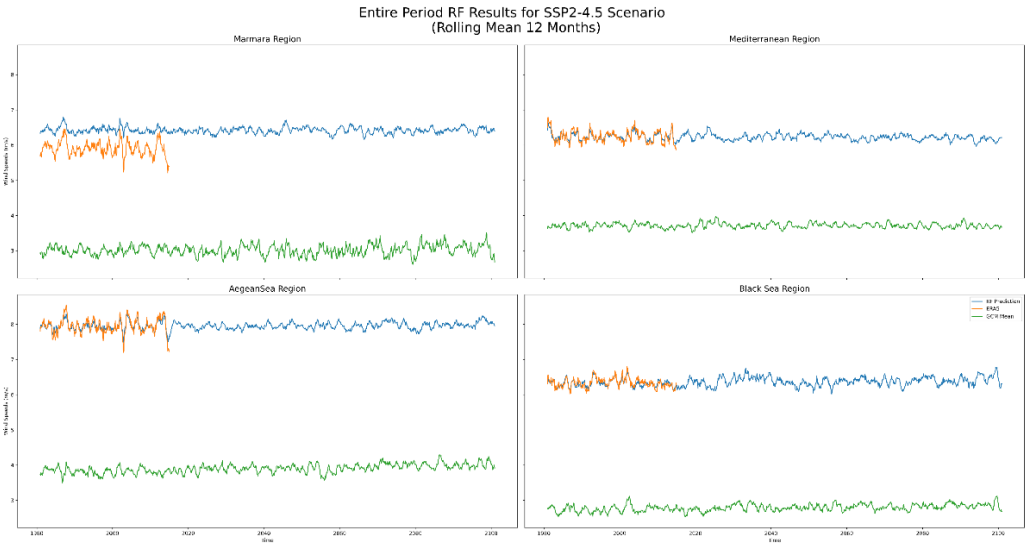



Figure 76 SSP2-4.5 Scenario 12 Months Rolling Means for RF Predictions, ERA5 and GCM Means

The same analysis is also done for the SSP 5-8.5 scenario. Increasing wind speeds by the end of the 21$^{st}$ century is apparent in this scenario. The variability in the region for inter-annual means can also be seen in Figures 77, 78,79, and 80 for 3,6,8, and 12-month moving averages.

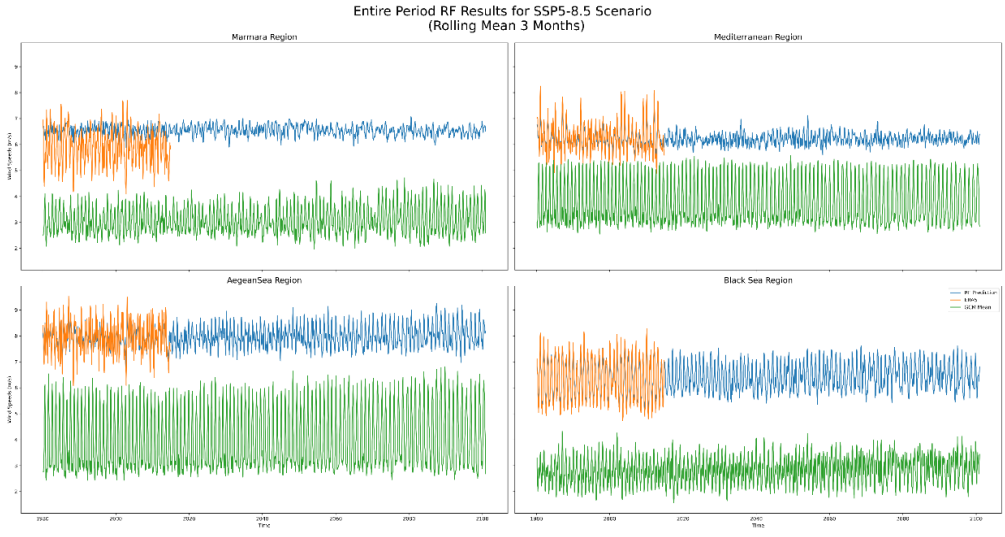



Figure 77 SSP 5-8.5 Scenario 3 Months Rolling Means for RF Predictions, ERA5 and GCM Means

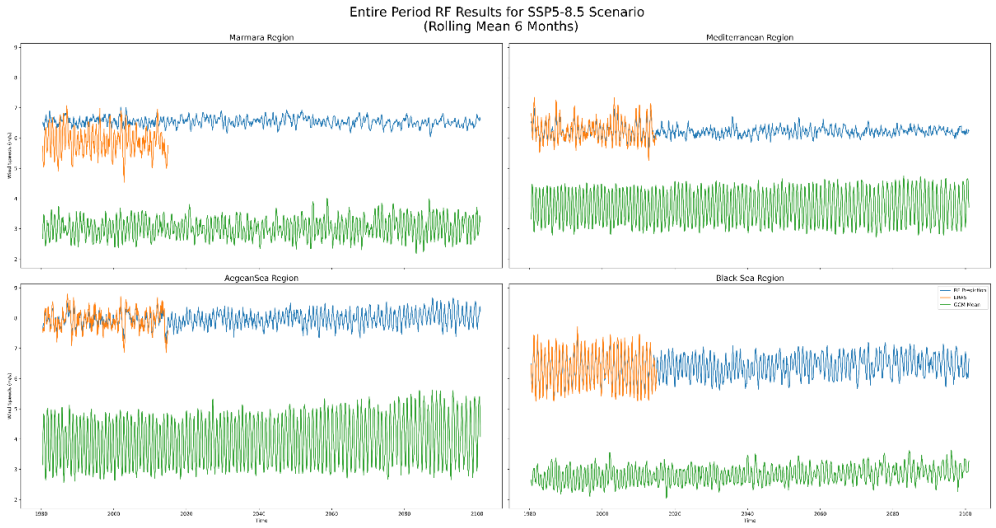



Figure 78 SSP 5-8.5 Scenario 6 Months Rolling Means for RF Predictions, ERA5 and GCM Means

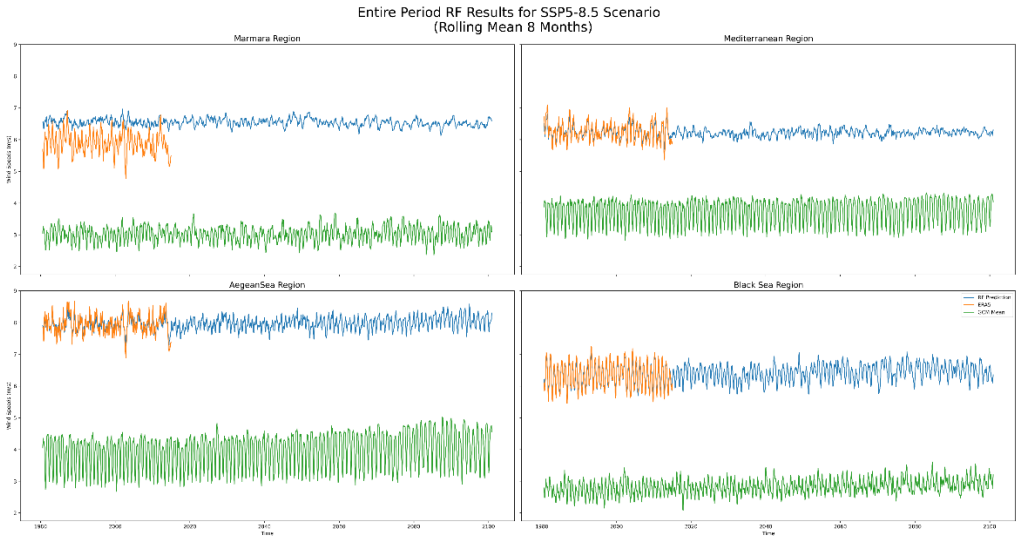



Figure 79 SSP 5-8.5 Scenario 8 Months Rolling Means for RF Predictions, ERA5 and GCM Means

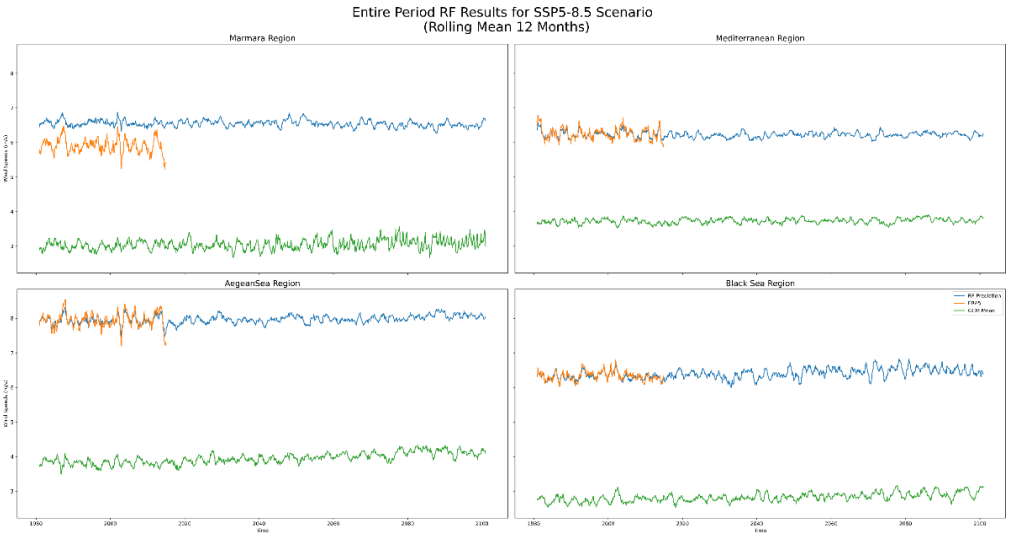



Figure 80 SSP 5-8.5 Scenario 12 Months Rolling Means for RF Predictions, ERA5 and GCM means

### 4.3.2 Changes in the wind resource on existing onshore Wind Power Plants (at 100 m.a.g.l)

#### 4.3.2.1 Calculation of Shear Exponent from ERA5 Data

The shear exponent between 10 m wind speeds and 100 m ERA5 wind speeds are calculated using the power law formula to determine the changes in the wind speeds with height (see fig.81). Shear exponents are expected to be close to zero in the offshore regions and changes with the roughness in the onshore sites. Even though the roughness length is not considered in this calculation, the map may reflect the roughness of the lands. It is in between 0.15-0.10 as it is expected over the seas.

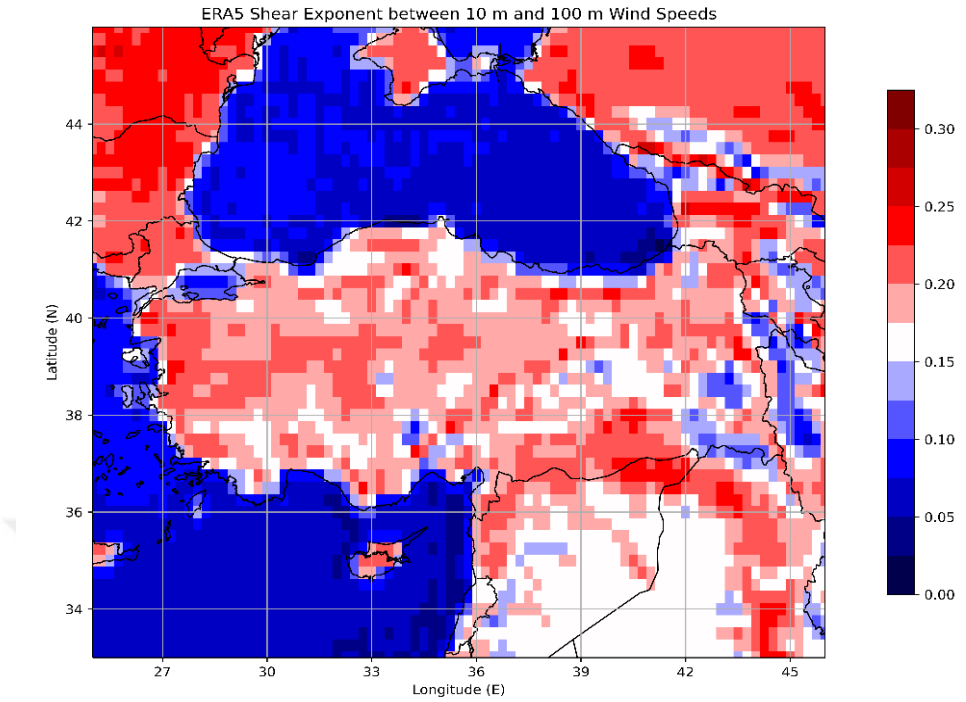



Figure 81 Shear exponent calculation from ERA5 Re-analysis data

The distribution of all three comparisons is given in Figure 82. As shown in the figure, the calculated 100 m wind speeds are similar to the original wind speed distributions. Constant share exponents do not adaquately depicit 100 m wind speeds.

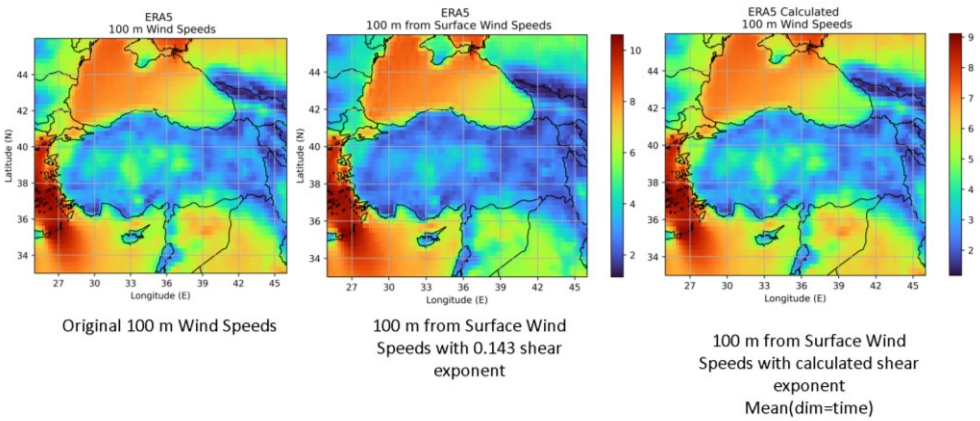



Figure 82 100 m wind speed comparisons for ERA5 re-analysis data

The wind speed distribution of all three comparisons at 100 m is shown in Figure 83 as histograms. As it can be seen in the figure, the calculated 100 m wind speeds are similar to the original wind speed distributions.

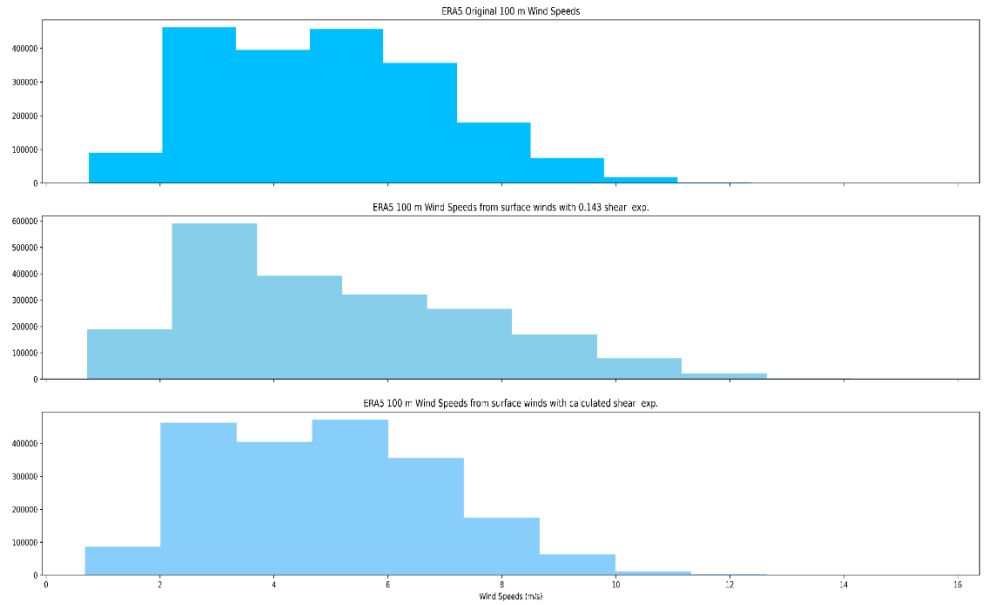



Figure 83 Histograms of ERA5 Wind Speeds at 100 m.a.g.l

Therefore, time average values of the calculated shear exponent from ERA5 are regridded to the resolution of each CMIP6 model in Table 9 for historical, SSP2-4.5, and SSP5-8.5 scenarios. Then wind speeds are extrapolated from 10 m to 100 m for each of them by using the power law. An example is given in Figure 84 (the same model is used: AWI-CM-1-1-M) to compare 10, and 100 m wind speeds 100 from the shear exponent. The difference between 10 m and 100 m wind speeds using the calculated the shear exponent. The difference between 10 m and 100 m wind speeds is also illustrated in Figure 85.

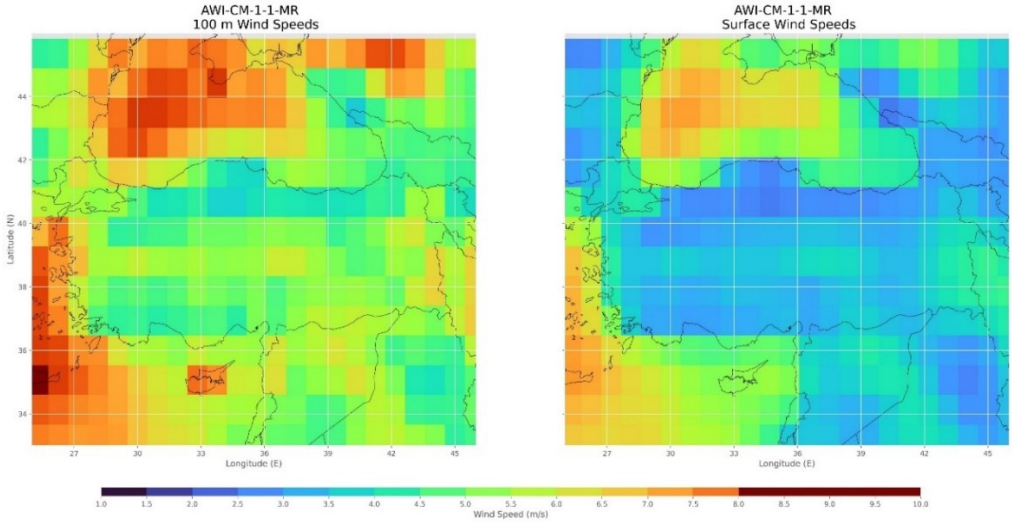



Figure 84 An example of 100-m wind speed from AWI-CM-1-1-MR calculated with extrapolation using the shear exponent and 10-m wind speed (m/s).

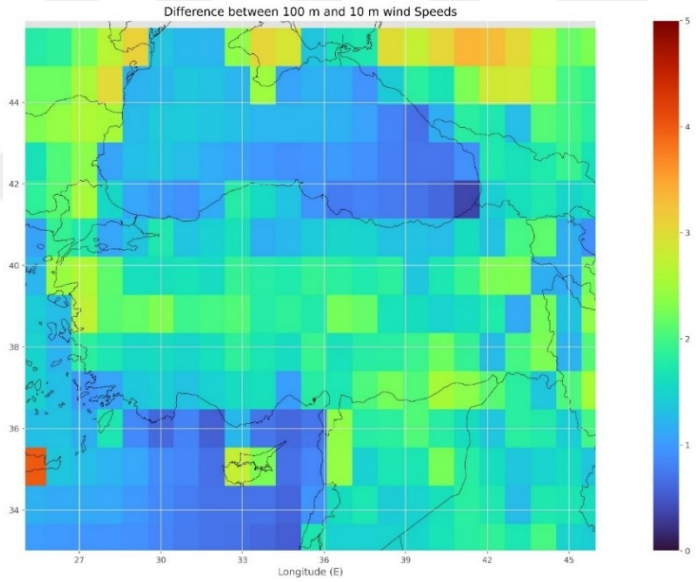



Figure 85 Difference between 10 m and 100 m wind speeds (m/s)

#### 4.3.2.2 Model Performances

The results are obtained by using centroid points for each WPP polygon. The nearest ERA5 and GCMs grids representing each centroid point of a polygon are obtained. The statistics between GCM grids and ERA5 grids are also illustrated in figure 86.

"y-axis" shows each CMIP6 GCM, and the x-axis shows each WPP number changing from 1 to 330. As can be seen from the figure, EC-Earth Models, CMCC-ESM2, HadGEM3-GC31-LL, MIROC6, and MPI-ESM1-2-LR showed a better correlation with ERA5. The lowest RMSE is determined for TaiESM1, UKESM1-0-LL, FIO-ESM2-0, and ACCES-CM2 models. SDE results are also similar and obtained higher errors for BCC-CSM2-MR, FGOALS-G3, FGOALS-F3L, IPSL-CM6A-LR, MIROC-ES2L, MPI-ESM1-2-LR, MRI-ESM2-0 models together with PBIAS.

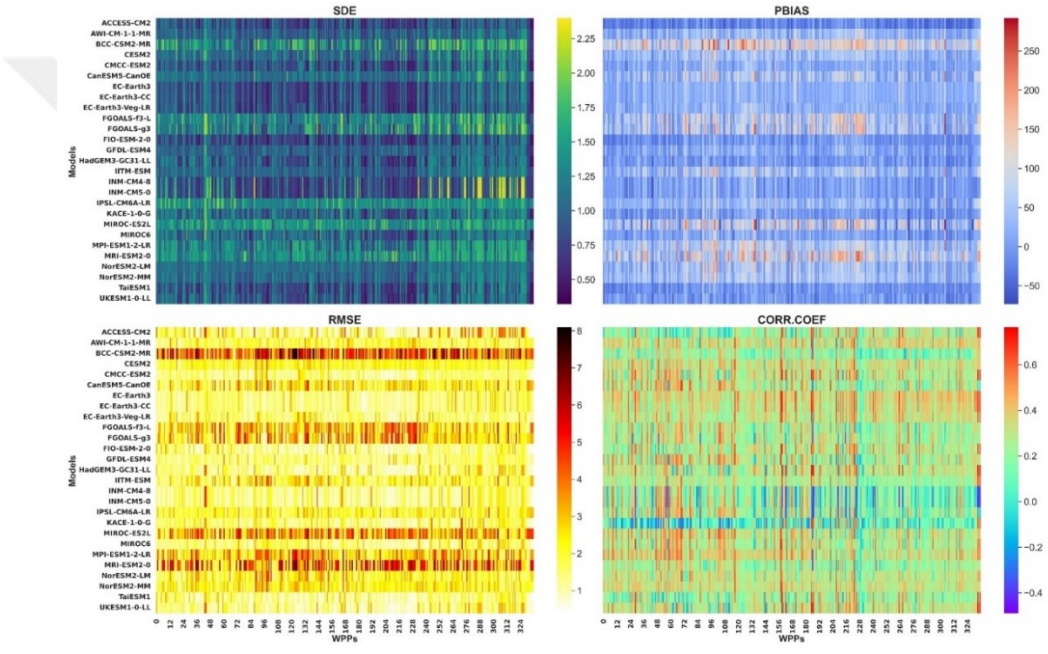



Figure 86 Statistics between GCMs and ERA5 data at 100 m.a.g.l. for each WPP

Overall performances of each GCM with ERA5 data are summarized in the Taylor diagram (see fig.87). Diagram demonstrating the successful representation of all data by EC-Earth3 models compares the entire dataset with the ERA5 and GCMs. HadGEM3-GC31-LL, UKESM1-LL, FI-ESM2-0, and TAIESM1have also good correlations with ERA5.

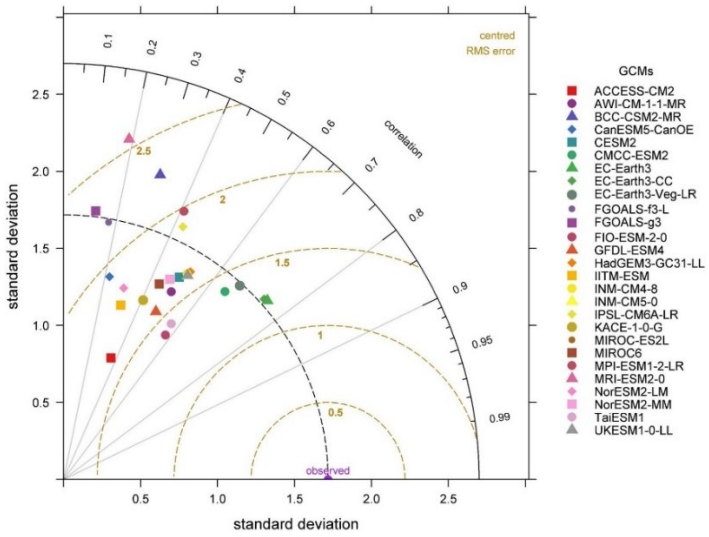



Figure 87 Taylor diagram for all WPPs at each GCMs vs ERA5

Seasonal Taylor diagrams (see fig.88) showed similar performance with the figure 87. Three EC-Earth models have the best performances with the ERA5 data. Spring and fall season errors are lower than the winter and summer seasons for all models.

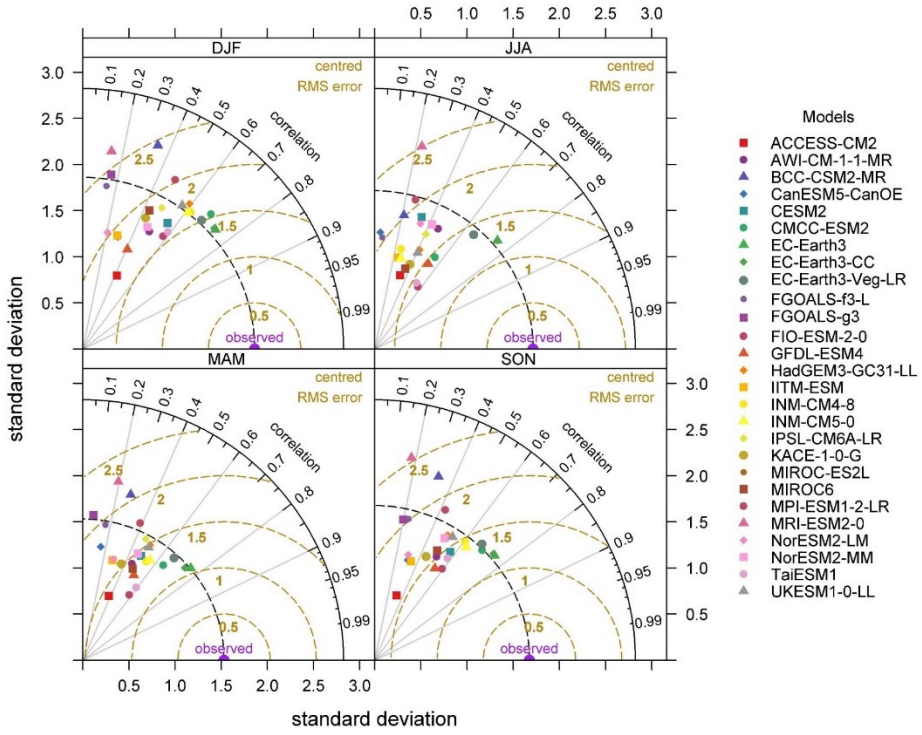



Figure 88 Seasonal Taylor diagrams for 27 GCMs with ERA5 (as an "observed") included all WPPs nearest grids in historical period (1980-2014)

Seasonal averages of each GCM in the spatial distribution over Türkiye are also investigated (see fig. 89). To comprehend the reflection of the changes in wind speed over the wind energy density, wind power density values (see fig. 90) are also calculated under the assumption that the air density is constant (1.225 $kg/m^3$). Seasonality is an obvious driver of wind resources, especially over the northern Marmara and the Aegean Sea in the ERA5 data. Winter is the season with the highest wind power density over the sea. However, although ERA5 wind speeds are higher in winter and summer, summer season variability is not followed by most of the GCMs except EC-Earth models, UKESM-1-0-LL, and HadGEM-GC31-LL models. These differences are obvious in the seasonal wind power density (figure 89), which uses a cube of wind speed.

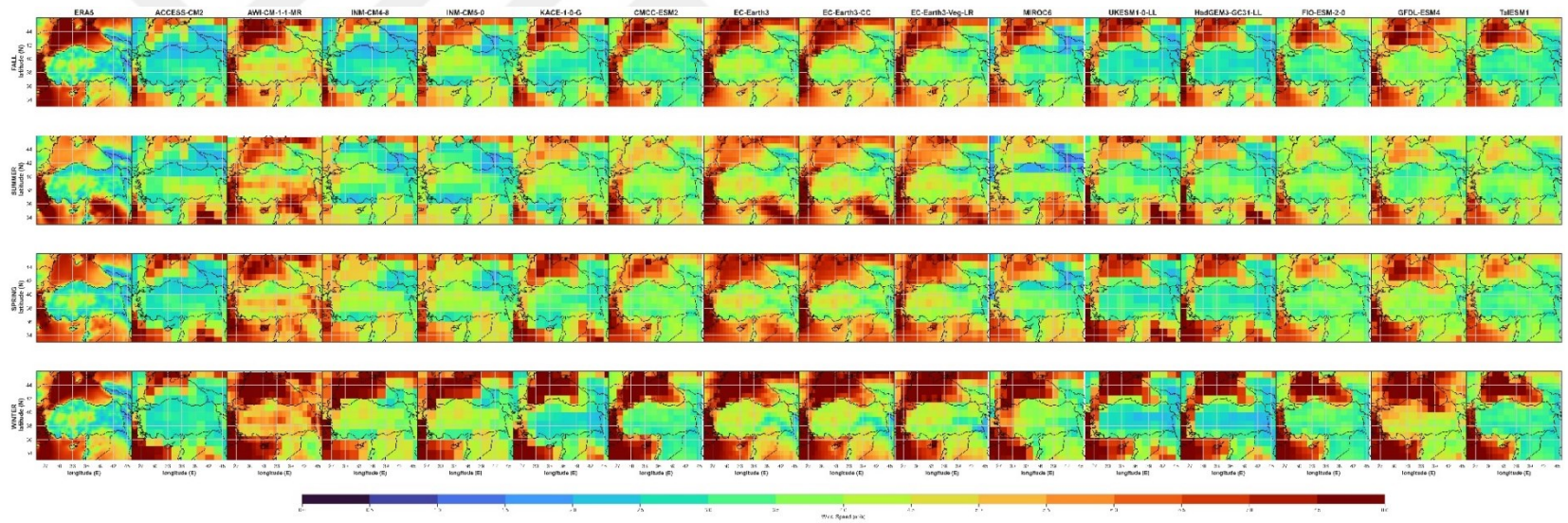





Figure 89 Seasonal average wind speeds (m/s) at historical period for selected 15 GCMs which has higher correlation with ERA5 at 100 m.a.g.l.

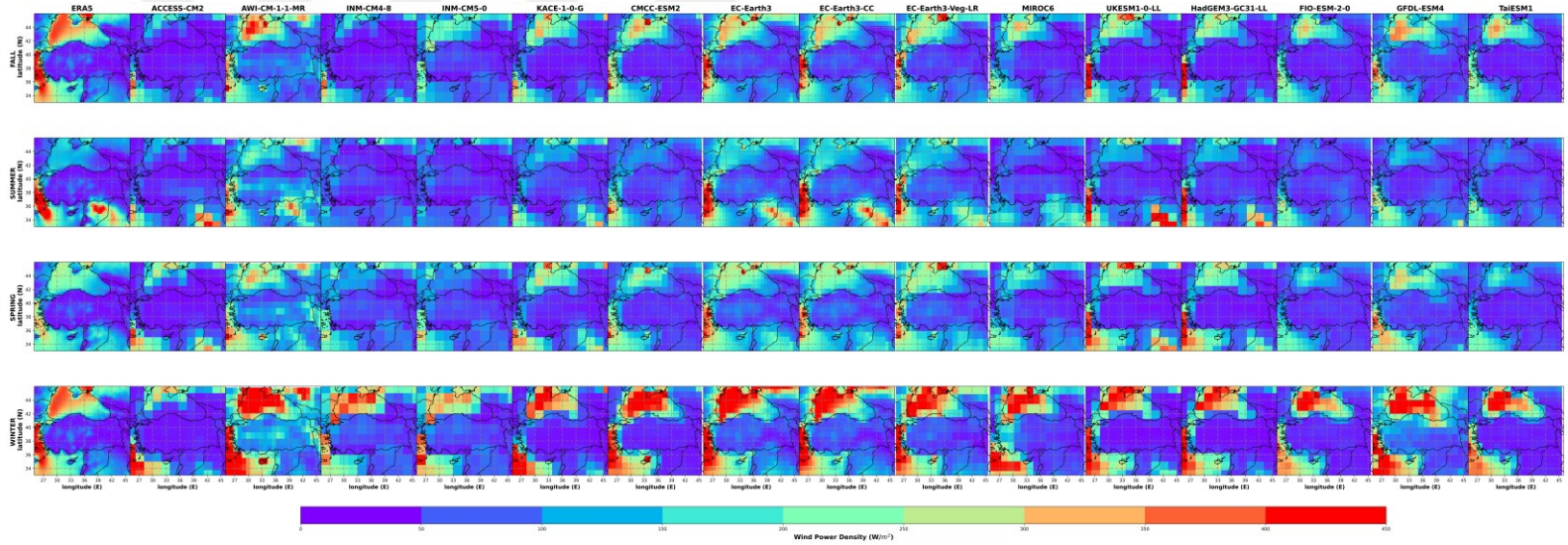



Figure 90 Seasonal average wind power density ($W/m^2$) at historical period for selected 15 GCMs which has higher correlation with ERA5 at 100 m.a.g.l.

#### 4.3.2.3 Performance Evaluation of RF Results for Train Period

RF prediction performances for the entire study period are illustrated in Figure 91. ERA5 data for the 1980-2014 period is also given in the figure to demonstrate the range of the historical period. RF prediction has the closest values to ERA5, while most of the individual GCMs overestimate the ERA5. The average wind speed is around 4.5 m/s for ERA5 and RF predictions. EC-Earth3 models, HadGEM3-GC31-LL, UKESM1-LL, FI-ESM2-0, GFDL-ESM4 and TAIESM1 have similar distribution with the ERA5 and RF predictions.

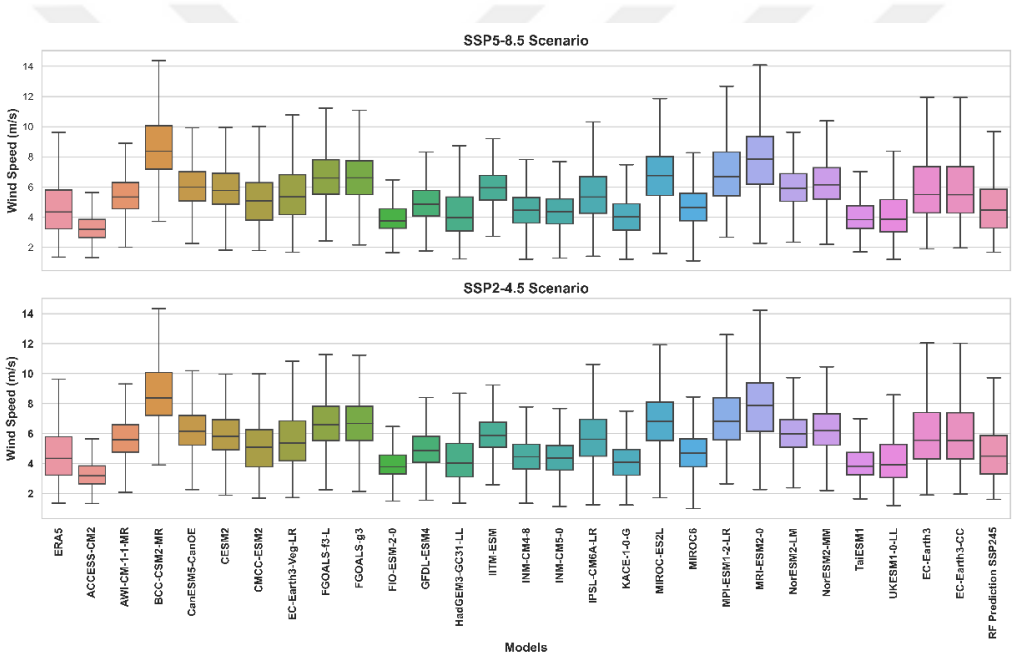



Figure 91 Entire study period RF results together with individual GCMs and ERA5 data

To obtain the wind speed distribution with ranges, a histogram of each season and region, including each WPP, is also demonstrated with Kernel Density Estimate (KDE) in Figure 92. It is determined that although ERA5 wind speeds are slightly higher than the RF predictions, the results of these two scenarios are very close. The histograms show the wind speed distribution. Therefore Aegean and Marmara region WPPs have higher wind speeds than other regions where the highest numbers are

accumulated in 5-7 m/s. WPPs in other regions have very low (2.5-5 m/s) wind speeds. However, the coarse resolution of GCMs is probably caused by the low wind speeds in those regions. But it also shows that, despite the coarse resolution from GCMs, Marmara and Aegean WPPs have promising wind resources.

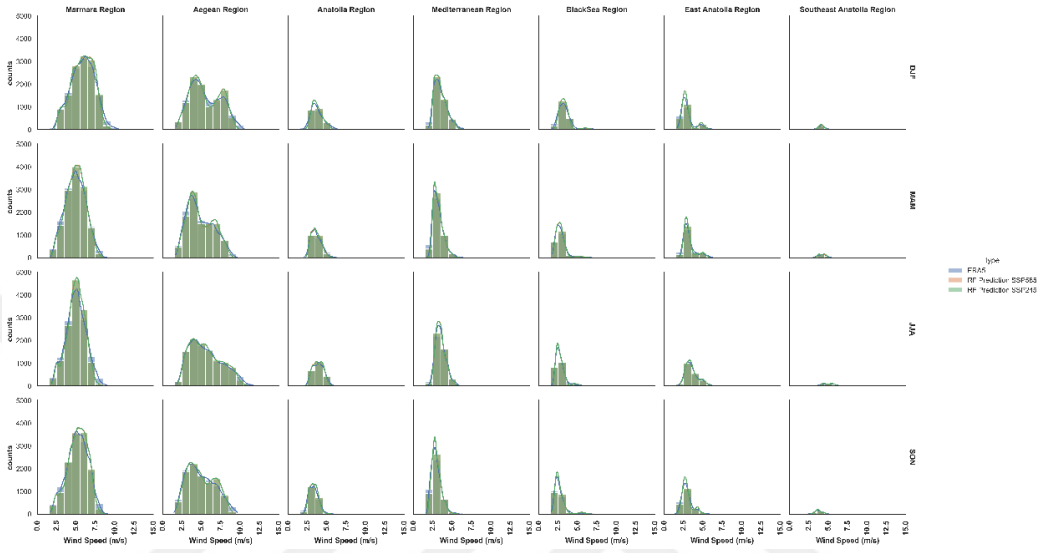



Figure 92 Histogram of train period with two scenarios and ERA5 data in terms of regions and seasons

Predicted wind speed differences from ERA5 data during the train period are also calculated and shown in Figure 93. As can be seen in the figure, wind speed differences are minor and change from -2 and 2 m/s for all regions and seasons. The highest number of differences is accumulated around zero.

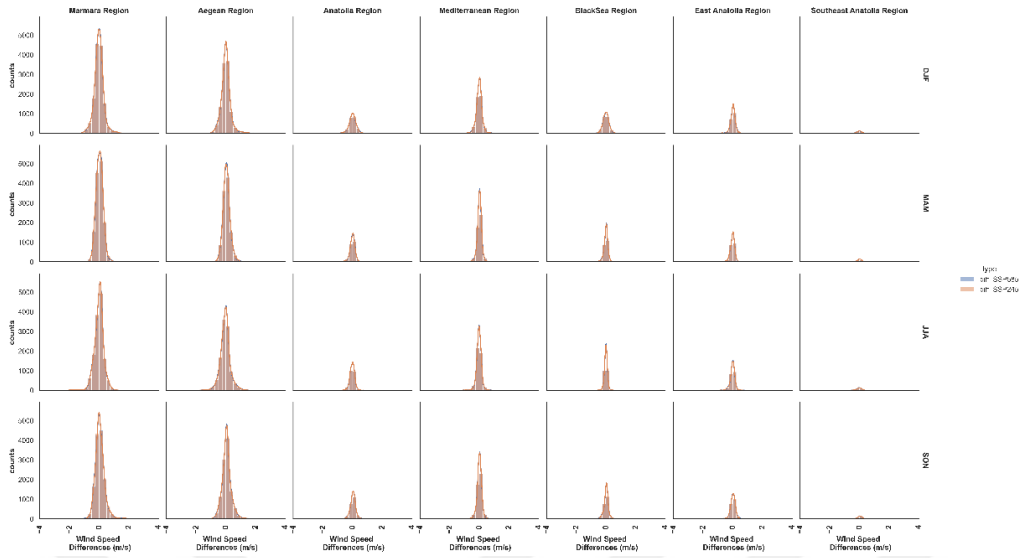



Figure 93 Histogram of wind speed differences between prediction and ERA5 data during the train period with two scenarios in terms of regions and seasons

WPP-based train period performances of RF predictions are evaluated with ERA5 during the same period. Figure 94 shows the correlation coefficients in terms of the region for each WPP. Since most WPPs are located in the Marmara and Aegean regions, it is difficult to determine the size of the corr. coefficients in those regions. However, correlations are changed from 0.96 to 0.98 for all WPPs. There are no location-specific changes for correlations.

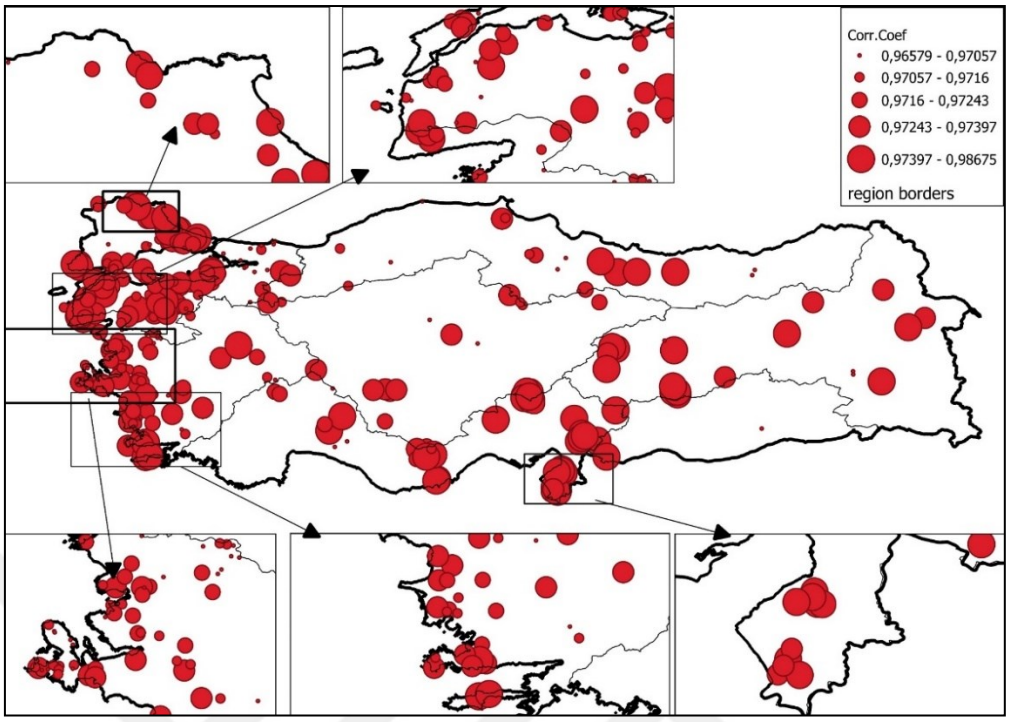



Figure 94 Corr. Coefficients between RF prediction and ERA5 during the train period, closed stations are zooms in some parts of the Marmara, Aegean and Mediterranean region

RMSE of each WPP is also calculated and illustrated in Figure 95. Due to the intensity of the WPPs in the northern Aegean and Marmara regions, it is difficult to determine regionality in the RMSEs. However, Figure 96 shows the detailed version of Figure 95 over the Çanakkale, İzmir, and Balıkesir regions with the largest number of WPPs. The highest RMSE can be seen on the İzmir shores.

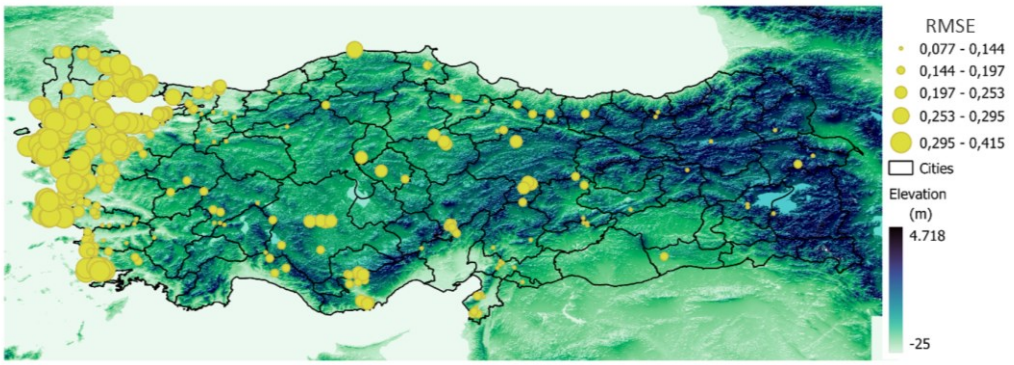



Figure 95 RMSE for all WPPs for train period

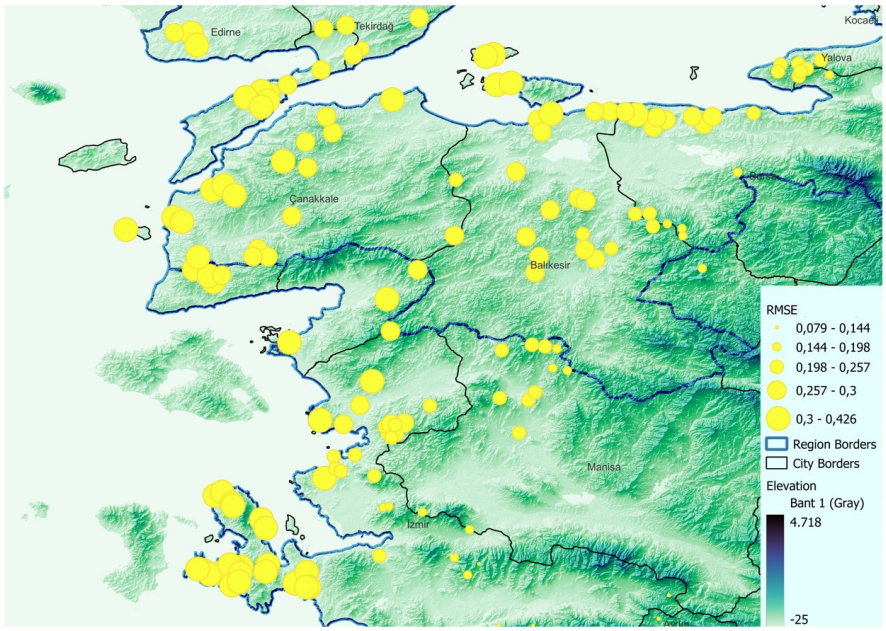



Figure 96 RMSE for Çanakkale, İzmir, Balıkesir cities

Bias is also calculated for all WPPs (Figure 97). Negative bias values can be seen in the internal parts of the Anatolia, Aegean, and Marmara regions. The same version of the RMSE is also illustrated in figure 98. As seen in the figure, negative and positive biases are close to each other. This might be because obtaining the closest grid for all WPPs may result in obtaining different grids for each WPP.

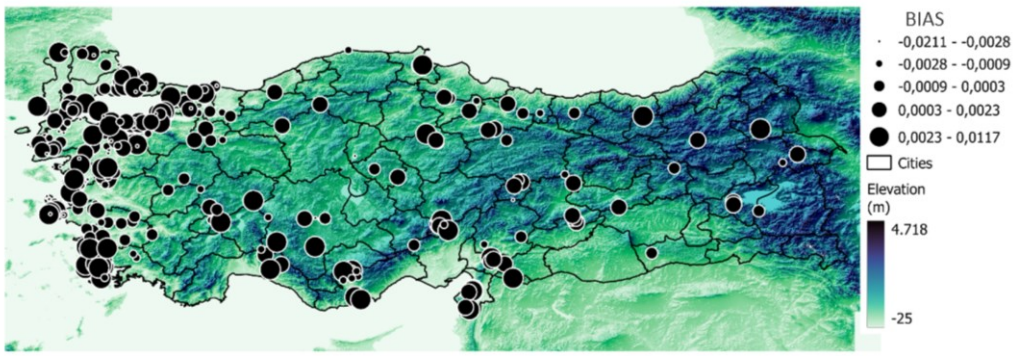



Figure 97 for all WPPs for train period

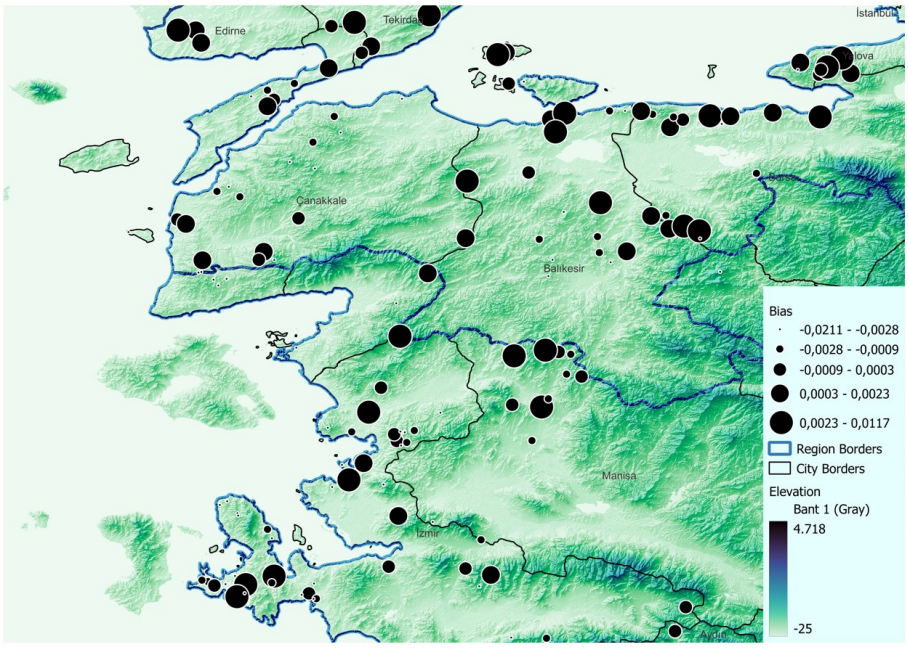



Figure 98 for Çanakkale, İzmir, Balıkesir cities

***Seasonal and Regional errors***

The overall performances of each WPP are also summarized in figure 99. High RMSE and SDE in the Aegean region WPPs may be associated with higher wind speeds. A couple of WPPs in the Mediterranean region have a correlation coefficient higher than 0.98.

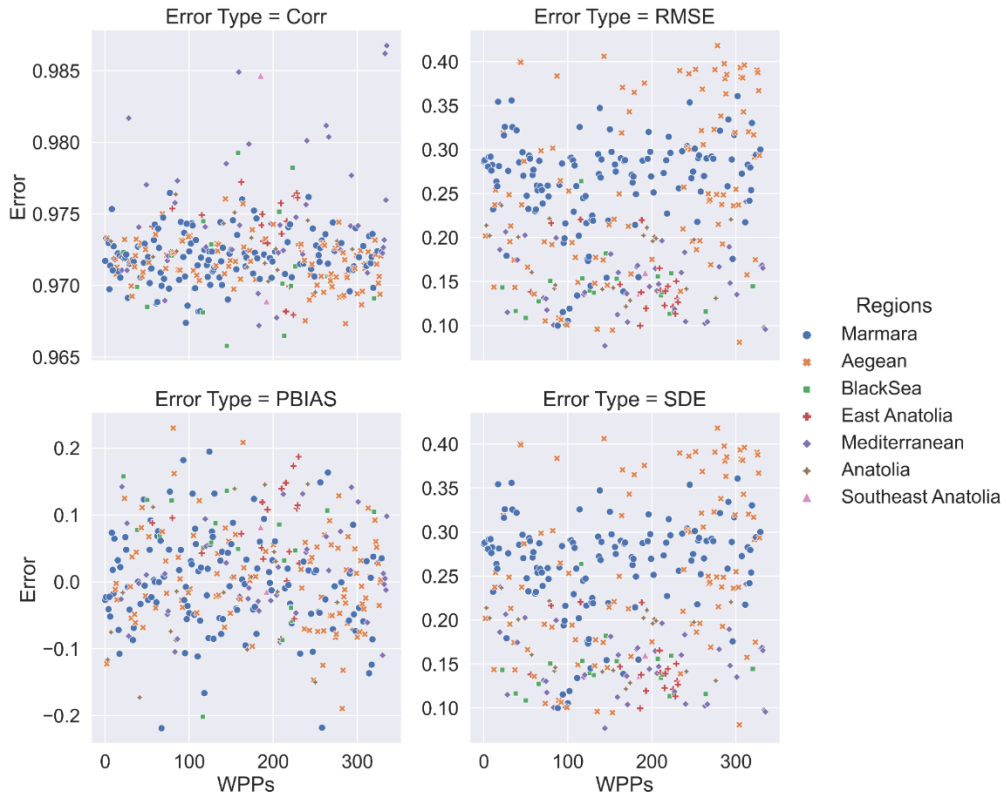



Figure 99 Train period errors of entire study area for each WPPs in terms of regions

Overall regional errors are also summarized in the Table-21.

Table 21 Averages of regional error for all WPPs

| **Regions** | **Corr** | **RMSE** | **Pbias** | **SDE** | **Number of WPPs** |
|---|---|---|---|---|---|
| Aegean | 0.971579 | 0.261683 | -0.02217 | 0.261635 | 102 |
| Anatolia | 0.971654 | 0.179702 | 0.000235 | 0.179677 | 21 |
| Black Sea | 0.971496 | 0.144124 | 0.016189 | 0.144113 | 20 |
| East Ant | 0.973432 | 0.147206 | 0.009362 | 0.1472 | 19 |
| Marmara | 0.971354 | 0.262021 | -0.0085 | 0.261995 | 125 |
| Mediterranean | 0.974885 | 0.150316 | 0.019304 | 0.150294 | 43 |
| Southeast Ant. | 0.976491 | 0.148821 | 0.025917 | 0.148802 | 2 |

RF prediction errors are also calculated in terms of seasons for each WPP (figure 100). Results indicated that the correlations are changed between 0.99-0.97 for the

winter season, 0.98-0.95 for the summer season, 0.98-0.96 for the spring season, and 0.98-0.965 for the fall season. RMSE and SDE are changed between 0.10-0.40. PBIAS is generally positive for the spring and fall seasons. However, most of the WPPs in the Marmara region and a few WPPs in the Aegean region showed negative PBIAS (%), which varies between -1-0.5 in the winter season. In summer, only a few WPPs have positive PBIAS from the Marmara, East Anatolia, and Black Sea regions.

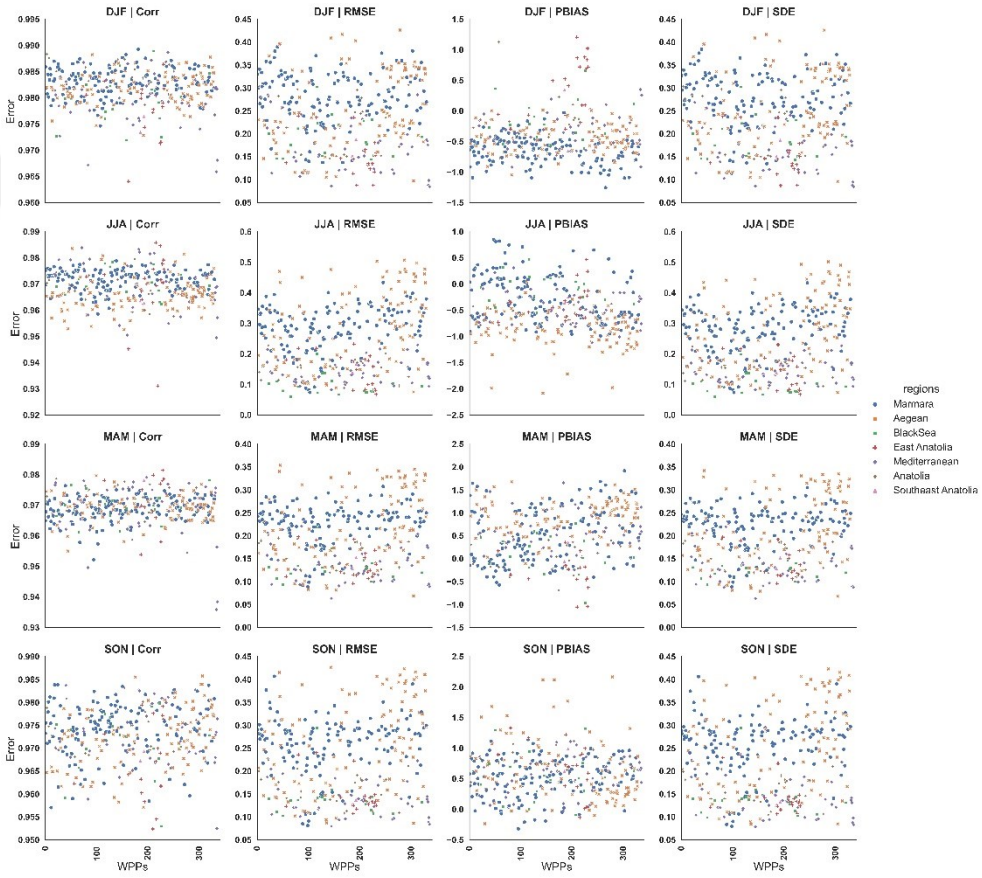



Figure 100 Regional and seasonal errors for RF predictions during the train period for each WPP, each point represents the each WPP and rows shows the seasons while the columns show the errors

#### 4.3.2.4 Time Series Analysis

Inter and intra-annual variability of wind speeds are analyzed in this part. The overall performance of RF predictions is evaluated in terms of regional averages in Figures 101 and 102, annually and monthly, respectively. ERA5 data is averaged for the entire Türkiye. There is no obvious change in the annual averages during the entire study period (1980-2100). However, the highest wind speeds are determined in the Aegean and the Marmara region, which have the highest number of WPPs located here. Black sea averages, outside of the ERA5 averages, have the lowest wind speeds. Inter-annual variability for all regions is similar to historical period variations.

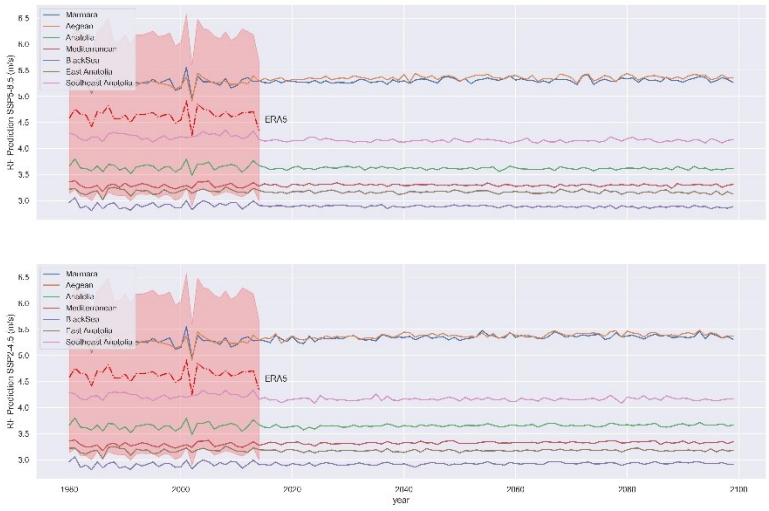



Figure 101 Annual average time series analysis for regional wind speed predictions during the entire period (shaded area shows the confidence interval related to ERA5 annual avarages with standard deviation)

Monthly variations of wind speeds associated with each wind power plant are also examined. In Figure 102, higher wind speeds in the summer and winter months in the Aegean and Marmara regions also exceed ERA5 averages. However, wind speeds of both the Marmara and the Aegean regions were around 5-6 m/s during the year. SPP2-4.5 and SSP5-8.5 showed similar results at annual and monthly average time scales.

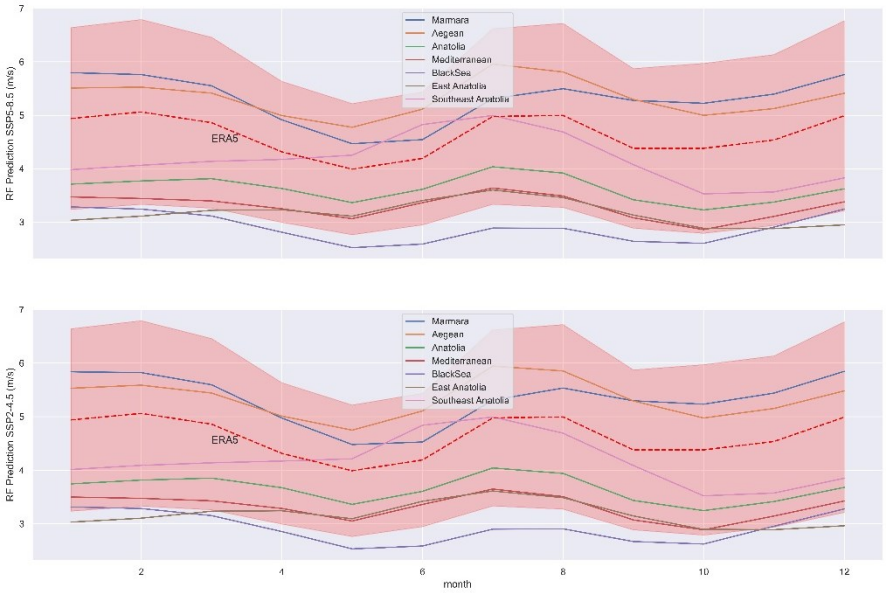



Figure 102 Monthly average time series analysis for regional wind speed predictions during the entire period (shaded areas shows the confidence interval with standard deviation) with ERA5 entire period averages

#### 4.3.2.5 Projected changes in the wind speeds for each WPP in Türkiye

Since the RF predictions showed better results with all 27 GCMs, changes in the wind speeds for each WPP are compared with the reference period ERA5 data. Figure 103 and 104 shows those changes during the 21$^{st}$ century for two different scenarios. WPPs in the Marmara region have positive changes in April, May, June, July, and August at three terms. Especially in April, June, and September, the change is greater than +5 %. WPPs in the Aegean region also have similar changes with the Marmara region except for negative changes up to -5 % in July and August months for three terms. Decreasing changes are determined in the winter months (Dec, Jan, Feb.) for all regions except from the East Anatolia region, where there are increasing wind speeds nearly reach % 5. However, the magnitude of the negative changes is smaller than the positive changes.

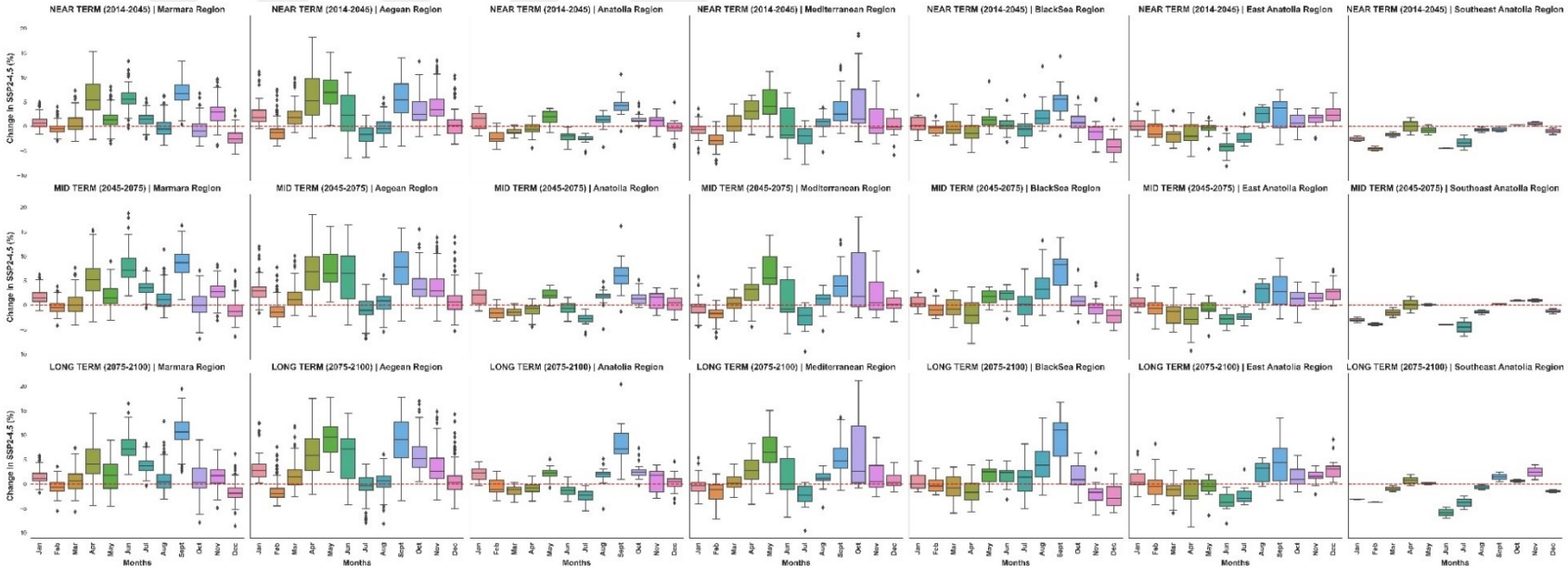



Figure 103 Changes in the wind speed (%) between RF predictions and ERA5 reference data for three period at SSP2-4.5 scenario: each boxplot includes WPPs, columns show the geographical regions while the rows show the near-term (2014-2045), mid-term (2045-2075), long-term (2075-2100) average differences from the reference data.

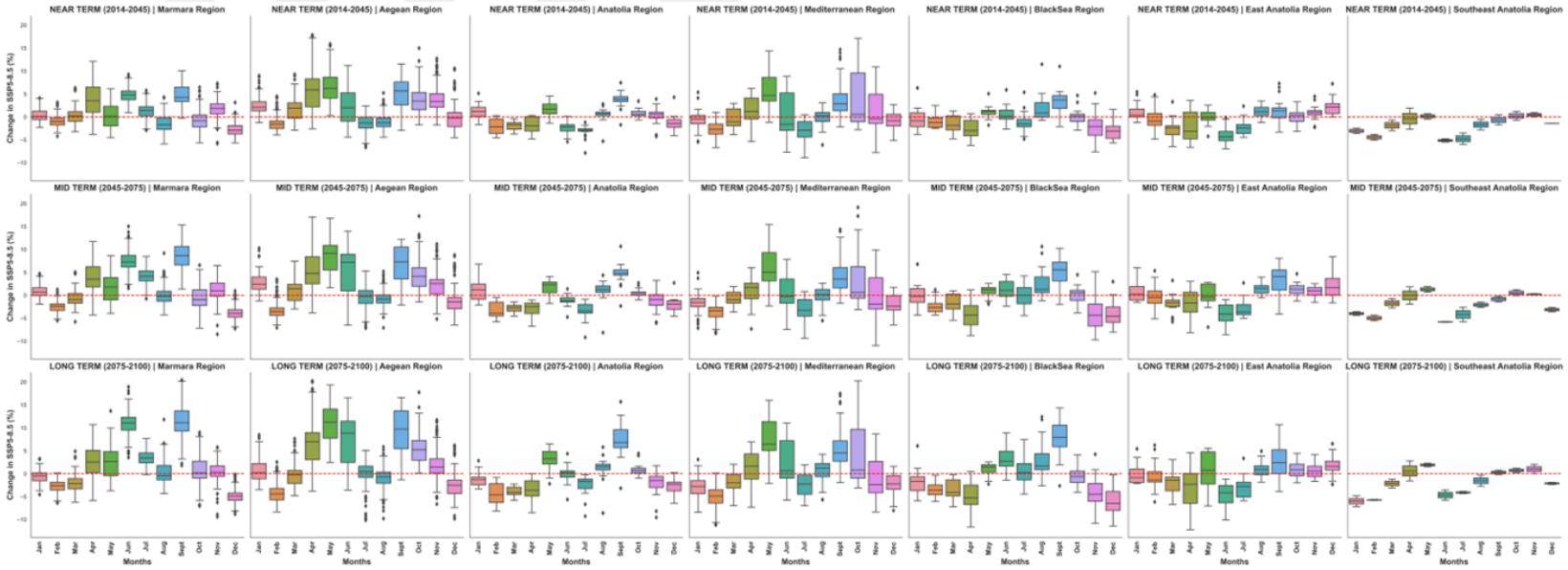



Figure 104 Same as figure 103 but for SSP5-8.5 scenario

Individual GCMs are also evaluated in terms of Mann-Kendall trends for historical SSP2-4.5 and SSP5-8.5 scenarios (fig.105). Most of the GCMs resulted in no significant trend. However, during the historical period, 20% of 27 GCM models have a decreasing trend for Anatolia and Mediterranean regions. % 20 of the models have an increasing trend for the SSP2-4.5 scenario, and the same percentage is valid for the decreasing trends in the SSP5-8.5 scenario.

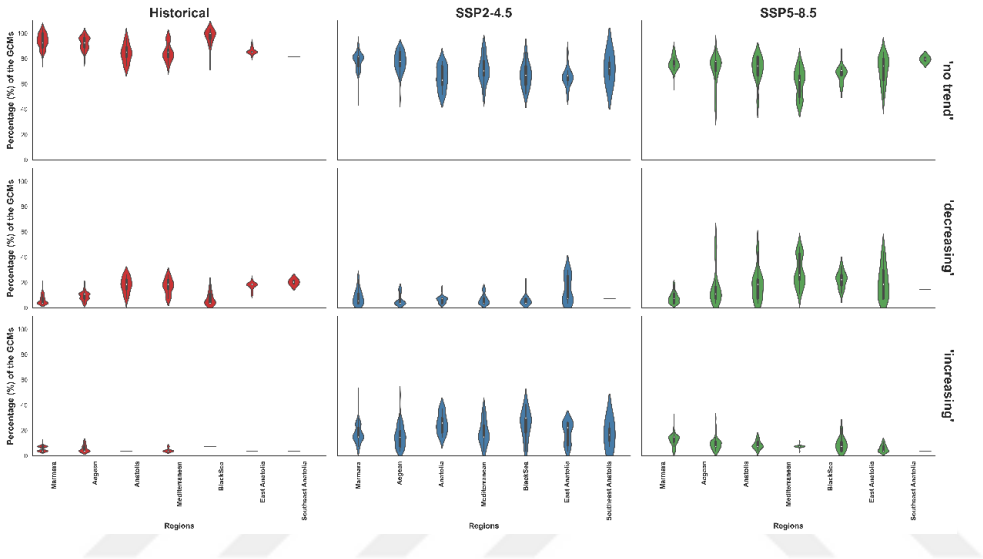



Figure 105 Trend results for scenarios and historical periods in terms of number of significant trends (p value < 0.05) and “no trends” for percentage of GCMs among 27 GCMs

WPD for each CMIP6 Model is also calculated for SSP5-8.5 future projections by separating the entire time series into three terms (near [2014-2045], mid [2045-2075], long [2075-2100] term) and illustrated in Figure 106 and 107 as two parts ( first 13 GCM are shown in Figure 106 and the last 14 GCM are shown in Figure 107) together with ERA5 data in the historical period.

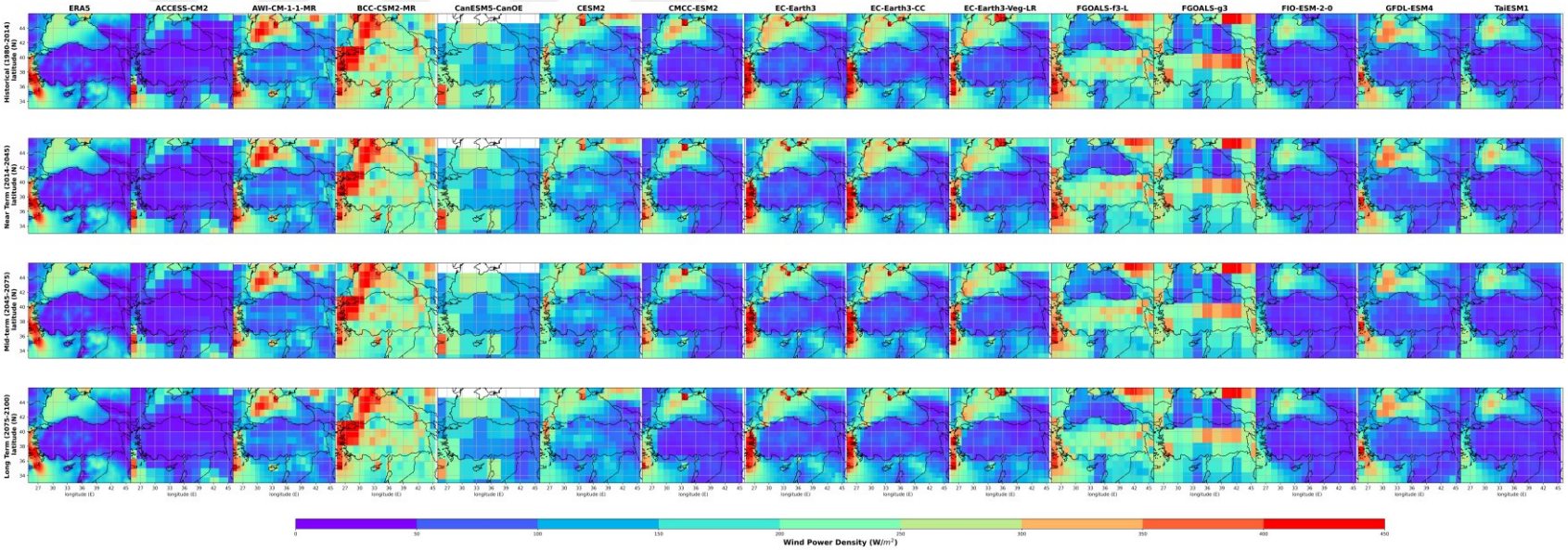



Figure 106 Wind power densities (W/m$^2$) at 100 m for 14 CMIP6 models in the Table-9, together with SSP5-8.5 scenario (Part-1)

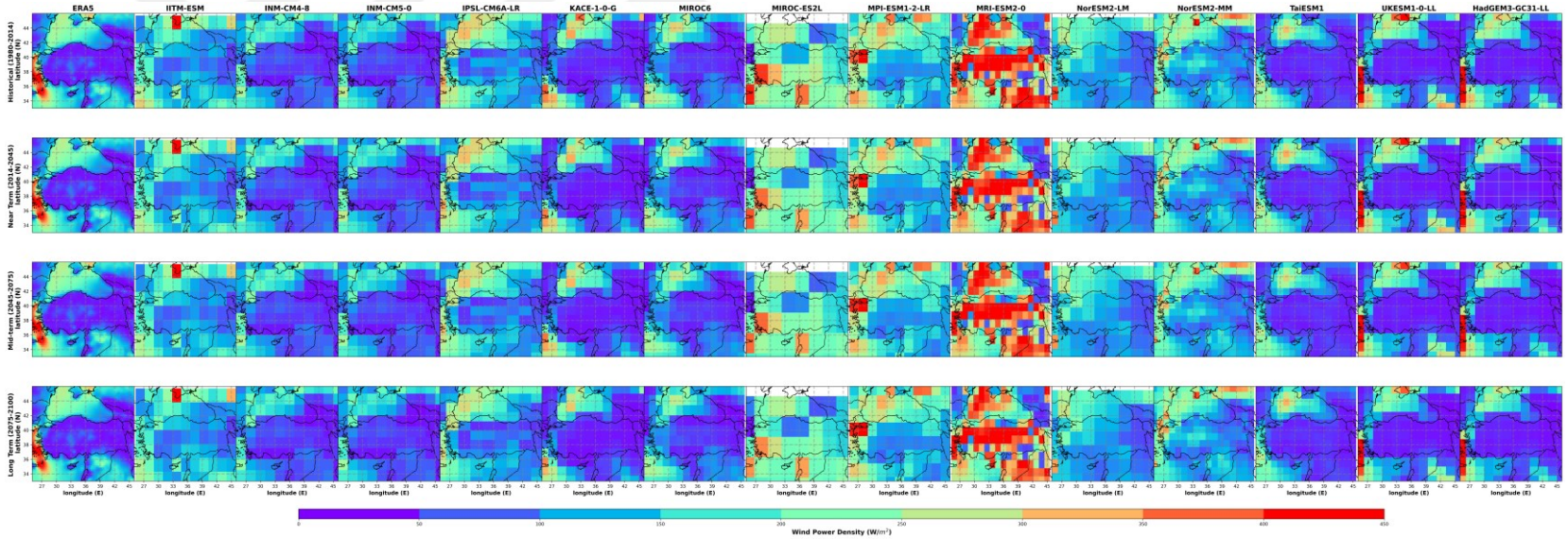



Figure 107 Wind power densities ($W/m^2$) at 100 m for 14 CMIP6 models in the table-9, together with SSP5-8.5 scenario (Part-2)

## 4.4 Mesoscale Model Output Analysis Results

WRF-PGW model wind speed outputs are analyzed in this part of the study. Model performances are evaluated by using observation data and WRF-ERA5 outputs during the reference period (1995-2014). The following parameters are obtained from WRF outputs: pressure, surface pressure, relative humidity, Temperature, u and v components of wind with ETA levels and 10 m.a.g.l.

### 4.4.1 Model performances

#### 4.4.1.1 Historical Period (1994-2014)

Wind climatology during the historical period is illustrated in figure 108 by using monthly averages from each GCM and WRF-ERA5 model for the 1995-2014 period. These GCMs are used in the ensemble projection that is conducted by WRF-PGW. Higher wind speeds blow from northern, western parts of the Aegean Sea to the southeast, while the Marmara and northern Aegean regions get the northeasterly winds for most models. Wind directions of GCMs are also parallel with the WRF-ERA5 results. The wind direction in the internal parts of the Türkiye is not the same for all models and regions. However, wind direction in the BCC-CSM-MR and FGOALS-F3l models over the Black Sea mostly blows from the eastern, while the other models agreed on the northeasterly winds.

Due to terrain complexity, the wind is distributed in different parts of the onshore parts. This complexity is evident in the WRF-ERA5, where the model's spatial resolution has the highest (4 km).

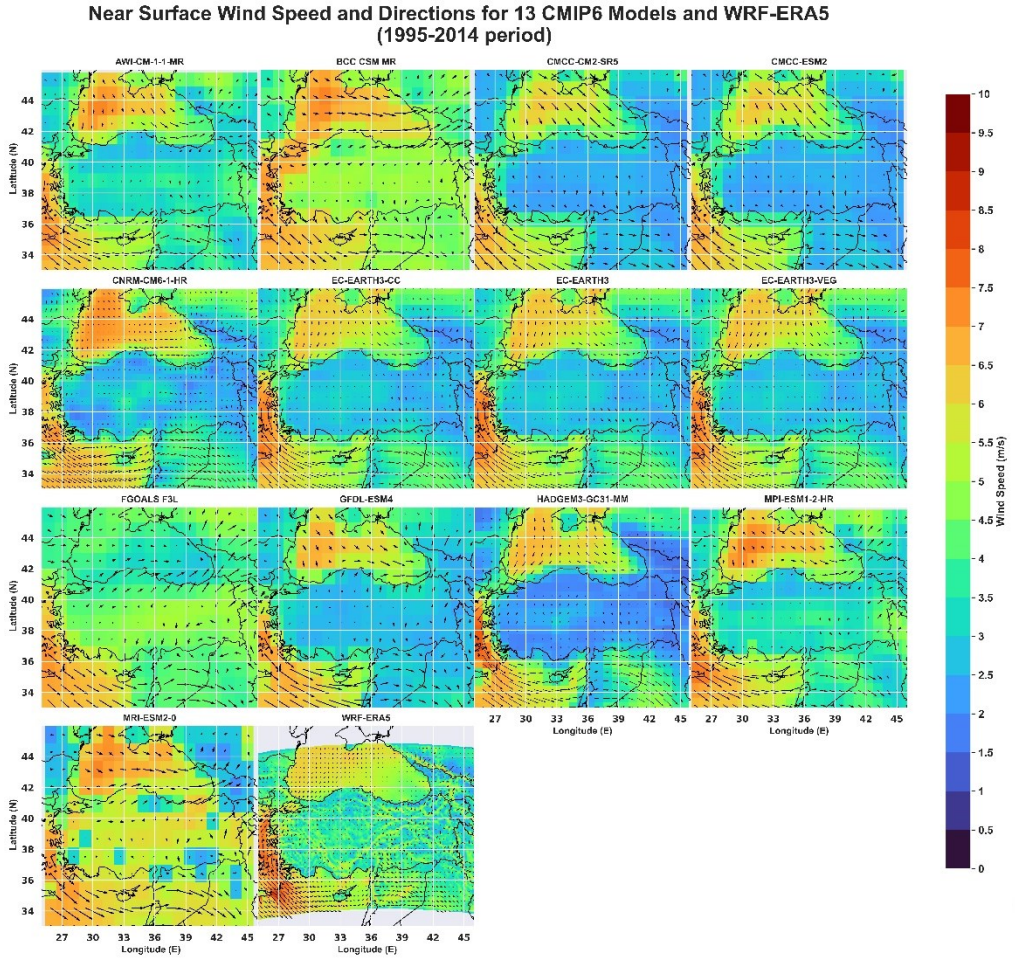



Figure 108 Wind speed and direction of 13 GCMs and WRF-ERA5

Mesoscale model performances are examined with the re-analysis and observation data during the available period (1995-2014) for WRF-ERA5 (Figure 109). Observation data is interpolated by using the IDW interpolation method in QGIS at 4 km horizontal resolution. While REPA [74], data is only available at long-term average time scales, it is also added to better comprehend the spatial relationships between REPA and WRF's high-resolution wind speed data. However, it should also be considered that REPA data has a 100 m horizontal resolution, and the results are at 100 m.a.g.l. However, higher wind speeds in the Taurus mountains and Eastern Black Sea are similar to WRF-ERA5. A more detailed demonstration of REPA and WRF is given in Figure 110. The WRF-ERA5 outputs in the figure are obtained from 2nd level of the model (approximately 80 m.a.g.l), where the higher wind speeds in the mountain regions are more obvious and the wind speeds are very smilar to each

other. It should also be considered that the REPA data is converted from pdf [74] to tiff by using georeferencing tools in QGIS and re-colored. The results also showed that MERRA2 and WRF results in historical and projection periods show overestimation comparing to observation and ERA5 reanalysis.However, it is also obtained that CMIP6 models have overestimations with the observations in the previous results.

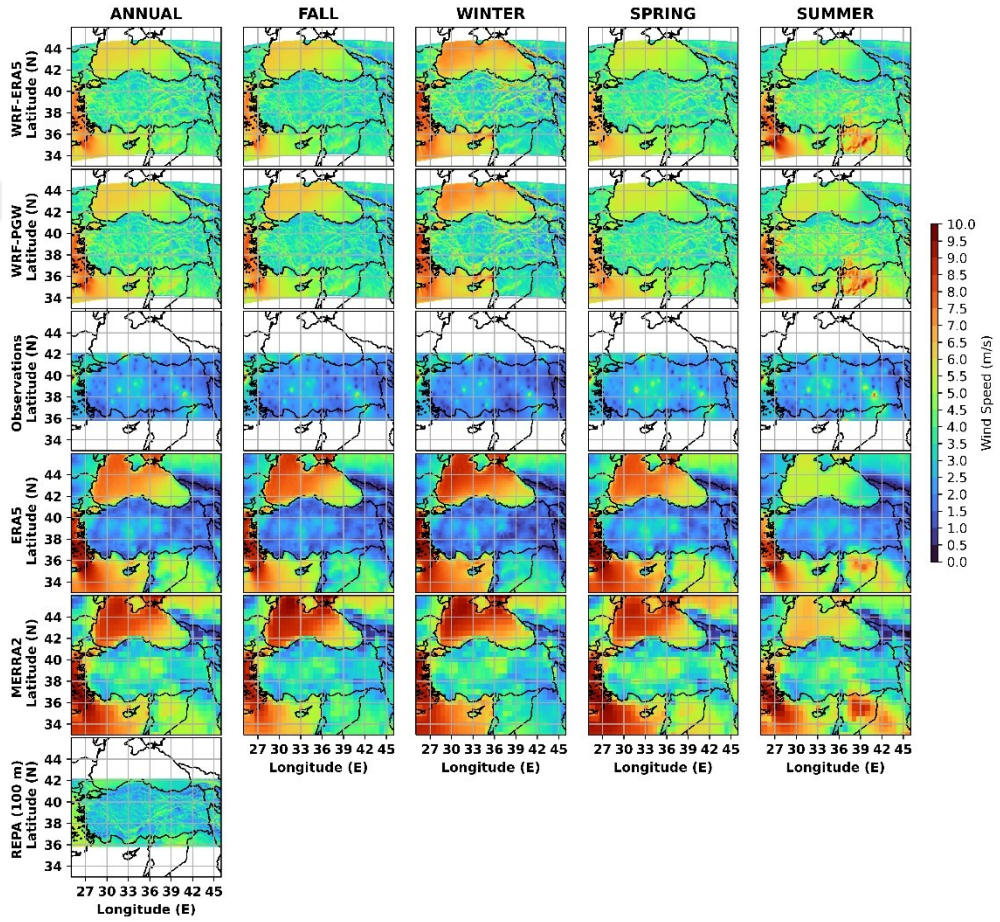



Figure 109 WRF and reference data comparisons at seasonal and annual scale

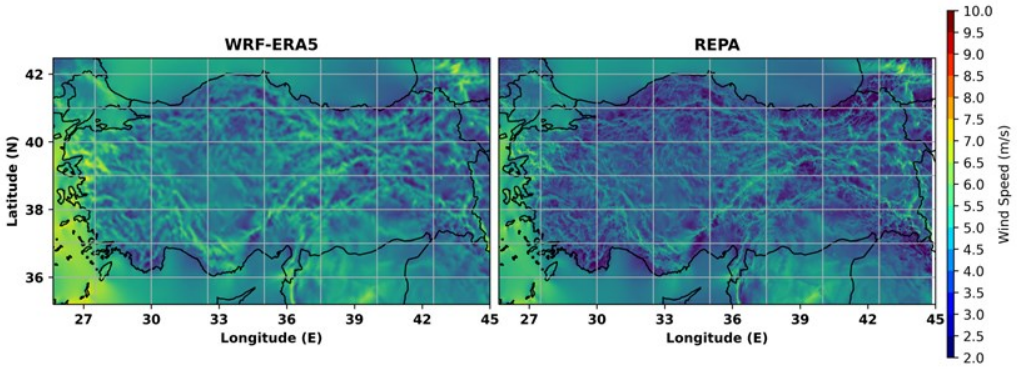



Figure 110 Detailed illustration of REPA [74], (100 m) and WRF-ERA5 (80 m.a.g.l) data

For each observation station, the nearest WRF grids are obtained from WRF-ERA5 data to calculate the error statistics. The heights above the sea level for both WRF grids and observation stations are illustrated in Figure 111 in order to evaluate the representativeness of WRF grids with the observations. Station elevations match appropriately with the topographic map provided at background.

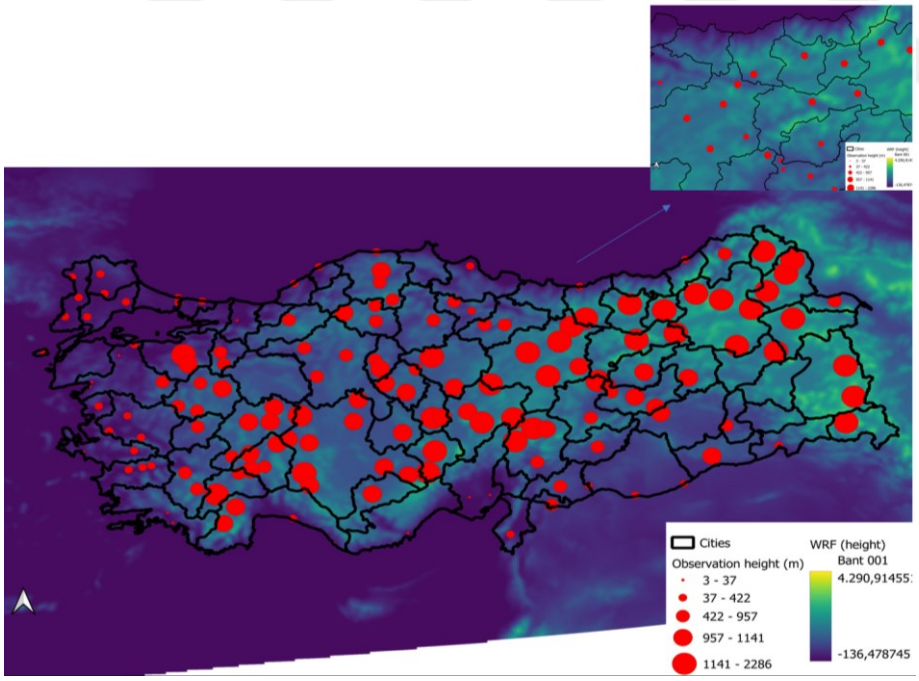



Figure 111 WRF topography and observation station heights (m.a.g.l.)

Taylor diagrams are also generated for all ensemble member CMIP6 models, ERA5 and MERRA2, and WRF-ERA5. Regional performances of each model and WRF-

ERA5 are illustrated in Figure 112. The grey dot representing WRF-ERA5 in the graph is closer to observations for all regions.

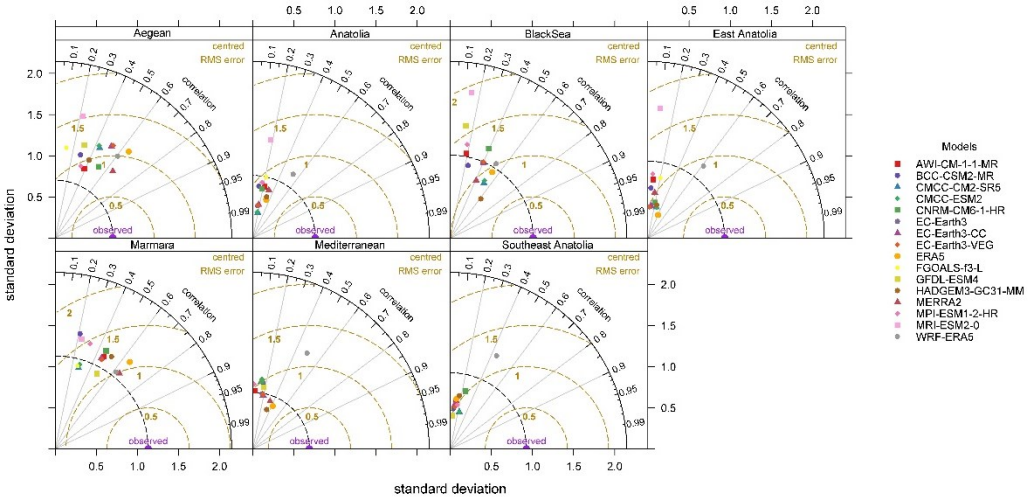



Figure 112 Regional Taylor Diagrams for between CMIP6 Models, WRF-ERA5, and two reanalysis data (MERAA2 and ERA5)

Heat maps (Figure 113) are generated by using the closest grid from all CMIP6 models and WRF-ERA5 to the observations for the historical period. ERA5 and MERRA2 are also included in the analysis to compare all models together. WRF-ERA5 and ERA5 have the lowest SDE (0.50-0.25). ERA5 and HADGEM3-GC31-MM have the lowest RMSE, and the highest correlations are determined for ERA5, MERRA2, and WRF-ERA5. PBIAS is lower for ERA5.

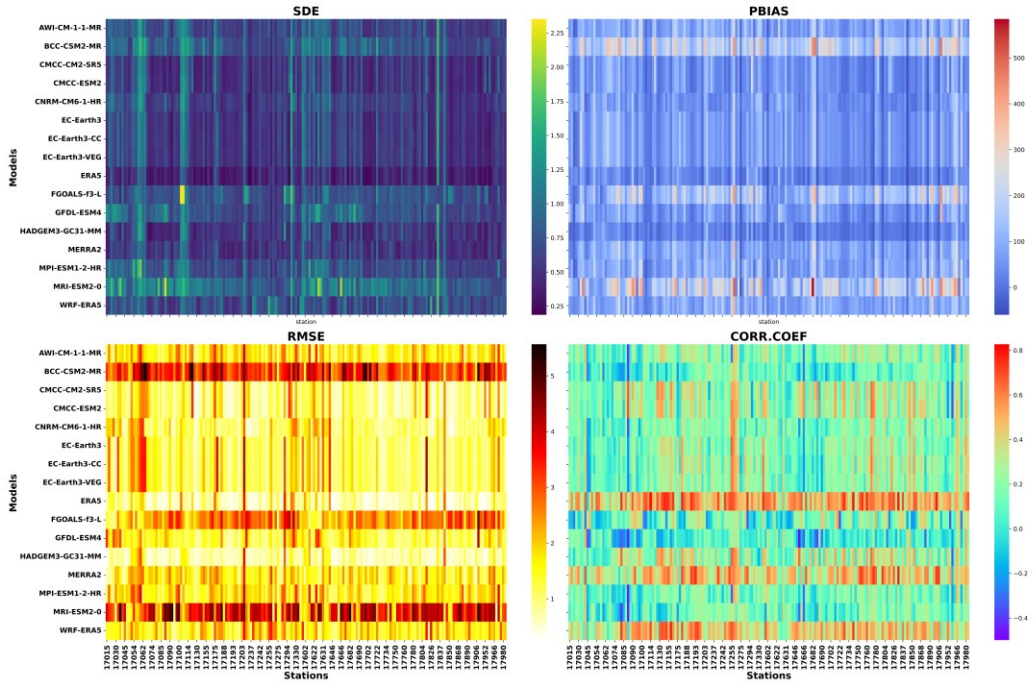



Figure 113 Error heatmaps prepared for CMIP6 Models, MERRA2, ERA5, WRF-ERA5 through and observation stations

Overall regional error results are given in Table 22. High RMSE, PBIAS, and SDE are determined in the Aegean, Mediterranean, and Southeast Anatolia Regions. The highest RMSE, SDE, and PBIAS are determined in the Mediterranean Region. Correlation coefficients are changed from 0.49 to 0.61. East Anatolia has the highest correlations.

Table 22 Statistical error metrics calculated for the closest WRF-ERA5 grid points

| **Regions** | **WRF-ERA5 Prediction Errors with Observations** | | | |
|---|---|---|---|---|
| | **RMSE** | **PBIAS** | **SDE** | **Corr.** |
| Aegean | 2.09 | 96.89 | 1.07 | 0.59 |
| Anatolia | 1.56 | 63.73 | 0.89 | 0.51 |
| Black Sea | 1.76 | 71.77 | 1.08 | 0.52 |
| East Anatolia | 1.51 | 65.16 | 0.97 | 0.61 |
| Marmara | 2.00 | 66.81 | 1.11 | 0.59 |
| Mediterranean | 2.27 | 108.03 | 1.27 | 0.51 |
| Southeast Anatolia | 2.21 | 93.63 | 1.21 | 0.49 |

The same computations are also made done for the regional-seasonal classifications and are given in Table 23. Winter season in the Mediterranean region has the highest errors with relatively low correlations. East Anatolia and Anatolia regions have lower errors during the spring season. The lowest correlations can be seen in Anatolia (0.45) during the winter season and in the Southeast Anatolia region during the summer (0.37) and spring (0.40) seasons. Marmara region has the highest correlations in the fall (077) and spring (0.74) seasons. High errors in the Southeast Anatolia region can also be related to a low number of observation stations.

Table 23 Statistical error metrics with observations and closest WRF-ERA5 grid points

| Regions | SEASON | WRF-ERA5 Prediction Errors with Observations | | | |
|---|---|---|---|---|---|
| | | RMSE | PBIAS | SDE | Corr |
| Aegean | DJF | 2.17 | 94.55 | 1.32 | 0.54 |
| | JJA | 2.31 | 101.09 | 1.04 | 0.61 |
| | MAM | 1.82 | 87.11 | 0.75 | 0.60 |
| | SON | 1.96 | 107.56 | 0.80 | 0.68 |
| Anatolia | DJF | 1.66 | 61.40 | 1.18 | 0.45 |
| | JJA | 1.73 | 68.75 | 0.79 | 0.50 |
| | MAM | 1.36 | 54.73 | 0.58 | 0.62 |
| | SON | 1.40 | 73.42 | 0.53 | 0.65 |
| BlackSea | DJF | 2.04 | 71.94 | 1.42 | 0.49 |
| | JJA | 1.64 | 73.58 | 0.81 | 0.50 |
| | MAM | 1.50 | 67.52 | 0.75 | 0.57 |
| | SON | 1.58 | 73.98 | 0.82 | 0.64 |
| East Anatolia | DJF | 1.69 | 70.25 | 1.30 | 0.47 |
| | JJA | 1.61 | 67.01 | 0.74 | 0.78 |
| | MAM | 1.23 | 50.52 | 0.66 | 0.60 |
| | SON | 1.33 | 72.64 | 0.64 | 0.71 |
| Marmara | DJF | 2.22 | 61.75 | 1.53 | 0.49 |
| | JJA | 1.99 | 72.91 | 0.83 | 0.69 |
| | MAM | 1.66 | 62.63 | 0.69 | 0.73 |
| | SON | 1.88 | 74.84 | 0.72 | 0.77 |
| Mediterranean | DJF | 2.63 | 119.21 | 1.73 | 0.46 |
| | JJA | 2.24 | 99.60 | 1.03 | 0.62 |
| | MAM | 1.90 | 91.59 | 0.82 | 0.49 |
| | SON | 1.94 | 117.27 | 0.74 | 0.60 |
| Southeast Anatolia | DJF | 2.09 | 84.00 | 1.40 | 0.47 |
| | JJA | 2.90 | 112.06 | 1.12 | 0.35 |
| | MAM | 1.80 | 77.31 | 0.83 | 0.40 |
| | SON | 1.98 | 106.39 | 0.83 | 0.55 |

#### 4.4.1.2 Future Period (2080-2100)

Wind climatology for near-surface wind speeds is also illustrated in figure 115 for the future period. The distribution of wind direction and magnitude of the wind speed is similar to the historical period (see fig.108). Existing differences between those periods are smoothed by taking the long-term means of the magnitude. However, in the following analysis, those differences are also examined.

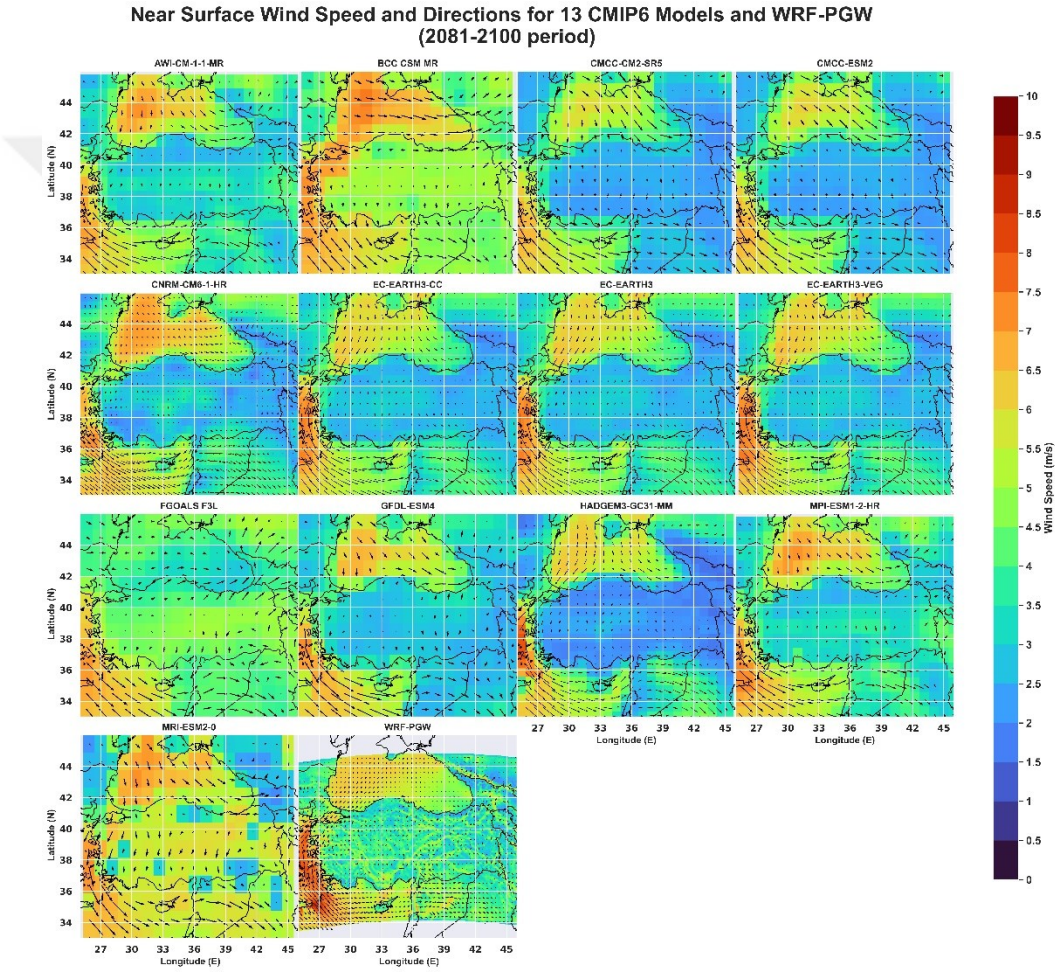



Figure 114 Wind speed and direction of 13 GCMs and WRF-PGW

The results are also compared with 13 CMIP6 models by calculating the ensemble mean of the models with CDO [249]. Figure 115 shows those ensembles' seasonal and annual average results and future estimates from WRF. For those calculations, each CMIP6 model is regrided to the coarse model resolution, which is 1.250x10.

Therefore, the success of the dynamical downscaling is obvious in the figure where the smooth wind speeds are distributed in the CMIP6 ensembles, and the detailed distribution of wind speeds can be seen in the WRF-PGW. Seasonality is similar but higher in the WRF-PGW.

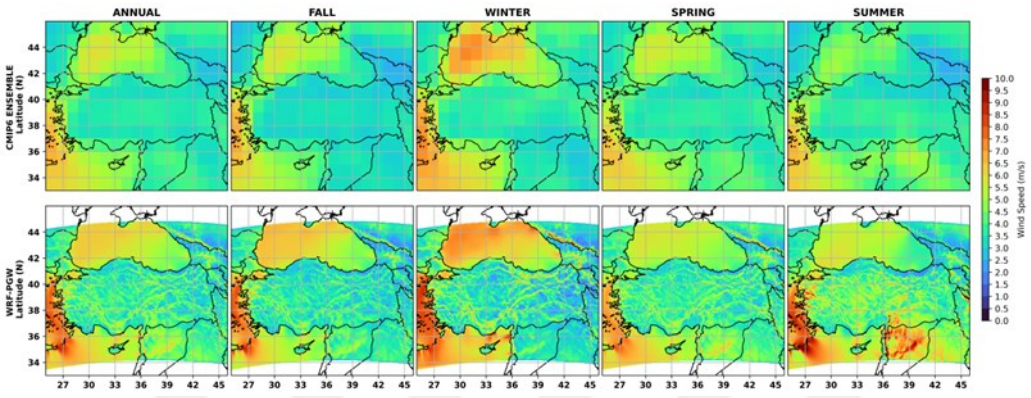



Figure 115 Annual and seasonal averages for future period for WRF-PGW and CMIP6 ensembles with 13 GCMs.

CDO seasonal multi-year variance and standard deviation analysis are used to determine multi-year variability in wind speeds [249]. Figure 116 and Figure 117 demonstrate the variance and standard deviation, respectively. As it can be understood from the figures, the CMIP6 ensemble mean has a very small variance for all seasons and annuals. However, WRF-PGW has high variance and standard deviation, particularly in winter and annual over the seas.

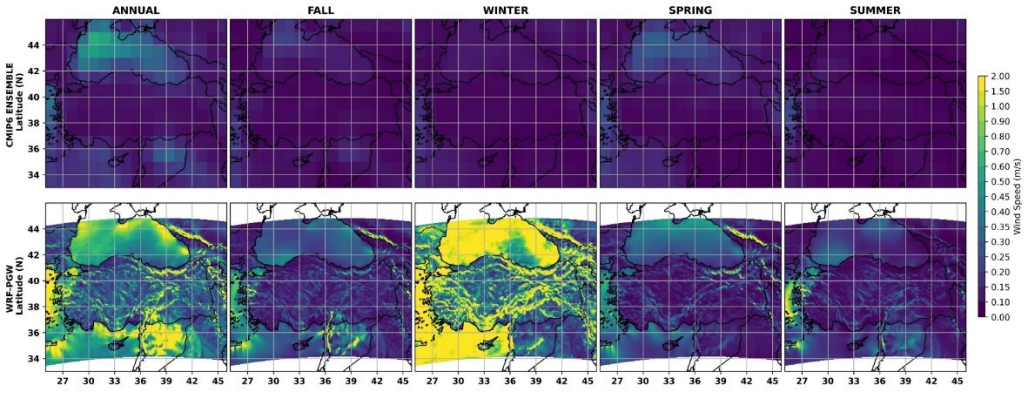



Figure 116 Annual and seasonal variability (variance) during the future period for WRF-PGW and CMIP6 ensembles with 13 GCMs.

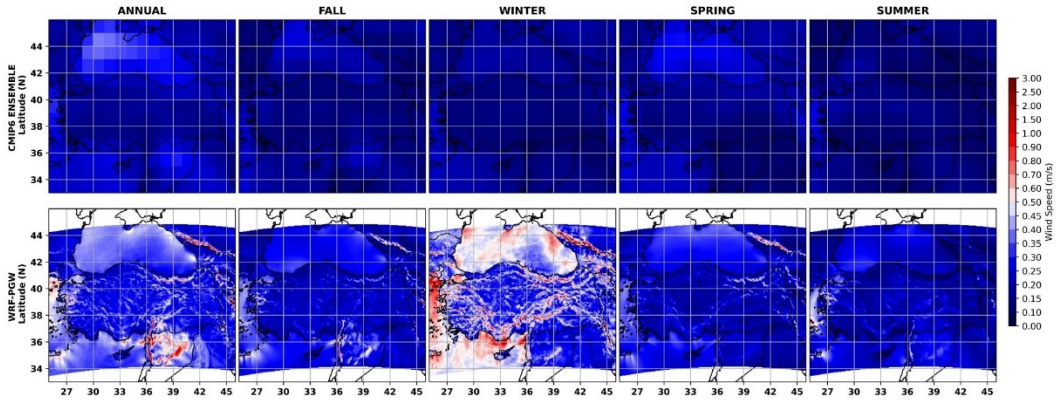



Figure 117 Annual and seasonal standart deviation for future period for WRF-PGW and CMIP6 ensembles with 13 GCMs.

### 4.4.2 Calculation of Wind Speeds at Hub heights

Since vertical levels of the WRF is terrain following [77], the heights of the ETA levels above the ground level are calculated by using perturbation heights to obtain wind speeds at the wind turbine's hub height. The height of each level is calculated by using the equation (26) [267] for a sample WRF output file where the "PH" is geopotantial perturbation ($m^2/s^2$) and "PHB" is the geopotantial ($m^2/s^2$) and "g" is the gravitational constant (9.81 $m/s^2$).

$$\text{Height above the ground (m)} = \frac{\text{PH} + \text{PHB}}{g} - \text{Terrain Height} \quad (26)$$

Based on these results, first, three levels' height above the ground level is found to be approximately 25, 81, and 152 m.a.g.l. The results are given in Figures 118, 119, and 120, respectively.

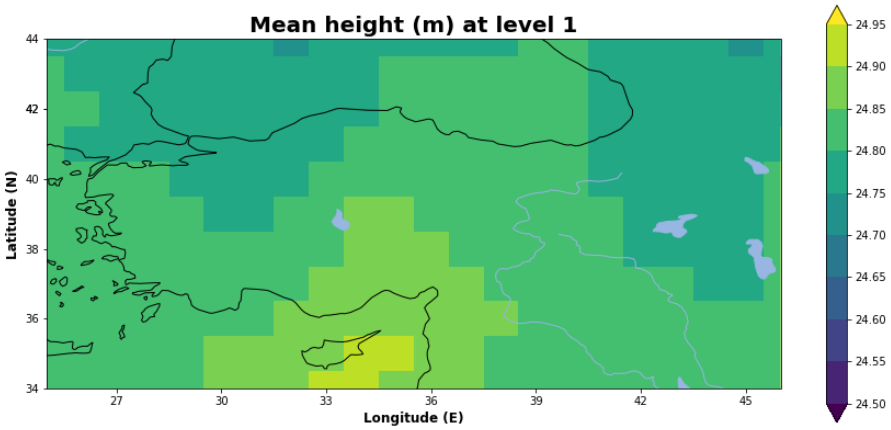



Figure 118 Mean height (m) at level-1 (bottom_top=0)

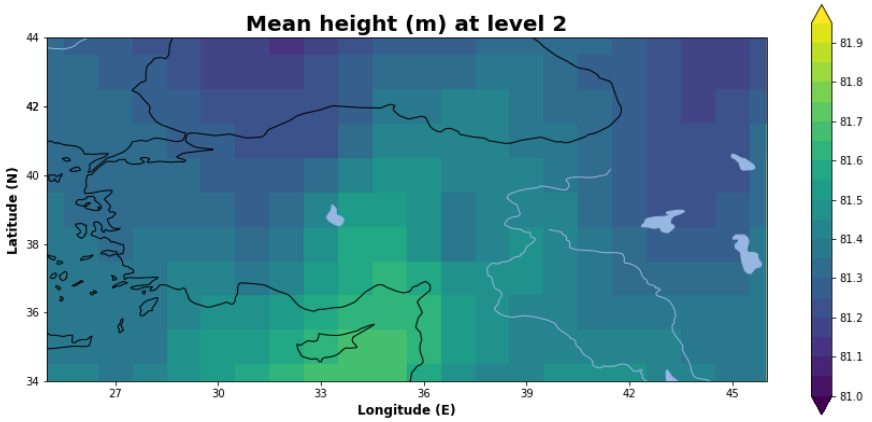



Figure 119 Mean height (m) at level-2 (bottom_top=1)

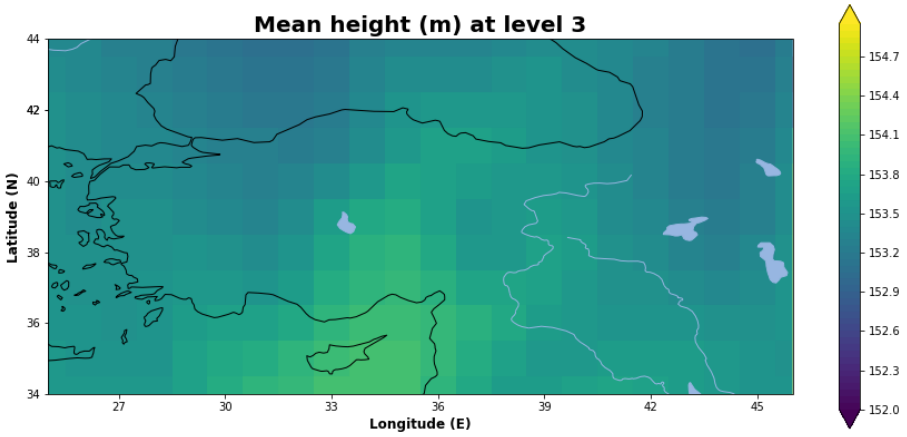



Figure 120 Mean height (m) at level 3 (bottom_top=2)

Therefore, wind speeds in the 2nd level are used to obtain wind resources at turbine hub height (Figure 121). Wind power density (figure 123) is also calculated at level 2 (approximately 80 m.a.g.l.) by calculating air density from equaion 22 (figure 122) with pressure and temperature at the same level (see equation 21).

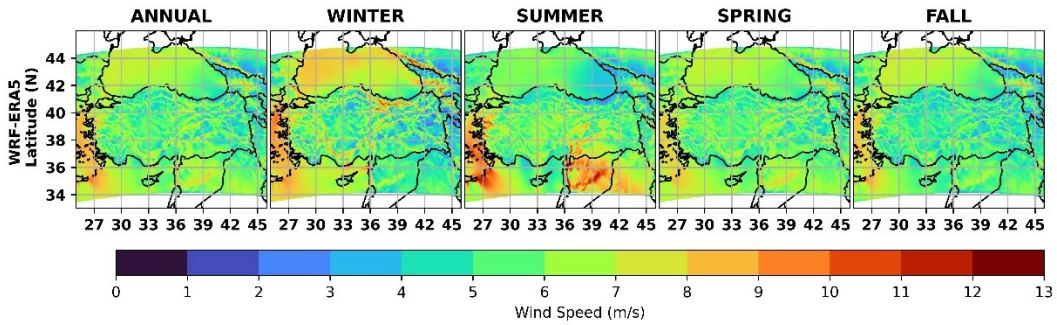



Figure 121 Wind Speeds at 80 m for seasonal time scale (1995-2014)

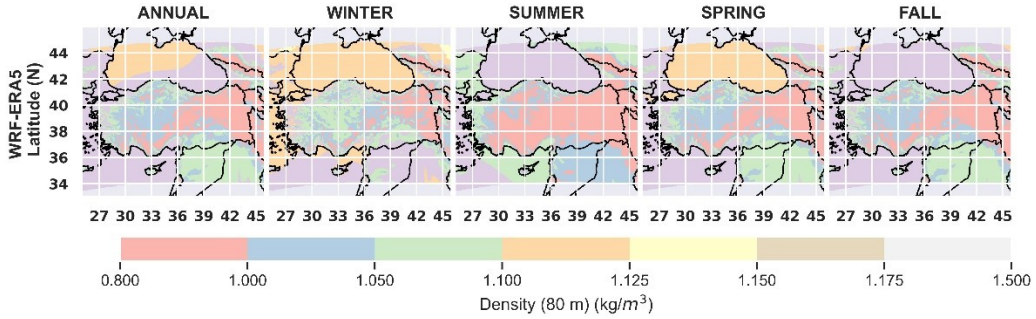



Figure 122 Air density at 80 m for seasonal time scale (1995-2014)

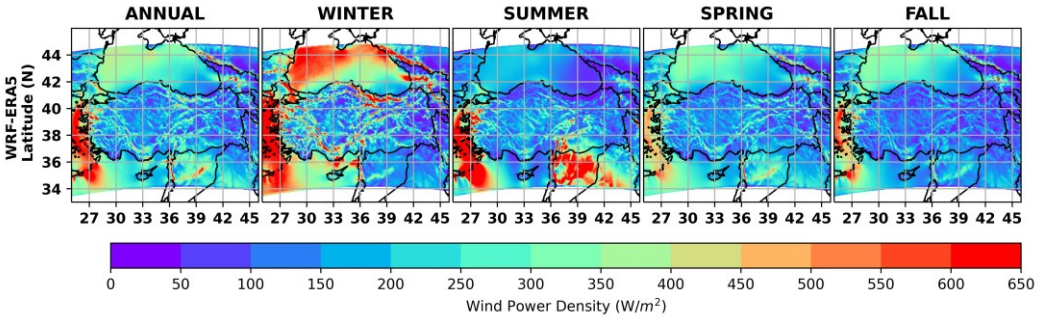



Figure 123 Wind power density at 80 m for seasonal time scale (1995-2014)

### 4.4.3 Inter-annual changes during the historical wind resource

Inter-annual wind resource evaluations are done by using the same monthly average data at 80 m.a.g.l. Figure 124 shows how the wind speed averages can be changed from year to year. As seen in the figure, some years have lower wind speeds than others. For example, while 2012 has generally higher wind speeds than 2014, 2011 shows the lowest winds overall.

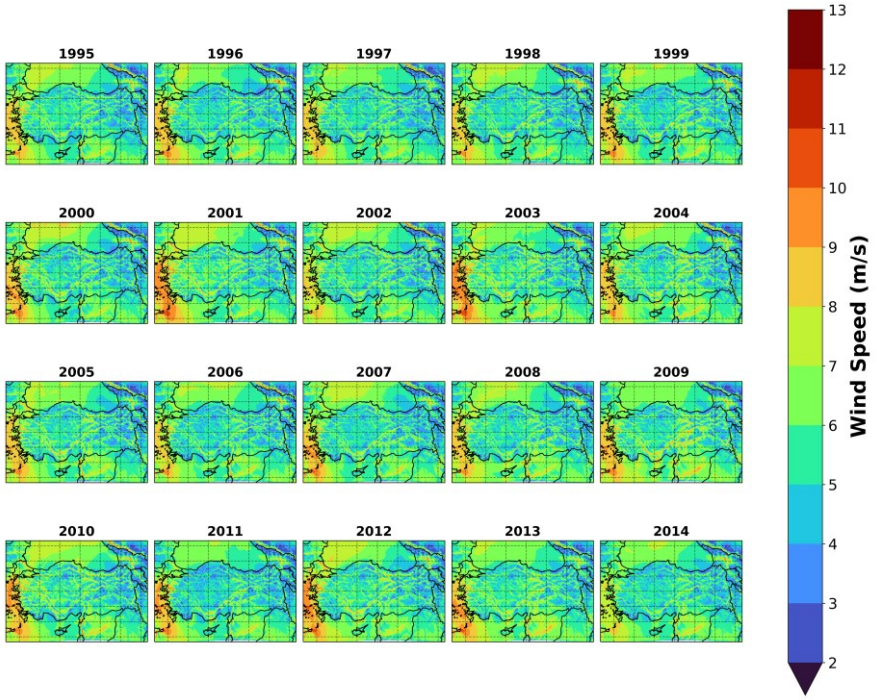



Figure 124 Annual mean wind speeds at 80 m

Annual statistical statistics are also prepared in terms of standard deviation (Figure 125) and variance (Figure 126) due to the difficulty in comprehending variations in wind speed. These results can give an idea of how wind speeds change yearly. The highest wind speed variability was seen in 2002,2003,2010,2012. The lowest wind speeds for 1995,1996,2013,2014 years are associated with low electricity production from wind. The locality of this variability is also shown in these figures.

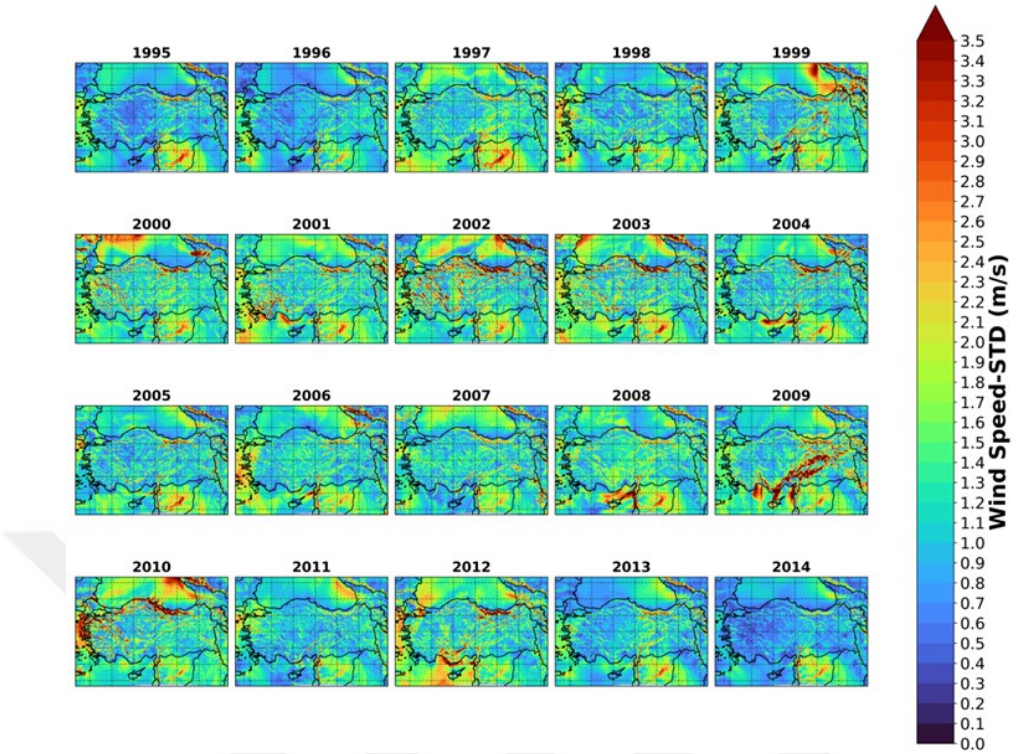



Figure 125 Annual standard deviation of monthly wind speed data at 80 m

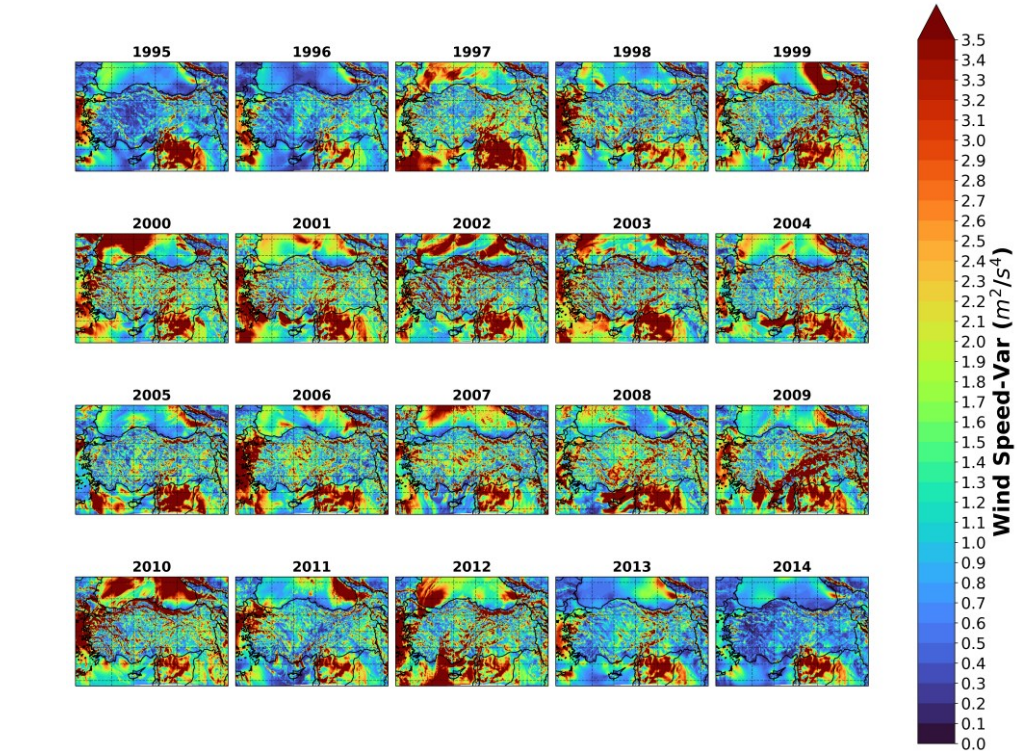



Figure 126 Annual variability (variance) of monthly wind speed data at 80 m

The same calculations are done for the wind power density and its average values, standard deviations, and variances are shown in figures 127, 128, and 129, respectively. Because it uses a cube of the wind speed, wind power density has the advantage that the change is more noticeable than wind speeds.

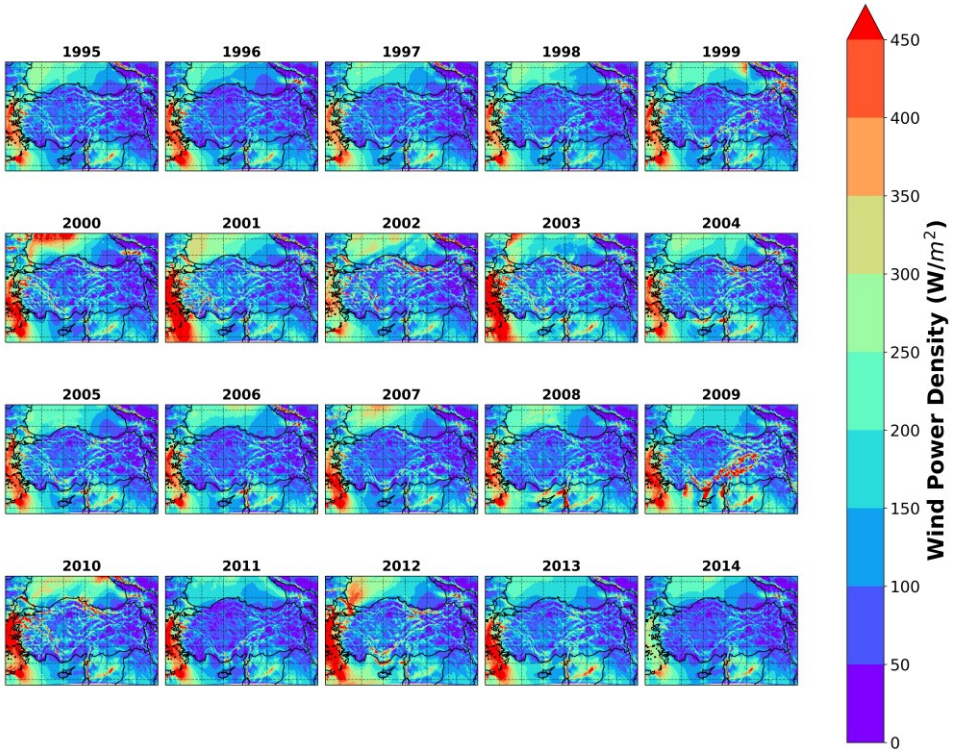



Figure 127 Annual mean wind power density at 80 m

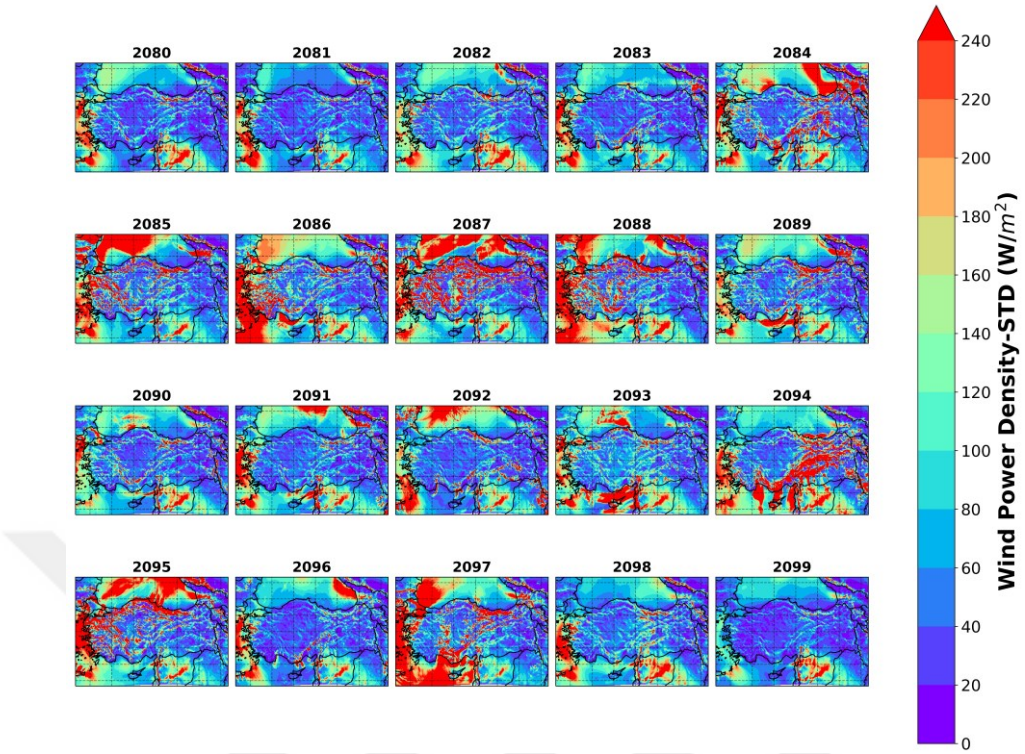



Figure 128 Annual standart deviation of monthly WPD at 80 m

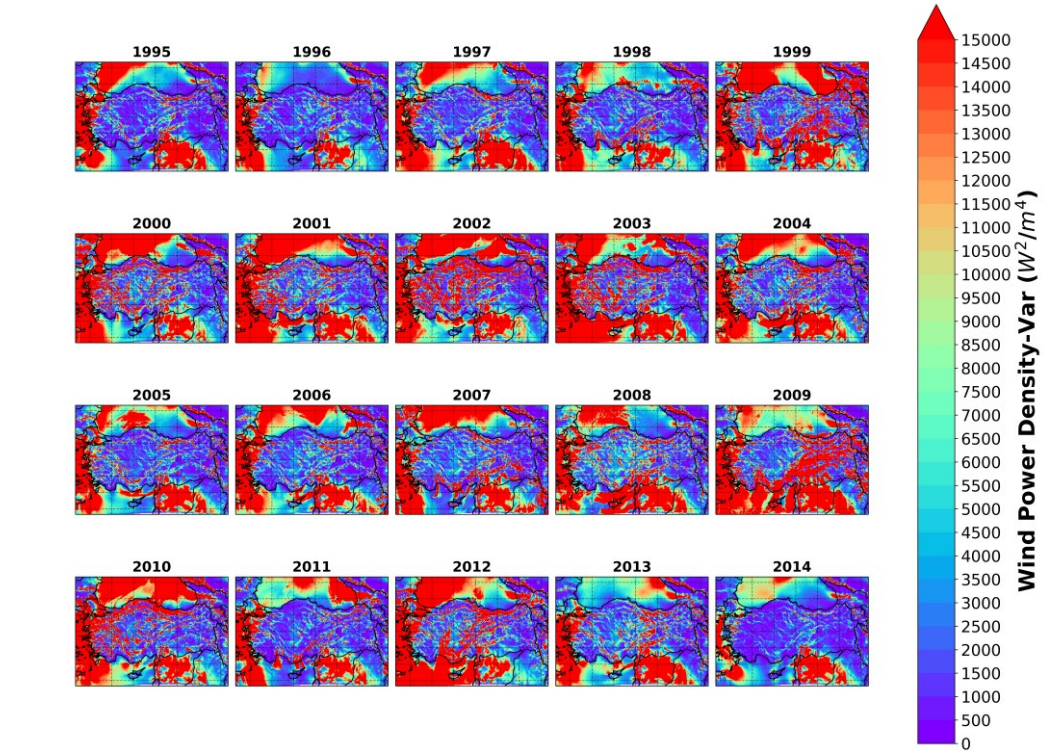



Figure 129 Annual variability of monthly wind power density at 80 m

### 4.4.4 Projected changes in the mesoscale wind resource

Since the WRF-PGW outputs are available for the 2081-2100 period, projected wind speed differences from the reference data (1995-2014) are also calculated. Figure 130 shows the seasonal and annual averages for the difference between "WRF-PGW"-"WRF-ERA5". Figure 131 shows the same results in terms of percentage. The general picture of the change is positive. However, especially in winter months, change is negative for the mountain regions in the eastern Anatolia region. Summer months' change is positive and reaches at 20 % for the Marmara region, western and eastern Black Sea shores, and around Cyprus.

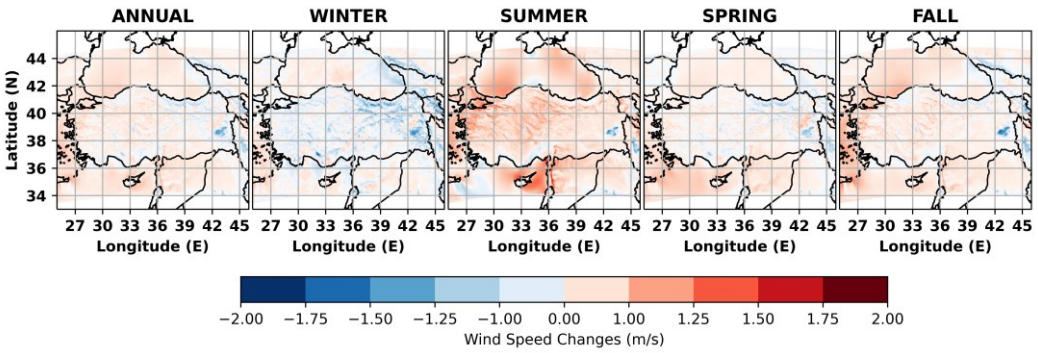



Figure 130 Difference between WRF-PGW and WRF-ERA5 (at 10 m)

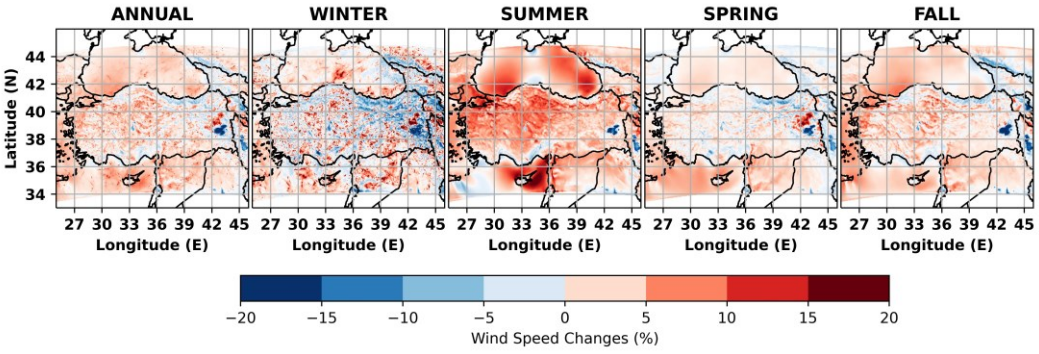



Figure 131 Projected wind speed changes in percentage (at 10 m)

The results that is obtained from mesoscale model are also compared with the simple mean ensemble of 13 GCMs. Figure 132 shows the anomalies of SSP5-8.5 scenario from the historical period based on 13 GCMs. As it can be seen in the figure, dynamically downscaled wind resource shows high spatial variability in terms of

magnitude. For example, there are some places in the Anatolia where the winter wind speed change is positive in the WRF anomalies, while the change is negative for entire Türkiye in the simple mean ensemble. The estimation from multi model mean ensembe shows very rough estimations.

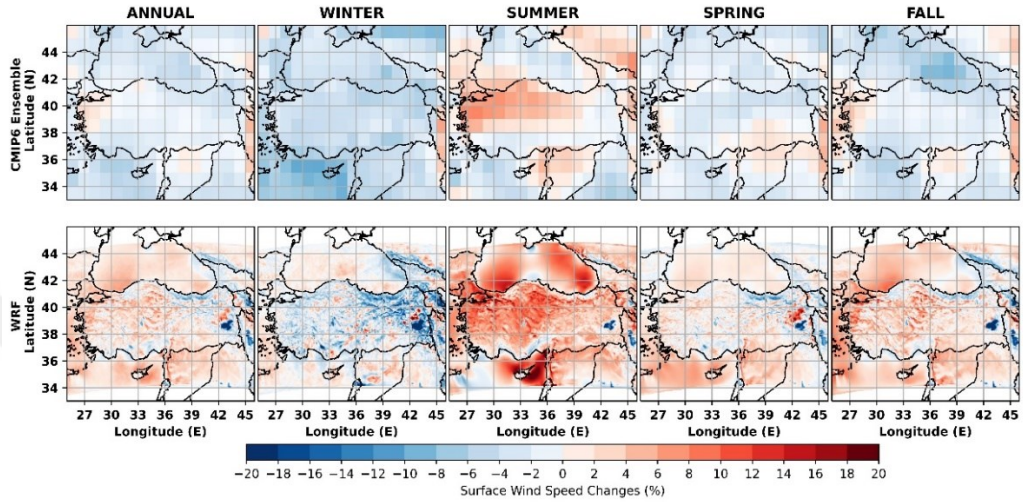



Figure 132 Simple mean ensemble and WRF outputs anomalies at seasonal and annual time scale (at 10 m)

### *Changes in Wind Speed at Turbine Hub Height (80 m) for Future Scenarios*

Changes in the wind resource at hub height (80 m usually) are also calculated to determine intra- and inter-annual changes in the wind resources. Figure 133 shows the seasonal and annual wind speed changes from thereference period. The change is positive in summer months and negative in winter for the eastern Black Sea region.

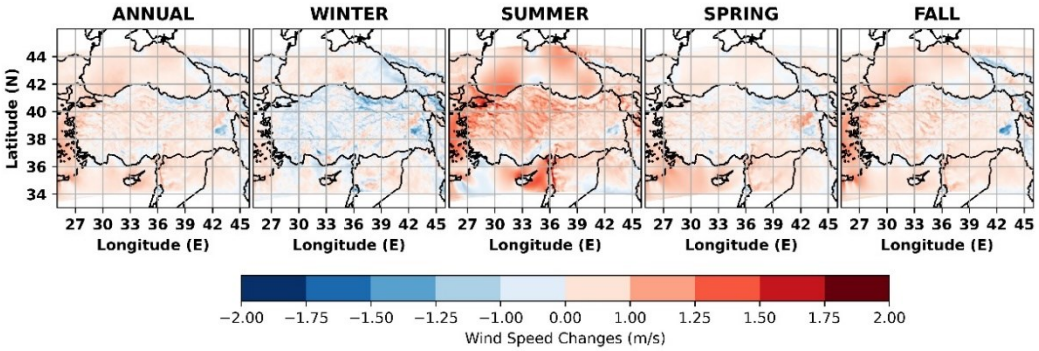



Figure 133 Changes in the future wind speeds (m/s)

Changes in the percentage of wind speeds prove that positive changes can reach up to 13 % for summer months (Figure 134). The northern part of the Marmara and the western Black Sea is also expected to have increased wind speeds higher than 13 %. Cyprus will also face 16 %- 19% positive changes for the same season. Winter wind speeds over the eastern black Sea are negative ( up to -10 %). The Aegean sea wind speeds are projected to change positively up to 10 % for nearly all seasons and annually.

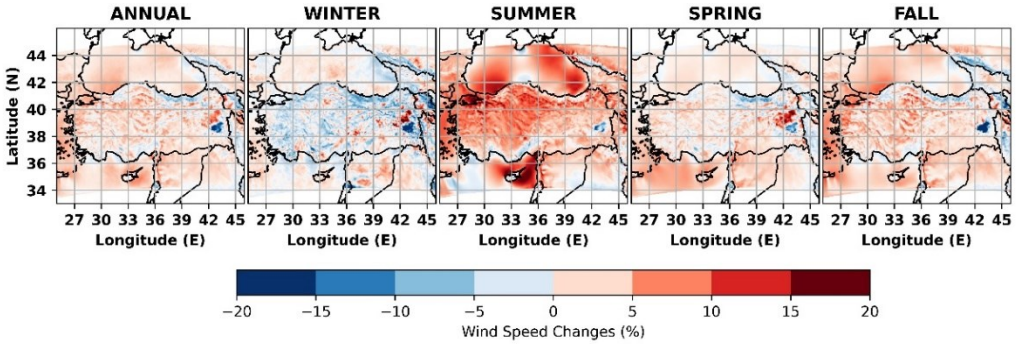



Figure 134 Changes in the future wind speeds (%)

WPD changes are also calculated by using the same “future-references” approach (Figure 135). Changes in the WPD seem more visible than wind speeds due to the fact that a cube of wind speed is used in the calculation. Aegean Sea wind power density is expected to increase to 40 W/m$^2$, especially in the southern part of the sea, for the annual, summer, and fall seasons. Winter season WPD changes seem negative for the Taurus mountains, interior Anatolia, and the eastern part of the black sea. However, the Aegean Sea and flat regions will have positive WPD changes.

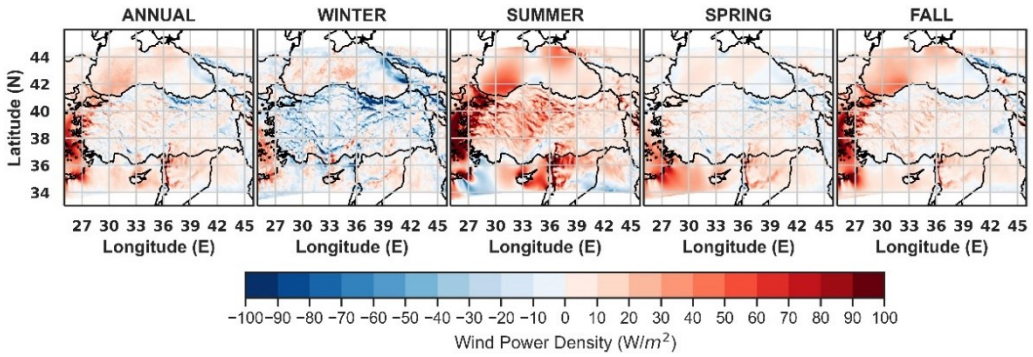



Figure 135 Wind power density ($W/m^2$) changes

Percentage changes are also given in the figure 136 where the positive grid-based changes are more apparent in the winter season.

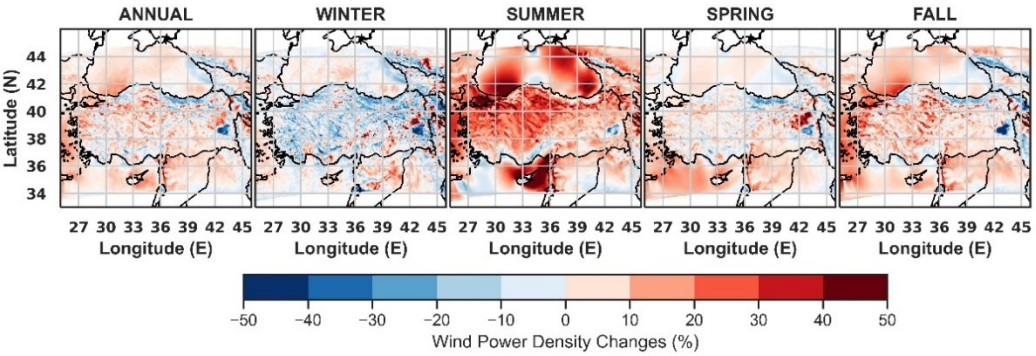



Figure 136 Wind power density changes (%)

## 4.5 Micro-scale modeling results of a selected WPPs

Due to computer and commercial software expenses, the micro-scale modeling part of the study is performed for one onshore site and one offshore site using WRF reference and projected results.The wind turbine power curve is selected as Vestas v90/2MW, which is one of the default wind turbines in the WindSIM [51]. Figure 137 shows the power curve and thrust coefficient of the turbine.

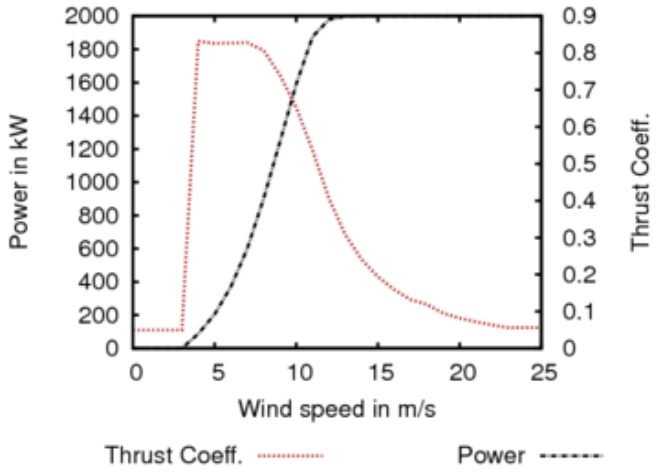



Figure 137 Vestas v90 wind turbine power curve and trust coefficient from WindSIM program

For the offshore wind micro-modeling part of the study, DTU wind turbine with 10 MW capacity [268] is also used in addition to Vestas v90. The power curve of the turbine is given in Figure 138.

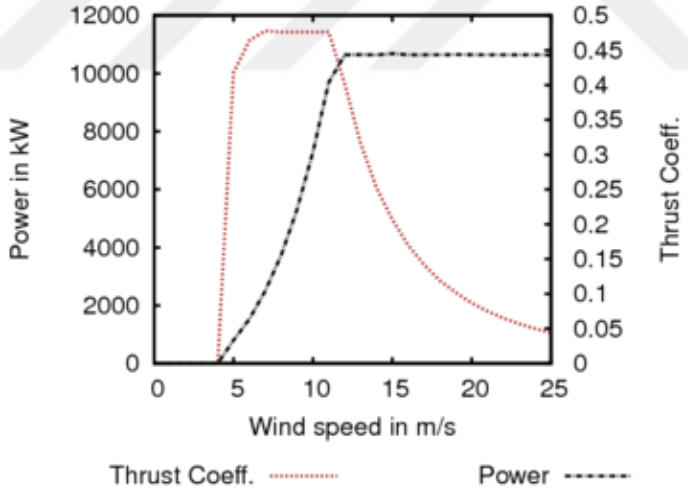



Figure 138 10 MW-DTU wind turbine power curve and trust coefficient from WindSIM

### 4.5.1 Offshore Area

Since there is no offshore wind power plant and offshore measurement in Türkiye yet, an area was selected based on the following criteria:

- Bathymetry ( up to 50 m)
- Wind Power density (400 W/m$^2$)
- Wind Speed ( > 7 m/s) (see Table 14)

Figure 139 illustrates the entire long-term average wind speed distribution over Türkiye together with bathymetry data from GEBCO (The General Bathymetric Chart of the Oceans) [269]. Figure 140 shows the long-term average of WPD obtained from WRF-ERA5 over the period of 1985-2014. Higher wind speeds and WPD can be seen in the Aegean Sea. However, the southern part of the Aegean Sea has limited sea depth for Türkiye's territorial waters.

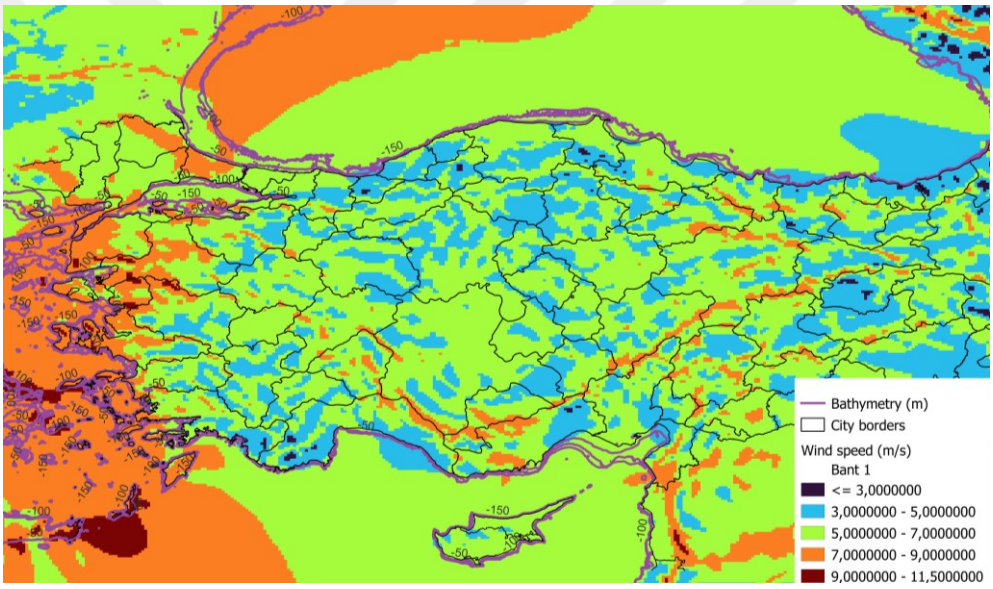



Figure 139 Wind speed distribution together with bathymetry data taken from GEBCO [269].

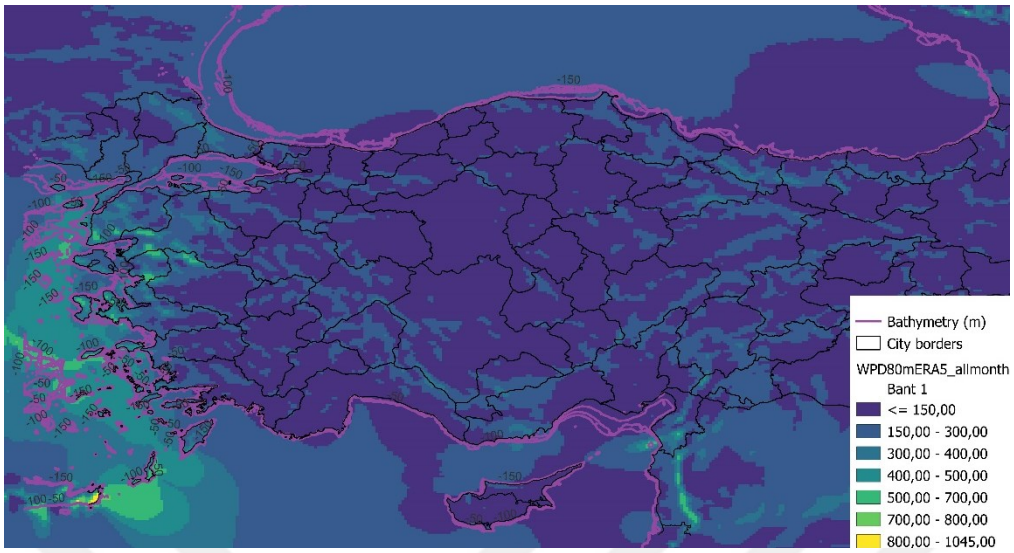



Figure 140 WPD distribution together with bathymetry data

A detailed version of the selected area around the Bozcaada is given in Figure 141. The western part of the island has 500-700 W/m$^2$ WPD, which is a very high value for wind power investments. The southern west part of the island has high WPD as well, but the sea depth of the area is higher than 150 m.

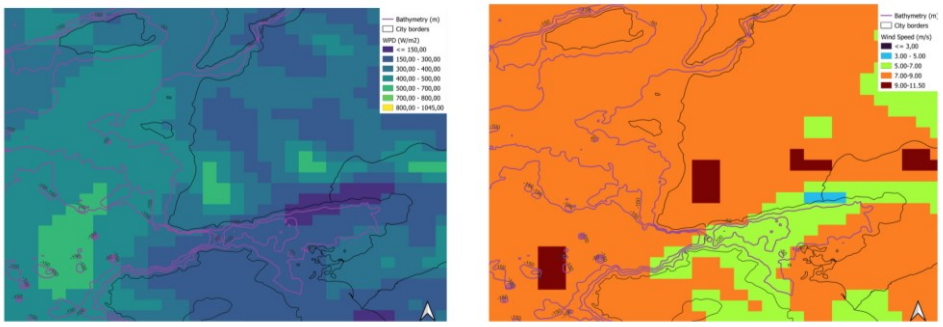


Figure 141 Wind Power Density (W/m$^2$) and wind speed (m/s) information over the selected area

An area in figure 142 is selected for offshore wind resource assessment. Hourly wind speed and wind direction data from WRF-PGW and WRF-ERA5 grids in the selected area were also obtained for the last three years. An overview of the selected area around Bozcaada and selected six grids in WRF outputs are also given in figure 142. Wind speed and direction are calculated from hourly time series for each grid point.




Figure 142 Overview of the WRF grid points and the selected area

Terrain data is generated using elevation and roughness maps and given to WindSIM as input. The terrain model setup is given in Figure 143.

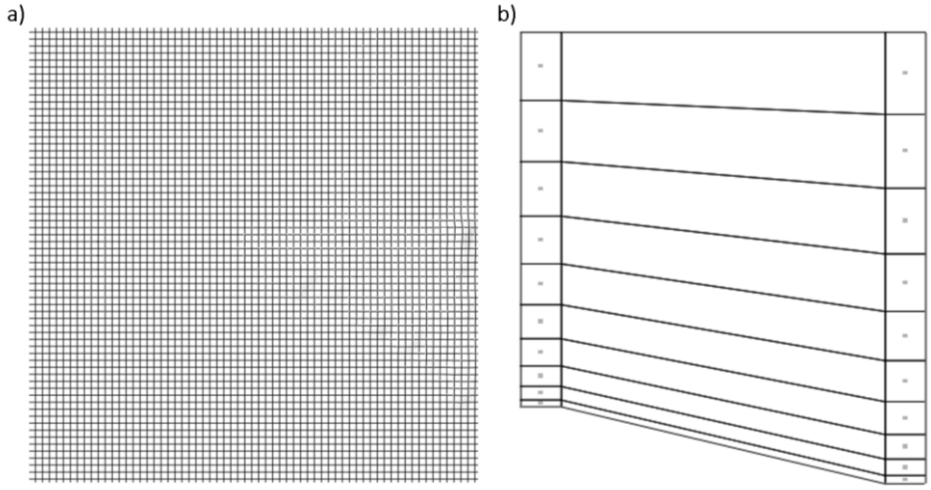



Figure 143 Terrain model set-up “a” is the horizontal mesh and “b” is the vertical gridding from surface to 800 m with 10 different vertical level

In the offshore runs, two different climatology data are used for the runs: WRF-PGW grid and WRF-ERA5 grid. Figure 144 and 145 gives the wind direction and the Weibull distribution of each grid point for the selected area for WRF-ERA5 and

WRF-PGW grids, respectively. The prevailing wind direction is the same for all grids and scenarios.

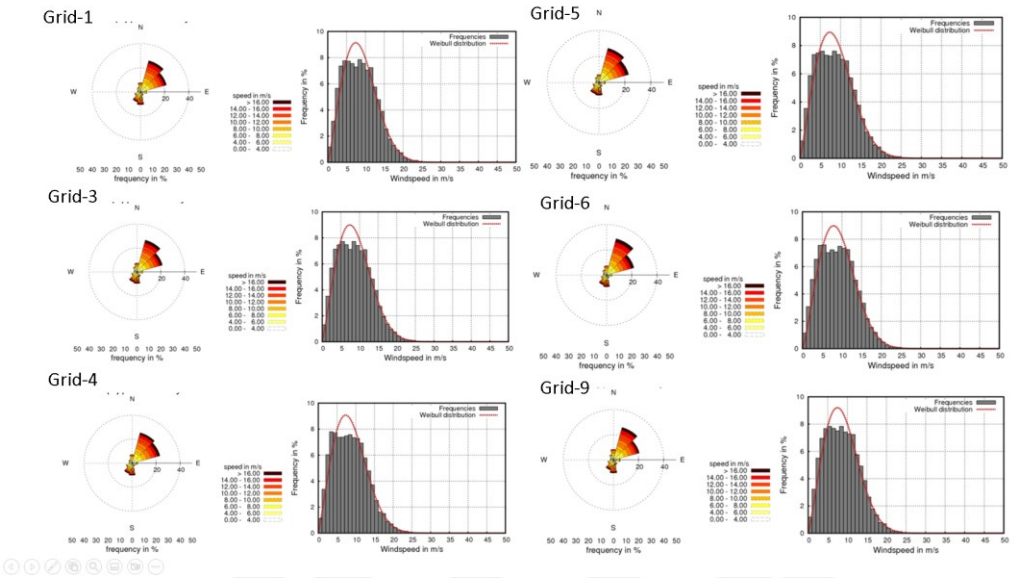



Figure 144 Wind rose and Weibull distribution of wind speeds for grid point at 80 m (WRF-ERA5 Grids)

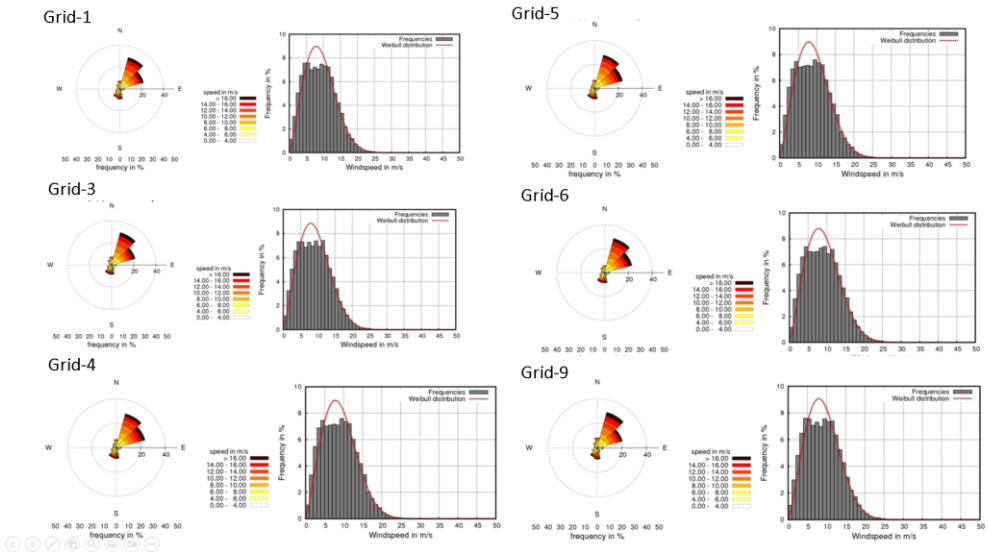



Figure 145 Wind rose and Weibull distribution of wind speeds for grid point at 80 m (WRF-PGW-GRIDS)

Wind resource distribution over the study area is also given in Figures 146 and 147 for WRF-ERA5 and WRF-PGW, respectively. Wind speeds over the southern part of the island are lower than the northern parts. This could be reasoned by the roughness and elevation on the island. PGW and ERA5 results are similar to each other.

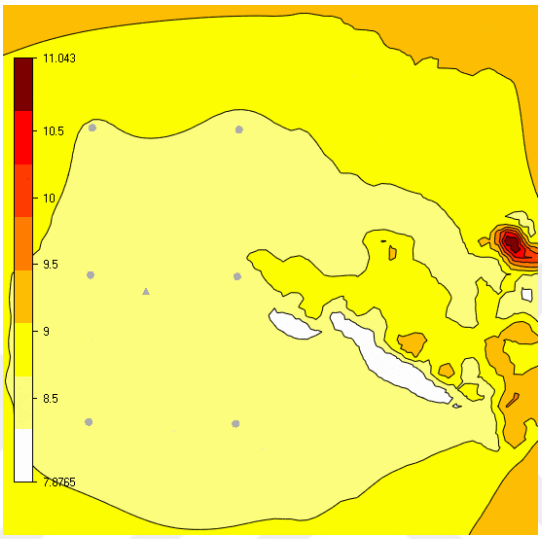



Figure 146 Wind speed distribution over the area with WRF-ERA5 from WindSIM program

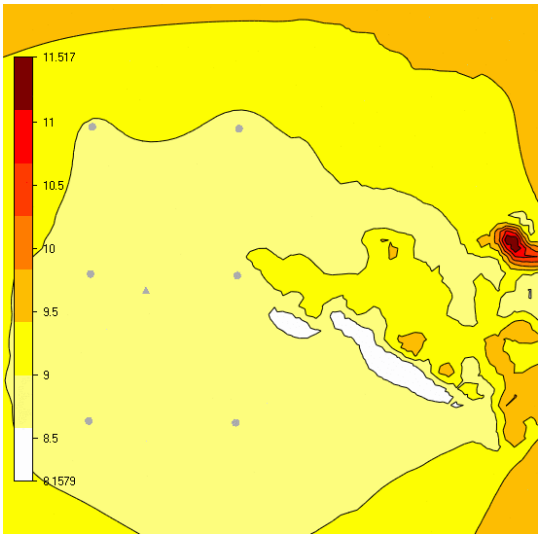



Figure 147 Wind speed distribution over the area with WRF-PGW from WindSIM program

Energy production results are given in Table 24 for WRF-PGW and WRF-ERA5. As can be seen in the table, WRF-PGW production is higher than WRF-ERA5 for both turbine types. The 10 MW DTU wind turbine's higher capacity factor than the V90.

Table 24 Energy production results for a single wind turbine

| Run-type | Turbine Type | Hub Height (m) | Capacity (MW) | Gross AEP (GWh/y) | Average wind speed (m/s) | Full load hours (hours) | Capacity factor(%) |
|---|---|---|---|---|---|---|---|
| WRF-PGW | DTU-10 MW | 119.0 | 10.0 | 50.2 | 9.5 | 5020.1 | 57.3 |
| WRF-ERA5 | DTU-10 MW | 119.0 | 10.0 | 47.7 | 9.1 | 4768.6 | 54.4 |
| WRF-PGW | V90 | 80.0 | 2.0 | 9.4 | 8.9 | 4698.6 | 53.6 |
| WRF-ERA5 | V90 | 80.0 | 2.0 | 8.9 | 8.6 | 4463.6 | 51.0 |

After evaluating different types of wind turbines, a wind farm layout is also generated by using the same wind climatology data. The wind farm contains 79 turbines which are sited according to 300 NE wind direction and 5xD (diameter of the wind turbine) from the horizontal side of the turbine and 10xD from the vertical site of the turbine.

DTU-10 MW wind turbines are used which has 178 m rotor diameter. The layout of the wind farm is given in Figure 148. White triangles show the wind turbine locations, and white dots show the WRF grid points.

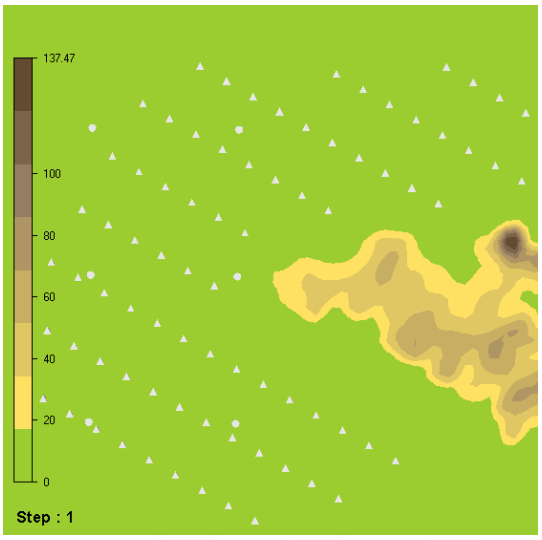



Figure 148 Wind farm layout from WindSIM program

Due to the existing wind farm layout, Wake-Model 1 is also selected as a wake model. Wind speed distribution of the area and turbines are also given in Figures 149 and 150 for WRF-ERA5 and WRF-PGW, respectively.

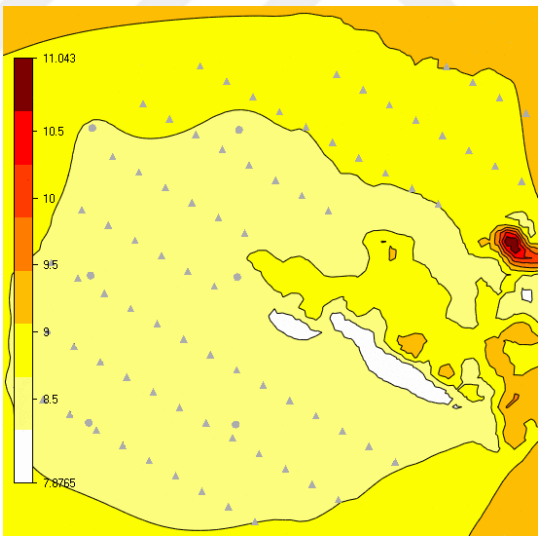



Figure 149 Wind Speed distribution with WRF-ERA5 outputs from WindSIM program

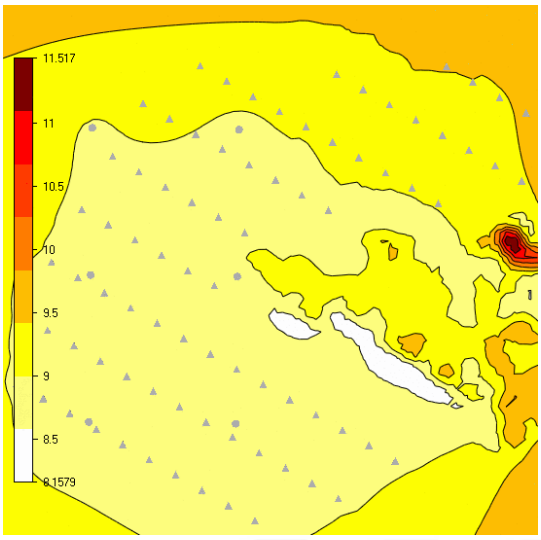



Figure 150 Wind Speed distribution with WRF-ERA5 outputs from WindSIM program

The annual energy production of this wind farm is also given in Table 25. As it is shown in the table, the capacity factor and AEP of WRF-PGW is higher than the WRF-ERA5. Wake losses are lower in the WRF-PGW than in WRF-ERA5. Therefore, the production (AEP) in an offshore wind farm in Bozcaada will be higher in the 2080-2100 period compared to the historical period.

Table 25 Energy Production of the Offshore Wind Farm

| Data | No. of turbines | Capacity (MW) | Gross AEP (GWh/y) | Average wind speed (m/s) | Wake losses (%) | AEP with wake losses (GWh/y) | Full load hours (hours) | Capacity factor(%) |
|---|---|---|---|---|---|---|---|---|
| WRF-ERA5 | 79 | 790.0 | 3780.0 | 9.2 | 2.0 | 3704.8 | 4689.6 | 53.5 |
| WRF-PGW | 79 | 790.0 | 3978.8 | 9.6 | 1.9 | 3904.3 | 4942.2 | 56.4 |

### 4.5.2 Onshore WPP

An onshore existing wind power plant is also selected to determine wind resource from WRF outputs in a complex terrain. Distribution of the turbines, WRF grids (4) and observation (OBS) is illustrated in the figure 151 from the WindSIM. Location

of the turbines are obtained from EMRA database [270]. More information about the WPP explained here as WPP-6 [271].

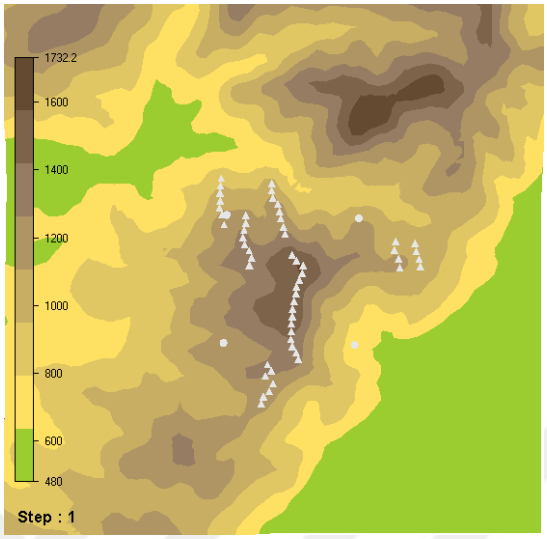



Figure 151 Selected onshore WPP layout and locations of the WRF grids and observation station

Terrain and roughness maps over the area are given in Figure 152. Roughness length (m) is high (up to 0.75), and elevation is also high over the wind farm.

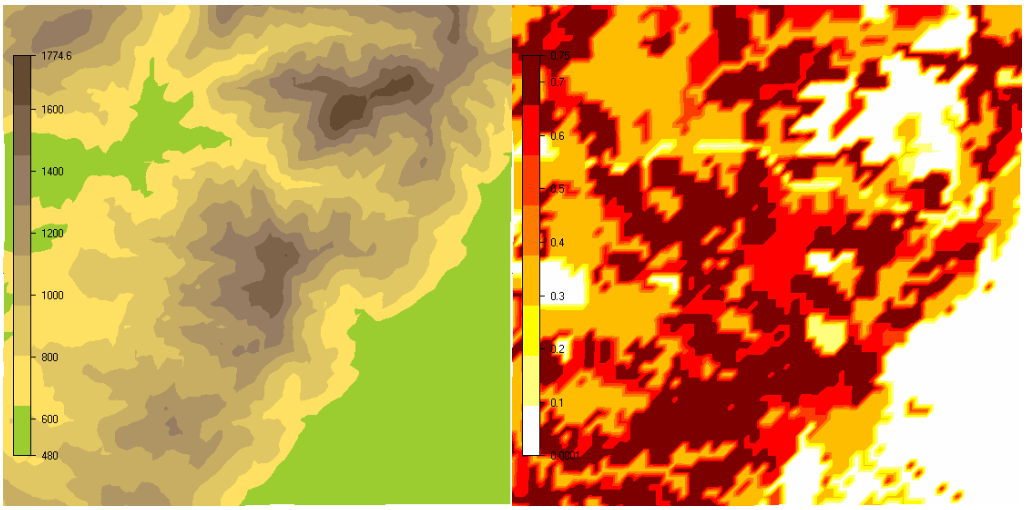



Figure 152 Terrain (left) and roughness maps (right) of the WPP

The terrain model set-up is also given in Figure 153. All options are the same with the offshore runs (including Wake model 1), which is selected to model wake effects between turbines.

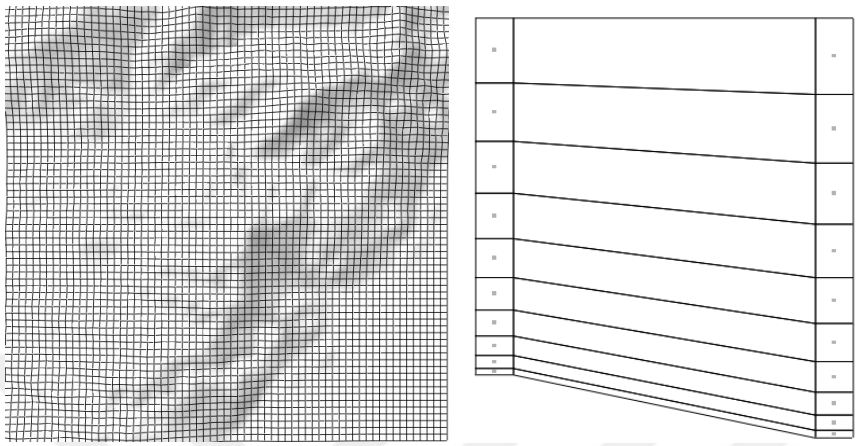


Figure 153 Terrain model setup

Three runs are performed for the complex onshore terrain: run with observation data, WRF-ERA5 and WRF-PGW. Figure 154, 155, and 156 illustrates the wind direction and Weibull distribution of those data, respectively. The prevailing wind direction in the observation data is from the west, while the WRF grids have northwesterly winds.

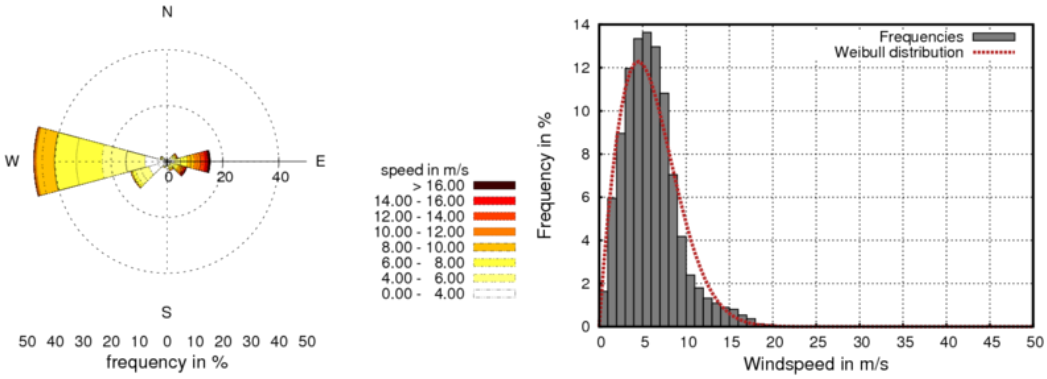



Figure 154 Obsevation at 80 m

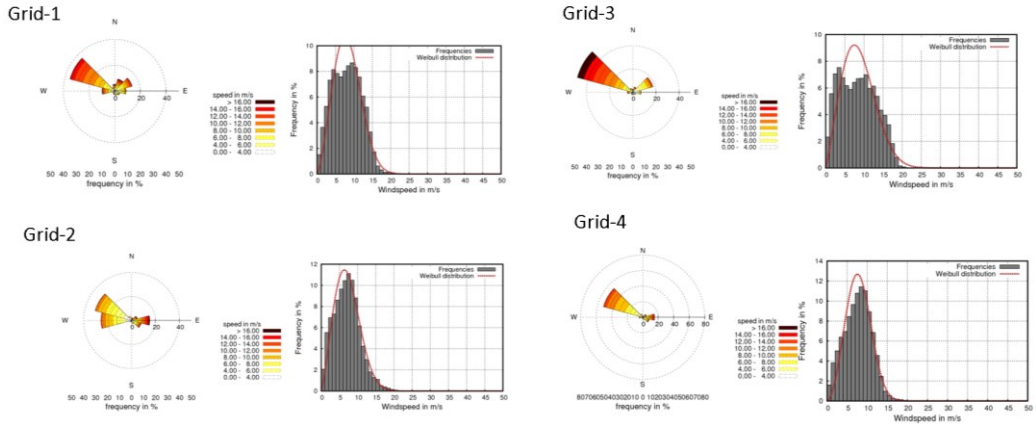



Figure 155 WRF-ERA5 Grids at 80 m

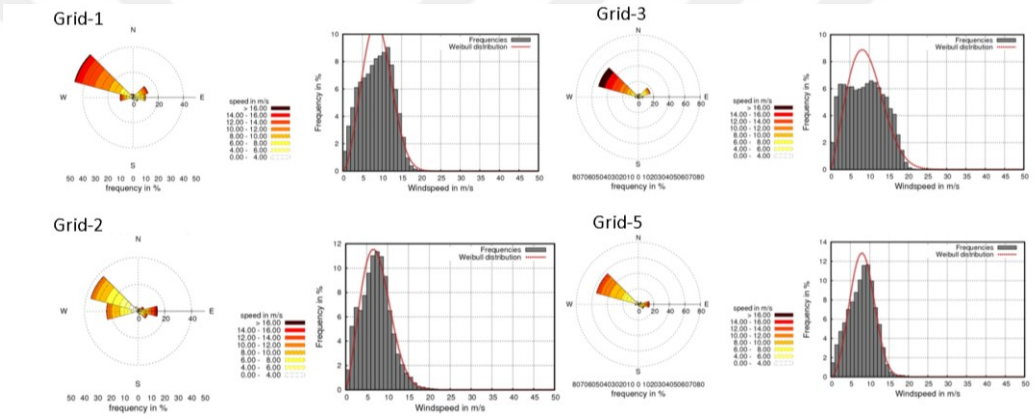



Figure 156 WRF-PGW Grids at 80 m

Wind speed distribution over the selected area is also presented in Figures 157, 158, and 159 for observation, WRF-ERA5, and WRF-PGW, respectively. Although their spatial distribution is nearly the same, observation data wind speeds reach approximately 8.1 m/s while the WRF grids are around 15 m/s.

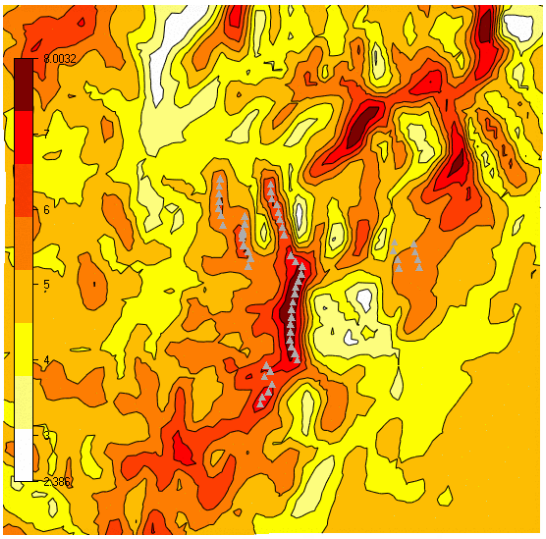



Figure 157 Observation wind speed

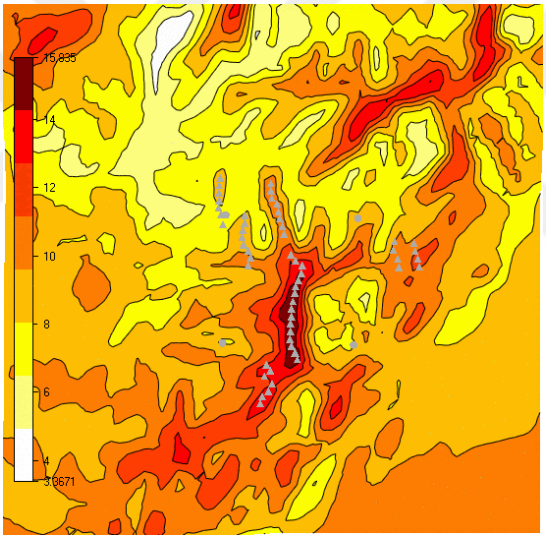



Figure 158 ERA5 all grids wind speed

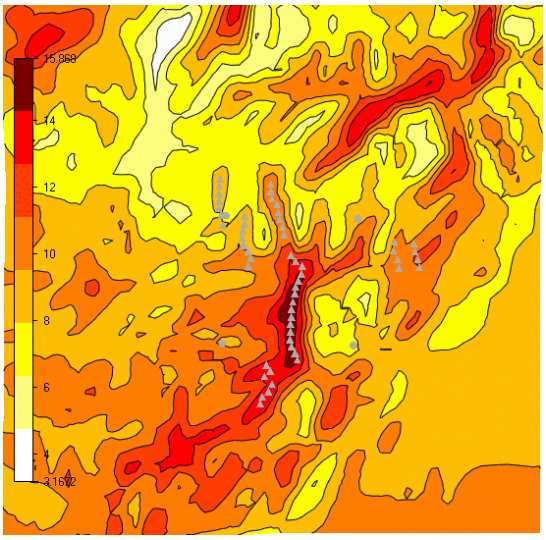



Figure 159 WRF-PGW all grid wind resource distribution

The same overestimation with WRF-PGW is also determined in the energy production results in Table 26. 54 wind turbine is used for the calculation of AEP and capacity factors with Vestas v90 wind turbine. The height of the wind turbine is assumed at 80 m.a.g.l.Wake losses are higher in the observations (2.6 %) than in the WRF-ERA5 and WRF-PGW. Due to overestimation in the model-derived wind speeds (11.6 versus 6.4), capacity factor differences are also high with the observations.

Table 26 Energy production results for a wind turbine

| Turbine Type | Hub Height (m) | No. of turbines | Capacity (MW) | Gross AEP (GWh/y) | Average wind speed (m/s) | Wake losses (%) | AEP with wake losses (GWh/y) | Full load hours (hours) | Capacity factor(%) |
|---|---|---|---|---|---|---|---|---|---|
| OBS | 80 | 54 | 108.0 | 271.5 | 6.4 | 2.6 | 264.5 | 2449.4 | 28.0 |
| WRF-ERA5 | 80 | 54 | 108.0 | 446.1 | 11.6 | 2.5 | 435.0 | 4027.6 | 46.0 |
| WRF-PGW | 80 | 54 | 108.0 | 517.5 | 11.6 | 1.9 | 507.8 | 4702.2 | 53.7 |

# CHAPTER 5

# DISCUSSION

Due to the increasing demand for energy consumption and the recent developments in climate change mitigation measures, renewable energy has become more important in recent years. Wind energy, among the other renewables, has rapidly grown over the last decade in Türkiye and the World. The wind has different advantages because it is a domestic resource and abundant in most regions of the World. However, determining wind resources is very important for producers and planners. Due to the chaotic nature of wind, wind resource prediction has also become an important topic in recent years.

On the other hand, renewable energy resources have high advantages in mitigating climate change. However especially, wind and solar are weather-depended renewable energy resources that cause drawbacks in combating climate change. Therefore, it is aimed to determine climate change's impact on wind resources over Türkiye, where it will be negatively affected by climate change in terms of precipitation and temperature.

Although overall results in this study agreed on increasing wind speeds in summer and decreasing wind speeds at winter season over Türkiye, the entire results should also be evaluated in terms of overall climate change perspectives. Changes in the wind resource variability is not alter the wind energy's positive contribution to mitigate climate change as it is mentioned in the [9]. However the results of the study contributes to long term planning of the wind energy in the electricity production. Because, wind is a complex parameter associated with uncertainties in electricity production. Those uncertainties are creating imbalances in the electricity grid as well. Availability, variability, and reliability of wind resources are also important for the long-term planning of grid investments. Since wind is an intermittent resource, the prediction of wind is also a significant topic for producers and regulators.

Depending on the recent developments in the climate change negotiations, Türkiye has to increase the share of renewables to reach the 2053 net zero emission targets. Türkiye has exceeded the 11 GW installed capacity [4]. However, the share of wind in the Türkiye's installed capacity is around 11% which is expected to be higher to reach the net-zero emission targets. With increasing wind speeds, it is also essential to conduct spatial planning studies within this context. Climate change will affect not only wind resources but also electricity consumption, infrastructure damage, etc. For example, in this study, it is concluded that wind speeds will be increased in the Aegean region and the Aegean Sea for the summer season. The territorial sea border issue is one of the problems between Türkiye and Greece. Due to the special circumstances in the Aegean Sea (Aegean Dispute between Türkiye and Greece) Türkiye did not sign the Third United Nations Convention on the Law of the Sea (UNCLOS III, 1973-1982) [272]. Territorial sea borders of Türkiye is declared as 6 nautical mile [273]. Therefore, maritime spatial planning for future investments should be well-planned to produce electricity with all regional stakeholders. It is also expected that the temperatures will be increased in the region, which will cause higher electricity demand during the summer season. Therefore, planning should be done earlier for wind investments in the region. The region also has high tourism potential, which should be considered for possible investments. Visual impacts of wind turbines could be a negative environmental impact on the residents around the region.

On the other hand, wind energy installations are done under the three different approval systems in Türkiye: licensed, unlicensed, and YEKA [123]. Licensed projects can be subject to the feed-in-tariff mechanism (YEKDEM) [121] , an incentive method for renewable energy investments in Türkiye. However, this mechanism will be finished in 2031. After that, the government can establish new incentives and support mechanisms or market structures to increase the use of wind energy. Determination of the future wind resource can also help to develop new models or regional incentives. For example, incentives can be planned depending on the region and available wind resources. Since wind speed is not the same for all regions and some regions have already reached high installed capacity, plans need

to be established by considering both spatial plans, available geographical conditions, and wind resources.

Although wind resources will be available in the future, current policies will shape future investments. Competitive prices in the wind energy market, nearly reaching the prices of fossil fuels, will be less in the future. The energy demand of Türkiye will be doubled in 2040 [274]. Long-term energy plans for Türkiye already exist. However, projected wind resource information should be included in these models as well. As the EU faced during the Russian invasion of Ukraine, supply security is very important for countries with import dependency. Today, approximately half of Türkiye's electricity production still depends on imported coal and natural gas. Renewables can help to reduce these dependencies due to the abundance of the resource. However, the domestic production of wind and solar manufacturers is also another important topic. Türkiye has supported the domestic production of wind turbines since 2005 with incentives [121]. However, those policies must be accelerated to produce locally manufactured wind turbines. Yet, long-term average and extreme wind speeds should also be considered for designing those wind turbines. For Türkiye, where lower wind speeds and wind power density are found in the middle and eastern parts of the country, the wind turbine designs for low wind speed locations should be evaluated.

Flexibility solutions in the traditional electricity grids for an increasing share of renewables in electricity production is another topic to consider for future investments. EU is also trying to integrate alternative methods for supply security. Hydrogen is one of the most important topics as an alternative resource and flexibility solution to carbon-based energy and economies. Green hydrogen, based on the electrolyzing of water by using electricity produced from wind and solar, is one of the most popular topics now. Wind can also help to produce green hydrogen, which will be a very important alternative secondary energy resource in the near future. Offshore wind-based hydrogen production is also under investigation for this purpose. Within this context, Türkiye's future wind energy potential over the seas or onshore regions is also promising for future hydrogen investments. Due to the

geographical location of Türkiye, producing green hydrogen and transporting it to the EU countries is another option.

Offshore wind is a critical player in the world's energy production. Especially the latest efforts and targets in the Northern European countries, USA, and China is very ambitious about offshore wind. ESMAP's report showed that the Türkiye has a 69 GW offshore wind power potential (12 GW is fixed, and 57 GW is for the floating foundation) [33]. This potential indicates that future offshore wind investments will be valuable for Türkiye's energy mix. However, the lack of wind resources or site characterization information was an important factor in the last unsuccessful offshore wind tender (YEKA) of Türkiye [125]. Wind resource assessment is a crucial parameter in reducing uncertainties about offshore wind. On the other hand, if the current prices of offshore wind are not feasible for investment in Türkiye, future opportunities should be investigated and well-planned. Another important factor in successful offshore wind investments is having a pipeline and a well-planned road map [125]. Those road maps also started with the wind resource assessment and followed by maritime spatial planning. Spatial planning should be done by considering all actors in the marine environment. Determination of the technical potential is the first step, but marine areas have a lot of stakeholders, including fishery, biodiversity, transportation, navigation, tourism, etc. Therefore, prohibited areas or areas to negotiate with stakeholders should be determined after determining the potential using wind resource and geological data.

New technologies, such as floating offshore wind, should also be considered for future offshore wind investments in Türkiye. Areas deeper than 60 meters can be considered for floating offshore wind. Although the technology is expected to be commercial by the mid-2020s to 2030s [3], future plans can be made with this technology. In addition, turbine designs should be made with consideration for changing wind resources.

Repowering policies are also important for countries like Türkiye, which has an approximately 25-year mature onshore wind energy market. Most of Türkiye's wind turbines are reaching the end of their life. The installed wind turbines have 49-year

licenses. Therefore, new wind turbines can be added to the same locations if there is capacity. This study also aimed to determine the future potential of existing wind power plants for their possibilities to repower their wind farms with new technologies based on wind resources. These kinds of studies are also crucial for determining foreseeable markets. Türkiye should publish a repowering roadmap for reaching net-zero targets. However, repowering potential should be considered when doing this.

To sum up, determining the future availability and variability of wind energy resources has many advantages, such as combating climate change, providing foreseeable markets, ensuring supply security, reducing uncertainties, and increasing transparency in the wind energy market. The study also aligns with two of the United Nations' Sustainable Development Goals: "Ensure access to affordable, reliable, sustainable and modern energy for all (SDG-7)" and "Take urgent action to combat climate change and its impacts (SDG-13)" [275]. As the SDGs outline, achieving these goals requires policy support as well. Policymakers use this type of information not only for planning but also for determining financial mechanisms. This kind of vision and perspective is also crucial for developing countries like Türkiye.

# CHAPTER 6

# SUMMARY, CONCLUSIONS and RECOMMENDATIONS

## 6.1 Summary and Conclusions

This study determines the current wind climatology as well as future variability and availability of wind resources in Türkiye due to changing climatic conditions. The study contains a multi-model ensemble, mesoscale model analysis, and micro-scale modeling. First, a multi-model ensemble technique (machine learning method and multiple linear regression) is applied to CMIP6 climate models with 28 GCMs over seven geographical regions during the historical period (1980-2014). Three different reference data are used in the historical part of the study to validate GCMs. ERA5 re-analysis data performed better than MERRA2 with observations, and only ERA5 data is used for WPP-based multi-model ensemble studies. Multi-model ensemble techniques are taken advantage of by individual GCMs and produce more accurate results with the random forest regression method. WPP-based onshore and offshore wind resource determination with two scenarios are also performed separately due to the lack of offshore wind power plants in Türkiye. Offshore parts are investigated using four seas around Türkiye, and four different RF regressions for each sea are produced. Each licensed/pre-licensed WPP in Türkiye is obtained, and 330 different RF predictions are produced for those wind power plants. Secondly, mesoscale modeling results are examined for the entire Türkiye with SSP5-8.5 scenario for the 2080-2100 period. Finally, due to limitations in computers, only a selected two (offshore and complex onshore) areas are studied at the micro-level. The offshore area is selected depending on the sea depth and wind speed conditions. The results related to each step of the study is summarized as follows:

***Hindcast results***

Machine learning ensemble approaches of RF and MLR are used to develop regression models among 28 CMIP6 GCMs for providing ensemble prediction of monthly wind speeds over seven different geographical regions of the Türkiye and Aegean offshore regions. Regression models are developed using two global re-analysis data and station based observation under three different categorizations: all GCMs, DVM, and WDVM. The key findings of the study are given as follows:

- ERA5 shows less bias and a higher correlation with observed winds. MERRA2 and ERA5 have low correlations (0.22-0.48 for ERA5, 0.15-0.31 for MERRA2) for Southeast Anatolia, where the number of ground stations is comparatively low.
- Aegean Sea Offshore wind speeds, even at 10 m, are higher than any onshore region in Türkiye (higher than the 6.0 m/s for all-time average classifications). These higher and consistent wind speeds, supported by Etesian winds, are promising for future offshore wind investment around the Aegean Sea. Onshore wind speed potential from high to low is respectively ordered as Marmara, Aegean and Mediterranean regions.
- Both global re-analysis data and observation winds showed significant negative trends over the Marmara and northern Aegean region during the wintertime. MERRA2 also showed negative trends in the internal part of the Anatolia lands except in the summer season. However Northeastern part of the Black Sea has significantly increasing wind speeds which are agreed by both global re-analysis data.
- CMIP6 model performances mostly overestimate ERA5 and observations, while most GCMs are close to MERRA2. GCM10 (EC-Earth3), GCM11 (EC-Earth3-Veg), and GCM 20 (KACE-1-0-G) were found closest to ERA5 data for all regions.
- Based on the three MME development (All, DVM, and WDVM), DVM classifications of MLR and RF also yielded better estimates (higher

correlation and lower error) than All and WDVM categories, particularly for Marmara, Aegean, and Mediterranean regions during the test period.

- RF predictions from all model classifications and datasets at all regions are much better (corr. coeff. is around 0.97 during the train period) than MLR (corr. Coef. Changes between 0.41 to 0.81 during the train period) estimates. ERA5-derived estimates yielded the smallest error throughout onshore regions, while MERRA 2-based estimates provided the highest error. Offshore region winds are higher and more variable than the onshore winds, but a similar skill for RF and MLR is obtained.
- MERRA 2 winds are higher than ERA5 and observation over onshore regions, while they are slightly lower than ERA5 winds over offshore regions.

***Impacts on Offshore wind resource results***

To evaluate the offshore wind resource over Türkiye, wind speeds are extrapolated at 100 m above the sea level by using pressure level data from CMIP6. Two different climate change scenarios' results for RF prediction are produced, and results showed that using individual GCMs cannot succesfully represent ERA5 re-analysis data for a region.

- RF prediction results performed better than GCMs, and correlations with the ERA5 data was high (changes from 0.85 to 0.98). The difference between scenarios is also found to be very small. However, SSP2-4.5 data are only higher than SSP5-8.5 for the summer months at Marmara and Black Sea.
- CMIP6 models underestimate the ERA5 data over the study area. Aegean Sea wind speeds change between 7 m/s to 10 m/s for the entire study period for ERA5 and RF predictions which promises a good opportunity for offshore wind power installations during the upcoming years. Although the projected wind speeds from RF predictions are expected to be decreased at winter and summer seasons (3% and 5 %) respectively (see figure 160), the potential is still good enough to wind power investments. Avarage wind speeds in the Black Sea change between 5-8 m/s, the winds in this region are also projected

to increase by approximately 20% in the near, mid, and long term, especially in the summer months (see figure 160). Mediterranean Sea wind speeds are expected to decrease in the winter months and increase in fall season by approximately 9 %. Seasonal variability of wind speed changes is also considered due to the increasing electricity demand for those regions in the summer months. Projected changes in the Marmara Sea are low, but the reasons can be varied due to the low number of grids in this region.

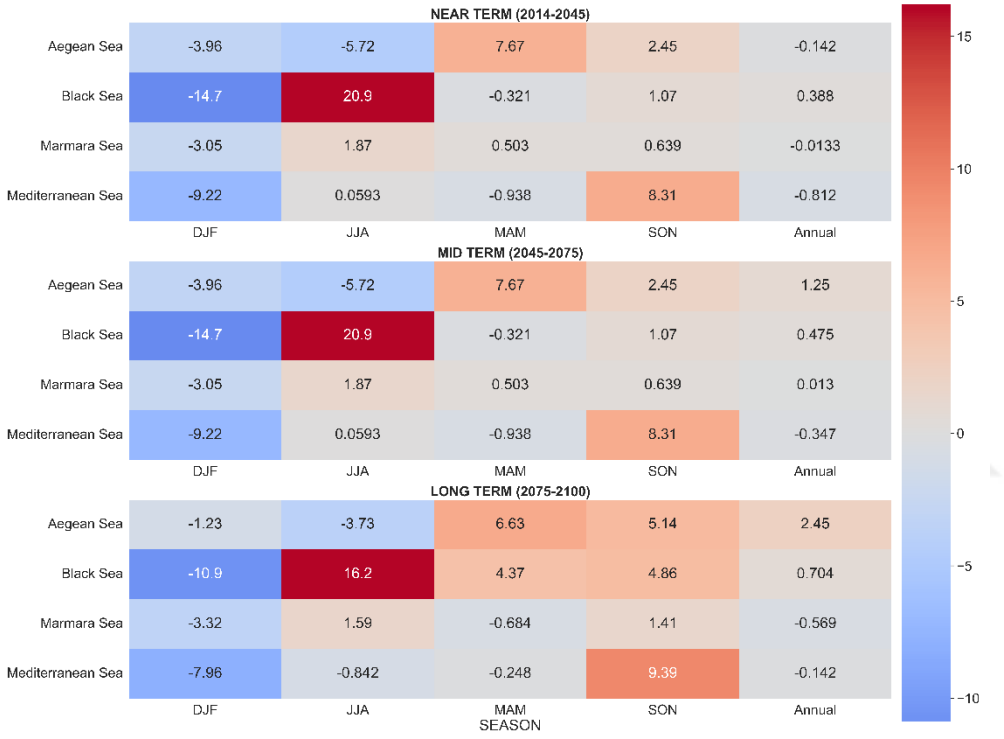



Figure 160 Regional changes (%) for offshore RF prediction anomalies

However, this study only includes the GCMs with coarse resolution, which gives a rough estimation of wind climatology. Therefore, further work is needed to establish to increase the resolution of the GCMs due to wind climatology requiring higher resolution for better representation of the area.

***Impacts on current Onshore Wind Power Plants' results***

These results are obtained by calculating wind speeds with power law at 100 m and getting the nearest grid point to each WPP in Türkiye from all models. RF predictions

are developed for each WPP for the SSP2-4.5 and SSP5-8.5 scenarios by using 27 GCMs. The results are summarized as follows:

- EC-Earth3 models, HadGEM3-GC31-LL, UKESM1-LL, FIO-ESM2-0, UKESM and TAİESM1have better performances with ERA5.
- Aegean and Marmara region WPPs have the highest wind speeds and wind power density.
- RF performances with ERA5 data are better than any individual models (correlation coefficients are higher than the 0.96, low RMSE (between 0.10 and 0.40 in RF predictions).
- RF prediction errors are also calculated in terms of seasons for each WPP. Results showed that winter correlations are between 0.97-0.99, summer 0.95-0.98, spring 0.96-0.98, and fall 0.96-0.98. RMSE and SDE are changed between 0.10-0. 40. PBIAS is generally positive for the spring and fall seasons. However, in winter: most of the WPPs in the Marmara region and a few WPPs in the Aegean region showed negative PBIAS (%), which varies between -1-0.5. In summer, only a few WPPs have positive PBIAS from the Marmara, East Anatolia, and the Black Sea region.
- There was no discernible change in the annual averages across the whole study period (1980-2100). However, the highest wind speeds are shown in the Aegean and Marmara regions, which have the highest number of WPPs installed. The lowest average wind speeds are seen in the Black Sea. Inter-annual variability for all regions is similar to historical period variations.
- Higher wind speeds (5-6 m/s in a year) in the Aegean and Marmara region's summer and winter months also exceed the ERA5 averages. SPP2-4.5 and SSP5-8.5 showed similar results at annual and monthly average time scales.
- Most of the GCMs resulted in no significant trend. However, During the historical period, 20% out of 27 GCM models have a decreasing trend for Anatolia and Mediterranean regions. % 20 of the models have an increasing trend for the SSP2-4.5 scenario, and the same percentage is valid for the decreasing trends in the SSP5-8.5 scenario.

- Overall changes from RF predictions for each WPP in Türkiye are summarized in the Figure 161. Projected wind speed changes is calculated as negative in winter at three term except from Aegean, Marmara and Mediterranean region at near term. Aegean region WPPs will have an increasing wind speeds in mid- and long-term at spring, fall, summer and annual. However the magnitude of the change is small.

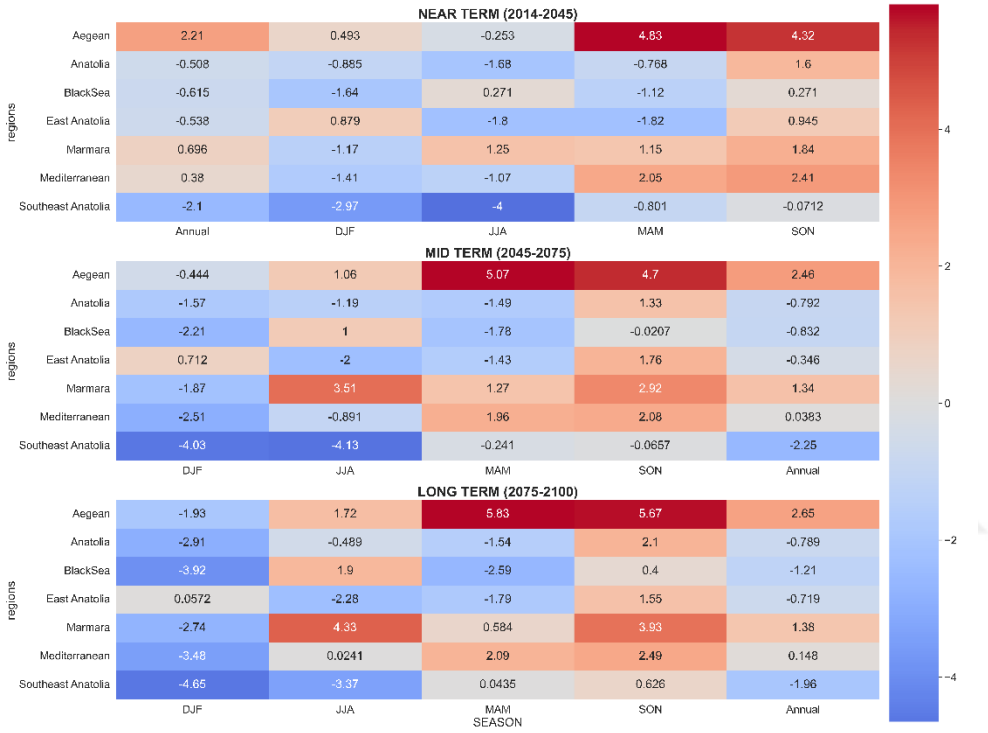



Figure 161 Regional avarages for onshore RF prediction anomalies (%)

***Mesoscale modeling results***

WRF-PGW and WRF-ERA5 outputs are analyzed in this part of the study. Model performances for wind speeds at 10 and 80 m.a.g.l. are evaluated. The following results are determined for the SSP5-8.5 scenario and historical period:

- WRF-ERA5 and ERA5 have the lowest SDE. While ERA5 and HADGEM3-GC31-MM have the lowest RMSE, the highest correlations are determined for ERA5, MERRA2, and WRF-ERA5.

- Winter season in the Mediterranean region has the highest errors with relatively low correlations. East Anatolia and Anatolia regions have lower errors during the spring season. The lowest correlations can be seen in Anatolia (0.45) during the winter season and in the Southeast Anatolia region during the summer (0.37) and spring (0.40) seasons. Marmara region has the highest correlations in the fall (077) and spring (0.74) seasons. High errors in Southeast Anatolia can also be related to a low number of regional observations.
- Inter-annual changes have been determined for the historical period. The highest wind speeds can be seen in 2002, 2003, 2010, 2012. The lowest wind speeds for 1994, 1995, 1996, 2013, 2014 years associated with low electricity production from wind.
- A simple mean ensemble of CMIP6 models produced more smooth results than WRF-PGW.
- The projected wind speed change is summarized in the figure 162 by taking avarage values of the each grid in the each region. The change is expected to be positive at annually. However, the change is negative for winter. Summer months are projected to change positively, and wind speed change will reach at 14.7 % for the Marmara Sea. The northern part of the Marmara and the western Black Sea are also expected to have increased wind speeds higher than 13 %. Cyprus island will likewise experience 16 %- 19% positive changes for the same season.
- WPD changes are also summarized in the figure 163. Winter season WPD changes seem negative for all regions except from Aegean Sea and Southeast Anatolia Region. Marmara Sea WPD is expected to increase 48 % at summer season. However the change is lower in the Spring season for this region 3.4%).

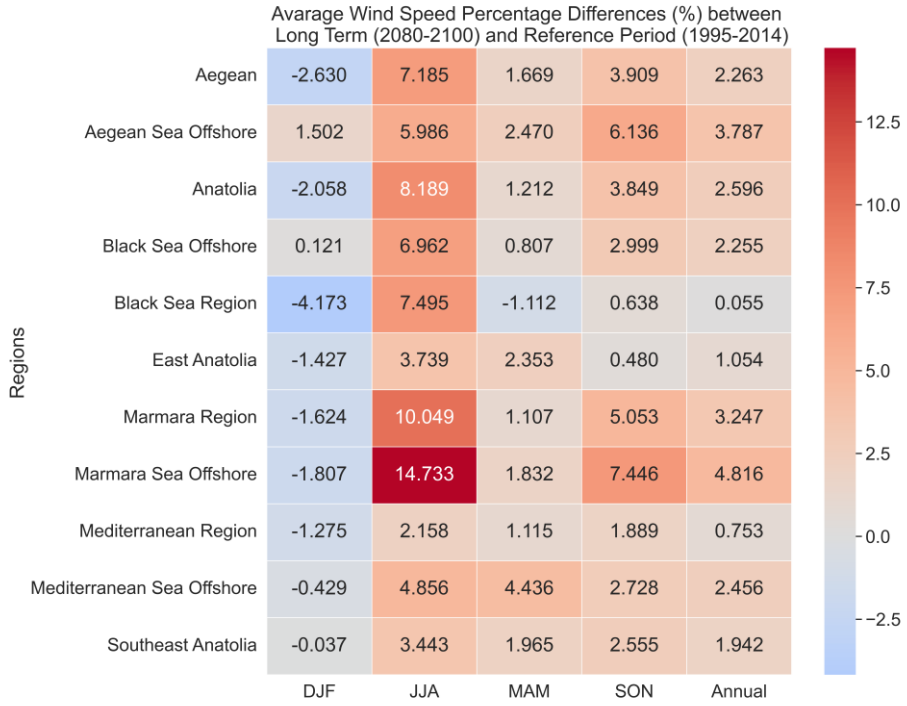



Figure 162 Regional avarages for WRF-PGW prediction anomalies (wind speed-%)

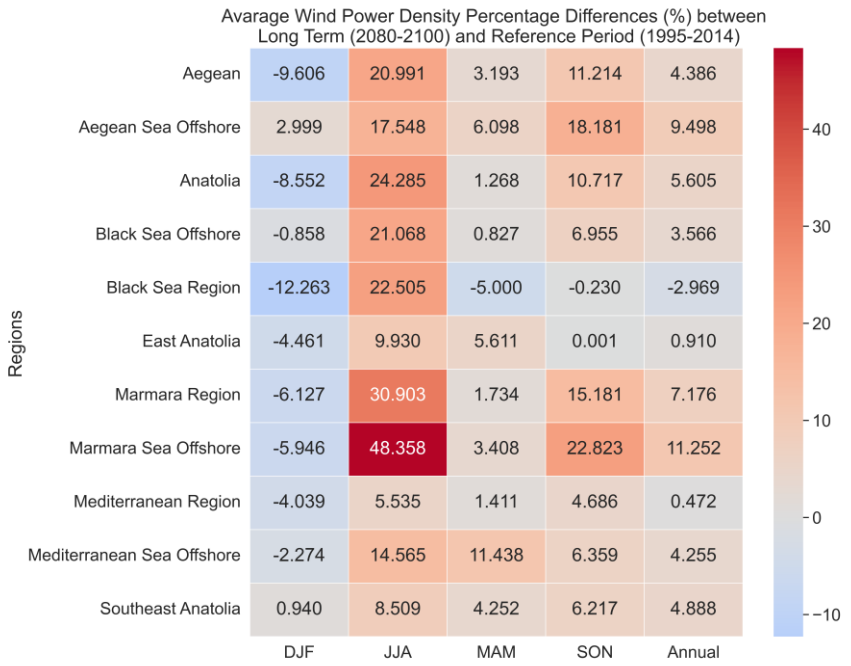



Figure 163 Regional avarages for WRF-PGW prediction anomalies (WPD-%)

To compare the RF results for each WPP with the mesoscale data, the nearest grid points in the mesoscale model to the 330 WPPs are also obtained. The avarage value of those grids are also calculated at each region and illustrated in the figure 164. The results showed that wind speeds around the WPPs in Marmara, Anatolia, Black Sea and Aegean region is expected to increase 10 %, 6.9%, 9%,6.1% respectively in long term. Black Sea wind speeds around the WPPs are expected to decrease.

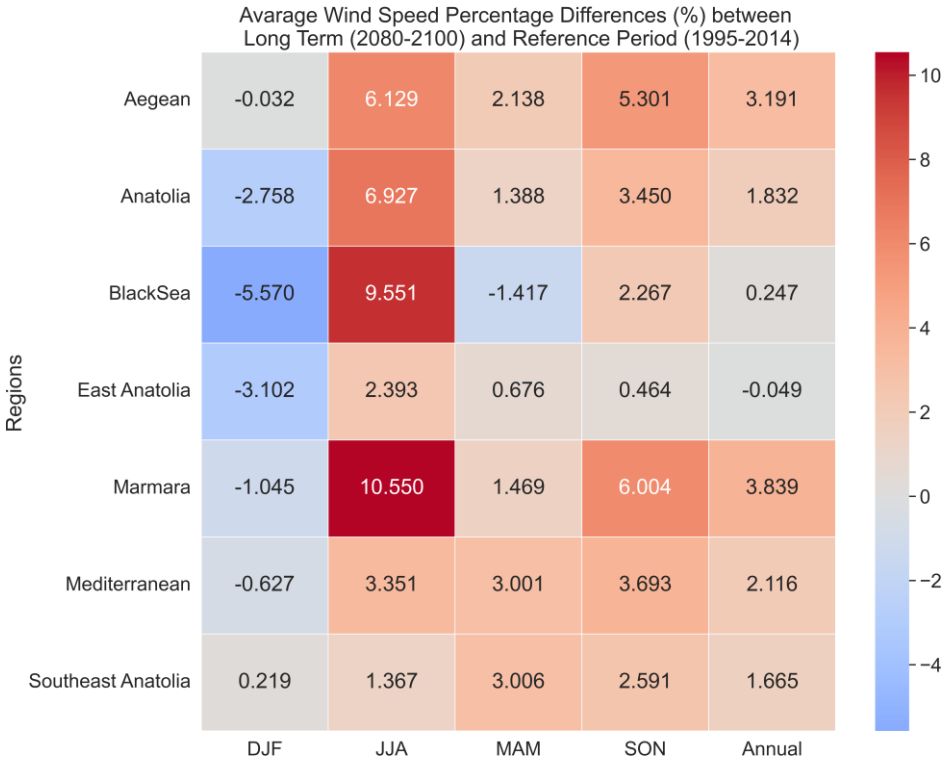



Figure 164 Summary of the mesoscale model outputs with the nearest onshore WPPs

***Micro-scale modeling results***

Two different terrain types are selected for micro-scale modeling. Capacity factor and energy production results with WRF-PGW is higher than the WRF-ERA5 for both onshore and offshore area.

Overestimation is determined in the complex onshore area with the observations. The capacity factor is 28.0 with the observations, while it is 46 % for the WRF-ERA5 runs and 53.7 for the WRF-PGW runs.

Offshore results are closer to each other. Unfortunately, it cannot be compared with the model results because there are no observational data in the offshore region. Two different wind turbines are used to calculate energy production in offshore wind resource investigations.

## 6.2 Recommendations

Although it is already used in this study, the dynamical downscaling method with the sensitivity studies for wind could be improved by mesoscale models and CMIP6 ensembles to predict future wind resources more appropriately.

Similar studies should be done for other renewable energy resources which are weather dependent such as solar energy.

Although they weren't the focus of this study, extreme winds are crucial for using wind energy to generate power.. It should be studied as well.

New technologies, such as airborne, are in the R&D phase now. Therefore, wind resource assessment for higher altitudes (> 500 m) above the ground level should also be studied to determine potential over these regions.

Micro-scale modeling is only performed for two sites. It should be done for the entire Türkiye by using statistical/dynamical downscaling methods to determine micro-scale changes for the entire Türkiye.

## REFERENCES


[1] O. Edenhofer, R. Pichs-Madruga, Y. Sokona, E. Farahani, S. Kadner, K. Seyboth, A. Adler, I. Baum, S. Brunner, P. Eickemeier, B. Kriemann, J. Savolainen, S. Schlömer, C. von Stechow, and T. Zwickel and J.C. Minx (eds.), Climate Change 2014: Mitigation of climate change Working Group III contribution to the Fifth Assessment Report of the Intergovernmental Panel on Climate Change. New York NY: Cambridge University Press, 2014.

[2] European Comission, Renewable energy targets. [Online] Available: https://energy.ec.europa.eu/topics/renewable-energy/renewable-energy-directive-targets-and-rules/renewable-energy-targets_en. Accessed on: Accessed Nov. 03 2022.

[3] GWEC, Global Wind Report 2022. [Online] Available: https://gwec.net/global-wind-report-2022/. Accessed on: Dec. 10 2022.

[4] Turkish Electricity Transmission System Operator (TEİAŞ), Load Dispatch Information Center Information System: Daily Statistics. [Online] Available: https://ytbs.teias.gov.tr/ytbs/frm_login.jsf. Accessed on: Mar. 18 2023.

[5] MENR, "National Energy Plan of Türkiye," Ministry of Energy and Natural Resources, 2022. [Online] Available: https://enerji.gov.tr//Media/Dizin/EIGM/tr/Raporlar/TUEP/T%C3%BCrkiye_Ulusal_Enerji_Plan%C4%B1.pdf. Accessed on: Jan. 22 2023.

[6] IEA, $CO_2$ Emissions from Fuel Combustion: Overview. [Online] Available: https://www.iea.org/reports/co2-emissions-from-fuel-combustion-2019. Accessed on: Oct. 12 2020.

[7] P. Lionello and L. Scarascia, "The relation between climate change in the Mediterranean region and global warming," (En;en), Reg Environ Change, vol. 18, no. 5, pp. 1481–1493, 2018.

[8] A. Tuel and E. A. B. Eltahir, "Why Is the Mediterranean a Climate Change Hot Spot?," Journal of Climate, vol. 33, no. 14, pp. 5829–5843, 2020.

[9] Clarke, L., Y.-M. Wei, A. De La Vega Navarro, A. Garg, A.N. Hahmann, S. Khennas, I.M.L. Azevedo, A. Löschel, A.K. Singh, L. Steg, "Energy Systems. In IPCC, 2022: Climate Change 2022: Mitigation of Climate Change. Contribution of Working Group III to the Sixth Assessment Report of the Intergovernmental Panel on Climate Change: [P.R. Shukla, J. Skea, R. Slade, A. Al Khourdajie, R. van Diemen, D. McCollum, M. Pathak, S. Some, P. Vyas, R. Fradera, M. Belkacemi, A. Hasija, G. Lisboa, S. Luz, J. Malley, (eds.)].," IPCC, Cambridge, UK and New York, NY, USA, 2022.

[10] Ali, E., W. Cramer, J. Carnicer, E. Georgopoulou, N.J.M. Hilmi, G. Le Cozannet, and P. Lionello, “Cross-Chapter Paper 4: Mediterranean Region. In: Climate Change 2022: Impacts, Adaptation and Vulnerability. Contribution of Working Group II to the Sixth Assessment Report of the Intergovernmental Panel on Climate Change: [H.-O. Pörtner, D.C. Roberts, M. Tignor, E.S. Poloczanska, K. Mintenbeck, A. Alegría, M. Craig, S. Langsdorf, S. Löschke, V. Möller, A. Okem, B. Rama (eds.)].,” IPCC, Cambridge, United Kingdom and New York, NY, USA, 2022.

[11] J. M. Gutiérrez, R.G. Jones, G.T. Narisma, L.M. Alves, M. Amjad, I.V. Gorodetskaya, M. Grose, N.A.B. Klutse, S. Krakovska, J. Li, D. Martínez-Castro, L.O. Mearns, S.H. Mernild, T. Ngo-Duc, B. van den Hurk, and and J.-H. Yoon, Interactive Atlas: In Climate Change 2021: The Physical Science Basis. Contribution of Working Group I to the Sixth Assessment Report of the Intergovernmental Panel on Climate Change [Masson-Delmotte, V., P. Zhai, A. Pirani, S.L. Connors, C. Péan, S. Berger, N. Caud, Y. Chen, L.Goldfarb, M.I. Gomis, M. Huang, K. Leitzell, E. Lonnoy, J.B.R. Matthews, T.K.Maycock, T. Waterfield, O. Yelekçi, R. Yu, and B. Zhou (eds.)]. [Online] Available: http://interactive-atlas.ipcc.ch/.

[12] Z. Zhang, K. Wang, D. Chen, J. Li, and R. Dickinson, “Increase in Surface Friction Dominates the Observed Surface Wind Speed Decline during 1973–2014 in the Northern Hemisphere Lands,” (EN), Journal of Climate, vol. 32, no. 21, pp. 7421–7435, 2019.

[13] F. Dadaser-Celik and E. Cengiz, “Wind speed trends over Turkey from 1975 to 2006,” Int. J. Climatol., vol. 34, no. 6, pp. 1913–1927, 2014.

[14] V. Eyring, S. Bony, G. A. Meehl, C. A. Senior, B. Stevens, R. J. Stouffer, and K. E. Taylor, “Overview of the Coupled Model Intercomparison Project Phase 6 (CMIP6) experimental design and organization,” Geosci. Model Dev., vol. 9, no. 5, pp. 1937–1958, 2016.

[15] S. Ç. Bağçaci, I. Yucel, E. Duzenli, and M. T. Yilmaz, “Intercomparison of the expected change in the temperature and the precipitation retrieved from CMIP6 and CMIP5 climate projections: A Mediterranean hot spot case, Turkey,” Atmospheric Research, vol. 256, p. 105576, 2021.

[16] F. Di Sante, E. Coppola, and F. Giorgi, “Projections of river floods in Europe using EURO-CORDEX CMIP5 and CMIP6 simulations,” (en), Int. Journal of Climatology, vol. 41, no. 5, pp. 3203–3221, 2021.

[17] A. A. Akinsanola, K. O. Ogunjobi, A. T. Abolude, and S. Salack, “Projected changes in wind speed and wind energy potential over West Africa in CMIP6 models,” (en), Environ. Res. Lett., vol. 16, no. 4, p. 44033, 2021.

[18] D. Carvalho, A. Rocha, X. Costoya, M. deCastro, and M. Gómez-Gesteira, “Wind energy resource over Europe under CMIP6 future climate projections: What changes from CMIP5 to CMIP6,” Renewable and Sustainable Energy Reviews, vol. 151, p. 111594, 2021.

[19] A. N. Hahmann, O. García-Santiago, and A. Peña, “Current and future wind energy resources in the North Sea according to CMIP6,” (English), Wind Energy Science 7, vol. 7, no. 6, pp. 2373–2391, 2022.

[20] A. S. Bhasuru, G. Nagababu, S. S. Kachhwaha, and H. Puppala, “Climate change impacts the future offshore wind energy resources in India: Evidence drawn from CORDEX-SA Regional Climate Models,” Regional Studies in Marine Science, vol. 56, p. 102717, 2022.

[21] H. Deng, W. Hua, and G. Fan, “Evaluation and Projection of Near-Surface Wind Speed over China Based on CMIP6 Models,” (en), Atmosphere, vol. 12, no. 8, p. 1062, 2021.

[22] D. Carvalho, A. Rocha, M. Gómez-Gesteira, and C. Silva Santos, “Potential impacts of climate change on European wind energy resource under the CMIP5 future climate projections”, Renewable Energy, vol. 101, pp. 29–40, 2017.

[23] K. Deng, C. Azorin-Molina, L. Minola, G. Zhang, and D. Chen, “Global Near-Surface Wind Speed Changes over the Last Decades Revealed by Reanalyses and CMIP6 Model Simulations,” Journal of Climate, vol. 34, no. 6, pp. 2219–2234, 2021.

[24] K. L. McInnes, T. A. Erwin, and J. M. Bathols, “Global Climate Model projected changes in 10 m wind speed and direction due to anthropogenic climate change,” Atmosph. Sci. Lett., vol. 12, no. 4, pp. 325–333, 2011.

[25] J. Najac, J. Boé, and L. Terray, “A multi-model ensemble approach for assessment of climate change impact on surface winds in France,” (En), Clim Dyn, vol. 32, no. 5, pp. 615–634, 2009.

[26] M. Reyers, J. Moemken, and J. G. Pinto, “Future changes of wind energy potentials over Europe in a large CMIP5 multi-model ensemble,” (en), Int. J. Climatol., vol. 36, no. 2, pp. 783–796, 2016.

[27] I. Tobin, S. Jerez, R. Vautard, F. Thais, E. van Meijgaard, A. Prein, M. Déqué, S. Kotlarski, C. F. Maule, G. Nikulin, T. Noël, and C. Teichmann, “Climate change impacts on the power generation potential of a European mid-century wind farms scenario,” (en), Environ. Res. Lett., vol. 11, no. 3, p. 34013, 2016.

[28] J. Wu, Y. Shi, and Y. Xu, “Evaluation and Projection of Surface Wind Speed Over China Based on CMIP6 GCMs,” (en), J. Geophys. Res. Atmos., vol. 125, no. 22, e2020JD033611, 2020.

[29] Ju Feng, “Artificial Intelligence for Wind Energy (AI4Wind): A state of the art report,” DTU Wind Energy, DTU Wind Energy E Vol, 2019. [Online] Available: https://orbit.dtu.dk/en/publications/artificial-intelligence-for-wind-energy-ai4wind-a-state-of-the-ar. Accessed on: Oct. 27 2021.

[30] C. Feng, M. Cui, B.-M. Hodge, and J. Zhang, “A data-driven multi-model methodology with deep feature selection for short-term wind forecasting,” Applied Energy, vol. 190, pp. 1245–1257, 2017.

[31] D. Niu, Di Pu, and S. Dai, “Ultra-Short-Term Wind-Power Forecasting Based on the Weighted Random Forest Optimized by the Niche Immune Lion Algorithm,” Energies, vol. 11, no. 5, p. 1098, 2018.

[32] D. Vassallo, R. Krishnamurthy, T. Sherman, and H. J. S. Fernando, “Analysis of Random Forest Modeling Strategies for Multi-Step Wind Speed Forecasting,” (en), Energies, vol. 13, no. 20, p. 5488, 2020.

[33] ESMAP, Ed., “Going Global Expanding Offshore Wind to Emerging Markets,” Dünya Bankası, Washington DC, 2019.

[34] H. H. Başaran and İ. Tarhan, “Investigation of offshore wind characteristics for the northwest of Türkiye region by using multi-criteria decision-making method (MOORA),” (en), Results in Engineering, vol. 16, p. 100757, 2022.

[35] Cem Öksel, Ali Koç, Yıldız Koç, And Hüseyin Yağlı, “Off-shore Wind Energy Potential Research for Antakya Bay,” (en), Selçuk Üniversitesi Mühendislik, Bilim ve Teknoloji Dergisi, vol. 4, no. 1, pp. 18–29, http://sujest.selcuk.edu.tr/sumbtd/article/view/313, 2016.

[36] U. Cali, N. Erdogan, S. Kucuksari, and M. Argin, “Techno-economic analysis of high potential offshore wind farm locations in Turkey,” (en), Energy Strategy Reviews, vol. 22, pp. 325–336, 2018.

[37] C. Anagnostopoulou, P. Zanis, E. Katragkou, I. Tegoulias, and K. Tolika, “Recent past and future patterns of the Etesian winds based on regional scale climate model simulations,” Clim Dyn, vol. 42, no. 7-8, pp. 1819–1836, 2014.

[38] S. Dafka, A. Toreti, J. Luterbacher, P. Zanis, E. Tyrlis, and E. Xoplaki, “Simulating Extreme Etesians over the Aegean and Implications for Wind Energy Production in Southeastern Europe,” Journal of Applied Meteorology and Climatology, vol. 57, no. 5, pp. 1123–1134, 2018.

[39] I. Logothetis, K. Tourpali, S. Misios, and P. Zanis, “Etesians and the summer circulation over East Mediterranean in Coupled Model Intercomparison Project Phase 5 simulations: Connections to the Indian summer monsoon,” International Journal of Climatology, vol. 40, no. 2, pp. 1118–1131, 2020.

[40] A. Poupkou, P. Zanis, P. Nastos, D. Papanastasiou, D. Melas, K. Tourpali, and C. Zerefos, “Present climate trend analysis of the Etesian winds in the Aegean Sea,” (En), Theor Appl Climatol, vol. 106, no. 3-4, pp. 459–472, 2011.

[41] B. Jourdier, “Evaluation of ERA5, MERRA-2, COSMO-REA6, NEWA and AROME to simulate wind power production over France,” in Advances in Science and Research, 2020, pp. 63–77.

[42] H. Arslan, H. Baltaci, B. O. Akkoyunlu, S. Karanfil, and M. Tayanc, “Wind speed variability and wind power potential over Turkey: Case studies for Çanakkale and İstanbul,” Renewable Energy, vol. 145, pp. 1020–1032, 2020.

[43] R. Kose, M. Ozgur, O. Erbas, and A. Tugcu, “The analysis of wind data and wind energy potential in Kutahya, Turkey,” Renewable and Sustainable Energy Reviews, vol. 8, no. 3, pp. 277–288, 2004.

[44] H. Serkendiz, H. Tatlı, and B. ÖZTÜRK, “Türkiye'deki Potansiyel Rüzgar Enerji Yoğunluğunun Yeniden Tanımlanması,” (tr scheme="ISO639-1";tr), joa, vol. 3, no. 5, pp. 739–750, https://dergipark.org.tr/en/pub/joa/article/534959, 2018.

[45] A. Ucar and F. Balo, “Investigation of wind characteristics and assessment of wind-generation potentiality in Uludağ-Bursa, Turkey,” Applied Energy, vol. 86, no. 3, pp. 333–339, 2009.

[46] R.K. Pachauri, M.R. Allen, V.R. Barros, J. Broome, W. Cramer, R. Christ, J.A. Church, L. Clarke, Q. Dahe, P. Dasgupta and N.K. Dubash, “Climate Change 2014: Synthesis report. Contribution of Working Groups I, II and III to the fifth assessment report of the Intergovernmental Panel on Climate Change” (p. 151). IPCC, 2014

[47] S. C. Pryor and R. J. Barthelmie, “Climate change impacts on wind energy: A review,” Renewable and Sustainable Energy Reviews, vol. 14, no. 1, pp. 430–437, 2010.

[48] O. Edenhofer, R. Pichs-Madruga, Ramón, and Y. Sokona, “Renewable Energy Sources and Climate Change Mitigation: Special report of the Intergovernmental Panel on Climate Change,” United Nations Environment Programme; World Meteorological Organization; Intergovernmental Panel on Climate Change; Potsdam-Institut für Klimafolgenforschung, New York, 2012.

[49] L. Landberg, Meteorology for wind energy: An Introduction. Chichester, West Sussex, England: Wiley, 2016.

[50] J. Sanz Rodrigo, R. A. Chávez Arroyo, P. Moriarty, M. Churchfield, B. Kosović, P.-E. Réthoré, K. S. Hansen, A. Hahmann, J. D. Mirocha, and D. Rife, “Mesoscale to microscale wind farm flow modeling and evaluation,” (en), Wiley Interdisciplinary Reviews: Energy and Environment, vol. 6, no. 2, e214, 2017.

[51] WINDSIM 10.0: Evaluation Version: WindSim AS.

[52] IPCC, “Climate Change 2022: Impacts, Adaptation and Vulnerability: ontribution of Working Group II to the Sixth Assessment Report of the Intergovernmental Panel on Climate Change,” 2022.

[53] United Nations (UN), ED., United Nations Framework Convention On Climate Change (UNFCCC), 1992.

[54] Gulev, S.K., P.W. Thorne, J. Ahn, F.J. Dentener, C.M. Domingues, S. Gerland, D. Gong, D.S. Kaufman, H.C. Nnamchi, J. Quaas, J.A. Rivera, S. Sathyendranath, S.L. Smith, B. Trewin, K. von Schuckmann, and and R.S. Vose, "Changing State of the Climate System. In Climate Change 2021: The Physical Science Basis. Contribution of Working Group I to the Sixth Assessment Report of the Intergovernmental Panel on Climate Change," IPCC, Cambridge, United Kingdom and New York, NY, USA 287–422, 2021.

[55] IPCC, "Climate Change 2021: The Physical Science Basis: Contribution of Working Group I to the Sixth Assessment Report of the Intergovernmental Panel on Climate Change," 2021.

[56] P. N. Edwards, "History of Climate Modeling," Wiley Interdisciplinary Reviews: Climate Change, vol. 2, no. 1, pp. 128–139, 2011.

[57] Stocker, T. (Ed.), "Climate change 2013: the physical science basis: Working Group I contribution to the Fifth assessment report of the Intergovernmental Panel on Climate Change", IPCC, Cambridge University Press,, Cambridge, United Kingdom and New York, USA, 2013.

[58] S. Solomon, D. Qin, M. Manning, K. Averyt, & M. Marquis (Eds.), "Climate change 2007: The Physical Science Basis Contribution of Working Group I to the Fourth Assessment Report of the Intergovernmental Panel on Climate Change," Intergovernmental Panel on Climate Change, IPCC, Cambridge University Press, Cambridge, New York, 2007.

[59] Heavens, N. G., Ward, D. S. & Natalie, M. M., "Studying and Projecting Climate Change with Earth System Models," Nature Education Knowledge, vol. 4, no. 5, 2013.

[60] K. Riahi, D. P. van Vuuren, E. Kriegler, J. Edmonds, B. C. O'Neill, S. Fujimori, N. Bauer, K. Calvin, R. Dellink, O. Fricko, W. Lutz, A. Popp, J. C. Cuaresma, S. KC, M. Leimbach, L. Jiang, T. Kram, S. Rao, J. Emmerling, K. Ebi, T. Hasegawa, P. Havlik, F. Humpenöder, L. A. Da Silva, S. Smith, E. Stehfest, V. Bosetti, J. Eom, D. Gernaat, T. Masui, J. Rogelj, J. Strefler, L. Drouet, V. Krey, G. Luderer, M. Harmsen, K. Takahashi, L. Baumstark, J. C. Doelman, M. Kainuma, Z. Klimont, G. Marangoni, H. Lotze-Campen, M. Obersteiner, A. Tabeau, and M. Tavoni, "The Shared Socioeconomic Pathways and their energy, land use, and greenhouse gas emissions implications: An overview," Global Environmental Change, vol. 42, pp. 153–168, 2017.

[61] E. J. Lantz, J. O. Roberts, J. Nunemaker, E. DeMeo, K. L. Dykes, and G. N. Scott, "Increasing Wind Turbine Tower Heights: Opportunities and Challenges," 2019.

[62] IRENA, Renewable Technology Innovation Indicators: Mapping progress in costs, patents and standards. Abu Dhabi, 2022.

[63] James F. Manwell (Author), Wind Energy Explained: Theory, Design and Application. John Wiley & Sons Ltd., 2009.

[64] Erik L. Petersen, Niels G. Mortensen, Lars Landberg, Jørgen Højstrup and Helmut P. Frank, Wind Power Meteorology. Risø National Laboratory, Roskilde, Denmark, 1997.

[65] Matthew Huaiquan Zhang, Wind Resource Assessment and Micro-Siting: Science and Engineering: John Wiley & Sons, 2015.

[66] E. L. Petersen and I. Troen, "Wind Conditions and Resource Assessment," WENE, vol. 1, no. 2, pp. 206–217, 2012.

[67] Peña, A., Hasager, C. B., Badger, M., R. J. Barthelmie, F. Bingöl, J.-P. Cariou, S. Emeis, S. T. Frandsen, M. Harris, I. Karagali, S. E. Larsen, Mann, J., Mikkelsen, P. T., P. M., S. S., A., Schlipf, D., Slinger, W. C., and R, Remote Sensing for Wind Energy: DTU, 2015.

[68] S. C. Pryor, J. T. Schoof, and R. J. Barthelmie, "Climate change impacts on wind speeds and wind energy density in northern Europe: empirical downscaling of multiple AOGCMs," Clim. Res., vol. 29, no. 3, pp. 183–198, 2005.

[69] D. J. Sailor, M. Smith, and M. Hart, "Climate change implications for wind power resources in the Northwest United States," Renewable Energy, vol. 33, no. 11, pp. 2393–2406, 2008.

[70] J. Najac, C. Lac, and L. Terray, "Impact of climate change on surface winds in France using a statistical-dynamical downscaling method with mesoscale modelling", International Journal of Climatology., vol. 31, no. 3, pp. 415–430, 2011.

[71] P. Donk, E. van Uytven, and P. Willems, "Statistical methodology for on-site wind resource and power potential assessment under current and future climate conditions: a case study of Suriname," (En), SN Appl. Sci., vol. 1, no. 8, pp. 1–15, 2019.

[72] A. N. Hahmann, B. Witha, D. L. Rife, N. Frouzakis, C. Junk, and T. Sile, "Description of the Probabilistic Wind Atlas Methodology, Deliverable D3.1: NEWA-New European Wind Atlas," 2017.

[73] A. N. Hahmann, T. Sile, B. Witha, N. N. Davis, M. Dörenkämper, Y. Ezber, E. García-Bustamante, J. F. González Rouco, J. Navarro, B. T. Olsen, and S. Söderberg, "The Making of the New European Wind Atlas, Part 1: Model Sensitivity," 2020.

[74] Ministry of Energy and Natural Resources, Wind Energy Potential Atlas of Türkiye. [Online] Available: repa.enerji.gov.tr. Accessed on: Mar. 27 2021.

[75] DTU Wind Energy, Global Wind Atlas. [Online] Available: https://globalwindatlas.info/about/resources. Accessed on: Oct. 12 2020.

[76] J. C. Hansen, N. G. Mortensen, T. Cronin, M. Nielsen, A. N. Hahmann, Badger, J., & Larsén, and X. G., "Wind Atlas for South Africa (WASA): Best practice guide for application of WASA," 2014.

[77] Skamarock, W. C., J. B. Klemp, J. Dudhia, D. O. Gill, D. M. Barker, M. G. Duda, X.-Y. Huang, W. Wang, et al., "A Description of the Advanced Research WRF Version 3. Tech. Rep," 2008.

[78] E. Tan, S. S. Mentes, E. Unal, Y. Unal, B. Efe, B. Barutcu, B. Onol, H. S. Topcu, and S. Incecik, "Short term wind energy resource prediction using WRF model for a location in western part of Turkey," (en), Journal of Renewable and Sustainable Energy, vol. 13, no. 1, p. 13303, 2021.

[79] T. Kaytancı, Ş. S. Menteş, and Y. Ünal, "Simulating the Impacts of Wind Farm Wake under the Changes in MYNN Planetary Boundary Layer Scheme in High Resolution Weather Research and Forecasting Model," (en), Atmosphere, vol. 13, no. 11, p. 1838, 2022.

[80] G. Ibarra-Berastegi, J. Sáenz, A. Ulazia, P. Serras, G. Esnaola, and C. Garcia-Soto, "Electricity production, capacity factor, and plant efficiency index at the Mutriku wave farm (2014–2016)," Ocean Engineering, vol. 147, pp. 20–29, 2018.

[81] Wind Atlas Simulation Programme (WASP): DTU Wind Energy, 2011.

[82] WindPRO: EMD.

[83] L. Landberg, Meteorology for wind energy: An introduction. Chichester UK, Hoboken NJ: John Wiley & Sons, 2016.

[84] OpenCFD Ltd, OPEN FOAM.

[85] OFWind CFD: EMD International.

[86] OrkunTemel, Laurent Bricteux, Jeroen van Beeck, "Coupled WRF-OpenFOAM study of wind flow over complex terrain," Journal of Wind Engineering and Industrial Aerodynamics, vol. 174, pp. 152–169, 2018.

[87] P. S. Arya, Introduction to Micrometeorology: Elsevier, 2001.

[88] S. Monin and A.M. Obukhov, Basic laws of turbulent mixing in the surface layer of the atmosphere, 1954.

[89] M. Optis, N. Bodini, M. Debnath, and P. Doubrawa, "New methods to improve the vertical extrapolation of near-surface offshore wind speeds," (English), Wind Energ. Sci., vol. 6, no. 3, pp. 935–948, https://wes.copernicus.org/articles/6/935/2021/, 2021.

[90] F. Bañuelos-Ruedas, C. Angeles-Camacho, and S. Rios-Marcuello, "Analysis and validation of the methodology used in the extrapolation of wind speed data at different heights," (en), Renewable and Sustainable Energy Reviews, vol. 14, no. 8, pp. 2383–2391, 2010.

[91] I. Troen and E. Lundtang Petersen, European Wind Atlas. Roskilde: Risø National Laboratory: Technical University of Denmark, 1989.

[92] N. Kasbadji Merzouk, “Wind energy potential of Algeria,” Renewable Energy, vol. 21, 553±562, 2000.

[93] Brasil, Atlas do Potencial Eólico Brasileiro. [Online] Available: http://www.novoatlas.cepel.br/. Accessed on: Apr. 04 2021.

[94] A. N. Starkov, P. P. Bezroukikh, M. M. Borisenko, and L. Landberg, “Russian wind atlas,” Denmark, 2000.

[95] Ministry of Energy and Natural Resources, “Wind Energy Potential Atlas of Türkiye,” MENR, 2006.

[96] Yüksel Malkoç, “Rüzgar Enerjisi Kaynaklarımız,” Elektrik Mühendisleri Odası, https://www.emo.org.tr/ekler/5237d34f69ddac7_ek.pdf.

[97] M. Dörenkämper, B. T. Olsen, B. Witha, A. N. Hahmann, N. N. Davis, J. Barcons, Y. Ezber, E. García-Bustamante, J. F. González-Rouco, J. Navarro, M. Sastre-Marugán, T. Sīle, W. Trei, M. Žagar, J. Badger, J. Gottschall, J. Sanz Rodrigo, and J. Mann, “The Making of the New European Wind Atlas – Part 2: Production and Evaluation,” 2020.

[98] Department of Climate and Agricultural Meteorology, Ed., “2020 Climate Evaluation of Turkey,” Turkish State of Meteorology Services, Ankara, Turkey, 2021. [Online] Available: https://www.mgm.gov.tr/FILES/iklim/yillikiklim/2020-iklim-raporu.pdf.

[99] Cetin S., Akgündüz A. S., Odabaşı E., Kılıç G., Çamalan G., Erkan A. M., Soydan M., and Güser Y., “Türkiye Meteorolojik Afetler Değerlendirmesi (2010-2021): Evaluation of Meteorological Disasters for Turkey (2010-2021),” Turkish State of Meteorology, Ankara, 2022. [Online] Available: https://media-exp1.licdn.com/dms/document/C4D1FAQHjPf9av2wurA/feedshare-document-pdf-analyzed/0/1650524797419?e=1664409600&v=beta&t=NzSbxj9YwNNsZqr_SBrumzft5V21kRzEc9jVSG9xG4A. Accessed on: Jul. 16 2022.

[100] NASA, Shuttle Radar Topographic Mission Data: SRTM-1 Arc-Second Global. [Online] Available: https://earthexplorer.usgs.gov/. Accessed on: Apr. 30 2021.

[101] Corine 2018-Land Cover. [Online] Available: https://land.copernicus.eu/pan-european/corine-land-cover/clc2018?tab=download. Accessed on: May 01 2021.

[102] A. Deniz, H. Toros, and S. Incecik, “Spatial variations of climate indices in Turkey,” Int. J. Climatol., vol. 31, no. 3, pp. 394–403, 2011.

[103] S. Sahin and M. Türkeş, “Contemporary Surface Wind Climatology of Turkey,” Theor Appl Climatol, vol. 113, no. 1-2, pp. 337–349, 2013.

[104] Serhat Sensoy, Mesut Demircan, Yusuf Ulupınar, “Climate of Turkey,” Turkish State Meteorological Service, Ankara, Turkey. [Online] Available: http://www.emcc.mgm.gov.tr/files/climateofturkey.pdf. Accessed on: Apr. 28 2021.

[105] Serhat Şensoy, Mesut Demircan, Yusuf Ulupınar, İzzet Balta, “Türkiye İklimi,” Turkish State Meteorological Service, Ankara, Türkiye. [Online] Available: https://www.mgm.gov.tr/FILES/iklim/yayinlar/turkiye_iklimi.pdf. Accessed on: Apr. 28 2021.

[106] Ministry of Environment, Urbanization and Climate Change, United Nations Framework Convention on Climate Change. [Online] Available: https://iklim.gov.tr/bm-iklim-degisikligi-cerceve-sozlesmesi-i-33. Accessed on: Oct. 20 2022.

[107] Law on the Ratification of the Paris Agreement by Türkiye, No: 7335, Official Gazette, dated 07.10.2021 numbered 31921.

[108] Republic of Türkiye, “Intended Nationally Determined Contribution,” 2015.

[109] Ministry of Environment, Urbanization and Climate Change, Paris Agreement. [Online] Available: https://iklim.csb.gov.tr/paris-anlasmasi-i-98587. Accessed on: May 01 2021.

[110] Ministry of Environment, Urbanization and Climate Change, Republic of Turkey Climate Change Strategy 2010-2023.

[111] Climate Council, “Comission Recomended Decisions,” Feb. 2022. [Online] Available: https://iklimsurasi.gov.tr/public/images/sonucbildirgesi.pdf. Accessed on: Jan. 17 2023.

[112] Reuters, Türkiye boosts greenhouse gas emission reduction target. [Online] Available: https://www.reuters.com/business/cop/Türkiye-boosts-greenhouse-gas-emission-reduction-target-2030-2022-11-15/. Accessed on: Nov. 21 2022.

[113] International Energy Agency, “Turkey 2021: Energy Policiy Review,” IEA, 2021. [Online] Available: https://www.iea.org/reports/turkey-2021. Accessed on: Oct. 20 2022.

[114] MENR, “Investor's Guide for Electricity”, Jun. 2022. [Online] Available: https://enerji.gov.tr/info-bank-investors-guide-for-electricity. Accessed on: Mar. 14 2023.

[115] Republic of Türkiye, 11th Development Plan, 2019.

[116] G. Florence, “OECD Economic Surveys: Turkey 2021,” Organisation for Economic Co-operation and Development (OECD), Jan. 2021.

[117] MENR, Turkey Electricity Demand Projection Report: 2020-2040. [Online] Available: https://enerjiapi.enerji.gov.tr//Media/Dizin/EIGM/Raporlar/Enerji_Talep_Projeksiy

onu/114176-turkiye_elektrik_enerjisi_talep_projeksiyonu_raporu.pdf. Accessed on: Feb. 20 2021.

[118] TurkStat, Greenhouse Gas Emissions Statistics, 1990 - 2020. [Online] Available: https://data.tuik.gov.tr/Bulten/Index?p=Sera-Gazi-Emisyon-Istatistikleri-1990-2020-45862#:~:text=Sera%20gaz%C4%B1%20envanteri%20sonu%C3%A7lar%C4%B1na%20g%C3%B6re,CO2%20e%C5%9Fd.%20olarak%20hesapland%C4%B1. Accessed on: Sep. 15 2022.

[119] OECD, "OECD Economic Surveys Turkey," OECD, 2021.

[120] Presidency of the Republic of Türkiye Investment Office, "Guide to investing in Turkish Renewable Energy Sector," [Online] Available: https://www.invest.gov.tr/en/library/publications/lists/investpublications/guide-to-investing-in-turkish-renewables-energy-sector.pdf. Accessed on: Mar. 18 2023.

[121] Law on Utilization of Renewable Energy Resources for the Purpose of Generating Electrical Energy, No: 5346, 2005.

[122] Republic of Türkiye, Presidential Decision No. 3453, 2021.

[123] Regulation on Renewable Energy Resource Zones, Official Gazette dated 09.10.2016, numbered 29852.

[124] MENR, Yenilenebilir Enerji Kaynak Alanları (YEKA) Modeli ve Uygulamaları. [Online] Available: https://enerji.gov.tr/eigm-yenilenebilir-enerji-uretim-faaliyetleri-yeka-modeli. Accessed on: Oct. 20 2022.

[125] World Bank Group, "Key Factors for Successful Development of Offshore Wind in Emerging Markets," ESMAP, World Bank, Washington, DC. License: Creative Commons Attribution CC BY 3.0 IGO, 2021.

[126] MENR, Duyurular. [Online] Available: https://enerji.gov.tr/medya-duyurular-liste. Accessed on: Oct. 18 2022.

[127] Regulation on Renewable Energy Guarantees of Origin in The Electricity Market, Official Gazette dated 14/11/2020, numbered 31304.

[128] International Energy Agency, "Renewables 2021 Data Explorer – Data Tools", IEA, [Online] Available: https://www.iea.org/data-and-statistics/data-tools/renewables-2021-data-explorer?mode=market&region=World&publication=2021&product=Total. Accessed on: Oct. 20 2022.

[129] Turkish Wind Energy Association (TWEA), Wind Database. [Online] Available: https://app.powerbi.com/view?r=eyJrIjoiNmFmYWY0MTYtNjUyNS00NzQ1LWIwMTMtOTI5ZTNkM2FlYWIxIiwidCI6ImU5YzY0NjU4LWFkMWQtNDUwOS1hODk0LTE2NWZhYjU2NjEyMyIsImMiOjl9. Accessed on: Dec. 21 2022.

[130] MENR, Info Bank: Resources,Wind Energy [Online] Available: https://enerji.gov.tr/eigm-resources-en, Accessed on: Dec. 10 2020.

[131] Law on Shore, No: 3621, Official Gazette dated 17.04.1990, numbered 20495.

[132] MENR, REZ Model. [Online] Available: https://enerji.gov.tr/eigm-yenilenebilir-enerji-uretim-faaliyetleri-yeka-modeli. Accessed on: Mar. 15 2021.

[133] Electricity Market Law, No:6446, Official Gazette, dated 30/3/2013 numbered 28603.

[134] Energy Market Regulatory Authority, Electricity Market Production Licences. [Online] Available: http://lisans.epdk.gov.tr/epvys-web/faces/pages/lisans/elektrikUretim/elektrikUretimOzetSorgula.xhtml. Accessed on: Apr. 29 2021.

[135] Turkish Wind Energy Association, Wind Energy Data Base. [Online] Available: https://app.powerbi.com/view?r=eyJrIjoiNmFmYWY0MTYtNjUyNS00NzQ1LWIwMTMtOTI5ZTNkM2FlYWIxIiwidCI6ImU5YzY0NjU4LWFkMWQtNDUwOS1hODk0LTE2NWZhYjU2NjEyMyIsImMiOjl9. Accessed on: Apr. 04 2021.

[136] J. O. Ebinger and W. Vergara, “Climate impacts on energy systems: Key issues for energy sector adaptation,” World Bank, Washington D.C., A World Bank study.

[137] W. Fan, Y. Liu, A. Chappell, L. Dong, R. Xu, M. Ekström, T.-M. Fu, and Z. Zeng, “Evaluation of Global Reanalysis Land Surface Wind Speed Trends to Support Wind Energy Development Using In Situ Observations,” (EN), Journal of Applied Meteorology and Climatology, vol. 60, no. 1, pp. 33–50, 2021.

[138] H. Miao, D. Dong, G. Huang, K. Hu, Q. Tian, and Y. Gong, “Evaluation of Northern Hemisphere surface wind speed and wind power density in multiple reanalysis datasets,” Energy, vol. 200, p. 117382, 2020.

[139] T. K. Laurila, V. A. Sinclair, and H. Gregow, “Climatology, variability, and trends in near-surface wind speeds over the North Atlantic and Europe during 1979–2018 based on ERA5,” (en), International Journal of Climatology, vol. 41, no. 4, pp. 2253–2278, 2021.

[140] T. K. Laurila, V. A. Sinclair, and H. Gregow, “Climatology, variability, and trends in near-surface wind speeds over the North Atlantic and Europe during 1979–2018 based on ERA5,” (en), International Journal of Climatology, vol. 41, no. 4, pp. 2253–2278, 2021.

[141] J. Ramon, L. Lledó, V. Torralba, A. Soret, and F. J. Doblas-Reyes, “What global reanalysis best represents near-surface winds?,” (en), Quarterly Journal of the Royal Meteorological Society, vol. 145, no. 724, pp. 3236–3251, 2019.

[142] T. Li, Z. Jiang, H. Le Treut, L. Li, L. Zhao, and L. Ge, “Machine learning to optimize climate projection over China with multi-model ensemble simulations,” (en), Environ. Res. Lett., vol. 16, no. 9, p. 94028, 2021.

[143] P. J. Gleckler, K. E. Taylor, and C. Doutriaux, “Performance metrics for climate models,” (en), J. Geophys. Res., vol. 113, no. D6, 2008.

[144] R. L. Wilby, “Evaluating climate model outputs for hydrological applications,” Hydrological Sciences Journal, vol. 55, no. 7, pp. 1090–1093, 2010.

[145] I. Barstad, A. Sorteberg, and M. -S. Mesquita, “Present and future offshore wind power potential in northern Europe based on downscaled global climate runs with adjusted SST and sea ice cover,” Renewable Energy, vol. 44, pp. 398–405, 2012.

[146] H. Hueging, R. Haas, K. Born, D. Jacob, and J. G. Pinto, “Regional Changes in Wind Energy Potential over Europe Using Regional Climate Model Ensemble Projections,” Journal of Applied Meteorology and Climatology, vol. 52, no. 4, pp. 903–917, 2013.

[147] A. A. Akinsanola, K O. Ogunjobi, A T. Abolude and Seyni, “Projected changes in wind speed and wind energy potential over West Africa,” 2021.

[148] A. Krishnan and P. K. Bhaskaran, “Skill assessment of global climate model wind speed from CMIP5 and CMIP6 and evaluation of projections for the Bay of Bengal,” (En;en), Clim Dyn, vol. 55, no. 9-10, pp. 2667–2687, 2020.

[149] P. B. Breslow and D. J. Sailor, “Vulnerability of wind power resources to climate change in the continental United States,” Renewable Energy, vol. 27, no. 4, pp. 585–598, 2002.

[150] L. Chen, “Impacts of climate change on wind resources over North America based on NA-CORDEX,” Renewable Energy, vol. 153, pp. 1428–1438, 2020.

[151] S. C. Pryor and R. J. Barthelmie, “Assessing climate change impacts on the near-term stability of the wind energy resource over the United States,” (eng), Proceedings of the National Academy of Sciences of the United States of America, vol. 108, no. 20, pp. 8167–8171, 2011.

[152] M. Segal, Z. Pan, R. W. Arritt, and E. S. Takle, “On the potential change in wind power over the US due to increases of atmospheric greenhouse gases,” Renewable Energy, vol. 24, no. 2, pp. 235–243, 2001.

[153] Y. Yao, G. H. Huang, and Q. Lin, “Climate change impacts on Ontario wind power resource,” (En;en), Environ Syst Res, vol. 1, no. 1, pp. 1–11, 2012.

[154] R. Davy, N. Gnatiuk, L. Pettersson, and L. Bobylev, “Climate change impacts on wind energy potential in the European domain with a focus on the Black Sea,” Renewable and Sustainable Energy Reviews, vol. 81, pp. 1652–1659, 2018.

[155] S. Kulkarni and H.-P. Huang, “Changes in Surface Wind Speed over North America from CMIP5 Model Projections and Implications for Wind Energy,” (en), Advances in Meteorology, vol. 2014, pp. 1–10, 2014.

[156] J. Moemken, M. Reyers, H. Feldmann, and J. G. Pinto, “Future Changes of Wind Speed and Wind Energy Potentials in EURO-CORDEX Ensemble Simulations,” J. Geophys. Res. Atmos., vol. 123, no. 12, pp. 6373–6389, 2018.

[157] S. C. Pryor, R. J. Barthelmie, and E. Kjellström, “Potential climate change impact on wind energy resources in northern Europe: analyses using a regional climate model,” (En;en), Clim Dyn, vol. 25, no. 7-8, pp. 815–835, 2005.

[158] S. C. Pryor, J. T. Schoof, and R. J. Barthelmie, “Winds of change?: Projections of near-surface winds under climate change scenarios,” Geophys. Res. Lett., vol. 33, no. 11, 2006.

[159] I. Tobin, R. Vautard, I. Balog, F.-M. Bréon, S. Jerez, P. M. Ruti, F. Thais, M. Vrac, and P. Yiou, “Assessing climate change impacts on European wind energy from ENSEMBLES high-resolution climate projections,” (En;en), Climatic Change, vol. 128, no. 1-2, pp. 99–112, 2015.

[160] C. Fant, C. Adam Schlosser, and K. Strzepek, “The impact of climate change on wind and solar resources in southern Africa,” Applied Energy, vol. 161, pp. 556–564, 2016.

[161] O. J. Matthew and O. S. Ohunakin, “Simulating the effects of climate change and afforestation on wind power potential in Nigeria,” Sustainable Energy Technologies and Assessments, vol. 22, pp. 41–54, 2017.

[162] P. de Jong, T. B. Barreto, C. A. Tanajura, D. Kouloukoui, K. P. Oliveira-Esquerre, A. Kiperstok, and E. A. Torres, “Estimating the impact of climate change on wind and solar energy in Brazil using a South American regional climate model,” Renewable Energy, vol. 141, pp. 390–401, 2019.

[163] A. F. Pereira de Lucena, A. S. Szklo, R. Schaeffer, and R. M. Dutra, “The vulnerability of wind power to climate change in Brazil,” Renewable Energy, vol. 35, no. 5, pp. 904–912, 2010.

[164] P. Nolan, P. Lynch, R. McGrath, T. Semmler, and S. Wang, “Simulating climate change and its effects on the wind energy resource of Ireland,” (en), Wind Energ., vol. 15, no. 4, pp. 593–608, 2012.

[165] M. Ohba, “The Impact of Global Warming on Wind Energy Resources and Ramp Events in Japan,” (en), Atmosphere, vol. 10, no. 5, p. 265, 2019.

[166] H. Koch and M. Büchner, “Is climate change a threat to the growing importance of wind power resources in the energy sector in Germany?,” Energy Sources, Part B: Economics, Planning, and Policy, vol. 11, no. 12, pp. 1128–1136, 2016.

[167] T. Katopodis, I. Markantonis, D. Vlachogiannis, N. Politi, and A. Sfetsos, "Assessing climate change impacts on wind characteristics in Greece through high resolution regional climate modelling," Renewable Energy, vol. 179, pp. 427–444, 2021.

[168] Kristopher B. Karnauskas, Julie K. Lundquist, and Lei Zhang, "Southward shift of the global wind energy resource under high carbon dioxide emissions,"

[169] M. Iturbide, J. Fernández, J. M. Gutiérrez, J. Bedia, E. Cimadevilla, J. Díez-Sierra, R. Manzanas, A. Casanueva, J. Baño-Medina, J. Milovac, S. Herrera, A. S. Cofiño, D. San Martín, M. García-Díez, M. Hauser, D. Huard, and Ö. Yelekci, Repository supporting the implementation of FAIR principles in the IPCC-WGI Atlas: Zenodo, 2021.

[170] Bloom, A., Kotroni, V., & Lagouvardos, K, "Climate change impact of wind energy availability in the Eastern Mediterranean using the regional climate model PRECIS," Natural Hazards and Earth System Sciences, vol. 8(6), pp. 1249–1257, 2008.

[171] D. Hdidouan and I. Staffell, "The impact of climate change on the levelised cost of wind energy," Renewable Energy, vol. 101, pp. 575–592, 2017.

[172] D.J. Sailor, T. Hu, X. Li, J.N. Rosen, "A neural network approach to local downscaling of GCM output for assessing wind power implications of climate change," Renewable Energy, vol. 19, 359±378, 2000.

[173] Yılmaz E., Türkiye Üzerinde 21. Yüzyılda Rüzgar Hızı ve Rüzgar Enerjisi Potansiyelinin İncelenmesi ve Wasp Modeli İle Seçili Bölge İçin Sonuçların Değerlendirilmesi, M.S. Thesis, Istanbul Technical University, 2016.

[174] J. Najac, "Impacts of climate change on wind energy resources in France: a regionalization study," Toulouse-3 Univ FRNC-TH--7848, 2008. [Online] Available: https://inis.iaea.org/search/search.aspx?orig_q=rn:42013904.

[175] Koch, H., & Büchner, M., "Is climate change a threat to the growing importance of wind power resources in the energy sector in Germany?," (en), Energy Sources, Part B: Economics, Planning, and Policy, 2016.

[176] S. C. Pryor, J. T. Schoof, and R. J. Barthelmie, "Winds of change?: Projections of near-surface winds under climate change scenarios," (en), Geophys. Res. Lett., vol. 33, no. 11, 2006.

[177] D. L. Johnson and R. J. Erhardt, "Projected impacts of climate change on wind energy density in the United States," Renewable Energy, vol. 85, pp. 66–73, 2016.

[178] D. Ren, "Effects of global warming on wind energy availability," (en), Journal of Renewable and Sustainable Energy, vol. 2, no. 5, p. 52301, 2010.

[179] R. Pašičko, Č. Branković, and Z. Šimić, “Assessment of climate change impacts on energy generation from renewable sources in Croatia,” Renewable Energy, vol. 46, pp. 224–231, 2012.

[180] J. S. Hosking, D. MacLeod, T. Phillips, C. R. Holmes, P. Watson, E. F. Shuckburgh, and D. Mitchell, “Changes in European wind energy generation potential within a 1.5 °C warmer world,” (en), Environ. Res. Lett., vol. 13, no. 5, p. 54032, 2018.

[181] J. P. Evans, M. Kay, A. Prasad, and A. Pitman, “The resilience of Australian wind energy to climate change,” (en), Environ. Res. Lett., vol. 13, no. 2, p. 24014, 2018.

[182] A. Bloom, V. Kotroni, and K. Lagouvardos, “Climate change impact of wind energy availability in the Eastern Mediterranean using the regional climate model PRECIS,” (English), Nat. Hazards Earth Syst. Sci., vol. 8, no. 6, pp. 1249–1257, https://nhess.copernicus.org/articles/8/1249/2008/, 2008.

[183] D. Sailor, T. Hu, X. Li, and J. Rosen, “A neural network approach to local downscaling of GCM output for assessing wind power implications of climate change,” Renewable Energy, vol. 19, no. 3, pp. 359–378, 2000.

[184] C. S. Cheng, E. Lopes, C. Fu, and Z. Huang, “Possible Impacts of Climate Change on Wind Gusts under Downscaled Future Climate Conditions: Updated for Canada,” (EN), Journal of Climate, vol. 27, no. 3, pp. 1255–1270, 2014.

[185] D. J. Rasmussen, T. Holloway, and G. F. Nemet, “Opportunities and challenges in assessing climate change impacts on wind energy—a critical comparison of wind speed projections in California,” (en), Environ. Res. Lett., vol. 6, no. 2, p. 24008, 2011.

[186] Copernicus Climate Change Service, “CMIP6 climate projections,” 2021. Accessed on: Aug. 01 2022.

[187] S. C. Pryor, R. J. Barthelmie, D. T. Young, E. S. Takle, R. W. Arritt, D. Flory, W. J. Gutowski, A. Nunes, and J. Roads, “Wind speed trends over the contiguous United States,” (en), J. Geophys. Res., vol. 114, no. D14, 2009.

[188] McVicar, Tim R., M. L. Roderick, R. J. Donohue, L. T. Li, T. G. van Niel, A. Thomas, J. Grieser, D. Jhajharia, Y. Himri, N. M. Mahowald, A. V. Mescherskaya, A. C. Kruger, S. Rehman, and Y. Dinpashoh, “Global review and synthesis of trends in observed terrestrial near-surface wind speeds: Implications for evaporation,” Journal of Hydrology, vol. 416-417, pp. 182–205, 2012.

[189] Katherine Klink, “Trends in mean monthly maximum and minimum surface wind speeds in the coterminous United States, 1961 to 1990,” vol. 13, pp. 193–205, 1999.

[190] Karl E. Taylor, “Summarizing multiple aspects of model performance in a single diagram,” Journal of Geophysical Research, vol. 106, pp. 7183–7192, 2001.

[191] M. Demircan, "Sıcaklık Verilerindeki Kırılma Tarihleriyle İklim İndekslerinin İlişkisi", PhD Thesis, Ankara University, Social Science Institute, Department of Geography, Ankara, 2019.

[192] QGIS Development Team, QGIS Geographic Information System: Open Source Geospatial Foundation, 2009.

[193] H. Hersbach, B. Bell, P. Berrisford, G. Biavati, A. Horányi, J. Muñoz Sabater, J. Nicolas, C. Peubey, R. Radu, I. Rozum, D. Schepers, A. Simmons, C. Soci, D. Dee, and J.-N. Thépaut, "ERA5 hourly data on single levels from 1979 to present," https://cds.climate.copernicus.eu/cdsapp#!/dataset/reanalysis-era5-single-levels?tab=form, 2018.

[194] Global Modeling and Assimilation Office (GMAO), "MERRA-2 tavg1_2d_slv_Nx: 2d,1-Hourly,Time-MERRA-2 tavg1_2d_slv_Nx: 2d,1-Hourly,Time-Averaged,Single-Level,Assimilation,Single-Level Diagnostics V5.12.4," Greenbelt, MD, USA,Goddard Earth Sciences Data and Information Services Center (GES DISC), 2015. Accessed on: Jun. 08 2022.

[195] T. Wu, M. Chu, M. Dong, Y. Fang, W. Jie, J. Li, W. Li, Q. Liu, X. Shi, X. Xin, J. Yan, F. Zhang, J. Zhang, L. Zhang, and Y. Zhang, "BCC-CSM2-MR: model output prepared for CMIP6 CMIP historical," (en), 2018.

[196] J. Zhang, T. Wu, X. Shi, F. Zhang, J. Li, M. Chu, Q. Liu, J. Yan, Q. Ma, and M. Wei, "BCC BCC-ESM1: model output prepared for CMIP6 CMIP historical," (en), 2018.

[197] X. Rong, "CAMS CAMS_CSM1.0: model output prepared for CMIP6 CMIP historical," (en), 2019.

[198] N. C. Swart, J. N. Cole, V. V. Kharin, M. Lazare, J. F. Scinocca, N. P. Gillett, J. Anstey, V. Arora, J. R. Christian, Y. Jiao, W. G. Lee, F. Majaess, O. A. Saenko, C. Seiler, C. Seinen, A. Shao, L. Solheim, K. von Salzen, D. Yang, B. Winter, and M. Sigmond, "CCCma CanESM5 model output prepared for CMIP6 CMIP historical," (en), 2019.

[199] Z. Chai, "CAS CAS-ESM1.0 model output prepared for CMIP6 CMIP historical," (en), 2020.

[200] G. Danabasoglu, "NCAR CESM2 model output prepared for CMIP6 CMIP historical," (en), 2019.

[201] G. Danabasoglu, "NCAR CESM2-FV2 model output prepared for CMIP6 CMIP historical," (en), 2019.

[202] G. Danabasoglu, "NCAR CESM2-WACCM model output prepared for CMIP6 CMIP historical," (en), 2019.

[203] D. C. Bader, R. Leung, M. Taylor, and R. B. McCoy, "E3SM-Project E3SM1.0 model output prepared for CMIP6 CMIP historical," (en), 2019.

[204] EC-Earth Consortium (EC-Earth), “EC-Earth-Consortium EC-Earth3 model output prepared for CMIP6 CMIP historical,” (en), 2019.

[205] EC-Earth Consortium (EC-Earth), “EC-Earth-Consortium EC-Earth3-Veg model output prepared for CMIP6 CMIP historical,” (en), 2019.

[206] Y. YU, “CAS FGOALS-f3-L model output prepared for CMIP6 CMIP historical,” (en), 2019.

[207] L. Li, “CAS FGOALS-g3 model output prepared for CMIP6 CMIP historical,” (en), 2019.

[208] H. Guo, J. G. John, C. Blanton, C. McHugh, S. Nikonov, A. Radhakrishnan, K. Rand, N. T. Zadeh, V. Balaji, J. Durachta, C. Dupuis, R. Menzel, T. Robinson, S. Underwood, H. Vahlenkamp, M. Bushuk, K. A. Dunne, R. Dussin, P. P. G. Gauthier, P. Ginoux, S. M. Griffies, R. Hallberg, M. Harrison, W. Hurlin, P. Lin, S. Malyshev, V. Naik, F. Paulot, D. J. Paynter, J. Ploshay, B. G. Reichl, D. M. Schwarzkopf, C. J. Seman, A. Shao, L. Silvers, B. Wyman, X. Yan, Y. Zeng, A. Adcroft, J. P. Dunne, I. M. Held, J. P. Krasting, L. W. Horowitz, P. Milly, E. Shevliakova, M. Winton, M. Zhao, and R. Zhang, “NOAA-GFDL GFDL-CM4 model output historical,” (en), 2019.

[209] NASA Goddard Institute for Space Studies (NASA/GISS), “NASA-GISS GISS-E2-1-G-CC model output prepared for CMIP6 CMIP historical,” (en), 2019.

[210] NASA Goddard Institute for Space Studies (NASA/GISS), “NASA-GISS GISS-E2.1G model output prepared for CMIP6 CMIP historical,” (en), 2018.

[211] NASA Goddard Institute for Space Studies (NASA/GISS), “NASA-GISS GISS-E2.1H model output prepared for CMIP6 CMIP historical,” (en), 2019.

[212] E. Volodin, E. Mortikov, A. Gritsun, V. Lykossov, V. Galin, N. Diansky, A. Gusev, S. Kostrykin, N. Iakovlev, A. Shestakova, and S. Emelina, “INM INM-CM4-8 model output prepared for CMIP6 CMIP historical,” (en), 2019.

[213] O. Boucher, S. Denvil, G. Levavasseur, A. Cozic, A. Caubel, M.-A. Foujols, Y. Meurdesoif, P. Cadule, M. Devilliers, J. Ghattas, N. Lebas, T. Lurton, L. Mellul, I. Musat, J. Mignot, and F. Cheruy, “IPSL IPSL-CM6A-LR model output prepared for CMIP6 CMIP historical,” (en), 2018.

[214] Y.-H. Byun, Y.-J. Lim, H. M. Sung, J. Kim, M. Sun, and B.-H. Kim, “NIMS-KMA KACE1.0-G model output prepared for CMIP6 CMIP historical,” (en), 2019.

[215] H. Tatebe and M. Watanabe, “MIROC MIROC6 model output prepared for CMIP6 CMIP historical,” (en), 2018.

[216] J. Jungclaus, M. Bittner, K.-H. Wieners, F. Wachsmann, M. Schupfner, S. Legutke, M. Giorgetta, C. Reick, V. Gayler, H. Haak, P. de Vrese, T. Raddatz, M. Esch, T. Mauritsen, J.-S. von Storch, J. Behrens, V. Brovkin, M. Claussen, T. Crueger, I. Fast, S. Fiedler, S. Hagemann, C. Hohenegger, T. Jahns, S. Kloster, S.

Kinne, G. Lasslop, L. Kornblueh, J. Marotzke, D. Matei, K. Meraner, U. Mikolajewicz, K. Modali, W. Müller, J. Nabel, D. Notz, K. Peters-von Gehlen, R. Pincus, H. Pohlmann, J. Pongratz, S. Rast, H. Schmidt, R. Schnur, U. Schulzweida, K. Six, B. Stevens, A. Voigt, and E. Roeckner, "MPI-M MPI-ESM1.2-HR model output prepared for CMIP6 CMIP historical," (en), 2019.

[217] K.-H. Wieners, M. Giorgetta, J. Jungclaus, C. Reick, M. Esch, M. Bittner, S. Legutke, M. Schupfner, F. Wachsmann, V. Gayler, H. Haak, P. de Vrese, T. Raddatz, T. Mauritsen, J.-S. von Storch, J. Behrens, V. Brovkin, M. Claussen, T. Crueger, I. Fast, S. Fiedler, S. Hagemann, C. Hohenegger, T. Jahns, S. Kloster, S. Kinne, G. Lasslop, L. Kornblueh, J. Marotzke, D. Matei, K. Meraner, U. Mikolajewicz, K. Modali, W. Müller, J. Nabel, D. Notz, K. Peters, R. Pincus, H. Pohlmann, J. Pongratz, S. Rast, H. Schmidt, R. Schnur, U. Schulzweida, K. Six, B. Stevens, A. Voigt, and E. Roeckner, "MPI-M MPI-ESM1.2-LR model output prepared for CMIP6 CMIP historical," (en), 2019.

[218] S. Yukimoto, T. Koshiro, H. Kawai, N. Oshima, K. Yoshida, S. Urakawa, H. Tsujino, M. Deushi, T. Tanaka, M. Hosaka, H. Yoshimura, E. Shindo, R. Mizuta, M. Ishii, A. Obata, and Y. Adachi, "MRI MRI-ESM2.0 model output prepared for CMIP6 CMIP historical," (en), 2019.

[219] Ø. Seland, M. Bentsen, D. J. L. Oliviè, T. Toniazzo, A. Gjermundsen, L. S. Graff, J. B. Debernard, A. K. Gupta, Y. He, A. Kirkevåg, J. Schwinger, J. Tjiputra, K. S. Aas, I. Bethke, Y. Fan, J. Griesfeller, A. Grini, C. Guo, M. Ilicak, I. H. H. Karset, O. A. Landgren, J. Liakka, K. O. Moseid, A. Nummelin, C. Spensberger, H. Tang, Z. Zhang, C. Heinze, T. Iversen, and M. Schulz, "NCC NorESM2-LM model output prepared for CMIP6 CMIP historical," (en), 2019.

[220] M. Bentsen, D. J. L. Oliviè, Ø. Seland, T. Toniazzo, A. Gjermundsen, L. S. Graff, J. B. Debernard, A. K. Gupta, Y. He, A. Kirkevåg, J. Schwinger, J. Tjiputra, K. S. Aas, I. Bethke, Y. Fan, J. Griesfeller, A. Grini, C. Guo, M. Ilicak, I. H. H. Karset, O. A. Landgren, J. Liakka, K. O. Moseid, A. Nummelin, C. Spensberger, H. Tang, Z. Zhang, C. Heinze, T. Iversen, and M. Schulz, "NCC NorESM2-MM model output prepared for CMIP6 CMIP historical," (en), 2019.

[221] S. Park and J. Shin, "SNU SAM0-UNICON model output prepared for CMIP6 CMIP historical," (en), 2019.

[222] D. Neubauer, S. Ferrachat, C. Siegenthaler-Le Drian, J. Stoll, D. S. Folini, I. Tegen, K.-H. Wieners, T. Mauritsen, I. Stemmler, S. Barthel, I. Bey, N. Daskalakis, B. Heinold, H. Kokkola, D. Partridge, S. Rast, H. Schmidt, N. Schutgens, T. Stanelle, P. Stier, D. Watson-Parris, and U. Lohmann, "HAMMOZ-Consortium MPI-ESM1.2-HAM model output prepared for CMIP6 CMIP," (en), 2019.

[223] M. Dix, D. Bi, P. Dobrohotoff, R. Fiedler, I. Harman, R. Law, C. Mackallah, S. Marsland, S. O'Farrell, H. Rashid, J. Srbinovsky, A. Sullivan, C. Trenham, P. Vohralik, I. Watterson, G. Williams, M. Woodhouse, R. Bodman, F. B. Dias, C. Domingues, N. Hannah, A. Heerdegen, A. Savita, S. Wales, C. Allen, K. Druken, B.

Evans, C. Richards, S. M. Ridzwan, D. Roberts, J. Smillie, K. Snow, M. Ward, and R. Yang, “CSIRO-ARCCSS ACCESS-CM2 model output prepared for CMIP6 CMIP historical,” (en).

[224] T. Semmler, S. Danilov, T. Rackow, D. Sidorenko, D. Barbi, J. Hegewald, D. Sein, Q. Wang, and T. Jung, “AWI AWI-CM1.1MR model output prepared for CMIP6 CMIP historical,” (en).

[225] T. Wu, M. Chu, M. Dong, Y. Fang, W. Jie, J. Li, W. Li, Q. Liu, X. Shi, X. Xin, J. Yan, F. Zhang, J. Zhang, L. Zhang, and Y. Zhang, “BCC BCC-CSM2MR model output prepared for CMIP6 CMIP historical,” (en).

[226] N. C. Swart, J. N. Cole, V. V. Kharin, M. Lazare, J. F. Scinocca, N. P. Gillett, J. Anstey, V. Arora, J. R. Christian, Y. Jiao, W. G. Lee, F. Majaess, O. A. Saenko, C. Seiler, C. Seinen, A. Shao, L. Solheim, K. von Salzen, D. Yang, B. Winter, and M. Sigmond, “CCCma CanESM5-CanOE model output prepared for CMIP6 CMIP historical,” (en).

[227] T. Lovato, D. Peano, and M. Butenschön, “CMCC CMCC-ESM2 model output prepared for CMIP6 CMIP historical,” (en).

[228] EC-Earth Consortium (EC-Earth), “EC-Earth-Consortium EC-Earth-3-CC model output prepared for CMIP6 CMIP historical,” (en).

[229] EC-Earth Consortium (EC-Earth), “EC-Earth-Consortium EC-Earth3-Veg-LR model output prepared for CMIP6 CMIP historical,” (en).

[230] Z. Song, F. Qiao, Y. Bao, Q. Shu, Y. Song, and X. Yang, “FIO-QLNM FIO-ESM2.0 model output prepared for CMIP6 CMIP historical,” (en).

[231] J. Ridley, M. Menary, T. Kuhlbrodt, M. Andrews, and T. Andrews, “MOHC HadGEM3-GC31-LL model output prepared for CMIP6 CMIP historical,” (en).

[232] A. D. Choudhury, K. Raghavan, P. A. Gopinathan, S. Narayanasetti, M. Singh, S. Panickal, and A. Modi, “CCCR-IITM IITM-ESM model output prepared for CMIP6 CMIP historical,” (en).

[233] E. Volodin, E. Mortikov, A. Gritsun, V. Lykossov, V. Galin, N. Diansky, A. Gusev, S. Kostrykin, N. Iakovlev, A. Shestakova, and S. Emelina, “INM INM-CM5-0 model output prepared for CMIP6 CMIP historical,” (en).

[234] T. Hajima, M. Abe, O. Arakawa, T. Suzuki, Y. Komuro, T. Ogura, K. Ogochi, M. Watanabe, A. Yamamoto, H. Tatebe, M. A. Noguchi, R. Ohgaito, A. Ito, D. Yamazaki, A. Ito, K. Takata, S. Watanabe, M. Kawamiya, and K. Tachiiri, “MIROC MIROC-ES2L model output prepared for CMIP6 CMIP historical,” (en).

[235] W.-L. Lee and H.-C. Liang, “AS-RCEC TaiESM1.0 model output prepared for CMIP6 CMIP historical,” (en), 2020.

[236] Y. Tang, S. Rumbold, R. Ellis, D. Kelley, J. Mulcahy, A. Sellar, J. Walton, and C. Jones, "MOHC UKESM1.0-LL model output prepared for CMIP6 CMIP historical," (en).

[237] T. Semmler, S. Danilov, T. Rackow, D. Sidorenko, D. Barbi, J. Hegewald, Pradhan, H. K., D. Sein, and Wang, Q. and Jung, T., AWI-CM-1.1-MR model output prepared for CMIP6 ScenarioMIP: links to SSP126, SSP245, SSP370, and SSP585 scenarios, 2018.

[238] N. C. Swart, J. N. Cole, V. V. Kharin, M. Lazare, J. F. Scinocca, N. P. Gillett, J. Anstey, V. Arora, J. R. Christian, Y. Jiao, W. G. Lee, F. Majaess, O. A. Saenko, C. Seiler, C. Seinen, A. Shao, L. Solheim, K. von Salzen, D. Yang, B. Winter, and M. Sigmond, "CCCma CanESM5-CanOE model output prepared for CMIP6 CMIP," (en), 2019.

[239] D. Peano, T. Lovato, and S. Materia, "CMCC CMCC-ESM2 model output prepared for CMIP6 LS3MIP," (en), 2020.

[240] Z. Song, F. Qiao, Y. Bao, Q. Shu, Y. Song, and X. Yang, "FIO-QLNM FIO-ESM2.0 model output prepared for CMIP6 GMMIP amip-hist," (en), https://doi.org/10.22033/ESGF/CMIP6.9165, 2019.

[241] E. Volodin, E. Mortikov, A. Gritsun, V. Lykossov, V. Galin, N. Diansky, A. Gusev, S. Kostrykin, N. Iakovlev, A. Shestakova, and S. Emelina, "INM INM-CM5-0 model output prepared for CMIP6 ScenarioMIP," (en), Earth System Grid Federation, 2019.

[242] A. Voldoire, "CNRM-CERFACS CNRM-CM6-1-HR model output prepared for CMIP6 HighResMIP," Earth System Grid Federation, 2019. Accessed on: Sep. 20 2021.

[243] T. Lovato and D. Peano, "CMCC CMCC-CM2-SR5 model output prepared for CMIP6 ScenarioMIP," 2020.

[244] J. Ridley, M. Menary, T. Kuhlbrodt, M. Andrews, and T. Andrews, "MOHC HadGEM3-GC31-MM model output prepared for CMIP6 CMIP historical," 2019. Accessed on: Sep. 20 2021.

[245] J. Jungclaus, M. Bittner, K.-H. Wieners, F. Wachsmann, M. Schupfner, S. Legutke, M. Giorgetta, C. Reick, V. Gayler, H. Haak, P. de Vrese, T. Raddatz, M. Esch, T. Mauritsen, J.-S. von Storch, J. Behrens, V. Brovkin, M. Claussen, T. Crueger, I. Fast, S. Fiedler, S. Hagemann, C. Hohenegger, T. Jahns, S. Kloster, S. Kinne, G. Lasslop, L. Kornblueh, J. Marotzke, D. Matei, K. Meraner, U. Mikolajewicz, K. Modali, W. Müller, J. Nabel, D. Notz, K. Peters-von Gehlen, R. Pincus, H. Pohlmann, J. Pongratz, S. Rast, H. Schmidt, R. Schnur, U. Schulzweida, K. Six, B. Stevens, A. Voigt, and E. Roeckner, "MPI-M MPI-ESM1.2-HR model output prepared for CMIP6 CMIP historical," Earth System Grid Federation, 2019. Accessed on: Sep. 10 2021.

[246] Energy Market Regulatory Authority (EMRA), Electricity Market Production Licenses. [Online] Available: https://lisans.epdk.gov.tr/epvys-web/faces/pages/lisans/elektrikUretim/elektrikUretimOzetSorgula.xhtml. Accessed on: Feb. 18 2022.

[247] Energy Market Regulatory Authority (EMRA), Electricity Market Pre-Licenses. [Online] Available: https://lisans.epdk.gov.tr/epvys-web/faces/pages/lisans/elektrikUretimOnLisans/elektrikUretimOnLisansOzetSorgula.xhtml. Accessed on: Feb. 18 2022.

[248] Rüzgar Kaynağına Dayalı Elektrik Üretim Başvurularının Teknik Değerlendirmesi Hakkında Yönetmelik, 2015.

[249] U. Schulzweida, CDO User Guide (2.1.0).

[250] Maurice G Kendall, Rank correlation methods. London :: Griffin, 1975.

[251] HENRY B. MANN, "Non-parametric tests against trend," pp. 245–259, 1945.

[252] M. Hussain and I. Mahmud, "pyMannKendall: a python package for non parametric Mann Kendall family of trend tests," JOSS, vol. 4, no. 39, p. 1556, 2019.

[253] P. K. Sen, "Estimates of the Regression Coefficient Based on Kendall's Tau," Journal of the American Statistical Association, vol. 63, no. 324, pp. 1379–1389, 1968.

[254] Wind Turbines Part 3: Design Requirements for Offshore Wind Turbines, 2009.

[255] G James, D Witten, T Hastie, and R Tibshirani, An introduction to statistical learning. New York: Springer, 2013.

[256] Scikit-learn: Machine learning in Python, 2011.

[257] R. Brogli, C. Heim, S. L. Sørland, and C. Schär, The pseudo-global-warming (PGW) approach: Methodology, software package PGW4ERA5 v1.1, validation and sensitivity analyses, 2022.

[258] Y. Li, Z. Li, Z. Zhang, L. Chen, S. Kurkute, L. Scaff, and X. Pan, "High-resolution regional climate modeling and projection over western Canada using a weather research forecasting model with a pseudo-global warming approach," (English), Hydrol. Earth Syst. Sci., vol. 23, no. 11, pp. 4635–4659, 2019.

[259] Dr. Catherine Meissner, "WindSIM | Getting Started: 12th Edition," 2019.

[260] USGS - United States Geological Survey, "Aster GDEM Version 1: 'ASTGTM: ASTER Global Digital Elevation Model V001.'' U.S.,"

[261] "Corine 2006: Version 13 (02/2010) - Raster data on land cover for the CLC2006 inventory," 2006. [Online] Available: https://www.eea.europa.eu/data-and-maps/data/clc-2006-raster. Accessed on: Apr. 15 2017.

[262] Global Mapper: Trial Software: Blue Marble, 2022.

[263] Prepared by AWS Scientific, Inc., Albany, New York, Wind Resource Assessment Handbook: Fundamentals for Conducting a Successful Monitoring. USA, 1997.

[264] D. C. Carslaw and K. Ropkins, "openair — An R package for air quality data analysis," Environmental Modelling & Software, vol. 27-28, pp. 52–61, 2012.

[265] R. Döscher, M. Acosta, A. Alessandri, P. Anthoni, T. Arsouze, T. Bergman, R. Bernardello, S. Boussetta, L.-P. Caron, G. Carver, M. Castrillo, F. Catalano, I. Cvijanovic, P. Davini, E. Dekker, F. J. Doblas-Reyes, D. Docquier, P. Echevarria, U. Fladrich, R. Fuentes-Franco, M. Gröger, J. v. Hardenberg, J. Hieronymus, M. P. Karami, J.-P. Keskinen, T. Koenigk, R. Makkonen, F. Massonnet, M. Ménégoz, P. A. Miller, E. Moreno-Chamarro, L. Nieradzik, T. van Noije, P. Nolan, D. O'Donnell, P. Ollinaho, G. van den Oord, P. Ortega, O. T. Prims, A. Ramos, T. Reerink, C. Rousset, Y. Ruprich-Robert, P. Le Sager, T. Schmith, R. Schrödner, F. Serva, V. Sicardi, M. Sloth Madsen, B. Smith, T. Tian, E. Tourigny, P. Uotila, M. Vancoppenolle, S. Wang, D. Wårlind, U. Willén, K. Wyser, S. Yang, X. Yepes-Arbós, and Q. Zhang, "The EC-Earth3 Earth system model for the Coupled Model Intercomparison Project 6," (English), Geosci. Model Dev., vol. 15, no. 7, pp. 2973–3020, 2022.

[266] B. Smith, LPJ-GUESS-an ecosystem modelling framework. INES, Sölvegatan, 12, 22362, 2001.

[267] D. E. K. Dzebre, A. A. Acheampong, J. Ampofo, and M. S. Adaramola, "A sensitivity study of Surface Wind simulations over Coastal Ghana to selected Time Control and Nudging options in the Weather Research and Forecasting Model," (eng), Heliyon, vol. 5, no. 3, e01385, 2019.

[268] Technical University of Denmark, DTU 10MW-178RWT Power Curve. [Online] Available: wind turbine power curve and trust coefficient from WindSIM. Accessed on: Dec. 20 2022.

[269] GEBCO Compilation Group, GEBCO 2020 Grid. [Online] Available: doi:10.5285/a29c5465-b138-234d-e053-6c86abc040b9. Accessed on: Nov. 18 2022.

[270] Energy Market Regulatory Authority (EMRA), Electricity Production Licences. [Online] Available: https://lisans.epdk.gov.tr/epvys-web/faces/pages/lisans/elektrikUretim/elektrikUretimOzetSorgula.xhtml. Accessed on: Jan. 05 2021.

[271] İ. Işık Çetin, "Effects of numerical weather predictions on wind power forecasts," Master of Science.

[272] United Nations, Third United Nations Conference on the Law of the Sea: UNCLOS III, (1973–1982).

[273] Law on Territorial Sea of Republic of Türkiye, No: 2674, Official Gazette dated: 29/5/1982 numbered 17708.

[274] Ministry of Energy and Natural Resources, Turkish Electricity Demand Projection Report: 2020-2040 Period. [Online] Available: https://enerji.gov.tr//Media/Dizin/EIGM/tr/Raporlar/ENTAP/114176-turkiye_elektrik_enerjisi_talep_projeksiyonu_raporu.pdf. Accessed on: May 26 2022.

[275] UN General Assembly, Transforming Our World: The 2030 Agenda for Sustainable Development. Draft resolution referred to the United Nations summit for the adoption of the post-2015 development agenda by the General Assembly at its sixty-ninth session, 2015.

## CURRICULUM VITAE

Surname, Name: Işık Çetin, İrem

### EDUCATION

| Degree | Institution | Year of Graduation |
|---|---|---|
| MS | METU Earth System Science | 2018 |
| BS | ITU Meteorological Engineering | 2013 |
| High School | Şehit Osman Altınkuyu Anadolu High School, Yalova | 2006 |

### FOREIGN LANGUAGES

Advanced English

### WORK EXPERIENCE

| Year | Place | Enrollment |
|---|---|---|
| 2022-Present | Turkish Energy, Nuclear and Min. Research Agency | International R&D Programmes Group Manager |
| 2019-2022 | MENR, Wind Energy Group | Coordinator |
| 2013-2019 | MENR, General Directorate of Renewable Energy | Engineer |

### PUBLICATIONS

1. Işık Çetin I., "Effects of Numerical Weather Predictions on Wind Power Forecasts", MS Thesis, 2018

2. Işık Çetin I., Yücel I., "CMIP6 Multi-model Ensemble Development for Future Offshore Wind Resources of Türkiye", 10th Int. Atmospheric Science Conferences, 2022

3. Işık Çetin I., Yücel I., M. T. Yilmaz, and B. Onol, "Multi-model ensemble evaluation of CMIP6-driven surface wind for eastern Mediterranean, Türkiye ", Int. Journal of Climatology, (Under Review)

4. Irem I. Cetin, Ismail Yucel, Soner Ç. Bağçaci, M. Tuğrul Yilmaz, "Climate Change Impacts On Wind Energy Resource Of Türkiye Usıng High-Resolutıon WRF Model with the Ensemble of CMIP6 GCMS", Oral Presentation, Wind Energy Science Conference-2023 (accepted)